Late Quaternary palaeoenvironmental reconstruction of northern Namibia using palaeolake sediments from Etosha Pan

---

Matjie Lillian Maboya

Supervisors: Professor D.S.G. Thomas and Dr S.L. Burrough

Green Templeton College

Thesis submitted for the degree of
Doctor of Philosophy (D. Phil)

University of Oxford

Michaelmas Term 2024

Abstract

Palaeoenvironmental reconstructions are an important tool in understanding major environmental and climatic changes from the past and into the future. They are critical in parts of southwestern Africa where existing records are sparse and future rates of climate change are predicted to be high. Etosha Pan is situated in the drylands of northern Namibia and has long attracted the interest of researchers who hypothesised changes in its geomorphological and palaeoenvironmental context over the late Quaternary. One of the reasons for uncertainty about the basin's palaeohydrological history is the lack of precision in age control to uncover the history of the pan over past millennia. In this thesis, a dual approach of optically stimulated luminescence (OSL) and radiocarbon dating of lakebed sediments and marginal sand ridges was adopted to better constrain the timing of major palaeoenvironmental changes. The work was undertaken by extracting samples from the north-western part of the pan and subjecting them to a range of sedimentological and geochemical analyses.

The new data from this study were used to reconstruct palaeoenvironmental and palaeohydrological dynamics in the Etosha basin from the last 40 ka. Key findings are that the pan underwent fluctuating lake levels in response to changing climate. This study proposes that, during the last glacial maximum (LGM, 23 - 19 ka), Etosha Pan sustained a deep lake under a wetter climate. The pan later experienced shallow lake levels at the start of the Holocene, which increased again due to a more humid climate during the mid-Holocene (7 - 5 ka). The key source of moisture during both periods is likely summer rainfall due to a temporary southward migration of the African tropical rain belt. These findings have implications for palaeoclimate modelling exercises for the LGM and mid-Holocene periods and assist in clarifying conflicting hypotheses of pan geomorphological evolution.

Acknowledgements

I would like to express gratitude to my supervisors, Prof. David Thomas and Dr. Sallie Burrough, and to Dr. Julie Durcan for guiding me in OSL dating. I appreciate your guidance, patience and for enabling my growth as a scientist throughout the past few years.

I am grateful to the following people for assisting with much needed resources and assistance for fieldwork: Mike Meadows, Martin Hipondoka, Anna Ambata and Andrew Baxter. Much appreciation to Szilvi, Mona, Hong and my lab mates Ella, Sam, Maike and Jiang for discussions and assistance in the lab.

Many thanks to the following organisations that supported tuition, fieldwork and laboratory work costs:

- Commonwealth Scholarship for Developing Countries
- Etosha Ecological Institute
- Green Templeton College
- iThemba LABS
- Namibia Ministry of Environment and Tourism
- National Environmental Isotope Facility (NEIF), funded by Natural Environment Research Council (NERC) at the Oxford Radiocarbon Accelerator Unit
- National Oceanography Centre (NOC) at University of Southampton
- Oppenheimer Memorial Trust
- Oxford University School of Geography and the Environment
- University of Cape Town Department of Environmental and Geographical Sciences
- University of Leicester School of Geography, Geology and the Environment

- University of Namibia Department of Geography, History and Environmental Studies
- University of Oxford's Wellcome Trust Palaeogenomics and Bio-Archaeology Research Network (PalaeoBARN)
- University of Witwatersrand Geography, Archaeology and Environmental Studies

Friends and family

I want to thank Mama, Papa, Morongoa, Tebello, Morategi, Alex, Geraldine, Kaisha, Khomotso, Kopo, Malose, Mogaleadi, Tshepo, Mpho, Olivia, Jimmy, Tonny, Jeffrey, Nteranya, Ramapulana, Takalani, Sebolaishi and many others. And to the Oxford Africa Society – thanks for the braais and consistent presence throughout this period. It truly takes a village!

Contents

List of Figures

List of Tables

List of Equations

Units

˚**C** Degrees Celsius

k cal BP Calendar years (thousands) before present (1950 AD)

g cm^{-3} Grams per centimetre cubed

Gy Gray (1 Gy = 1 J kg-1)

Gy ka-1 Grays per thousand years

ka Thousand years

km Kilometre

m Metre

masl metres above sea level

Ma Million years

mm Millimetre

ppm Parts per million

‰ Per mille (parts per thousand)

s Second

µm Micrometre

yr Year

Abbreviations

^{14}C Carbon-14 (radiocarbon)

^{90}Sr Strontium-90

^{90}Y Yttrium-90

CAB Congo Air Boundary

CAM Central Age Model

CMIP Climate Modelling Intercomparison Project

De Equivalent Dose

DRAC Dose Rate and Age Calculator

DRC Dose Response Curve

H_2O_2 Hydrogen peroxide

H_2SiF_6 Fluorosilicic

HCl Hydrochloric acid

HF Hydrofluoric acid

ICP-MS Inductively Coupled Plasma Mass Spectrometry

ITCZ Intertropical Convergence Zone

IRSL Infra-red stimulated luminescence

K Potassium

LED Light-emitting diode

LGM Last Glacial Maximum

LIA Little Ice Age

Lx Natural or regenerative dose

Lx/Tx Sensitivity-corrected OSL signal

MAAD Multiple Aliquot Additive Dose

MAM Minimum Age Model

MG Multigrain

MH Mid-Holocene

NERC Natural Environment Research Council

OSL Optically Stimulated Luminescence

PCA Principal Component Analysis

PH Preheat

PMIP Palaeoclimate Modelling Intercomparison Project

SAA South Atlantic Anticyclone

SAR Single Aliquot Regenerative

SG Single grain

SST Sea surface temperature

TL Thermoluminescence

Tx Test Dose

VPDB Vienna Pee Dee Belemnite

XRF X-ray fluorescence

α Alpha radiation

β Beta radiation

γ Gamma radiation

$\delta^{13}C$ Ratio of carbon-12 and carbon-13

$\delta^{18}O$ Ratio of oxygen-16 and oxygen-18

σ Standard deviation

Chapter 1: Introduction

1.1. Introduction

At a time of unprecedented climate uncertainty linked to global warming, it is essential to have better data on natural system dynamics for the full range of past environmental states to be established. Climate is a long-term and changing phenomenon that is better understood by analysing palaeoclimate archives. Saltpans and palaeolakes are integral to palaeoenvironmental reconstruction studies because they often contain records of environmental and climatic changes that persisted for significantly long periods. Quaternary palaeoenvironmental lacustrine studies have indeed been a rich source of data on past environments and climate in Africa. Most studies on the continent have been conducted in tropical East Africa where a range of factors, including topography and median long term climate conditions, can favour preservation of proxies (e.g., Street-Perrott *et al.*, 2007; Levin *et al.*, 2011; Njagi *et al.*, 2021). However, basins in dryland areas have the potential to yield significant data as shown in the case of the Makgadikgadi basin in Botswana (Burrough *et al.*, 2009; Burrough *et al.*, 2022). Etosha Pan in northern Namibia has yielded some important palaeoenvironmental data in the drylands through research that has uncovered lake-level changes, geomorphological evolution and sediment mobility on the pan (Brook *et al.*, 2007; Hipondoka *et al.*, 2014). Such research has allowed important questions on the pan's development and palaeohydrological history to be partially addressed. Investigating Etosha pan sediments will help to enhance current understanding of the potential impacts of rising temperatures to develop more accurate predictions for future climate conditions.

To assess critical points of change and the resilience of sensitive ecosystems such as those in the Etosha Pan (Figure 1.1), there is an urgent need to draw on insights from available palaeo-archives to understand how the basin has responded to or been influenced by climatic changes in the past. Palaeoenvironmental reconstruction studies utilise proxy evidence to provide information on how the landscape and its ecosystems responded to acute and long-term climate and hydrological change. However, in southwestern Africa, there is still limited information on how the environment responded to palaeoclimatic change in the late Quaternary period. Therefore, this thesis aims to investigate sediments from Etosha Pan to reconstruct climate and environmental changes over multi-millennial timescales. An improved analysis of palaeoenvironmental evidence from the basin can enhance our understanding of complex atmospheric circulation systems that control climate over this large palaeolake.

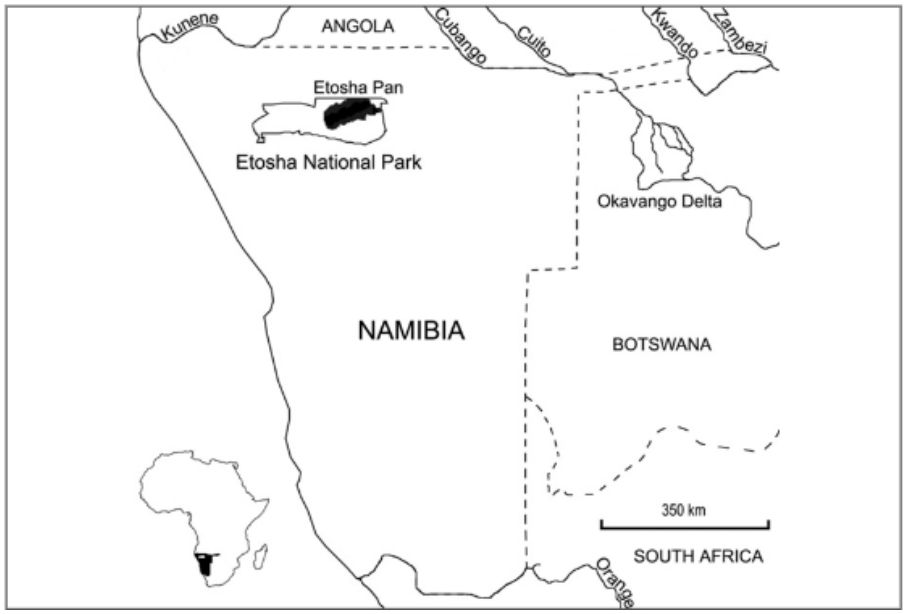

Figure 1.1: Etosha Pan's location in southern Africa. Adapted from Hipondoka (2005).

This project advances the palaeoenvironmental evidence base for Etosha by generating new data from basin floor sediments to investigate: 1) the nature of geomorphological evolution, i.e., whether it was dominated by aeolian processes since the Miocene (Miller, 2008), or underwent dynamic hydrological changes that included lacustrine states in the late Quaternary (Brook *et al.,* 2007); 2) the palaeoenvironmental context of the marginal sand ridges on the western part of the pan; 3) the potential magnitude and frequency of lacustrine dynamics in the late Quaternary. In an effort to answer the outstanding hydrological dynamism of the system and what it preserves about palaeoenvironmental change, optically stimulated luminescence (OSL) data have been used to build a sedimentological history of the pan's marginal sand ridges and sediment cores from a spring mound on the pan-floor. This chapter introduces the present-day climate of northern Namibia and includes a short overview of the current literature of Etosha that has necessitated this research. The chapter ends with an outline of the aims and objectives of the study.

1.2. Climate setting of northern Namibia

Etosha Pan is situated in central northern Namibia, an area that is presently semiarid and towards the northern limits of southern Africa's Kalahari dryland. An exploration of the current climate context of Etosha offers insights into the potential contributions of past climate change to basin hydrology. Namibia is characterised as semi-arid to hyper-arid with an easterly rainfall gradient where some areas on the west coast receive under 100 mm of precipitation per year, and up to 470 mm at Etosha in central northern Namibia (Lancaster, 2002). The headwaters of the Ekuma Delta that enter Etosha Pan from the northwest emerge from southern Angola, where the Cuvelai-Etosha drainage basin forms iishana (dozens of drainage channels) that flow north-south into the pan (Huntley *et al.,* 2019). As such, the majority of water entering Etosha

travels a considerable distance. The Zambezi low-level jet acts as a conduit for moisture from the Indian Ocean into the continental interior and is crucial for precipitation in the southwestern Africa region during wet seasons (Munday *et al*., 2021). The jet is more pronounced during the austral summer when it can contribute to increased precipitation in southern Angola and episodic flooding in northern Namibia where Etosha is located (Pereira *et al.,* 2024).

In addition, the South Atlantic Anticyclone situated over the ocean to the southwest (in summer) or west (in winter) of Namibia is a high-pressure system that advects moist air in an easterly direction towards the south-west coast of Africa (Tyson, 1986). Also contributing to the aridity on the coast, the cool Benguela current flows northwards in the South Atlantic (Figure 1.2) and maintains low humidity due to the low sea surface temperatures (SST) that prevent convection (Eckardt *et al*., 2013). Occasionally, the Benguela upwelling system diminishes, and this is associated with a weakening of the high-pressure inversion, which allows the penetration of Indian Ocean air masses to north-western Namibia where it produces rainfall. These negative anomalies in the pressure field also allow the southward migration of the African tropical rain belt, creating more rainfall events in the summer (Tyson, 1986; Nicholson, 2000). The convergence area of air masses from the tropical southern hemisphere Atlantic and Indian Ocean is commonly called the Congo Air Boundary (CAB) and its position is determined by pressure cells over both oceans. As such, Etosha Pan humidity is influenced by moisture from the rain-bearing systems from the Indian Ocean, when the CAB penetrates southwest and from the tropical air mass when the African tropical rain

belt migrates southwards (Tyson, 1986). The past cycles of aridity and humidity at Etosha were, therefore, likely influenced by the extent to which these systems were expressed or how they interacted. Moreover, the climate drivers of these cycles are worth investigating in order to have an improved understanding of the mechanisms that influence hydrological conditions at Etosha in the past, and which may be important in the future.

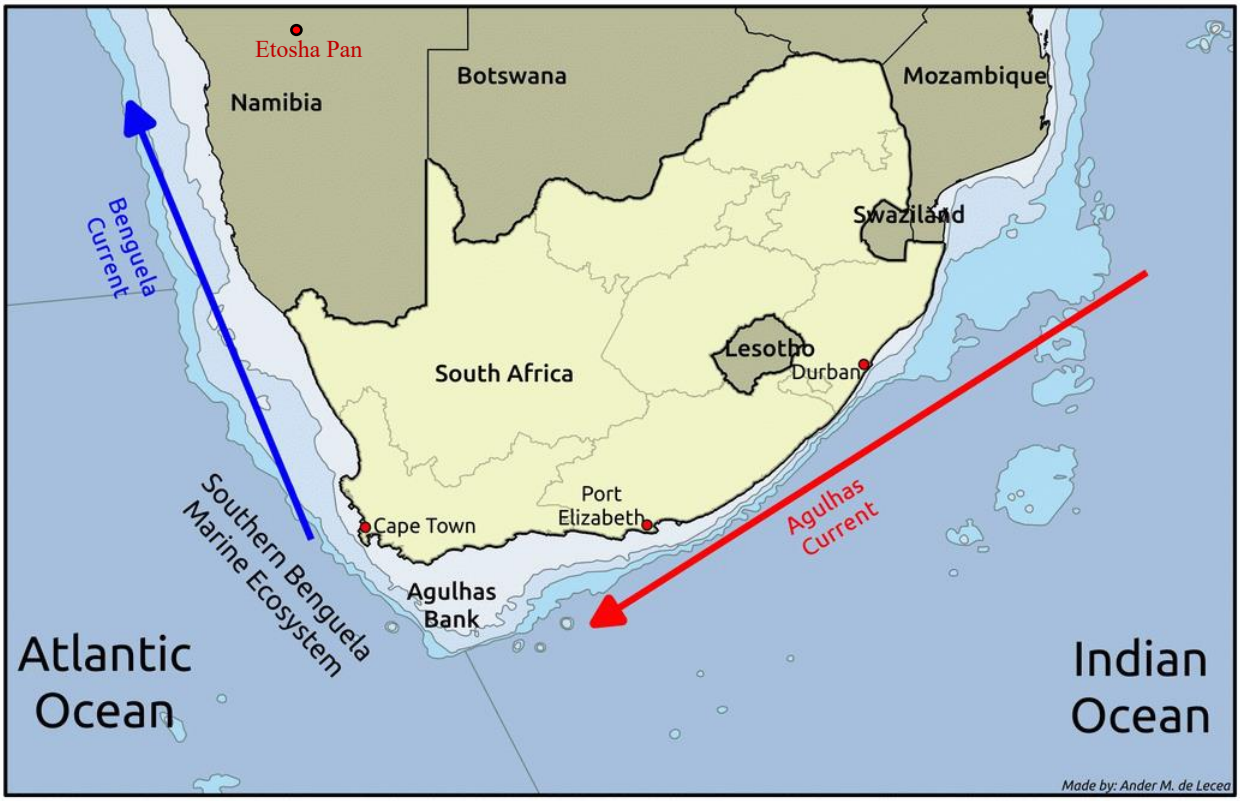

Figure 1.2: Southern Africa with the Benguela Current on the west coast. Adapted from (de. Lecea, 2016)

Namibia has a long history of palaeoenvironmental research, though the majority of investigated sites are located in the southern and western parts of the country. These include rock hyrax middens near the west coast (Scott *et al.*, 1996; Chase *et al.*, 2009; Chase *et al.*, 2011; Chase *et al.*, 2013; Chase *et al.*, 2023), speleothems from south of Etosha at Dante Cave (e.g., Railsback *et al.*, 2022), and the westward draining river systems from the Namibian highlands that form part of southern Africa's Great escarpment, separating coastal and inland regions (Walsh *et al.*, 2022). There have also been palaeoecological and sedimentary studies from pan sediments in the southeast of Namibia (Belz *et al.*, 2020; Schuller *et al.*, 2018) and dune accumulation analyses more broadly in the Namibian Kalahari (Stone and Thomas., 2008; Stone *et al.*, 2022). At Etosha, previous palaeoenvironmental studies have been limited, but include investigations of faunal remains such as the Miocene-Pliocene fossils from the western river delta (Pickford *et al.*, 2009). Prominent sand ridges on the western margins have long sparked fascination and a number of studies have attempted to understand their formation using thermoluminescence dating (Buch and Zoller, 1992), and later OSL (Brook *et al.*, 2007; Hipondoka *et al.*, 2014) and have had a handful of studies conducted on them. Brook *et al.* (2011) have additionally carried out studies on stromatolites found on the eastern side of Etosha for their potential to provide hydrological lake status information. These studies have been extremely valuable in providing critical information on palaeoenvironmental and palaeohydrological change. New tools and techniques, however, offer the potential to provide both greater chronological precision and additional information on how local conditions have been

impacted by regional climate changes. This study investigates pan-floor sediments on western side of the pan, which have historically received no research.

The Last Glacial Maximum (LGM; considered here as 23-19 ka, following Hughes *et al.* (2013)) and the Holocene (11.7 ka to present) have been commonly used in palaeoclimate modelling experiments such as PMIP and CMIP as periods against which the success of the models is tested. The LGM is understood to be a period of the most recent large ice extent across high latitudes on the globe (Yokoyama *et al.*, 2000). There is also a need to improve understanding of the manifestation of LGM and Holocene changes in drylands, which have been under-researched relative to more temperate and tropical regions.

Empirical data from ephemeral lakes in southern Africa have been used to test some of the models' abilities to simulate past climate (James *et al.*, 2018; Williams *et al.*, 2020; Dee *et al.*, 2021). As a result, these periods, which arguably represent the extremes of glacial and interglacial conditions, have become important points of investigation. Our ability to understand climate during these periods has the potential to enhance our capability to accurately project future climate changes. However, places such as northern Namibia, which are arid in the modern-day, remain poorly understood in terms of regional responses to extreme changes in climate.

In an effort to understand southern Africa's climate and environmental dynamics during the LGM and the Holocene, Etosha Pan is well-suited for palaeoenvironmental

reconstructions. This is due to its geographical position at the confluence of several atmospheric circulations such as Indian and Atlantic Ocean-sources moisture, penetration of tropical moisture from the African tropical rain belt, with additional complexity from the Kalahari Discontinuity and Congo Air Boundary (Howard and Washington, 2019). In this study, a suite of geochemical, sedimentological and palaeoecological proxies was used to build an improved chronology of palaeoenvironmental change at Etosha Pan.

1.3. Etosha Pan

Etosha Pan is the second-largest salt pan in southern Africa and is one of Namibia's most important national parks for both wildlife and tourism and is currently on UNESCO's tentative list of World Heritage Sites (Figure 1.1). The pan lies at the tail of the Cuvelai-Etosha Basin, which stretches 450 km north to south between Angola and Namibia, covering 160,000 km² (Mendelsohn *et al*., 2013). The pan has a surface area of about 5,000 km^2 at a mean floor elevation of 1080 m (Hipondoka *et al.*, 2014).

As noted in the previous section, the sparse data available on past hydrological conditions at Etosha has sparked a lively debate. Rust (1984) and Miller (2008) hypothesised that the Etosha basin is not a former Quaternary period lake at all but instead developed as a pan from long-term aeolian deflation that began in the Miocene and has remained dominantly influenced by aeolian conditions ever since. Others, including Schwarz (1920) and Hipondoka *et al.* (2014) have proposed a more complex

history. In essence, they argue that Etosha was formerly a large lake system that has periodically recorded fluctuating levels in relation to regional climate changes.

Related to these ideas, there is also a fundamental debate about the palaeoenvironmental context of sand ridges that lie parallel to the western pan margin today. Brook *et al.* (2007) and Hipondoka *et al.* (2014) have used what they interpreted as shoreline records from the Etosha sand ridges to demonstrate late Quaternary hydrological dynamism in the pan. Other scholars, however, interpreted the ridges to be of aeolian origin (lunette dunes) and used thermoluminescence dating to reconstruct palaeoenvironmental conditions with numerous periods of aridity to have occurred intermittently since 140 ka (Buch and Zoller, 1992). The nature of sediment accumulation at the basin margins remains contested. This leaves a gap in understanding the Etosha basin and the palaeoenvironmental context of its sand ridges on the western margin. Pan floor sediments have the potential to fill in some of the gaps in the record to improve the lake level reconstruction history. This thesis aims to collect new data from both the pan floor and the basin margins to investigate the palaeoenvironmental changes and create a more synchronous geomorphological history of the pan.

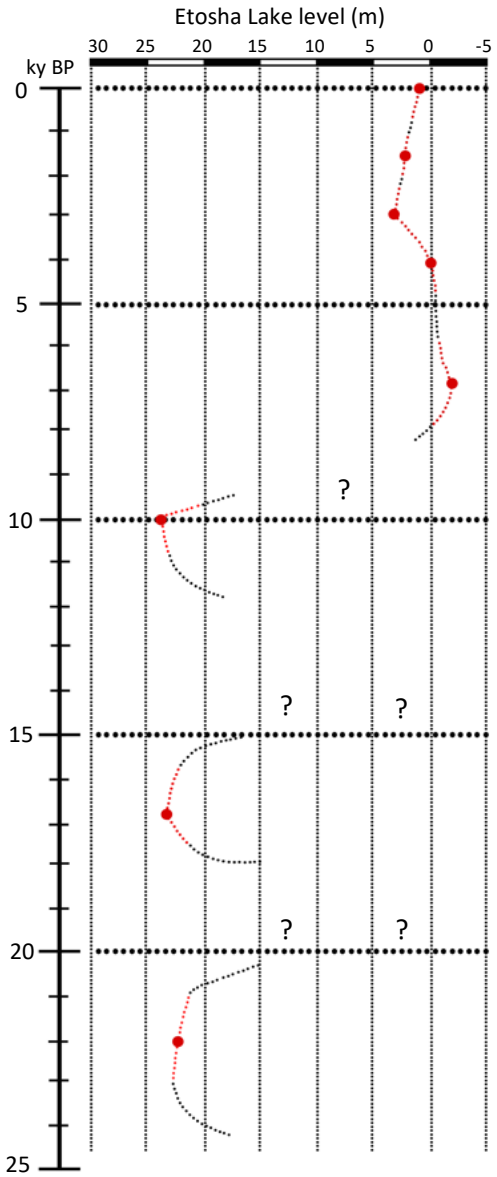

Figure 1.3: In red are the estimated lake levels at Etosha Pan over the last 25 ka BP (Figure adapted from Hipondoka *et al*., 2014). Red dots indicate the estimated lake level based on sediment ages from sand ridges, while the red curved lines are the relative uncertainties in the lake depth with 0 m as the modern-day shoreline. Question marks indicate gaps in the literature where no information is available regarding lacustrine levels at Etosha.

The present study aims to fill significant gaps within the lake-level reconstruction record at Etosha by analysing higher resolution sediment cores and exposures in test pits from the western basin floor (Figure 1.3). To date, no clear understanding of the long-term hydroclimate controls of the Etosha system and basin floor sediments have been investigated for their potential to provide robust data to address questions of basin origin or hydroclimate responses. At the same time, existing data remains both controversial and too poor in terms of temporal resolution to enable climate model-driven hypotheses to be tested e.g., various models within PMIP suggest differing past hydroclimate changes in the system. Therefore, a new palaeoenvironmental record from Etosha is needed to supplement existing data mainly focused on the shoreline reconstruction and lake-level status data from the sand ridges. In response, this project has investigated, for the first time, sediments from the basin floor system through a multiple-proxy approach to test hypotheses about pan chronology and hydrology. Samples from a series of lakebed marginal sand ridges, two sediment cores from the lakebed and pits on the lakebed have been subject to a range of field sampling and laboratory analyses to determine the chronology and environmental contexts of deposition.

It is poorly understood how different sources of water have influenced the hydrology of the salt pan or how they varied in the past. Specifically, the links between the Ekuma Delta and the spatial distributions of sediments and water over the pan remain unresolved. The Ekuma Delta has been the main inlet of riverine sediments and fluvial inflows into the pan during the late Quaternary and is located on the north-western part

of the pan. Other ephemeral river inflows in the modern-day occur on the eastern part of the pan through the Omarumba Owambo and Omuthiya rivers. Archibald and Nott (1987) noted that flooding of the pan today occurs on the east due to local rainfall (direct precipitation) and incoming floodwaters from the north. Moreover, it has been hypothesised that sediments from the Ekuma Delta are transported to the marginal sand ridges through complex aggradation processes during the late Quaternary (Hipondoka *et al.*, 2014). As the ridges remain a point of contestation, a record of environmental change from the pan could help to contextualise the role of the delta in sediment accumulation at the western end of the pan. Water is a limited resource at the Etosha Pan, and this can be seen in the short spells of unpredictable rainfall between October and May. However, the modern-day hydrological conditions continue to be a key attraction for wildlife. Therefore, a deep understanding of this setting and how it has changed in the past is important for managing the National Park and its sensitive ecological resources.

1.4. Aim and objectives

*This project **aims** to generate a robust dataset to establish the chronology and palaeohydrology of Etosha Pan through multi-proxy analyses of sediment cores, lakebed and marginal ridge sediments to reconstruct late Quaternary palaeoenvironmental change in northern Namibia.*

1.4.1. Primary Research Objectives:

Objective 1:

Produce a new, robust chronology of sedimentary accumulation of the Etosha lakebed and of the marginal sand ridges using modern dating protocols (OSL and Radiocarbon Dating) (Chapter 4 and Chapter 5).

Objective 2:

To characterise the nature and stratigraphy of pan floor sediments, and thereby environmental controls on their accumulation, at four sites on the northwestern end of the pan. This objective aligns with informing the timing and nature of the development of the three sand ridges parallel to the modern-day shoreline of the Etosha Pan (Chapter 4 and Chapter 6).

Objective 3:

To reconstruct the palaeoecological and palaeohydrological history of a spring mound on the basin floor by applying a range of geochemical and sedimentological analyses on sediment cores extracted from it (Chapter 5 and Chapter 6).

Objective 4:

To establish a record of palaeohydrological change within Etosha Pan through various landforms: sand ridge, basin floor and spring mound sediments and their respective chronologies (Chapter 7).

Objective 5:

To establish and contextualise the new palaeoenvironmental record from Etosha Pan within the growing regional record established from recent literature (Chapter 7).

1.5. Thesis structure

The remainder of this thesis is structured as follows:

Chapter 2 is a review of the context of Etosha within the wider literature, providing the grounds for the basis of this study and a comprehensive outlook of the importance of Etosha's palaeoenvironmental context in southwestern Africa. Previous work at Etosha and other parts of northern Namibia are described.

Chapter 3 outlines the methodological approach used to collect data in the research, starting with justification for the choice of field techniques and followed by a description of the laboratory analyses applied.

In Chapter 4, the new chronology of lakebed and ridge sediments is presented, underpinned by OSL dating. This record is placed within the context of earlier studies reported in Chapter 2.

Following this, Chapter 5 offers palaeoecological insights obtained from eggshells found in sediment cores from a spring mound on the basin floor. The eggshells were analysed through stable isotopes and ancient DNA analyses. These findings help to

build a more coherent palaeohydrological history of the pan during and after the last glacial maximum (LGM) in terms of the timing of lacustrine phases and lake levels.

Chapter 6 presents $\delta^{13}C$ data from sedimentary sequences preserved in pan-floor cores with the chronology of their deposition constrained by radiocarbon dating. These data are used to reconstruct lake levels on the pan over the last 40 k cal BP.

Chapter 7 integrates the new information about the pan into a holistic record of the pan's geomorphological history and its controls. The Chapter also allows for a comparison with other studies to improve the regional understanding of the Etosha Basin and its surrounds. In this Chapter, an integration of the new data from this project will be assessed within a regional analysis comprising existing published records from southwestern Africa.

Chapter 8 concludes the study with an assessment of the project's success in addressing the goals and gives a final summary of the study.

Chapter 2: Literature Review

2.1. Introduction

Drylands occupy 40 % of the earth's land surface and are home to more than two billion people who rely on them to support their livelihoods (Goudie and Wells, 1995; Safriel *et al.*, 2005; Middleton, 2011; Gudka *et al.*, 2014; Cooke and Warren, 2023). Most drylands in Namibia are likely to experience significant environmental, including hydrological, changes due to future temperatures projected to increase by up to 6 °C by the end of the century (in low-climate-mitigation scenarios) (Niang *et al.,* 2014). Drylands are particularly vulnerable due to their sensitivity to changes in temperature and rainfall (Engelbrecht, 2019). To make predictions about how such changes might impact these environments in the future, it is important to understand how they have responded to climate changes in the past millennia. This chapter will review late Quaternary palaeoenvironmental change literature from Etosha, northern Namibia and southwestern Africa more broadly. It is focused on studies that examine the period from the late Pleistocene until the late Holocene. Throughout this chapter, the gaps and inconsistencies in existing research will be highlighted. These include differences in interpreting the spatial extent of palaeoenvironmental change and the driving mechanisms of large-scale change. In addition, in this chapter a rationale is generated for investigating Etosha Pan as a promising site for reconstructing palaeoenvironmental change in northern Namibia. This is due to its geographical positioning and rich information stored in its sedimentary sequences demonstrated in research by Brook *et al.* (2007) and Hipondoka *et al.* (2014). Furthermore, examining new sediments from the Etosha Pan floor will help contribute to existing hypotheses about the late Quaternary palaeoclimate extent, which is crucial for understanding

long-term climate change in the region. The first section of the review gives an outline of the geomorphological context and methods commonly used in palaeoenvironmental studies in Namibia such as sedimentological and luminescence dating. The second part of the Chapter focuses on interpretations from prominent palaeorecords at Etosha, northern Namibia, the Namib Desert on the west coast, and marine offshore records.

2.2. Pans as proxies for palaeoenvironmental change

The geomorphology of pans in the Kalahari has long attracted paleoenvironmental Quaternary scientists. Pans are important features in dryland areas because some have been shown to act as zones of sediment accumulation that can serve as geoarchives which store information about past environmental change in the region (Thomas and Burrough, 2012; Burrough and Thomas, 2013; Schuller *et al.*, 2016; Schuller *et al.*, 2018). These closed landforms with low relief occur widely in the Kalahari Desert and are formed from complex processes and preconditions that can include bedrock geology, groundwater flows and climatic conditions (Goudie and Thomas 1985; Goudie and Wells, 1995). Some pans in the Kalahari are formed from wide network drainage systems, and some of them have undergone significant changes in the late Pleistocene and Holocene (Lancaster, 1986). For example, Etosha Pan (4,730 km^2), comparable in size to Sua Pan (4,921 km^2) and Ntwetwe Pan (4,700 km^2) (the two main components of the Makgadikgadi basin, Botswana), and the Great Salt Lake in the United States of America (4,662 km^2), is an example of a large saline pan that contains alkaline clays, with little to no vegetation (Trippner, 1997).

Etosha is an endorheic basin that is located within the larger Cuvelai-Etosha sedimentary basin which covers 173 000 km^2 and crosses the Namibian and Angolan political boundaries equally (Beyer *et al.,* 2018). The Cuvelai-Etosha basin is composed by dozens of iishana, an extensive shallow channel and pan system feeding the Etosha Pan. The rivers flow from north-south, beginning in the more humid southern Angola, to the drier northern Namibia (where Etosha is located) (Mendehlson *et al.,* 2013). Another source of water for the pan enters on the northeast through the Omarumba Owambo which drains the Tsintsabis area in the distal northern portion of Otavi Highlands. This has implications in interpreting the sources of water, sediments and understanding geomorphological processes that have shaped the pan during the late Quaternary.

Significant interest in Etosha has fuelled a suite of studies that have used various tools available at the time of investigation to try to understand the pan's geomorphological evolution (Buch and Zoller, 1992; Buch and Rose, 1996; Buch, 1997; Buch and Trippner, 1997; Brook *et al.*, 2007). A number of these studies have brought up important questions, notably regarding the formation processes of sand ridges and the driving mechanisms that may have formed them. This study uses samples from the lakebed and marginal sand ridges to reconstruct hydrological changes in the late Pleistocene and Holocene.

Recent research in southern Africa has highlighted the preservation of a range of organic proxies in sediments from dryland salt pans that can be investigated for

palaeoenvironmental change. These proxies can be used to reconstruct paleoenvironmental and palaeoclimatic change. In southern Africa, sites such as the Lebatse Pan (Holmgren and Shaw, 1997), Witpan (Telfer and Thomas, 2007; Telfer *et al*., 2009), Makgadikgadi Salt Pans (Burrough *et al.,* 2009; Franchi *et al.,* 2022) and Omongwa Pan in Namibia (Belz *et al.*, 2020) have been investigated for their potential to archive sedimentary records of environmental change. At some of these sites, organic proxies such as pollen, phytoliths and ostracods have shown enormous potential for preserving palaeoproxy records. Moreover, obtaining detailed information about specific events or brief periods is particularly challenging. This difficulty can be attributed to two primary factors: firstly, the dating of samples from the late Pleistocene continues to fall short of the precision required to capture rapid climate shifts, hindering the ability to constrain the exact timing of these events. Secondly, there is an inherent shortage of continuous records that allow for placing specific events within the context of ongoing climate fluctuations.

2.3. Location of the study area

Etosha Pan is located in southwestern Africa, northern Namibia between -18.91 S, 15.85 E and -18.68 S, 16.89 E near the border between Namibia and southern Angola. It is the second-largest pan in southern Africa after the Makgadikgadi basin in Botswana (1,100 km southeast of Etosha). Etosha National Park, in which the pan is the central feature, because of the pristine plant and animal communities it hosts. Etosha Pan is completely contained within the national park. The park supports a population of some of the last remaining black rhino species in Africa and more than

450 species of mammals and migratory birds (Sullivan *et al.*, 2024). Furthermore, the hypersaline and drought conditions present during most parts of the year makes it challenging for the wild animals that reside there. It is therefore important to develop a deeper understanding of past environmental conditions on the pan, which can be established through thorough palaeoenvironmental research.

2.4. Geological history of Etosha Pan

According to Buch (1997), extended periods of erosion and uncovering of the Damara Orogeny through denudation processes shaped the evolution of the Owambo Basin, in which Etosha lies.

Buch (1997) further stated that the long-term evolution of the basin was generated from three main stages:

- A Precambrian to early Palaeozoic (570 to 290 Ma) period of mountain-building
- A prolonged phase of geological stability
- The dominance of terrestrial erosion and denudation processes and limited tectonic activity

In the mid-to-late Cenozoic (65 to 1.8 Ma) period, the ’Palaeolake Etosha’ was the single collection point of three drainage systems namely: Cubango, Kunene and Cuvelai (Miller *et al.*, 2010). The pan is understood to be underlain by 50 m of saline olive clay which contains potassium feldspar and glauconite (Stuart-Williams, 1992;

Miller *et al.*, 2010). Modern Namibia has variable topography, starting at the coastline in the Namib Desert, to more than 2000 m high on the escarpment. There are two deserts on either side of the escarpment: the Kalahari Desert on the far east, and the Namib on the extreme western end. The escarpment is traversed by numerous rivers, some of which disappear into the Namib while a few (e.g., Hoanib River and Huarusib) flow into the ocean.

The lower layer of the Andoni Formation in the Owambo Basin (at Etosha) is composed of sand, clay and nodules of calcrete and dolcrete. The upper part has four lithological units (Miller, 2008; Miller *et al.*, 2010): Poachers Point Carbonate, Ekuma Delta Sandstone, Etosha Pan Clay (interbedded with Oshigambo) and Sandstone Members near the top – this was based on borehole samples conducted in a study by Miller *et al.* (2010). The Kalahari Group of the Owambo Basin hosts four more formations made of siliclastic sediments, but those are not the focus of this study and shall not be elaborated on. The Etosha Pan Clay member has been studied by researchers including Buch and Rose (1996), Buch and Trippner (1997) and Hipondoka (2005). It is the oldest member and main stratigraphic unit at the centre of the current Etosha Pan. It contains sand and silt that is almost completely composed of quartz (Miller *et al.*, 2010), making it suitable for quartz based OSL dating. According to Buch and Rose (1996), the Etosha pedogenic calcrete, formed in the early to mid-Pleistocene, is found up to a depth of 3 m where it is reported to contain reworked sediments.

2.5. Proxy methods overview

Proxies are measurable changes in a variable that are used as a “stand in” for changes in the environment. They are often preserved in geoarchives (Thomas and Burrough, 2012) and have different limitations and assumptions. Therefore, it is important to use an array of them where possible. This section of the review will give a brief summary of the proxies widely used in drylands and their contribution to scientific endeavours to investigate the past. The proxies include physical, biological and chronological methods. Chapter 3 will detail how the specific methods were applied in this thesis.

2.5.1. Sedimentological proxies

Sedimentological analyses have long taken place in southern Africa’s dryland environments (Thomas, 1987). They are one of the most common scientific tools to reconstruct past environmental dynamics recorded in sediments to unveil the physical properties of the sediments that have accumulated over thousands of years and older (Lukich *et al.* 2020). The physical dimensions of sediment particles serve as a crucial indicator for understanding shifts in pathways by which they were transported into palaeolakes and other water bodies with capacities to store sediments (Tooth and McCarthy., 2007; Schillereff *et al.*, 2014; Yanes *et al.,* 2019). Samples can be sieved, chemically pre-treated or mixed directly into a water solution for grain size analysis using a laser diffractor. Laser diffraction is the preferred method because it is relatively affordable, employs replicate measurements using relatively small samples (<50 mg), and because the measurements are underpinned by robust statistical analysis (Blott

and Pye, 2001). In Namibia, grain size analyses have taken place in pans (Schuller *et al.*, 2018; Belz *et al.*, 2020), where they were conducted on short sediment cores and helped to uncover different sediment deposition regimes such as aeolian versus fluvial inflows. Grain size analysis has also been used in studies at Etosha Pan and its use helped identify structural changes in sediment deposits and transport within the pan (Hipondoka *et al.*, 2004; Hipondoka *et al.,* 2014). Through analysis of sedimentary grain size data, it is possible to elucidate patterns and statistical characteristics such as sorting, skewness, kurtosis, mean and median (Folk and Ward, 1957). These parameters can help to identify and interpret depositional environment and sediment transport processes (Boggs, 2012). For example, well sorted sediments can often indicate aeolian sources while poorer sorting is typical of debris flow.

The sediment processes are associated with the Ekuma Delta which has been an area of debate, particularly in its role in building the ridges on the western margin of the pan (Brook *et al.*, 2007; Hipondoka *et al.*, 2014). Preliminary investigations of sand ridges sampled with a limited resolution were conducted by Hipondoka *et al.* (2004) and Hipondoka *et al.* (2014), leaving open the possibility of missing sedimentary changes. Hence it is important to widen sampling sites at Etosha to include the pan floor and to ensure high resolution sampling in order to capture sedimentary signals and improve understanding of the overall sediment transport mechanisms at the pan.

2.5.2. Palaeoecological proxies

Palaeoecological proxies used in palaeoenvironmental research include those from previously living organisms that are sensitive to shifts in environmental processes such as in water availability, temperature and geochemistry. Examples of these proxies used at Makgadikgadi include phytoliths (Burrough *et al.*, 2012), diatoms (Schmidt *et al.*, 2017) and ostracods (Franchi *et al.*, 2022). The use of biological proxies at Etosha so far only include stromatolites on the eastern part of the pan and Miocene-Pliocene animal fossils retrieved from the Ekuma Delta (Pickford *et al.*, 2009). The present study expands this by using late Pleistocene eggshells preserved in the sediment cores from a spring mound near Logan's Island.

Overall, Namibia's terrestrial palaeoclimate records have poor preservation of biological proxies (Schuller *et al.*, 2018). Due to high salinity and alkalinity, microfossils of pollen and diatoms in Namibian pans are scarce. Studies based on pollen have mainly taken place in the central Namib (e.g., van Zinderen Bakker, 1984; Dupont *et al.*, 2004; Scott *et al.*, 2004; Gil-Romera *et al.*, 2007), leaving sites in northern and eastern Namibia poorly understood with regards to palaeoenvironmental conditions in the late Pleistocene and the Holocene. Furthermore, the studies have limited chronological control, are sparsely distributed and the sites can be difficult to access, making it difficult to unpick Holocene environmental shifts at a high resolution. However, newer studies are beginning to address this deficit by using ostracods to reconstruct palaeohydrological change in pans. For example, Belz *et al.* (2020) extracted sediments from Omongwa Pan in a study that shows potential to reconstruct palaeoecological conditions using biological proxies (ostracod assemblages) in

Namibian pans. With regards to applying palaeoecological reconstruction using ostracods, challenges include the possibility of mixing that can result from wind-driven erosion and flash floods which can redistribute the microfossils, thus complicating their interpretations (Horne *et al.*, 2012). Secondly, in arid areas, high alkalinity can lead to chemical and physical alterations that can damage the ostracod taphonomy and lead to misinterpretation of their geochemistry (Smith and Palmer *et al.*, 2012). Moreover, the occasional lack of modern analogues of non-marine ostracods and other palaeoecological proxies in large pans can lead to homogeneity in the samples, which make the data interpretations to be complicated (Jackson and Williams, 2004; Smith *et al.*, 2012). Thus, the discovery and use of other biological proxies can help to build a more synchronous understanding of palaeoenvironmental change along with other proxies.

2.5.2.1. Diatoms

The abundance and species assemblage of diatoms in the sediment record can be used as an indicator of lacustrine conditions in the pan, succeeded by suitable environmental conditions for their preservation (Flower and Ryves, 2009). Some diatom species tend to be sensitive to localised changes in water geochemistry such as salinity and nutrient availability (Leterme *et al.,* 2013). Assemblages of different species can therefore provide an indication of these conditions in the Quaternary (Flower and Ryves, 2009). At Makgadikgadi pans in Botswana diatoms in a back flooded area of the basin, provided insights into hydrological conditions during a brief period of Marine Isotope Stage 5 (Schmidt *et al.*, 2017). The potential for Etosha Pan

to preserve diatoms is still to be investigated. As an ephemeral lake, it would be expected that some diatoms would be present during the wet phases in response to the changes in water availability and nutrient availability.

2.5.2.2. Leaf wax n-alkanes

The waxy coatings of plants contain long chain (C_{21} to C_{37}) n-alkanes (a straight chain hydrocarbon molecule) that are among the most long-lived and widely utilised terrestrial plant biomarkers. The stable isotopic compositions ($\delta^{13}C$ and δD) of n-alkanes and their applications in paleoecology and paleoclimatology have been studied extensively. Leaf waxes contain a complex array of compounds including of n-alkanes, n-alkanols and aldehydes that are formed by plants to manage, among others, water retention and protection from pathogens (Jenks and Ashworth, 1999). Analyses can show average chain length distribution (ACL) of leaf-wax n-alkanes as well as their hydrogen and carbon isotopic compositions (δD_{wax} and $\delta^{13}C_{wax}$). Both the ACL and carbon isotope compositions can be used to infer grass-dominated landscapes and have utility as aridity indicators (Carr *et al.,* 2014). They are widely distributed in the environment and often used in palaeoenvironmental studies due to their extreme durability and excellent preservation relative to other organic proxies that are often very poorly preserved in deserts (Cheung *et al.*, 2015; Inglis *et al.*, 2022).

Leaf waxes extracted from lake basin sediments in southern Africa have been used to study past climate and environmental changes (e.g., Carr *et al.*, 2014; Carr *et al.,* 2015). Strobel *et al.* (2019) used a multi-proxy approach, including leaf wax n-alkanes,

to reconstruct late Quaternary palaeoenvironmental changes on the south coast of South Africa. Tierney *et al.* (2010) further demonstrated the potential of leaf wax n-alkanes, in combination with other proxies, to reconstruct past environmental changes in East Africa. Leaf wax n-alkanes can record and distinguish between distant and local moisture sources of rainfall (Hou *et al.*, 2008). They can also help reveal the patterns of palaeorainfall that can give an indication of precipitation-evaporation ratios (e.g., Strobel *et al.*, 2019) which are helpful in understanding past climate.

2.5.2.3. Ancient DNA (aDNA)

The use of ancient DNA (aDNA) has greatly improved palaeoenvironmental reconstruction and ecosystem dynamics (Brown *et al.*, 2015). Dussex *et al.* (2021) and Djurhuus *et al.* (2020) highlight the potential of aDNA to identify changes in plant and animal communities and so infer past environmental shifts. Bista *et al.* (2017) further demonstrates the utility of aDNA in tracking seasonal diversity at the ecosystem scale, while Revéret *et al.* (2023) showcases the power of sedimentary aDNA in reconstructing the species assemblages of past aquatic habitats and environmental conditions. aDNA analysis assists in identification of species and taxonomies which otherwise do not leave fossils that can last thousands of years. However, the method is limited because DNA typically becomes denatured at high temperatures due to cumulative effects of thermal exposure over thousands of years (Lindahl, 1993). Another limitation is the availability of species data in the reference databases which is critical in identification of the species. Furthermore, contamination from modern sources of DNA, preservation potential and biases differ from one species to another

(Crump, 2021). These challenges do not, however, prevent utility of the method when the conditions are suitable. At Etosha, there are no published palaeoenvironmental studies that have applied aDNA analysis. This is primarily due to the lack of a detailed taxonomic reference database that can enable matching organisms to species with similar DNA (Rawlence *et al.*, 2014). Another challenge with aDNA analysis is the possible contamination from modern samples (Brown and Barnes, 2015), and mechanical damage of the DNA at the water-sediment interface (Capo *et al.,* 2021). The success of this method can help unveil ecosystem change and how specific flora and fauna respond to changes in hydroclimate in northern Namibia over the late Quaternary.

2.5.2.4. Stable isotopes

Stable carbon isotopes have been utilised extensively for palaeoenvironmental studies, especially in archaeological excavations using avian eggshell to reconstruct diet and vegetation changes over time in the interior landscape of southern Africa (e.g., Lee-Thorp and Ecker, 2015). $\delta^{13}C$ values in ostrich eggshells from controlled feeding experiments from South African wild ostriches (*Struthio camelus australis)* were shown to reflect dietary (plant) $\delta^{13}C$ values offset by biological fractionation i.e., the trophic effect so that changes in eggshell carbon isotopes are interpreted to reflect changes in the available dietary vegetation (Johnson *et al.*, 1998). For example, Lee-Thorp and Ecker (2015) found evidence of shifts in C_3/ C_4 dominance within vegetation which they have interpreted in terms of aridity in the late Pleistocene and noted a shift to moister conditions (indicated an increase in C_3 vegetation) around 6 ka at Wonderwerk Cave

in South Africa. Normally C_3 grasses predominate under more temperate conditions as C_4 grasses are arid adapted and outcompete C_3 vegetation in dryland contexts. The main controlling factors on C_3 or C_4 vegetation are not only moisture availability, but also temperature and partial pressure of atmospheric CO_2. For example, during the LGM, Heinrich Stadial 1 and Younger Dryas, C_3 grasses had a greater advantage because they are better adapted to lower temperature (Braun *et al.,* 2020). C_3 signals in southern Africa mostly come from trees and shrubs rather than grasses (Cowling, 1983; Ecker *et al.,* 2020). Southern Africa's savanna biome, including Lesotho, South Africa, ESwatini and Namibia is currently dominated by sub-tropical grasses that follow the C_4 photosynthetic pathway, which are favoured by the warm seasonal climate (Ellis, *et al*., 1980; Ehleringer *et al*., 1997; Mucina *et al*., 2006). Moreover, C_4 plants thrive in average temperatures above 22 degrees Celsius, which are common in southern Africa (Vogel, 1978). Finally, C_4 grasses have greater water use efficiency than C_3 grasses, enabling them to dominate the modern day grass distribution in southern Africa (Ellis *et al*., 1980).

Niespolo *et al*. (2020) emphasized the potential of avian eggshell (ostrich, in particular) isotopes in providing site-specific paleoenvironmental records (because in ostriches, home ranges rarely extend beyond 85 km^2). Where they have been applied, ostrich eggshells have not yet been used to reconstruct palaeohydrological change in pans, particularly at Etosha Pan.

Moreover, there has been extensive debate among scholars of sediment records about the subsequent climatic interpretation of stable isotopes analyses, particularly on the kind of vegetation changes (C_3 vs. C_4 vegetation ratios) that document environmental change and the way these ecological signals are reflected by stable carbon isotopes. Most grasses in Africa use the C_4 pathway whereas trees, herbs and shrubs normally use the C_3 pathway. Grasses are annual or perennial plants, better adapted to environments with short wet seasons compared to perennial C_3 woody plants which need access to some moisture year-round. Depending on the prevailing climate conditions, a shift towards a C_4 grass-dominated ecosystem at the drier end of the spectrum in a semi-arid environment typically signifies a brief yet relatively humid wet season with high seasonality. For example, Chase *et al.* (2009) and Collins *et al.* (2014) interpreted less depleted $\delta^{13}C$ values as representative of a shift towards C_4 plants under moist conditions as water availability permits the expansion of grasses into areas previously devoid of vegetation. A study by Railsback *et al*. (2022) also recognises that in arid areas, C_4 grasses are scarce, while C_3 shrubs remain on the landscape and do not make a significant change in the speleothem $\delta^{13}C$, therefore more negative $\delta^{13}C$ values are indicative of drier conditions (Belz *et al.*, 2020; Railsback *et al.*, 2022). In semi-arid areas, C_4 plants are commonly found in summer, and they generate higher $\delta^{13}C$ values that are interpreted to represent moist conditions (Railsback *et al.*, 2022). The palaeorecords of Etosha are yet to be analysed using carbon, oxygen or nitrogen stable isotopes. Probing such archives could lead to more robust interpretations of paleoenvironmental change.

2.6. Chronological methods

Establishing the age of deposition of physical and chemical proxies is essential for palaeoenvironmental studies. Accurate and precise dating techniques are required in reconstructing past environmental changes. There are methods that utilise organic matter (e.g., radiocarbon dating), and those that target the inorganic part of sediments such as quartz (e.g., OSL dating). Radiocarbon ages are generally more precise in most contexts but are limited to dating approximately the last 50 ka after which they may become inaccurate. OSL is accurate over a much longer time period of the Quaternary but is generally much less precise making it inappropriate to tackle questions addressing rapid climate changes. The following section briefly describes dating methods that were key to establishing a robust chronological framework for this project.

2.6.1. Radiocarbon dating

Radiocarbon dating of bulk sediments has proven to be a reliable method for establishing downcore chronology in numerous late Quaternary studies of salt pans (e.g., Schuller and Wehrmann, 2016; Schuller *et al.*, 2018; Belz *et al.*, 2020; Franchi *et al.*, 2022). Accumulation of organic matter over time is an essential requirement for the success of radiocarbon dating. In this project, bulk sediment samples were preferred due to the absence of plant macrofossils. Mobility of humic and fulvic acids was accounted for during the alkali rinses for pre-treatment of radiocarbon dating samples (Brock *et al*., 2010). However, some preservation issues can arise from reworked

material that can contain organic samples affected by the reservoir effect, when older carbon from soil organic matter could make the ages appear older (Broecker and Walton, 1959; Strunk, *et al.*, 2020). Chapter 3 will detail the processes used to analyse samples from this study using radiocarbon dating.

2.6.2. Optically Stimulated Luminescence (OSL) dating

OSL is an absolute dating method that measures the period of time passed since the burial of mineral grains such as feldspar and quartz to infer palaeoenvironmental change. It takes advantage of the phenomenon that light exposure on sediment transport 'resets' displaced electrons within particular minerals to their ground state. Once buried, radiation damage from natural radioactivity of sediment again causes a slow build-up of 'trapped' electrons (Duller, 2008). In the laboratory, light (controlled blue/green wavelengths) is used to stimulate electrons that may be trapped or unstable in the crystal defects of the mineral grains analysed (usually quartz or feldspar) (Murray and Wintle, 2000). The electrons can return to their 'ground state' after the stimulation and emit a light that can be measured precisely in the laboratory to estimate its intensity. The intensity of the light resulting from the release of the total trapped population is calibrated against that produced from known laboratory radiation doses to establish the equivalent dose, (*De*) to the total radiation dose the sediment has received since burial. Because it is possible to measure the rate at which this dose was delivered to the minerals (by assessing the radioactivity of the sediment in which it was buried), it is possible to calculate the time since burial (i.e., its estimated depositional age) using the following equation (Duller, 2004):

$$Estimated\ Age\ (ka) = \frac{Equivalent\ Dose\ (Gy)}{Estimated\ Dose\ Rate\ (Gy.ka^{-1})} \qquad \text{(Equation 1)}$$

OSL dating has been used in drylands to mostly date dunes and sedimentary beds that contain a sufficient amount of sand. Its wide use in drylands is because there is often insufficient organic material to use radiocarbon dating, which would otherwise be much more preferable dating method in most circumstances because of its higher precision. In salt pans in southern Africa, the OSL dating method has been used less frequently on pan-floor sediments (Telfer *et al*., 2009 and Burrough *et al.,* 2022 are rare examples) for palaeoenvironmental reconstruction studies. A collation of past luminescence dates from Etosha Pan is given in Table 2.1. Reliable OSL dates from Etosha Pan will underpin the interpretation of other proxy data such as from diatoms and leaf wax n-alkanes which are crucial in meeting the other objectives of the project. A key part of this thesis is to generate new OSL dates by finding a suitable means to collect field samples and ensure that the generated ages are analysed and interpreted using advanced protocols. The precise method followed to conduct OSL dating to the samples from this study will follow in Chapter 3 (*Methods*). It will detail materials used and methods followed for sampling, laboratory preparation and data analyses on samples from the sand ridges and pan floor.

2.7. Late Quaternary climate records from Namibia

Ongoing research using a variety of proxy records, such as marine sediments, lake sediments, and speleothems, continues to refine our understanding of how large-scale

changes have influenced Namibia's environmental history over different timescales. This part of the review will discuss regional findings from Namibia by referring to selected existing records and assessing their contributions towards the current understanding of late Quaternary palaeoenvironments of the region.

2.7.1. Terrestrial Archives: Lake sediments, speleothems and hyrax middens

2.7.1.1. Lake sediments

The arid climate, shifting rainfall zones in the past and extended dune systems in Namibia make the preservation of a suite of palaeoenvironmental proxies in continuous records challenging (Collins *et al.*, 2011; Zhu, 2016). Pans in Namibia have been a longstanding source of data, particularly on the south-western part of the country where they have held water bodies for significant periods of time enabling them to become, temporary net accumulators of sediment.

In the northern part of the country, Lake Otjikoto has yielded data from pollen assemblages as a proxy for humidity (e.g., Scott *et al.*, 1991; Mapani *et al.*, 2021). The lake is a 50 m deep freshwater dolomitic sinkhole that has been hypothesised to have accumulated sediments for over 6 ka and its water levels have varied over time (Scott *et al.*, 1991). Overall, the period between 8 .7 ka and 6 ka was characterised by a larger expansion of grass pollen, which was interpreted to represent wetter conditions than present (Scott *et al.*, 1991). However, this palynological study conducted by Scott *et al.* (1991) was limited by the chronology which made it difficult to constrain changes

in the three vegetation zones observed in their record. Nevertheless, it was one of the first detailed palynological studies of Lake Otjikoto sediments and was conducted on a sediment core with a depth of 1.3 m. Moreover, the Holocene radiocarbon dates that were obtained demonstrated that the lake had potential for research that would follow decades later. Scott *et al.* (1991) interpreted the record as an indication that there was a prolonged dry climate after 3.5 ka and was slowly replaced by a wetter one that lasted until 1 ka.

Namibia has a complex palaeoenvironmental history, some of which is preserved in pans. During wet periods, some pans hold permanent or semi-permanent bodies of water, and it is during these times that sediments are able to accumulate allowing records from these times to be preserved. Pan sediments do however bear complexities in palaeoenvironmental reconstruction studies due to accumulation vs. deflation processes which create potential for discontinuous records. These can include gaps reflecting periods of deflation or non-accumulation. In arid regions, pans are frequently net loss systems as opposed to temperate lacustrine basins which are classically net accumulators (Shaw and Bryant, 2011). However, there are periods in the past when conditions were wetter when sediments were able to accumulate. Schuller *et al.* (2018) conducted a comprehensive study on pans located in south-west Namibia and some in the north-western margin of South Africa. In their study, Schuller *et al.* (2018) investigated geochemical data from multiple sediment cores from pans in Namibia using 57 radiocarbon dates on 5 pans: Omongwa, Toasis, Koes, Branddam East Pan and Witpan (in the north-eastern part of South Africa). They used

geochemical proxies ((Ti/Al, K/Al, (Zr+Ti)/(Al+Ca)) ratios to infer changes in rainfall and wind strength over time. Their study reconstructed palaeoenvironmental change in the southwest Kalahari for the past 34 ka. In the study, increased sedimentation rates at some of the pans were interpreted to indicate wetter conditions in Namibia due to the expansion of the winter rainfall zone, which in studies further south has been associated with a northward expansion of the Antarctic sea-ice (Schuller *et al.*, 2018). However, due to the shallow and clayey nature of most of the pan sediments, they could only extract relatively short cores. Etosha Pan in the north integrates a much wider catchment and can provide some insights on the behaviour of the sensitive air masses from the Indian and Atlantic Oceans as well as moisture from migrations of the tropical rain-belt.

2.7.1.2. Cave deposits

Cave calcite, or speleothems, are another key proxy that has been used to reconstruct climate and environmental dynamics in Namibian caves and rock shelters. The use of ^{230}Th/U Thermal Ionization Mass Spectrometry (TIMS) absolute dating has enabled accurate chronological frameworks which have been applied to speleothems for palaeoclimate reconstruction studies. Due to its arid nature, preservation of cave and archaeological sites in Namibia is scarce. However, there are some primary cave sites in the Namib desert, including Rossing cave (Geyh and Heine, 2014), Narabeb, an open-air interdune pan (Stone *et al.*, 2024), Pockenbank rockshelter (MSA site; Schmidt *et al.*, 2016) and Apollo 11 cave (Vogelsang *et al.*, 2010). At Rossing cave, ^{30}Th/U dates (TIMS) from a large stalagmite captured the longest chronological

reconstruction that spans the last 420 ka and were found to follow the Milankovitch cycle (Geyh and Heine, 2014). Furthermore, they found the Holocene to have been dry due to the lack of stalagmite growth in the absence of drip water (Geyh and Heine, 2014). Some of these caves require an improvement of the chronological methods to adopt OSL where possible, while others contain evidence of paleoenvironmental change outside the study period of the current project (from 40 ka). Therefore, the thesis covers the findings from the Apollo 11 rockshelter that has captured human occupation at different periods since 47 ka (Vogelsgang *et al.*, 2010). In addition, radiocarbon data from Apollo 11 rockshelter suggest occupation phases between 47 - 28 ka, 24.5 - 20 ka and 18 - 14, 11 - 10 ka and 8 - 6.5 ka (Vogalsang *et al.,* 2010).

Caves in the central Namib Desert on the western part of the country (e.g., Rössing Cave) and at Dante Cave (located 435 km northeast of Windhoek), continue to improve our understanding of regional palaeoclimate change (Sletten *et al.*, 2013) (Figure 2.1). For example, a Dante cave stalagmite (DP1) captured changes in $\delta^{13}C$ which have been linked to the global 4.2 ka event, a period they interpret as being wet (e.g., Railsback *et al.*, 2019; Railsback *et al.*, 2022). Stalagmite DP1 from Dante Cave and stalagmite ORUM-1 from Orumana Cave suggested four wetter periods at 92 ka, 47–39 ka, 20–14 ka, and 4.5–0 ka from analysing isotope ratios of $\delta^{13}C$, $\delta^{18}O$ and Uranium (Railsback *et al.*, 2019). Other caves near borders of South Africa and Botswana including Wonderwerk (Brook *et al.*, 2010; Brook *et al.*, 2015) and Drotsky's (Brook *et al.*, 1996) have often been used to infer wide palaeoclimate environmental change. From both sites, the authors resolved that the identified wet period were driven by the

southward migration of the tropical rain-belt that brought higher rainfall to northern Namibia. At Wonderwerk, wetter conditions were observed at ca. 33 ka and 23 - 17 ka (Brook *et al.,* 2010). In addition, Brook *et al.* (2015) found the mid-Holocene (6.2 – 4.5 ka) to have been wetter. The mid-Holocene wetness was supported by palynological evidence which suggested that there was a change from dry asteraceous, karroid vegetation during the early Holocene (12.5 - 6.5 ka) to humid, grassy vegetation during the mid-Holocene (5.9 – 4.3 ka) which was attributed to an increase in summer rainfall (Brook *et al.,* 2010; House *et al.,* 2022). The corresponding change in isotopic data suggested that lighter $\delta^{13}C$ values (more negative) were found during wetter periods due to higher CO_2 production resulting from increased vegetation and biological activity (Brook *et al.*, 2010).

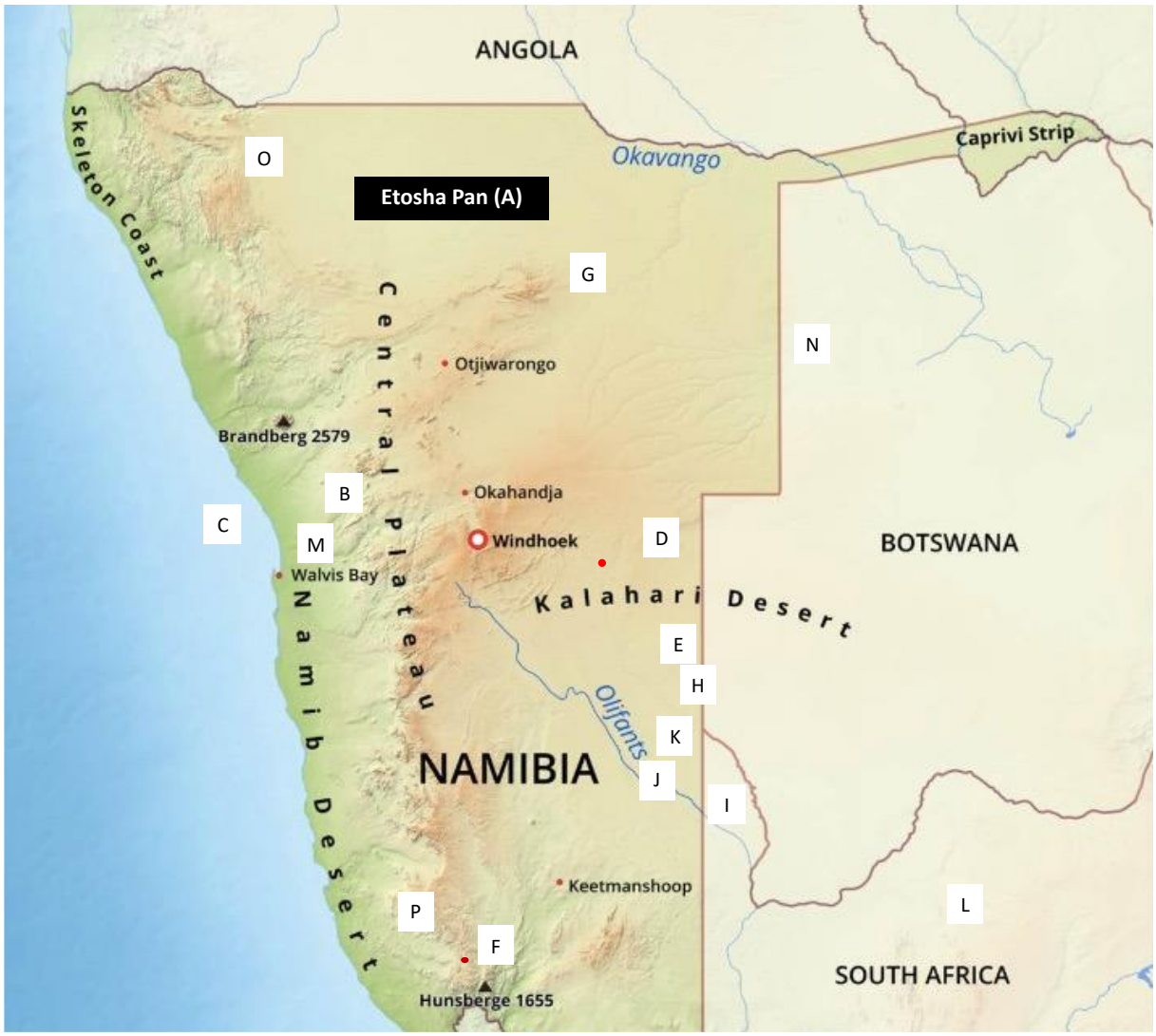

Figure 2.1: Map of key sites discussed in the text. A = Etosha Pan (This study). B = Spitzkoppe (Chase *et al*., 2009). C = MD08-3167 (off-shore marine core by Collins *et al*., (2014)). D = Dante Cave (Railsback *et al*., 2022). E = Omongwa Pan (Belz *et al*., 2020). F = Apollo 11 Cave (Vogelsgang *et al*., 2010). G = Lake Otjikoto (Scott *et al*., 1991; Tabares *et al*., 2019). H= Toasis Pan (Schuller *et al*., 2018). I = Witpan (Schuller *et al*., 2018). J = Branddam East (Schuller *et al*., 2018). K = Koës Pan (Schuller *et al*., 2018). L = Wonderwerk (Brook *et al*., 2010). M = Rossing Cave (Sletten *et al*., 2013). N= Drotsky's Cave (Brook *et al*., 1996). O = Orumana Cave (Railsback *et al*., 2016). P = Pockenbank Rockshelter (Schmidt *et al*., 2023). Map adapted from: https://www.freeworldmaps.net/africa/namibia/map.html

Overall, and in southern Africa more broadly, palaeoenvironmental studies have provided information about changes in humidity, but very few of them have reconstructed changes in palaeotemperature (Meadows and Holmes, 2018). Orumana cave on the north-western part of Namibia, covering the last 47 ka, recorded shifts in petrography and stable isotopes of carbon and oxygen whereby, lower $\delta^{18}O$ values and increased precipitation of calcite in the speleothems were interpreted to indicate wetter conditions during the LGM (Railsback *et al.*, 2016). Furthermore, the authors interpreted less-depleted $\delta^{13}C$ values of stalagmite carbonate to suggest that drier climate conditions that took place between 20 – 14.5 ka indicate the shift of the tropical rain belt further south of Orumana cave, leaving the northern part of Namibia with dry conditions (Railsback *et al.*, 2016). Using multi-proxy analyses on the cave deposits can help improve the findings at the different cave sites given how complex speleothem formations can be. These rare cave sites have provided crucial information towards understanding long-term environmental changes in the Namib Desert, helping to build a more comprehensive picture of this arid region.

2.7.1.3. Archaeological findings in caves and rock shelters

A firm chronology is important for making palaeoenvironmental interpretations. However, in caves and rock shelters within drylands, there is limited organic material available due to the highly oxidising environments. This makes it difficult to date evidence of environmental change using radiocarbon dating. OSL dating targets minerals that retain their chemical and structural integrity over thousands of years and therefore is suitable for studying caves with limited organic material. Excavations in

some caves in Namibia have added insights to deciphering late Pleistocene and Holocene environmental change through archaeological studies. For example, according to Railsback *et al*. (2022) the Dante cave in northeast Namibia records indicated evidence for a wetter period during the 4.2 ka event (4.1 - 3.9 ka). The values underwent a negative shift in $\delta^{13}C$ data (from -6.3‰ to -7.5‰) during the 4.1-3.9 ka period. The authors interpreted the low $\delta^{13}C$ data in stalagmite DAN1 and largest change in $\delta^{13}C$ (1.2‰) during that period to have suggested wetter conditions. Moreover, the greater deposition of clay and sand size particles during the 4.2 ka event also suggested increased water flow over the stalagmites, indicating wetter than normal conditions. Meanwhile the $\delta^{18}O$ recorded in the study exhibited only slight increases. The advancement of OSL in the past few decades has opened up a new avenue to using different minerals to enrich studies in caves and rock shelters (Zhu *et al.*, 2016).

Data from cave and archaeological sites can provide paleoenvironmental information linked to human occupation. The Apollo 11 Rockshelter, situated in southwest Namibia, has attracted research over the last few decades (e.g., Wendt, 1976; Miller *et al.*, 1999; Vogelsang, 2008; Murray-Wallace *et al.*, 2015; Lombard *et al.*, 2018) (Figure 2.1). Increased sedimentation during the Holocene at the site was interpreted to indicate episodes of human occupation (Vogelsang *et al.*, 2010). Moreover, archaeobotanical and faunal remain analyses suggest that human occupation at the Apollo 11 rockshelter may have been influenced by changing environmental conditions (Vogelsang *et al.,* 2010). Radiocarbon dating from Apollo 11 rockshelter suggests

occupation phases between 47-28 ka (Late MSA III-I), 24.5-20 ka (Early LSA II) and 18-14 ka (Early LSA I), 11-10 ka (LSA III) and 8-6.5 ka (LSA II and I). For example, the absence of occupation between 20 and 18 ka at Apollo 11 rockshelter may have occurred due to lower temperatures during the LGM that made the human occupation unsuitable under those conditions.

Moreover, charcoal analyses at the site contains evidence of a cool and wet LGM due to the appearance of dwarf shrubland concurrent with *Artemisia* pollen which are indicative of moist conditions (Vogelsang *et al.*, 2010). The *Olea* plant species at Apollo 11 also represents the replacement of plants that are less tolerant to frost and drought (i.e., the *Olea europaea ssp. Africana*), but did not necessarily give insights into the changes in moisture. During the same period at Pockenbank Rockshelter, also in northwest Namibia, there is evidence of a wet LGM. According to the study, human occupation intensity at the site during the LGM is ascribed to the northward extension of the westerlies that bought winter rainfall to the area (Schmidt *et al.*, 2023). Most periods with no apparent human occupation over the last 50 ka at the shelter are associated with arid conditions (Schmidt *et al.*, 2023).

2.7.1.4. Hyrax middens

The use of hyrax middens to reconstruct palaeoenvironmental and palaeoclimatic change has been established for decades (e.g., Scott *et al.*, 1990; Scott, 1996; Gil-Romera *et al.*, 2007). Numerous studies were conducted in Namibia and South Africa,

including Chase *et al.* (2009) who applied radiocarbon dating, stable isotopes of carbon ($\delta^{13}C$) and nitrogen ($\delta^{15}N$) on hyrax middens found at Spitzkoppe on the western part of Namibia. Their study reconstructed late Pleistocene and Holocene vegetation, and palaeorainfall changes reflected through the herbivorous diet of the dassies. Moreover, pollen assemblages and carbon isotope data from hyrax dung that suggested increased winter rainfall at c. 42 ka, and during the LGM (Scott *et al*., 2018). Similarly, Lim (2017) found that the LGM was characterised by greater water availability and low temperatures that favoured the mesic Nama-Karoo vegetation using evidence from southern Namib. Many studies have been carried out using the same proxy including Carr *et al.* (2010), Quick *et al.* (2011) and Chase *et al.* (2012, 2013, 2022, 2023), at different sites in Namibia and South Africa. However, there are challenges about the use and interpretation of results from using rock hyrax middens. For example, there is a possibility of contamination with modern vegetation, and this can affect radiocarbon dating data, potentially making the middens appear younger than they are (Corrión *et al.*, 1999). Secondly, the record might not be fully continuous because some time periods with no occupation might be absent from this record, and this might lead to their under-representation. Equally, there might be less representation by certain types of vegetation due to diet preference by the dassies (Scott and Vogel, 2000). Moreover, the signal preserved by rock hyrax middens is localized to dassie home territories and might not represent broader regional palaeoclimatic changes (Meadows, 2014). Despite these limitations, refinements in the methods used for analysing rock hyrax middens in subsequent studies have occurred and there has been increasing

confidence of their use in palaeoenvironmental reconstruction studies e.g., Horisk *et al.* (2023).

2.7.2. Etosha Pan formation

To date, a coherent explanation of the hydrological status of the Etosha basin during the late Quaternary has not been developed. Previous studies that have attempted to answer questions regarding its formation have largely focused on the marginal ridges rather than on the sediments in the basin itself. Similar debates have arisen in the Makgadikgadi basin, in Botswana, where recent investigations have also targeted basin floor sediments with some success in retrieving detailed environmental information (Burrough, 2022). This study is the first to examine sediments from within the Etosha basin floor. It also investigates a new higher resolution transect from three marginal ridges in an attempt to address questions regarding the Quaternary hydrological evolution of the system.

As mentioned above, the late Quaternary geomorphic evolution of Etosha Pan has been an area of contention, with two contrasting hypotheses emerging. Etosha Pan has received a long history of research (see, for example, Buch 1997; Stuart-Williams, 1992; Hipondoka, 2005; Hipondoka *et al.*, 2006; Brook *et al.*, 2011), yet the pan floor sediments for palaeorecords are still to be systematically investigated (Hipondoka, 2005). Contemporary Etosha Pan has a contested palaeoenvironmental history that has resulted in two main views encompassed in the hypotheses that this study aims to test. The first considers the Etosha basin to have remained dry during the Quaternary period, predominantly shaped by deflationary processes and regards the pan as an

erosional landform and its marginal ridges as lunette dunes (Buch and Rose, 1996; Beugler-Bell and Buch, 1997). The alternative view is of a system whose history demonstrates dynamic hydrological change through the Quaternary, characterised by both stable lake conditions that contributed sediment to shoreline ridges and periods of lake desiccation (Hipondoka *et al.*, 2014). These views are discussed in more detail below.

2.7.2.1. 'Deflation only' hypothesis

One view is that the modern Etosha Pan was formed during the late Tertiary (4 Ma) period from the coalescence of many smaller pans that were deflated through seasonal wetting and drying that eroded the pan in the land surface (Buch, 1997; Miller *et al.*, 2008). The proponents of Etosha's mode of development as an erosional landform, that has not seen significant subsequent water influx have suggested that the climate at Etosha was semi-arid and seasonal during the Miocene as it is today. Some of these scholars e.g., Buch and Rose (1996) based their theory on geomorphological observations on the pan and its marginal ridges which they interpreted as lunette dunes, as well as geochemical analyses of the pan surface (which at that time lacked age control). An implication of this hypothesis is that climatic changes during the Quaternary have not impacted significantly on the hydrology of the basin, nor left a strong sedimentary signature.

2.7.2.2. 'Fluctuating Quaternary hydrology' hypothesis

The alternative hypothesis emerged earlier in the 1920s (Schwarz, 1920; Jaeger, 1926) and proposed that Etosha is a remnant of a larger palaeolake that began shrinking in the Pleistocene. This hypothesis envisaged that the Etosha basin was much larger in the Pliocene due to its connection to the Cunene River as its major fluvial source. After the Cunene underwent river capture and diversion to the Atlantic Ocean, mega Etosha Palaeolake reduced significantly in size until it reached its current pan size since c 35 ka (Stuart-Williams, 1992). Subsequent reduction and final desiccation were ascribed to climatic change when the pan hosted high lake levels as late as the mid-Holocene (Hipondoka, 2005). Recently, Brook *et al.* (2007) and Hipondoka *et al.* (2014) examined the sand ridges on the west of Etosha, which they interpreted as shorelines using luminescence ages to date the deposition of the sediments. They argued in support of Etosha as a fluctuating palaeolake, with dynamic hydrological changes in the late Quaternary.

2.8. Etosha basin margin ridges; the focus of previous research

Previous studies of Etosha's Quaternary development have largely focused on the prominent sand ridges of the western basin margin but often contain active debate about their formation (Figure 2.2). Rust (1984) used radiocarbon dating analyses on calcrete samples from various sites including Logan's Island on the west of Etosha Pan and was first to describe the ridges as 'lunette dunes', formed by the accumulation of deflating pan floor sediments. Rust (1984) further interpreted Logan's Island as a residual from a former innermost lunette, and Miller *et al.* (2010) supported the lunette dune interpretation. A study by Buch and Zoller (1992) used thermoluminescence

dating and pedostratigraphy on ridges at 1100 masl, indicating aeolian erosion of the very old (Miocene) basin floor and a redeposition of sediments within the ridges beginning as early as 140 ka. However, in contrast, Brook *et al.* (2007) interpreted the ridges as relict shorelines, stating that they represented remnants of a larger palaeolake that existed in varying sizes during the Late Quaternary. When the ridges are interpreted as shorelines, (e.g., Brook *et al.*, 2007; Hipondoka *et al.*, 2014), rather than as aeolian dunes, they are thought to represent evidence of wetter, rather than drier phases. Moreover, ridge sediment grain size analyses by Brook *et al.* (2007) found, on average, 13 % more sand fractions in the ridges than in the pan surface sediments. This finding, along with better sorting in their grain size data, was interpreted to indicate exposure to wave action due to higher lake levels that occupied the pan in the mid and late Holocene. Hipondoka *et al.* (2014) highlighted the importance of riverine deposits by suggesting that the ridges were composed from sediments derived from Ekuma Delta which has a sediment load with high concentration of fines (38 %). The formation processes of the bounding basin ridges continue to be inconclusive and challenging.

By focusing only on ridges, it is not possible to validate one hypothesis over the other because of the difficulties in distinguishing between fluid driven processes (i.e., water vs. wind), sediment accumulation could be relevant to either hypothesis. By focusing on both basin floor sediments and those from sand ridges, this study reveals new information, which contributes to answering questions about basin evolution in the late Quaternary. On the one hand, if the erosional model holds true, it would be expected

that basin floor sediments would predominantly date to the Miocene. On the other hand, if the palaeolake model is confirmed, then we would expect some preservation of lacustrine sediment deposition concurrent with beach ridge formation during periods of the late Quaternary. Burrough *et al.* (2009) argue that the ridge building processes associated with dryland palaeolakes can commonly be attributed to both wind-driven and wave-driven action akin to coastal shoreline systems but that their construction is intimately linked to the presence of a large body of water. Therefore, a third possibility is a combination of both hypotheses, with one dominating at different points in time.

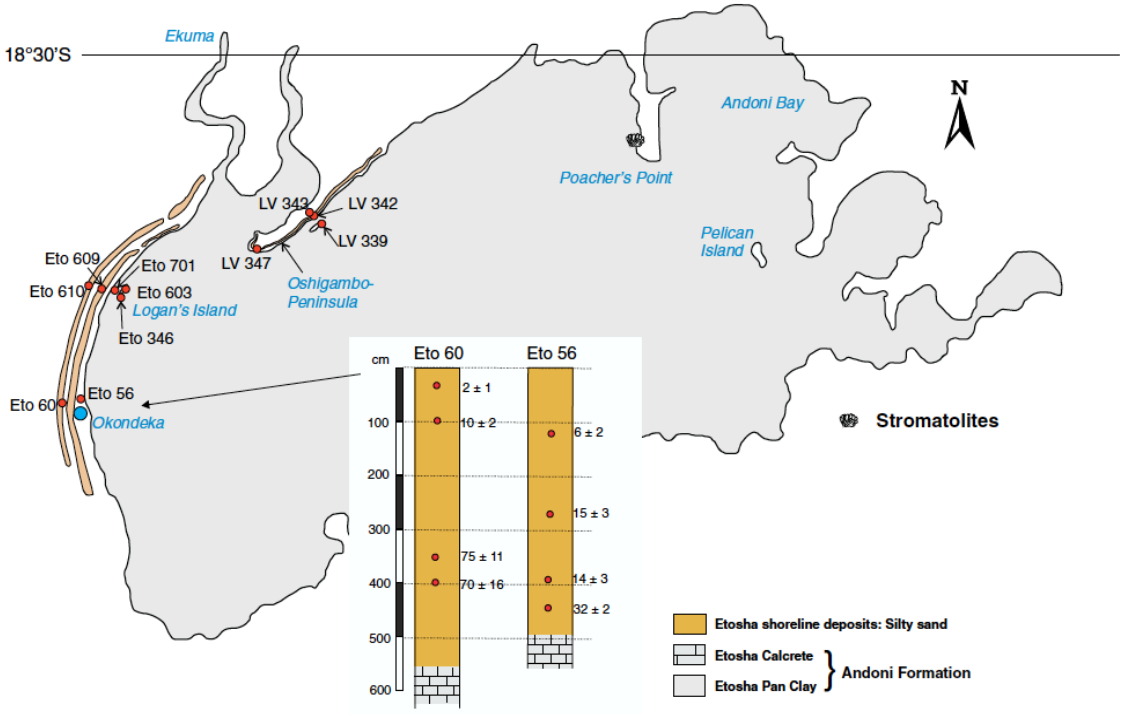

Figure 2.2. Etosha Pan and its marginal sand ridges showing sites that have been sampled in this study on the western part of the pan (Adapted from Hipondoka *et al.*, (2014). Eto 60 and Eto 56 are sites with thermoluminescence ages from Buch and Zoller (1992).

2.9. Palaeoenvironmental reconstructions at Etosha

Palaeoclimate reconstructions of the late Pleistocene in southwestern Africa are often constituted from sparsely distributed data. These spatial disparities, which may represent pronounced spatial heterogeneity within the palaeorecord, can inadvertently contribute to contradictory interpretations for the same period. The research has been conducted using a variety of methods, including, among others, cave speleothems, offshore marine records, pan sediments, and rock hyrax middens. The discussion below starts with outlining past palaeoenvironmental research at Etosha.

2.9.1. Last Glacial Maximum at Etosha

If the basin's western sand ridges are interpreted as shorelines formed during lake high-stands, (Hipondoka *et al.*, 2014) rather than lunette dunes (Buch and Zoller, 1992), then depositional ages suggest that Etosha experienced a wet climate during the last glacial maximum (LGM; referring to the period 23 - 19 ka). Earlier studies suggest that the dry phase persisted much longer as indicated by stromatolites on the east of Etosha which have been interpreted to reflect shallow lacustrine conditions at times due to intermittent growth of stromatolites on the Etosha Pan in the periods 15.4 - 13.5 ka and 10.6 ka (Brook *et al.*, 1996). However, like many early studies employing radiocarbon dating (e.g., Rust, 1985), the chronology presented by Brook *et al.* (1996) was based on radiocarbon ages from soil/sediment carbonates which might be influenced by the uptake of 'old' carbon and could include additional complications associated with bleaching and recrystallisation (Geyh and Eitel, 1997). Reassessment of radiocarbon dates sourced from stromatolites collected at Poacher's Point at Etosha

by Brook *et al.* (2011) indicated that previously published OSL ages were significantly older than organic residue ages contained by the host carbonate. As such, it is important to create a reliable chronology to underpin paleoclimatic studies at Etosha. As a result, this study used a multi-dating approach with luminescence and radiocarbon dating.

2.9.2. Etosha Pan during the Holocene

In palaeoenvironmental reconstruction dry lake basins are necessarily biased towards recording wet periods that facilitated net accumulation of sediments. In addition, there is the possibility of interspersed drying periods being largely absent from the record due to net deflation or lack of preserved landforms associated with these conditions (Burrough and Thomas, 2008; de Cort *et al.* 2021). Using OSL data from the sand ridges in the west of Etosha, which were interpreted as shorelines, Brook *et al.* (2007) found four periods of basin inundation in the Holocene at 7 - 5 ka, 4.5 - 3.5 ka, 2.5 - 1.7 ka and 1.0 ka. During these periods, the lake is believed to have carried larger amounts of water due to increased precipitation in the region. Using additional OSL dates from the ridges bounding the western margin of the pan, Hipondoka *et al.* (2014) suggested that a shallow water body occupied the basin between 10 ka and 7 ka. Hipondoka *et al.* (2014) further argued that Etosha experienced periodic shallow-water pan inundation after 7 ka, with a moist mid-Holocene inferred from rare mammal bone finds from the Ekuma Delta, in the northwest of the basin. A sitatunga *(Tragelphus spekei)* metacarpal, a wetland adapted species, interpreted to suggest wet, swampy conditions has a radiocarbon age of 4500 cal BP (Hipondoka *et al.*, 2005; Hipondoka

et al., 2006). Hipondoka *et al.* (2014) furthered the studies of palaeoenvironmental reconstructions by conducting sediment analysis and OSL dating to sand ridges on the west of the pan. Their record revealed existing gaps in Etosha's hydrological history during the lake high stands.

2.9.3. The palaeoenvironmental context of Logan's Island and the marginal sand ridges

The sand ridges on the western margin extend to as far as Okondeka (~ 40 km north-south distance from the Ekuma Delta) and some of them have been dated through luminescence dating. However, the ridges have been but reported as dunes in earlier papers (Buch and Zoller, 1992; Hipondoka *et al.,* 2004; Miller *et al.,* 2010) and reinterpreted as shorelines by Hipondoka (2014). Okondeka is a natural water hole located 23 km south-west of Logan's Island. Logan's Island is a geomorphological unit that stretches 900 m length and is 108 m wide. Based on the postulations from the earlier work, Logan's Island may be a remnant of a former shoreline (Hipondoka *et al.*, 2014) or it could be a lunette dune, the mode of formation proposed by others for the ridges, i.e., the "inner" and "outer" dunes of Buch and Zoller (1992). Robust evidence is required to understand its palaeoenvironmental context and place it within the wider geomorphology of the pan.

Logan's Island has been a site of palaeoenvironmental research, although the chronology establishment lacks precision. According to Hipondoka (2005), Logan's Island represents a shallow shoreline exposed during low lake levels, through the

erosion of the “beach ridges” that formed during extensive lake phases, suggesting that the island has an increasing sediment load that accumulates during lacustrine phases. Sand-sized particles (68 %), and comparable heavy minerals content (Buch *et al.*, 1992), were found within sediments of Logan’s Island as well as the marginal sand ridges on the west, suggesting similar formative processes between them (Hipondoka, 2005). Rust (1984) radiocarbon-dated pedogenic calcrete from Logan’s Island at a depth of 80 cm and found an age of 37 900 ± 100 BP. In addition, Heine (1982) dated molluscs (*Xerocerastus sp.)* and obtained an age of 10 6700 ± 465 BP from the eastern margin which was interpreted to have been deposited during wet conditions, but does not stipulate the sedimentary type, exact location or depth where the sample was taken.

Furthermore, karstic processes play a role in modern-Etosha Pan, though they remain poorly understood. There is an inflow of carbonate-rich water from the north (through fluvio-lacustrine processes), bordering the Otavi Mountains where water rises to the surface from groundwater flow and artesian springs on the southern parts of the pan (Hipondoka, 2005). Buch *et al.* (1992) sampled the southern part of the island, the outer dune (ETO 15/1 in this study), and the interdune depression across Logan’s Island. They found similar assemblage of heavy minerals that included garnet, amphibole and tourmaline and suggested that the sand ridges and Logan’s Island have similar origins (Buch *et al.*, 1992). Of the few springs on the pan, one is located 3.5 km to the west of Logan’s Island (Hipondoka, 2005), and formed where calcrete thickness decreases (Miller *et al.,* 2010). This spring mound was sampled by the present study

using two continuous sediment cores of 1.6 and 2 m depths that were extracted from the site.

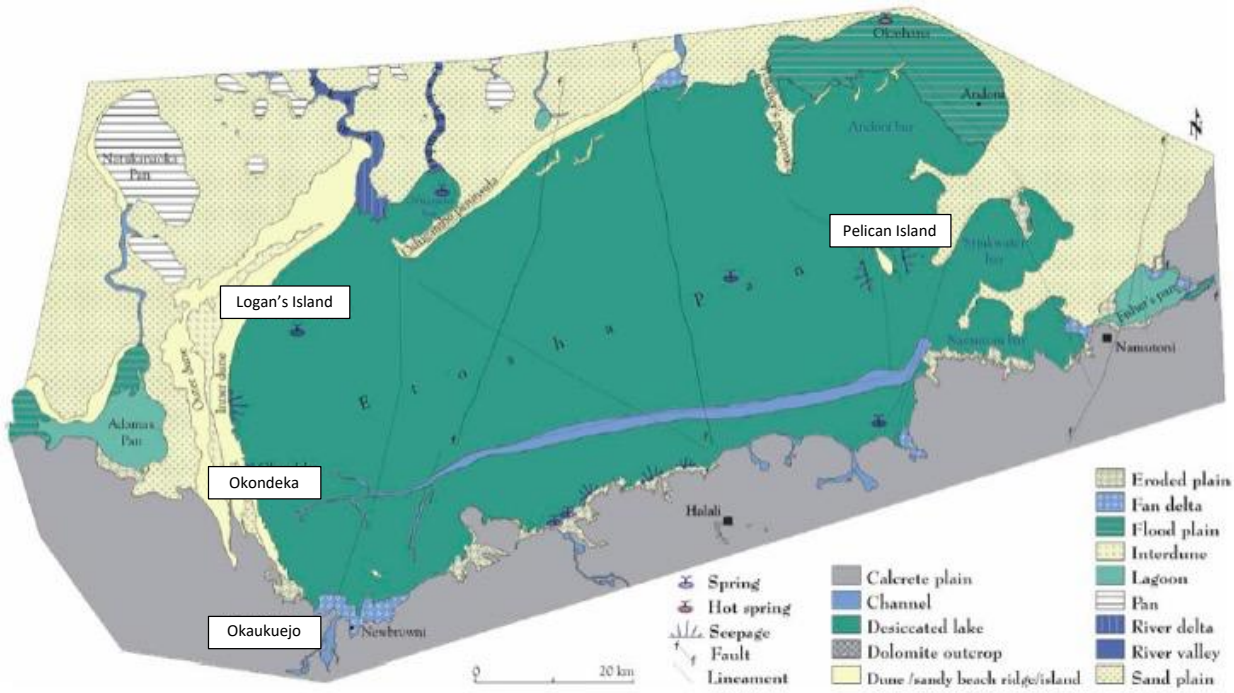

Figure 2.3: Etosha Pan geomorphology highlighting key locations discussed in the text including Logan's Island and Okondeka with sand ridges (referred to as "dunes" on the figure) laying parallel to the western margin of the pan. Adapted from Hipondoka (2005).

2.10. Previous luminescence dating studies at Etosha Pan

Only a handful of luminescence dates have been generated from Etosha Pan since the pioneering study by Buch and Zoller (1992) using thermoluminescence signals. Since then, methods progressed to using OSL mainly on the western sand ridges (Brook *et al.*, 2007; Hipondoka *et al.*, 2014), while radiocarbon dating was used on calcrete and stromatolite samples on the east (Brook *et al.*, 2011). This section of the review will collate OSL dates in previous studies that were obtained by different authors.

Table 2.6: Published chronologies from Etosha Pan

Age (ka)	Dated Material	General Location	Depth	Author's Interpretation	Dating Method	Source
2 400 ± 500	Sand	Okondeka (outer dune) (ETO 15/1 in this study)	20 cm	Dry	TL	(Buch and Zoller, 1992; Buch *et al.*, 1992)
5 600 ± 2 200	Sand	Okondeka (inner dune) (ETO 15/2 in this study)	120 cm	Dry	TL	(Buch and Zoller, 1992; Buch *et al.*, 1992)
10 000 ± 2400	Sand	Okondeka (outer dune) (ETO 15/1 in this study)	95 cm	Dry	TL	(Buch and Zoller, 1992; Buch *et al.*, 1992)
13 000 ±2 700	Sand	Okondeka (inner dune) (ETO 15/2 in this study)	390 cm	Dry	TL	(Buch and Zoller, 1992;

						Buch *et al.*, 1992)
14 800 ±2 800	Sand	Okondeka (inner dune) (ETO 15/2 in this study)	250 cm	Dry	TL	(Buch and Zoller, 1992; Buch *et al.*, 1992)
19 700 ±4 100	Sand	Okondeka (inner dune) (ETO 15/2 in this study)	>400 cm	Dry	TL	(Buch and Zoller, 1992; Buch *et al.*, 1992)
70 400 ±1 620	Okondeka III Soil	Okondeka Dune (unspecified)	450 cm	Dry	TL	(Buch and Zoller, 1992; Buch *et al.*, 1992)
140 000 +312/-45 ka (sic)	Sand	Okondeka (outer dune) (ETO 15/1 in this study)	>500 cm	Dry	TL	(Buch and Zoller, 1992; Buch *et al.*, 1992)

6.4 ± 1.0 ka	Sand	ETO 15/1 in this study	500 cm	Both dry and wet. Authors refer to sand ridges as lunette dunes but use "shorelines" in the discussion section, to represent wet phases	OSL	(Brook *et al.*, 2007)
4.0 ± 1.4 ka	Sand	ETO 15/2 in this study	250 cm	Both dry and wet. Authors refer to sand ridges as lunette dunes but use "shorelines" in the discussion section, to represent wet phases	OSL	(Brook *et al.*, 2007)
2.1 ± 1.0 ka	Sand	ETO 15/3 in this study	100 cm	Both dry and wet. Authors refer to sand ridges as lunette dunes but use "shorelines" in the discussion section, to represent wet phases	OSL	(Brook *et al.*, 2007)

9.70 ± 0.60 ka	Sand	Sand Ridge 1 (ETO 15/2 in this study)	50 cm	Wet	OSL	(Hipondoka *et al.* 2014)
16.70 ± 1.00 ka	Sand	Sand Ridge 1 (ETO 15/2 in this study)	80 – 90 cm	Wet	OSL	(Hipondoka *et al.* 2014)
19.10 ±1.60 ka	Sand	Sand Ridge 1 (ETO 15/2 in this study)	200 – 210 cm	Wet	OSL	(Hipondoka *et al.* 2014)
21.80 ± 2.10 ka	Sand	Sand Ridge 1 (ETO 15/2 in this study)	230 – 240 cm	Wet	OSL	(Hipondoka *et al.* 2014)
0.27 ± 0.04 ka	Sand	Sand Ridge 2 (ETO 15/1 in this study)	20 – 30 cm	Wet	OSL	(Hipondoka *et al.* 2014)
3.50 ± 0.20 ka	Sand	Sand Ridge 2 (ETO 15/1 in this study)	200 – 210 cm	Wet	OSL	(Hipondoka *et al.* 2014)
18.25 ± 1.24 ka	Not specified	Pan floor	20 – 30 cm	Wet	OSL (No further analysis took place)	(Hipondoka *et al.* 2014)
>58 ka (saturated)	Not specified	Pan floor	200 – 210 cm	Wet	OSL	(Hipondoka *et al.* 2014)

					(No further analysis took place)	
3.12 ± 0.24 ka	Sand	Logan Island (ETO 15/3 in this study)	55 – 65 cm	Wet	OSL	(Hipondoka *et al.* 2014)
4.04 ± 0.25 ka	Sand	Logan Island (ETO 15/3 in this study)	239 – 249 cm	Wet	OSL	(Hipondoka *et al.* 2014)
7.40 ± 0.30 ka	Sand	Logan Island (ETO 15/3 in this study)	425 – 435 cm	Wet	OSL	(Hipondoka *et al.* 2014)

2.11. Key Debates in southern Africa's palaeoclimate reconstructions

The key debates in southern African palaeoenvironmental reconstruction are largely related to differences in scale, shifts of the winter and summer rainfall zones (Chase and Meadows, 2007) and limitations relating to spatial heterogeneity. Etosha is not exempt from these debates and therefore requires new, continuous records to help shed light on how the basin has been affected by some of these phenomena.

Latitudinal shifts of the African tropical rain belt are known to have impacted palaeoclimatic conditions in Namibia for at least the last 100 ka (Collins *et al.*, 2014) the last glacial cycle, and there is no reason to suppose that equivalent shifts did not occur over prior glacial-interglacial cycles. The southern limit of the tropical rain belt is crucial for Namibia's seasonal rainfall and can determine which parts of the country receive rainfall in the austral summer (Figure 2.4). Furthermore, seasonal migration of the tropical rain-belt results in a rainfall gradient between the north and southern parts of the country, whereby, the northern part of the country experiences greater rainfall on average than the south, which receives shorter rain belt excursions. This rainfall gradient adds spatial complexity to Namibia's climate and, by extension, the palaeoclimate changes being studied in the past decades.

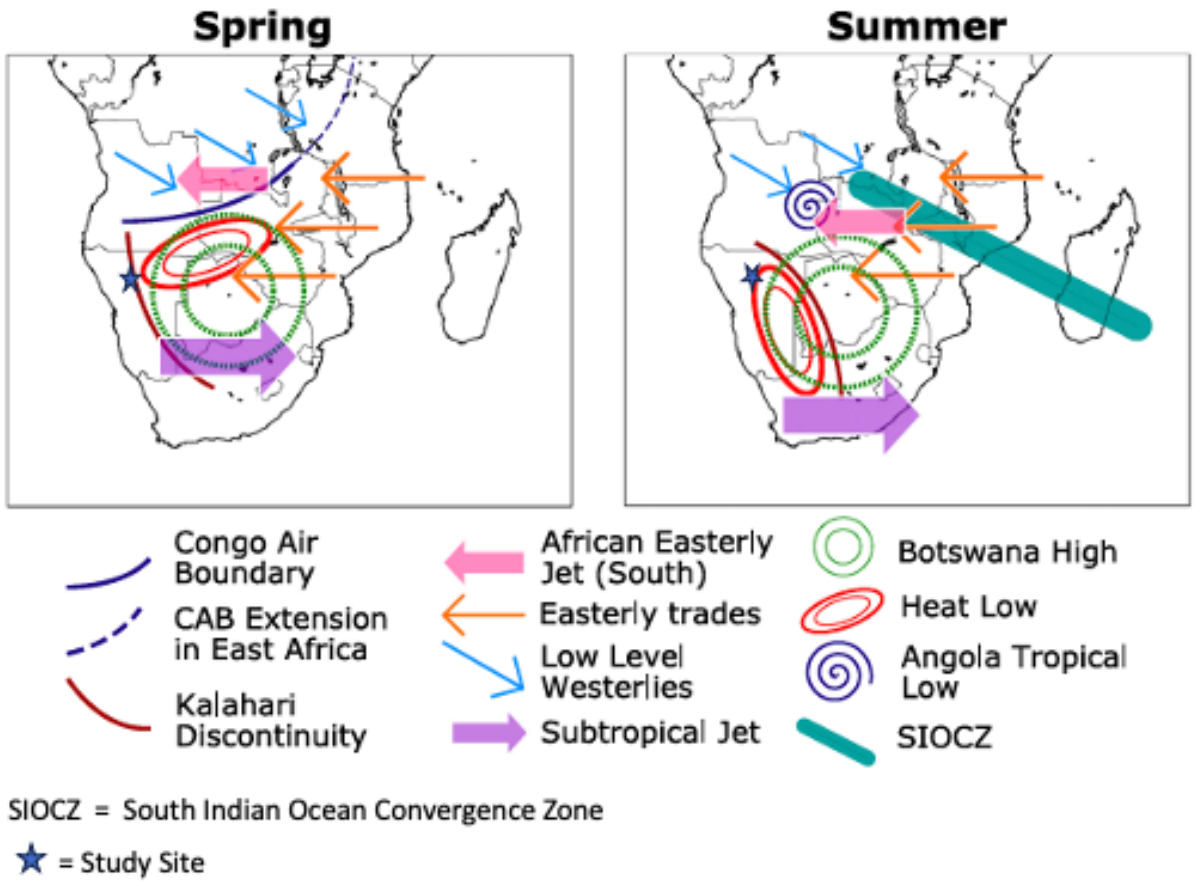

Figure 2.4: Schematic representation of key atmospheric circulation systems relating to the Congo Air Boundary (CAB). (Adapted from Howard and Washington, 2019)

In addition, the rainfall gradient in the country is also affected by the influence of the Benguela current on Atlantic precipitation generation. Precipitation amounts increase steeply eastwards from the coast, such that Gobabeb in the central Namib Desert has a mean annual figure of 15 mm, (Eckardt *et al.*, 2013; Viles *et al.*, 2013) while in the north-east rainfall ranges between 350 – 500 mm per annum (Mendelsohn *et al.*, 2002). It is worth investigating on how different oceanic moisture sources have differed in the past, and how the summer and winter rainfall zones have shifted, expanded or

contracted in the late Quaternary. This will help to contextualise present and future climatic changes.

The Congo Air Boundary (CAB) serves as the convergence zone of moisture sources from the Atlantic and Indian Oceans in southern Africa (Figure 2.4). The breakdown of the CAB can lead to the formation of tropical-temperate-toughs (TTTs) that are a key source of moisture for Namibia in summer (Railsback *et al.*, 2022). Tropical moisture sourced from the Indian Ocean is known to influence rainfall on the east coast of South Africa, however, there are debates about the extent to which Indian Ocean moisture reached Namibia to influence its palaeoclimate. Studies analysing compound-specific isotopes found in leaf waxes have contributed to disentangling the complexity of this argument particularly through the use of δD Hydrogen isotopes which can distinguish different hydrological sources that affect palaeorainfall patterns (Collins *et al.*, 2014). Collins *et al.* (2014) demonstrated the impact of a strong precessional forcing and cyclicity (23 - 19 ka), by providing evidence from vegetation changes and variations in hydrological sources preserved in the isotopes of Hydrogen and Carbon-13 ($\delta^{13}C$) from offshore sediments. Moreover, these atmospheric circulation systems do not act in isolation and are made more complex in their expressions and interactions between each other. There are delays in the response of vegetation and ocean hydrological dynamics due to the differences in lag time to respond to large-scale change.

Marine sediment cores found offshore of Namibia have often been investigated to reconstruct changes in vegetation and humidity using marine sediment cores (e.g.,

Gingele, 1996), pollen (Shi *et al.*, 1998) and leaf-wax n-alkanes (e.g., Collins *et al.*, 2014). These studies have taken place at different latitudes, with some near Angola and others further south. Collins *et al.* (2014) inferred increased summer precipitation during the LGM in the western Kalahari region of Namibia based on leaf wax analyses from downwind marine cores. Their study suggested that majority of the sediments were sourced from the Kalahari (Collins *et al.,* 2014), and the increased precipitation has been predicated by some palaeoclimate models e.g., Kageyama *et al.* (2013). However, in other studies, including those focused on the strength of the Benguela current and its impact on southwestern Africa, moisture regimes suggest the period to have been relatively dry. Off-shore marine core data from Gingele (1996) suggested that the late Pleistocene was likely dry between 21.7 ka and 18.2 ka in southwestern Africa and then progressed to wet conditions until 11.5 ka.

Schefuß *et al.* (2005) suggested that the low sea-surface temperature (SST) gradient that results from direct insolation in the southern hemisphere leads to warm subtropical conditions and cold tropics, coupled with weak trade winds produced wetter conditions for southwestern Africa. Singarayer and Burrough (2015) compare model and empirical data along the southwestern coast of Africa to demonstrate the effect of the 20 ka cycle, but infer a difference in behaviour of the tropical rain belt over the oceans and the near coastal region of Namibia when compared with Nambian interior. Like Collins *et al.* (2014), they suggest that the direct influence of any precessional signal will be strongest inland and during glacial periods.

Another mechanism that highlights the importance of the Atlantic-sourced moisture in southwestern Africa especially during glacial periods was initially proposed by Van Zinderen Bakker (1967) and later supported by Tyson (1986). It is understood that the moisture stems from the migration of the polar front north of Antarctica. The expansion of Antarctic sea-ice during glacials leads to a northward migration of the polar front, which displaces the moisture-bearing mid-latitude cyclones to move northwards to bring wetter conditions to southwestern Africa. Indeed, shifts in the southern hemisphere westerlies are thought to have been significant as demonstrated by studies from Stuut *et al.* (2002) and Chase and Meadows (2007). Other scholars bring the role of Indian Ocean moisture to light in southwestern Africa on a longer timescale, as shown through the shifts in the Congo Air Boundary (CAB). They argued that during glacials, tropically sourced moisture had a greater influence on increased precipitation in southwestern Africa than Atlantic Ocean sourced westerlies precipitation (Collins *et al.*, 2014). These postulations remain to be tested. Furthermore, Brook *et al.* (2007) argued that the Etosha wetness between 7 - 5 ka was due to the incursion of the Indian Ocean moisture through shifts in the CAB due to a lower SST gradient between the tropics and subtropics in the southern hemisphere.

Etosha Pan lies at the confluence of different atmospheric circulation systems that might have interacted in the past. For example, both the north-south and west-east rainfall gradients can influence the palaeoclimate and environmental change at Etosha, adding to its complexity as a palaeoarchive of environmental change.

2.12. Synthesis of the reviewed literature on current understanding of late Quaternary palaeoenvironments at Etosha Pan

Over several decades, available dating techniques and protocols have significantly improved. For example, Hipondoka *et al.* (2014) used single aliquot regenerative OSL which is better suited for analysing sedimentary quartz than that of Buch and Zoller (1992) who had to base their interpretations of sand ridges on data from thermoluminescence dating, which generally has low precision. The studies by Hipondoka *et al.* (2014) and Brook *et al.* (2007) were limited to the sand ridges on the western part of the pan. Furthermore, the ages of the sand ridges were interpreted to be shorelines (by both studies) without much evidence to contrast them being of aeolian origin as has been proposed by other scholars. Hipondoka *et al.* (2005) and Hipondoka *et al.* (2014) noted that there are gaps in the reconstruction of Etosha's palaeohydrological history and this hinders the ability to pinpoint the exact timing of these events.

It is essential to explore datasets of Etosha beyond the marginal sand ridges, and at a greater temporal resolution. Furthermore, a combined use of independent dating approaches across the sand ridges, pan-floor sediment cores and lakebed samples systematically will help improve understanding of past and present hydrological change on the pan.

In addition, the studies based at Etosha often point to periods when the pan contained large volumes of water, but are unable to quantify lake size or depth, except for that of

Brook *et al.* (1996) which interpreted the growth of stromatolites to indicate a period when the pan contained water >8 m in depth. Some studies at Etosha, e.g., Miller *et al.* (2010), made postulations about the palaeoenvironmental context of the basin, as well as the mode of formation of the marginal sand ridges, without the use of clear proxy data. Hipondoka *et al.* (2005) assessed these studies and found that there are still outstanding questions about the formation and evolution of Etosha Pan. Changing atmospheric carbon dioxide levels over interglacial and glacial periods in the past might have also influenced Namibia's vegetation dynamics because the trees, shrubs and grasses are very sparce but often respond to large-scale change.

2.13. Conclusion

Etosha Pan has been subject to relatively few palaeoenvironmental studies in the past. Of the few that have taken place, they are limited by chronology, short time span and focussed on basin margin deposits. There exists an opportunity to contribute additional information to this existing dataset through a multi-dating approach at different locations of the pan, which is undertaken by this study. In Namibia more broadly, multi-proxy terrestrial research is needed in order to give a clearer picture of the climate and environmental changes during the LGM and the Holocene. It is worth probing the dataset at Etosha to test whether it can contribute information to some of the major debates in palaeoenvironmental studies in southern Africa.

Chapter 3: Methods

3.1. Introduction

Identifying suitable sites in the Etosha Pan for fieldwork was a critical aspect of the thesis. This chapter introduces the sampled sand ridges and lakebed, justifies their selection, sampling strategy, and the number of samples collected for dating. Furthermore, it outlines methods used for geochemical and palaeoecological proxies using relevant protocols. The current chapter details the laboratory procedures for extracting a dateable quartz component and the instrumentation used to measure 19 samples for Optically Stimulated Luminescence (OSL) dating. It also outlines the chosen dating protocol, quality assessment tests, and signal analyses conducted to determine a sample's equivalent dose *(De),* as well as the measurement and calculation of the environmental dose rate (Ḋ). Radiocarbon dating analyses were also conducted on 17 bulk sediment samples to establish better chronological precision upon which the palaeoenvironmental interpretations could be made. By establishing a reliable chronology for Etosha Pan, the study aimed to constrain the timing of the region’s major palaeoenvironmental changes.

3.1.1. Fieldwork design

The fieldwork was designed with the goal of obtaining high resolution sediment deposits for multi-proxy analyses. The equipment, locations, and timing (late dry season for better basin access) were selected strategically to collect sediments that would reveal environmental changes across wide temporal and spatial scale.

3.1.1.1. Site selection

To choose an appropriate site for palaeoenvironmental research, several factors must be considered such as basin geomorphology, suitability for dating the samples and the type of underlying lithology. Accessibility is also a key issue, especially in a national park where, even with a research permit, there are strict controls on movement. This study focused on the north-western margin of Etosha Pan, a strategic location selected to optimize data collection and achieve the research objectives, and accessible by a track along the modern pan surface margin. The area provided ideal conditions for investigating the basin's chronological development and formation processes, specifically because:

1) **Proximity to the Ekuma Delta:** The coring sites needed to be relatively close to the Ekuma Delta, since it is the primary source of river sediment deposits. River capture of the Kunene and subsequent diversion to the Atlantic Ocean played an integral role in Etosha's development as it deprived the pan of its main fluvial source and led to the reduction to its current size in the mid-Pleistocene (Hipondoka, 2005; Stuart-Williams, 1992). Since this project includes investigating key aspects of the geomorphic evolution of the pan, an assumption was made that the Kunene's contribution of sediments to the pan was through the Ekuma Delta as it is the main river inlet from the Cuvelai-Etosha drainage system. Stuart-Williams (1992) estimated that the Kunene River was cut off from Etosha's main drainage basin at 35 ka. Therefore, sites capturing the deposition of those sediments would potentially contain data regarding such

hydrological changes as the Ekuma Delta has been the main river inlet on the pan during the late Quaternary (Hipondoka *et al.,* 2004).

2) **Sampling the existing sand ridges:** as this project aims to contribute to debates about basin development and the palaeoclimatic context of Etosha, it was important to choose a site close to those that have already been studied to allow for comparative analysis. For example, Buch and Zoller (1992) and Hipondoka *et al.* (2014) studied the ridges on the northwest margins of the pan (as explained in Chapter 2), which are also a target area for this project.
3) **Preservation of older sediments:** Samples investigated by Hipondoka *et al.* (2014) and Brook *et al.* (2007) from the sand ridges mostly dated to the Holocene. Brook *et al.* (2007) had a maximum sampling depth of 100 cm on the ridges, while Hipondoka *et al.* (2014) also encountered a Holocene age from a maximum depth of 425-435 cm from Logan's Island, and maximum depth of 240 cm on the other ridges. Therefore, extracting deeper cores would increase the likelihood of encountering older sediments. This would therefore create an opportunity to extend the record of ridge deposition beyond the Holocene.
4) **Generation of a pan-floor sediment palaeoenvironmental record:** The Etosha's pan floor has not been previously sampled to help answer questions of origin, palaeoenvironmental context or palaeohydrological histories. As such, this research took an opportunity to sample the pan floor for the first time with the expectation that the new dataset would add insights to existing understanding of the pan geomorphology. This was achieved using two methods of sediment retrieval i) through the use of pits into hard compacted clay

(where coring was impossible), and ii) extracting sediment cores from the wetter, less compact sediments of a spring mound. In the latter case, radiocarbon dating was applied to core samples to achieve a higher resolution chronology (typical precision on ^{14}C is 1 - 3 % compared to 10 % with OSL dating). The use of radiocarbon dating within the Etosha basin has been limited to stromatolite formations (Brook *et al.* 2016), and mid-Holocene ungulate remains found at the Ekuma Delta (Hipondoka, 2006). Radiocarbon dating of bulk sediments in other southern African salt pans (Nash *et al.*, 2006; Schuller *et al.*, 2018) provided good insight for the successful application of this technique to pan sediments.

5) **Research permissions:** The research permit allowed access to the west of the basin along an existing track, with access not permitted to the eastern and more central locations within the pan.

Taken together, the north-western area had sedimentary and landscape contexts pertinent to the aims and was an area where it was possible to access and sample within the constraints of the permissions granted.

3.2. Field data collection

Two field campaigns were conducted to collect data from the pan. One took place in 2015 prior to the conception of this thesis, and the second one followed in 2019. The 2015 fieldwork focused on the sand ridges and was conducted by a team of researchers from the University of Oxford and the University of Turku, Finland guided

by Dr. Martin Hipondoka from the University of Namibia, Windhoek. Eight samples from the 2015 field campaign were dated and the preliminary results revealed that they were of Holocene age. The 2019 field work involved researchers from the University of Oxford, the University of Windhoek and the University of Cape Town and targeted the pan-floor sediments. It was scheduled for the first week of September 2019 (at the end of winter) because the pan is at its driest during that period, enabling the team to transport equipment across the pan to the selected sample sites.

3.2.1. Lakebed sediment sampling

Five sampling sites of approximately 1 metre depth were excavated at different locations on the pan as shown in Figure 3.1. A layer of hard calcrete and dense clay at the sampling sites prevented deeper sampling, as the vibracorer could not penetrate through these materials (The vibracorer is shown in Figure 3.1 and described in detail in section 3.2.2.). The advantage of pit sampling sites was the exposure of the vertical pan profile, allowing the identification of different sediment facies and deposition zones to sub-sample from.

Figure 3.1: Photographs of fieldwork in Etosha. Left: OSL Sample collection from a site on the lakebed (Credit: A. Nagendji). Right = Photograph of vibracorer during sample collection of Core B (ETO 19-4V).

From each sampling site, samples were collected at a 10 cm vertical resolution for grain size, leaf-wax n-alkanes and diatoms analyses until a maximum depth was reached. Sampling was determined by the nature of the exposed internal stratigraphy. Therefore, OSL samples were taken at specific depths where clear sediment facies were identified. This enabled capture of both changes in sediment deposition and changes in dose rate that might affect the OSL age. Samples are specified in Table 3.1 below. The spatial spread was ~1 km for samples on the lakebed and the sand ridges, except the sediment cores which were 2 m apart (Figure 3.2).

Table 3.1: Depth and locations of samples excavated from the lakebed

Sample ID	Depth (cm)	Latitude	Longitude
ETO 19/5/1	8 cm	18.77571 S	15.91786 E
ETO 19/5/2	26 cm	18.77571 S	15.91786 E
ETO 19/7/1	39 cm	18.66558 S	15.99347 E
ETO 19/7/2	61 cm	18.66558 S	15.99347 E
ETO 19/7/3	88 cm	18.66558 S	15.99347 E
ETO 19/8/1	37 cm	18.66921 S	15.99567 E
ETO 19/8/2	58 cm	18.66921 S	15.99567 E
ETO 19/8/3	67 cm	18.66921 S	15.99567 E

3.2.2. Lakebed core samples

The vibracorer was selected as the preferred tool for this site for several reasons. Firstly, it is non-destructive to the pan surface (creating only a small hole and being relatively portable, requiring limited vehicle access) which allows it to be safely used in a National Park without leaving permanent damage to the environment. Secondly, a vibracorer has been used extensively in Quaternary studies in southern Africa (e.g., Baxter and Meadows, 1999; Quick *et al.,* 2016; Du Plessis *et al.,* 2021; Burrough, 2022) and has a proven ability to retain the stratigraphy of the sediments in aluminium tubes after coring and transportation. The corer can easily be managed by 3 - 4 people during operation and is relatively easy to transport to remote locations. For this project, a vibracorer was loaned from the University of Cape Town and transported to Etosha National Park for the 2019 fieldwork. Two parallel cores were taken for replication and

to ensure that there were enough samples for the various analyses planned. Table 3.2 below shows the locations where each core was retrieved.

Table 3.2: Location and depth of each sediment core retrieved from the modern-day spring on the lakebed

Core ID	Length of core (cm)	Latitude	Longitude
ETO 19/3V	163 cm	18.77545° S	15.91835° E
ETO 19/4V	194 cm	18.77545° S	15.91836° E

Figure 3.2: Locations of sampling sites on the lakebed and the sand ridges on the north-western margin of Etosha Pan.

The two sediment cores were split lengthwise and described lithologically at the University of Witwatersrand (Figure 3.3). The University of Witwatersrand was selected for the availability of a dark lab which was essential for core splitting within conditions

that would preserve the OSL signal. One core was sent to University of Oxford where further analyses and subsampling would take place. Notes were made on discernible sediment facies, texture, colour and macrofossils on one half of each core while the other half was kept in the dark for the collection of OSL samples. Colour comparisons were made with a Munsell Colour Scheme (Munsell, 2000).

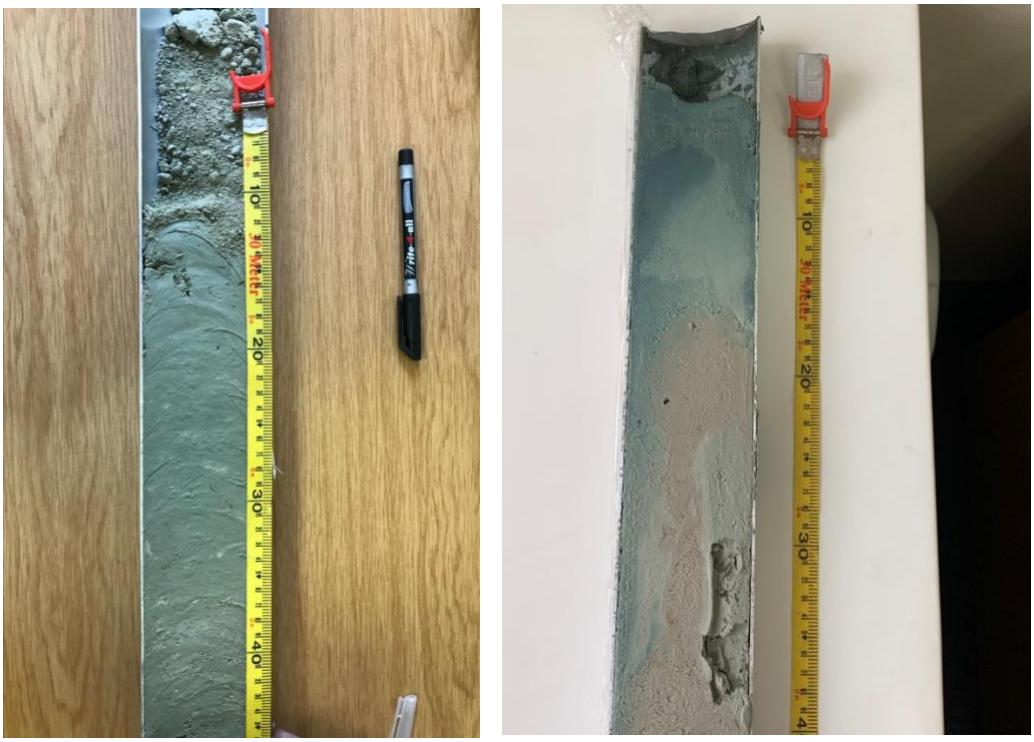

Figure 3.3: Photographs of ETO 19-4V (Core B) sediment core after splitting in the laboratory at the University of Witwatersrand.

3.2.3. Sand ridge samples

The work for the thesis included completing initial analyses on OSL samples collected during a coring programme in 2015. Preliminary OSL analysis on those samples

revealed that they were of Holocene age, thus laboratory work in 2019 was extended to those previously unprocessed samples collected during the 2015 field campaign. The three prominent sand ridges that run parallel to the north-western edge of the pan were targeted as they had been a key area of past research that investigated the palaeoenvironmental context of Etosha. Logan's Island at Etosha Pan, Namibia, is a significant site for understanding the region's depositional context and formation. Therefore, the island was sampled for similar reasons as the ridges. However, the argument is about the depositional context of the ridge: whether it is an aeolian structure that accumulated during the lake's dry phases, or if it is an island with net sediment accumulation during high lake phases (Hipondoka, 2005).

Table 3.3: Location and maximum depth reached on each sampling site on the sand ridges

Sand Ridge ID	Maximum Depth (m)	Latitude	Longitude
ETO 15/1/1	0.5	18.78607 S	15.7715 E
ETO 15/1/2	1.0	18.78607 S	15.7715 E
ETO 15/2/1	1.0	18.78584 S	15.83575 E
ETO 15/2/2	1.2	18.78584 S	15.83575 E
ETO 15/2/3	1.9	18.78584 S	15.83575 E
ETO 15/2/5	3.0	18.78584 S	15.83575 E
ETO 15/2/6	4.0	18.78584 S	15.83575 E
ETO 15/3/1	0.3	18.78189 S	15.88568 E
ETO 15/3/4	3.0	18.78189 S	15.88568 E
ETO 15/3/6	5.0	18.78189 S	15.88568 E

3.3. Laboratory work

Analysis of samples from the sediment cores and pit samples was primarily carried out in Oxford, with additional work undertaken in several specialist labs at other institutions in the UK. These included University of Leicester for leaf wax n-alkane analysis and diatom analysis at the University College London Department of Geography.

3.3.1. ICP-MS

ICP-MS analyses for this project were conducted in the School of Geography and the Environment Geolab at the University of Oxford and used to measure concentrations

of Uranium (^{238}U), Thorium (^{232}Th), and Potassium (^{40}K) to determine dose rate information. For the measurements, the Perkin Elmer 2000B ICP-MS system was used. Approximately 25 mg of each sample was collected and prepared for the ICP-MS measurement by digesting it in a solution of 1 ml concentrated HNO_3 and 1 ml of HF was then evaporated on a hot plate after the mixture was left to react overnight and then the samples were diluted in 2 % HNO_3. The elements were quantified using SPS-SW2 reference material on the 19 samples analysed for OSL dating.

3.3.2. Grain size

The Malvern Mastersizer 2000 Laser Particle Analyser was used for the grain size analyses. For each sample, 1 cm^3 of sediment was added to 1 litre of water and given 10 seconds of ultrasonic treatment. 360 samples were collected at a 1 cm resolution from both cores to reveal fine scale sedimentological changes. Three repeat measurements were averaged before undergoing statistical analysis using Gradistat (version 9.1) (Blott and Pye, 2001) to quantify sediment particle size distributions. Grain size data were analysed using the geometric methods of moment and were based on geometric graphical measures based on original Folk and Ward (1957) method. These provided information on the mean, mode, sorting (standard deviation), skewness and kurtosis.

High-resolution subsampling enabled reconstruction of changes in sediment characteristics through the samples. In addition, grain size analysis was conducted on each OSL sample collected and used in dose rate calculations, as well as to analyse the sediment depositional environment for each sample.

For grain size data analysis, End-Member Modelling Analysis (EMMA) was used in this project as a statistical technique to identify distinct grain size populations using an unmixing technique (Dietze *et al*., 2012). EMMA is particularly helpful in paleoenvironmental reconstruction because it provides robust, objective results that can be used to interpret complex sedimentary records such as lake sediments (Kumar *et al.,* 2022). EMMA enables quantitative reconstruction of past changes in sediment sources, wind patterns and fluvial processes over time. The method uses algorithms such as end-member analysis to identify the minimum of groups in the dataset required to explain variance observed in the samples (Dietze *et al*., 2012; Dietze *et al*., 2022). The subgroups, known as end-members, can represent specific sedimentary processes that possess a unique grain size signature to quantitatively reconstruct past sediment deposition and transport mechanisms.

In addition, principal component analysis (PCA) and biplots applied to grain size data have been utilised in this project to identify key characteristics about sedimentary environments. PCA can reveal relationships between energy conditions, depositional process signatures, and temporal environmental changes (Chambers and Upchurch, 1979; Ikhane, *et al.,* 2019). For example, high energy environments such as deep river channels can be explained by heavy loading of coarser fractions often indicated by PC1. Bimodal signatures are common in aeolian environments due to separate saltation and suspension sediment groups (Ikhane, *et al.,* 2019). Higher order principal components such as PC2 and PC3 can reflect different sediment sources. For example, clusters in PCA can reflect provenance and processes influencing sediment supply

variations (Chambers and Upchurch, 1979). Finally, temporal changes in the environment's evolution can help track samples along PC axes along with progradational cycles (Yang *et al.,* 2017). In this project, PCA analysis has assisted in correlating sedimentary facies as visual analysis was not always possible.

3.3.3. Diatoms

Diatom analysis was intended as a contribution to Objective 3 by understanding how diatom assemblages have varied at Etosha in the past to help make inferences about changes in lake status. To test the viability of this method, ~ 0.5 grams of sediment was diluted into an equal amount of distilled water. Smear tests were conducted using samples from 8 depths: 2 from each sediment Core and 2 from 2 sample pits. The samples were used to make smear slides by taking a small amount of sediment mixed in water, taking a drop of that, and diluting to 5ml to make a wet mount as described here: (https://www.microscopemaster.com/microscope-slides.html). The suspension was then dried on a coverslip, taking care to not trap any air bubbles, and fixed using Naphrax to make permanent slides. Excess water was removed with a paper towel. Naphrax (synthetic resin) is a specially formulated solution for detecting and embedding diatoms. The samples were then examined from under a light microscope to search for the presence of diatoms with increasing magnification from 40x to 1000x.

3.3.4. Leaf-wax n-alkanes

Ten subsamples of unidentified modern plant leaves were collected directly from the Etosha Pan surface during field work were sent to the University of Leicester where they were freeze-dried upon arrival. They served as reference material for modern-day

leaf wax n-alkane distributions in the Etosha Basin as not much is known about them. 16 samples from the two sediment cores (Core A = ETO 19-3V and Core B = ETO 19-4V) and 8 pit samples on the lakebed were later sent to the lab for analysis. The 8 samples collected from the pits are:

- ETO 19-5-B (28 cm)
- ETO 19-5-C (40 cm)
- ETO 19-7-A (10 cm)
- ETO 19-7-B (20 cm)
- ETO 19-7-E (40 cm)
- ETO 19-8-A (15 cm)
- ETO 19-8-C (45 cm)
- ETO 19-9-A (10 cm)

Sample preparation and analysis took place at the University of Leicester Environmental Stable Isotope Laboratory. Soxhlet extraction took place, with samples subjected to Soxhlet extraction for 24 hours in methane (MeOH with a ratio of 2:1 to the samples) as described in Collins *et al.* (2014). The samples were then evaporated on a rotary tube and purified using column chromatography. The columns were conditioned with hexane for collection of the n-alkanes. Samples were then isolated and coupled to a mass spectrometer (GC-MS) for identification of n-alkanes with reference standards (n-tetracosane (C24)/n-tetratriacontane (C34))

3.3.5. Stable carbon isotopes

Stable carbon isotopes have been utilised extensively for palaeoenvironmental studies, especially in archaeological excavations using avian eggshell to reconstruct diet and vegetation changes over time in southern Africa, particularly in the interior landscape (e.g., Lee-Thorp and Ecker, 2015). Niespolo *et al.* (2020) emphasised the potential of avian eggshell (ostrich in particular) isotopes for providing site-specific paleoenvironmental records. Ostrich eggshells have not been used to reconstruct palaeohydrological change in most pans located in southern Africa, including Etosha Pan. For analysis, 18 eggshell samples from the spring mound cores (Core A = ETO 19-3V, and Core B = ETO 19-4V) were sent in for stable isotopes analysis with the goal of extracting information about past vegetation changes at Etosha. The isotope analysis of carbon-13 ($\delta^{13}C$) was conducted at the University of Cape Town Stable Isotopes Laboratory. For each sample, 0.1 mg was used for the $\delta^{13}C$ measurements. The samples were reacted with 100 % phosphoric acid at 70°C to release carbon dioxide gas, which was then collected and analysed in an isotope ratio mass spectrometer (IRMS) mass spectrometer to determine $\delta^{13}C$ values.

3.3.6. Ancient DNA

Genomic DNA was extracted from 5 – 50 mg of six powdered eggshell fragments from five depths in both spring mound cores following a protocol adapted from Oskam *et al.,* (2010) and Grealy *et al.,* (2017) and optimised for fossil avian eggshell. aDNA analyses for current study was conducted at the Palaeogenomics & Bio-Archaeology Research Network (PalaeoBARN) at the University of Oxford. Extracts were then converted into double-indexed libraries (Meyer and Kircher, 2010), and sequenced (at low-depth) on

an Illumina HiSeq X Series (Macrogen, South Korea) using 150bp paired-end sequencing chemistry. Following this, downstream computational analyses were performed in HAYSTAC (Dimopoulos *et al.,* 2022) under default settings. Databases were constructed for both taxonomic identification ("Aves" mitochondrial genomes; 1,019 species) and characterisation of microbial diversity ("Prokaryote Reference"; 5,636 species) using references available on the NCBI Nucleotide database.

3.4. Chronology

3.4.1. Radiocarbon dating

Radiocarbon dating of bulk sediments has proven to be a reliable method for establishing downcore chronology in numerous late Quaternary studies of salt pans (e.g., Schuller *et al.,* 2018; Belz *et al.,* 2020). Accumulation of organic matter over time is an essential requirement for the success of radiocarbon dating. As some research has indicated that Etosha Pan has seasonal water inundations, organic matter from these periods is likely preserved in the sediments, making them suitable for radiocarbon dating. A radiocarbon dating chronology from Etosha is fundamental to this project's ability to meet Objective 1 and lays the foundation to achieve Objective 2 and 3.

Radiocarbon sample preparations and analyses were carried out at iThemba LABS in Johannesburg in October 2019 on Core B (ETO 19-4V) that was opened at the University of the Witwatersrand. 17 samples (bulk sediment and eggshell) from sediment Core B were used for radiocarbon dating at iThemba, while 11 from Core A

(ETO 19-3V) were analysed at the University of Oxford Research Laboratory for Archaeology and the History of Art (RLAHA). No organic macro fossils were found and identified from the sediment cores, thus bulk samples were dated. A limitation of dating bulk sediment samples is that it averages organic matter that is accumulated over a long period, unlike plant macro fossils, which capture a specific short-lived period. These, in conjunction with luminescence dating, helped to create a solid chronology to establish the timing of sediment deposition (age) and major environmental changes of Etosha Pan. The radiocarbon dating methods at iThemba and Oxford Radiocarbon dating labs are similar and thus described below.

The procedure for analysing sediment samples for radiocarbon dating involved several steps to isolate the organic carbon from the sediment and convert it into a suitable form for Accelerator Mass Spectrometry (AMS) measurements. Firstly, samples were freeze-dried overnight and then ground to fine powder using pestle and mortar the following day. The samples were then pre-treated in acid (HCl), alkali solution (NaOH) and another acid (HCl) (acid-alkali-acid also known as A-A-A) rinse for 20 minutes in each and rinsed with deionized water after each cycle to prevent further contamination with secondary organic acid (Brock *et al.,* 2010). The HCl rinse helps to remove any carbonates formed during the analysis. The final acid is used to neutralise the solution again. Due to the high carbonate content (seen in the continuous fizzing during acid treatment) in the Etosha sediment cores, the bulk samples were reacted with HCl for 24 hours instead of the usual 60 minutes used in the analysis.

Cryogenic distillation then follows to prepare the samples for combustion in the presence of iron oxide and silver wool catalysts under a vacuum (Vogel *et al.,* 1984). Liquid nitrogen was used to freeze out the CO_2, while dry ice removed the H_2O, and other unwanted gases were flushed out from the line. Following this, quartz sample tubes were baked at 600 °C for four hours to prepare them for sample graphitisation. The samples (in gaseous form) were purified and collected for stable isotope measurements using two Europa Scientific instruments (mass spectrometers) that measure the $\delta^{13}C$ and $\delta^{15}N$ ratios under continuous flow of helium gas (Figure 3.4). Finally, the graphite samples were pressed into a target holder suitable for accelerator mass spectrometry (AMS) measurement. After graphitisation, the samples (now in graphite form and referred to as targets) are pressed onto a clean aluminium holder and then transferred to the AMS for analysis. The proportion of radiocarbon atoms is determined by measuring ratios of $^{14}C/^{12}C$ and $^{13}C/^{12}C$ using six standards and two samples of known age along with regular checks to ensure high precision.

An age model for the radiocarbon dated cores was constructed in BACON (v.2.2) (Blaauw and Christen, 2011; Blaauw and Christen, 2021) which produced best estimate modelled ages for each 1 cm section of the cores. BACON uses Bayesian statistics to produce robust age-depth models that account for accumulation histories of the sediments. Prior information provided to the model assumed no depositional hiatuses. Specific data of each BACON model used for the sediment cores are presented in Chapter 5 along with other model calibration tools.

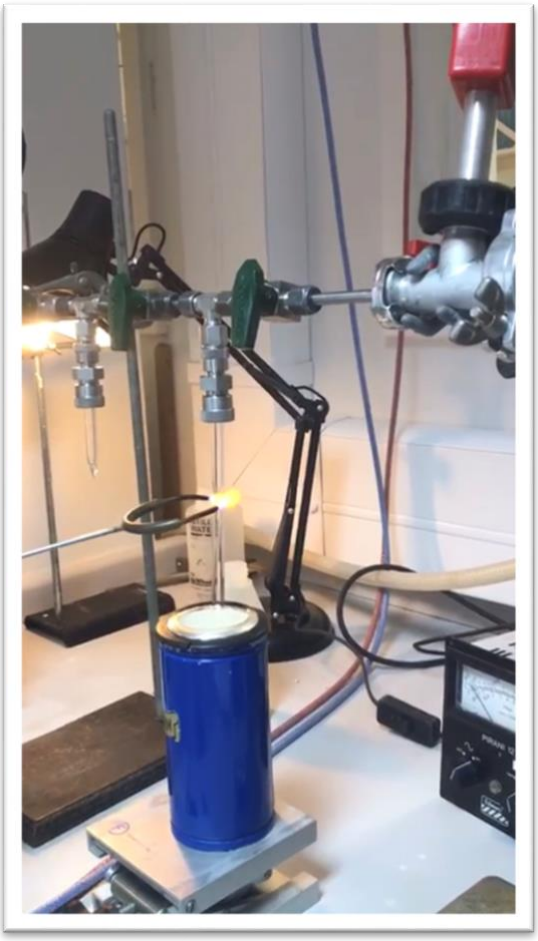

Figure 3.4: Radiocarbon sample in a sealed test tube containing CO_2 collected in the dry ice to ensure that no gas escapes during the transfer from the line to the mass spectrometer. (Picture taken from RHALA during sample analyses)

3.4.2. OSL dating

Luminescence dating is a well-established dating methodology that measures the period of time passed since sediments were exposed to sunlight (Figure 3.5). OSL can typically date samples ranging from a few decades to several hundred thousand years old, depending on the environmental conditions and the properties of the mineral grains (Wintle, 2008). This method has advanced the study of sedimentary deposits, providing valuable insights into past environmental changes and landscape dynamics

beyond the absolute limits of radiocarbon dating and in regions where organic material is often lacking.

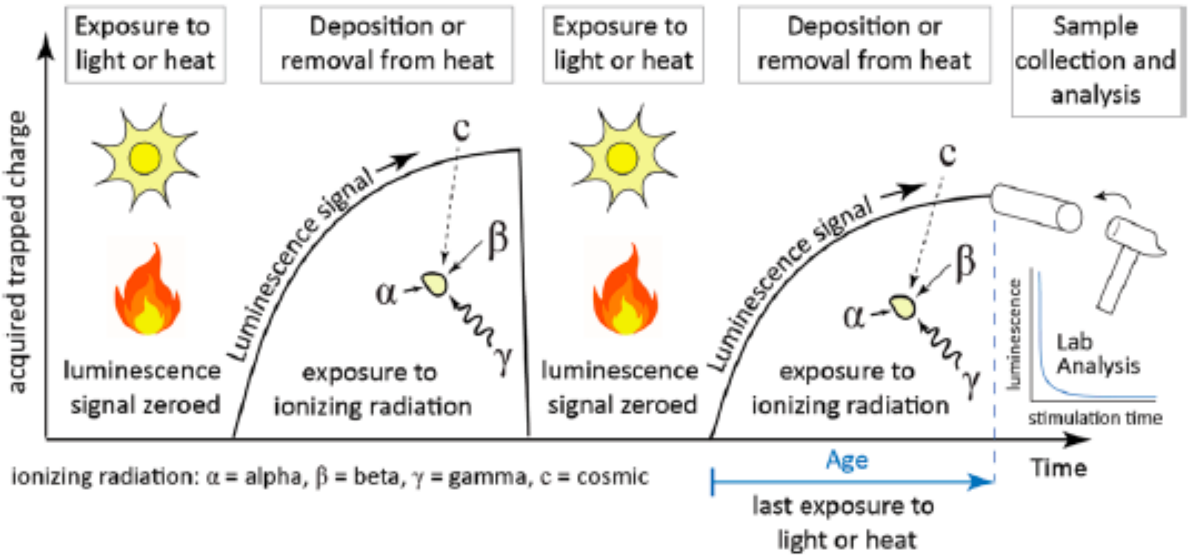

Figure 3.5: Illustration of OSL process over time. The luminescence signal is zeroed each time the sediments are exposed to light and accumulates the luminescence signal again until it is analysed in a laboratory (Adapted from Mahan *et al*., 2023).

Luminescence dating is a key method for achieving Objective 1 and has been used in conjunction with data from radiocarbon dating to establish robust chronological control. At Etosha, luminescence dating has been used to reconstruct the timing of sediment deposition at using sediments from the bounding basin ridges (e.g., Rust, 1984; Buch and Zoller, 1992; Brook *et al.,* 2007; Hipondoka *et al.,* 2014) but had not been carried out on samples from the pan floor sediments. However, the work by Buch and Zoller (1992) was conducted using thermoluminescence dating, while others (e.g., Brook *et al.,* 2007; Hipondoka *et al*., 2014) used the more advanced OSL. Reliable OSL dates from Etosha Pan underpin interpretation of other proxy data such as that from diatoms and leaf-waxes which are crucial in meeting the other objectives of this project.

3.4.2.1. OSL dating strategy

From ETO 15/1 (sand ridge one), the two available samples were dated while ETO 15/2 (sand ridge two) had seven samples collected. However, they were not all dated simultaneously. The top, middle and bottom-most samples were dated first through a quick range-finder test (Roberts *et al.*, 2009; Durcan *et al.,* 2010). If there was a difference in ages between the three samples, then the other samples in-between would also be dated in order to help understand the depositional history at that particular site. This helped to save resources (machine time and labour) and to avoid extensive dating at a site where, for example, the OSL samples measured were all contained in one sedimentary layer. Three samples from ETO 15/1 and ETO 15/2 underwent range finder tests with two aliquots of each sample reacted with quickly: 1 hour in concentrated HCl, followed by treatment in 40-minute HF and 45-minute HCl treatments (Durcan *et al.*, 2010). This was done instead of the usual chemical pre-treatment involving HCl and H_2O_2 treatments over a 2 – 4 week process. For example, in ETO 15/3 (Logan's Island) gave rough ages: the top-most sample was dateable (late Holocene), and the bottom-most sample also gave an age (early Holocene). These data provided strong basis for further analyses of the samples in-between. A similar strategy was followed for ETO 15/2 where the top-most sample yielded one Holocene age and a saturated sample at the bottom-most subsample. Further analyses of the samples between them were thus warranted.

3.4.2.2. Sample collection

OSL samples were collected in opaque tubes and transported to the Oxford Luminescence Dating Laboratory (Figure 3.6), University of Oxford where the sample preparation took place under subdued red light.

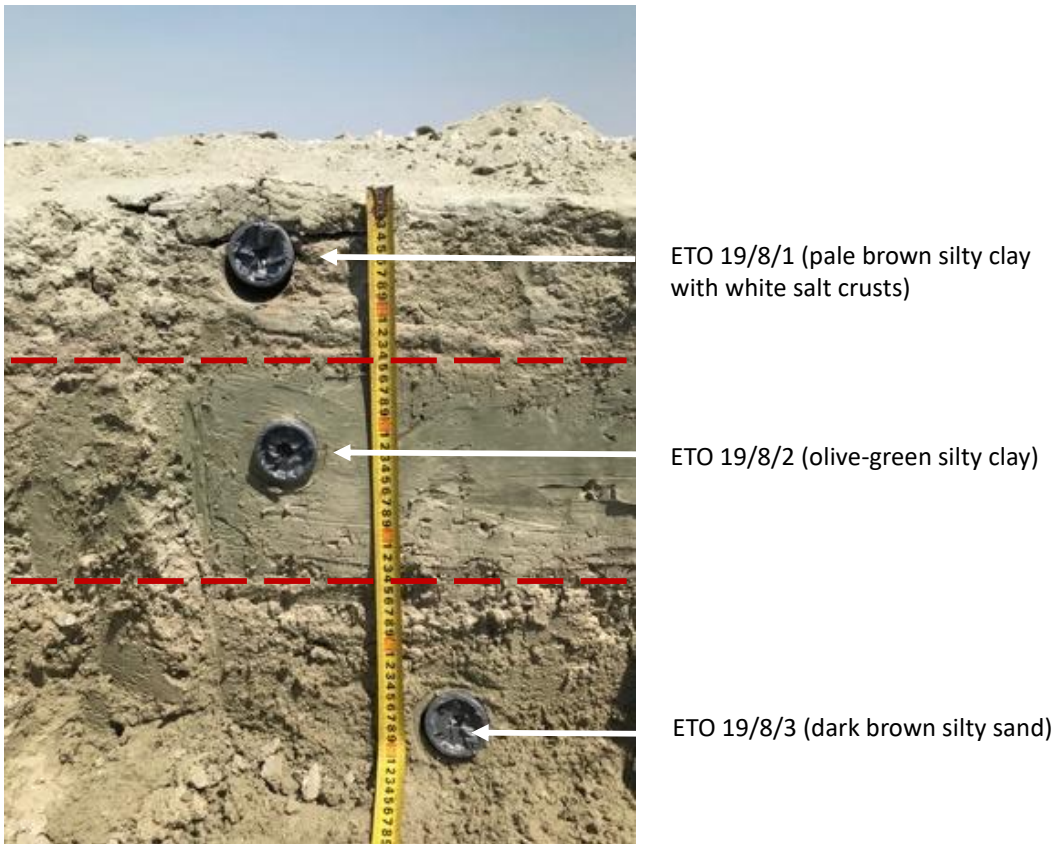

Figure 3.6: Example of an excavated lakebed sample site, ETO 19/8, showing the different sediment facies where the OSL samples were collected.

A total of 15 samples for OSL dating were collected in the field in light-tight sample tubes using a hydraulic auger on the three sand ridges during the 2015 fieldwork season. A further 15 samples were collected from four exposed sediment profiles at

sites on the lakebed in 2019. 18 of the samples were analysed for this project using laboratory procedures outlined below. The other 11 samples remained in storage. The OSL data were included geochemical data from ICP-MS (measurements of U, Th, K) for environmental dose rate calculation. The text below describes in detail the procedure followed in this study to determine the chronology based on OSL.

3.4.2.3. Chemical pre-treatment

All samples were handled within subdued orange light conditions (~ 600 nm) at the Oxford Luminescence Dating Laboratory (OLD). Samples were chemically pre-treated with 37 % HCl and 30 % H_2O_2 to remove carbonates and organic material. Sodium polytungstate was used to isolate quartz grains through density separation (<2.7 g cm^2), which were then sieved to 180 - 210 microns. The quartz grains were then etched with 40 % HF for 50 minutes to remove remaining feldspars and etch the outer alpha-irradiated quartz rind. Following this, they underwent another HCl rinse to remove any remaining soluble fluorides that may have formed during etching and were re-sieved to the original grain size range (Wintle, 1997).

3.4.2.4. Luminescence measurement

All luminescence measurements took place at the Oxford Luminescence Dating Laboratory (OLD) using four TS/OSL-DA-15 automated readers. A EMI9235QA photomultiplier tube with two 3 mm thick U-340 filters was used. Beta irradiations were carried out using $^{80}Sr/^{90}Y$ beta sources calibrated individually against known gamma-doses. Stimulation was carried out with blue light producing diodes (with a peak

emission at 470 ± 20 nm) (Wintle and Murray, 2006; Murray and Wintle, 2003). Infra-red (IR) stimulation, used to monitor feldspar contamination, was carried out at 875 nm ± 10 nm.

3.4.2.5. Equivalent dose determination

The Single Aliquot Regenerative (SAR) protocol by Murray and Wintle (2000, 2003), has become the standard method for determining the Equivalent Dose (*De*) in luminescence dating. The *Des* represents the laboratory calibrated total radiation dose equivalent to the total dose it received since burial (palaeodose), and it is a critical component in calculating the age of the sample using luminescence dating techniques, such as Optically Stimulated Luminescence (OSL) dating. The SAR protocol offers a significant advantage over previous methods by utilising the same sample for dose measurements while simultaneously providing a way to detect, track, and correct for any changes in the sample's sensitivity during the measurement process. The protocol involves several steps, as illustrated in Figure 3.7.

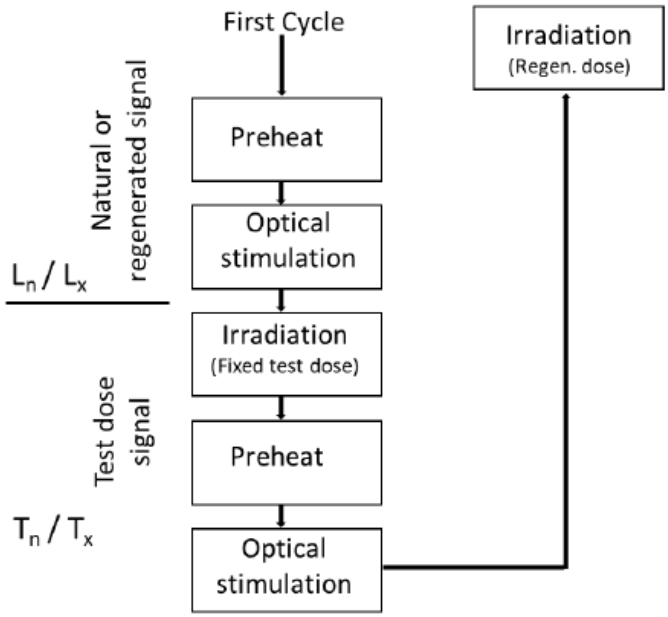

Figure 3.7: Overview of the SAR protocol of Murray and Wintle (2000)

First, the sample is pre-heated to eliminate any unstable signals from shallow, OSL traps. Then, the natural luminescence signal (Ln) is measured during stimulation with blue wavelength light. After this, the sensitivity of the sample is measured using a fixed laboratory irradiation (test dose) applied to the sample, followed by pre-heating and measurement of the test dose signal (Tn). To establish the relationship between laboratory irradiation and the luminescence signal, known as the Dose Response Curve (DRC) multiple SAR cycles were performed, each applying different laboratory regenerative doses followed by a sensitivity change measurement. The sensitivity-corrected luminescence signal (Ln/Tn) was then interpolated onto the DRC (Lx/Tx) to determine the *De.* By normalising for sensitivity changes in the sample and creating a Dose Response Curve for each subsample (aliquot) the SAR protocol has greatly enhanced the precision and accuracy of luminescence dating.

For the equivalent dose measurements, quartz grains were mounted onto 2 mm multi-grain aluminium discs using silicon spray, and the SAR Protocol described above (Murray and Wintle, 2000) was used. For analysis, the Lx/Tx data were fitted using the exponential curve on Analyst Software. Post IR-OSL tests were conducted in each SAR cycle to check for the presence of IR-response minerals such as feldspar (Duller, 2003).

3.4.2.5. Combined dose recovery and pre-heat plateau tests

Preheat plateau tests were used to optimise the accuracy of the SAR protocol during analyses. The SAR protocol involves thermal treatments that can remove charge from unstable traps in the mineral grains, consequently making the samples more sensitive to further measurements. The preheat plateau tests help to establish any dependence of the *Des* on preheat temperatures and inform the optimum temperature of the pre-heat and cut-heat measurements (Murray and Wintle, 2000). Once a suitable preheat temperature was selected, dose recovery tests were conducted to recover a known dose to assess the robustness of the SAR protocol with Etosha sediments and its ability to correct for any laboratory sensitivity change (Galbraith *et al.,* 1999; Wintle and Murray, 2006). The success of the test is in how well the measured dose replicates the given dose whereby 10 % unity in the ratio of the doses represents suitability of the SAR to determine the *Des* (Duller, 2008). As explained above, for this project, combined dose recovery and pre-heat plateau tests were conducted on one sample per site i.e., for the three samples at site ETO 19/7 on the lakebed, one test was

conducted, similar to the five samples at ETO 15/2 and others. Pre-heat tests were conducted (on both lakebed and sand ridge samples), following which a measurement temperature of 220 °C at which the sample was held for 10 seconds was deemed appropriate, with a cut-heat (hold of zero seconds) of 160 °C following the application of the test dose. The results of these tests are presented in Chapter 4 where the new ridge and lakebed chronologies are presented.

3.4.2.6. Dose rate calculations

The environmental dose rate represents the total amount of radiation absorbed by the mineral (quartz in this case) (Duller, 2008; Guérin, 2013). It is a key part of calculating the time passed since burial of sediments. It can be calculated using the equation below, whereby:

$$Dose\ rate\ (\dot{D}) = D_{\alpha} + D_{\beta} + D_{\gamma} + D_{cosmic} \qquad \text{(Equation 1)}$$

$D\alpha$ = total alpha radiation assumed to be zero as it was removed during the HF process, $D\beta$ = total beta radiation, $D\gamma$ = total gamma radiation, $Dcosmic$ = total cosmic radiation contributions to the dose rate

Light-exposed sample ends of OSL tubes were removed and used for ICP-MS analyses for dose rate calculation: ^{238}U, ^{232}Th and ^{40}K concentrations. The other portion of the light-exposed samples in the tube was reserved for grain size analysis. Dose rates were calculated using DRAC software (Dose Rate and Age Calculator for

trapped charge dating; Durcan *et al.,* 2015) and attenuated for grain size (Guérin *et al.,* 2012), water content (Aitken, 1985) and chemical etching (Bell, 1979). The factors used to calculate the cosmic dose rate on DRAC follow those of Prescott and Stefan (1982), taking into account the altitude and geomagnetic latitude of the samples.

3.4.2.7. OSL age calculation

OSL dating can provide improved chronology in areas where most other tools such as radiocarbon dating have limitations e.g., radiocarbon dates are generally limited by the half-life of ^{14}C to ages younger than 45 ka. OSL, on the other hand, can be used to date older sediments but are often less precise. Within OSL dating, multiple *Des* measurements are generated for each sample. To obtain a representative *Des* from the sample, a number of considerations are taken into account to inform the age model used to calculate a final *Des* used in the age Equation 1. The commonly used age models are the central age model (CAM), Minimum age model (MAM) and the finite mixture model (FMM).

The Central Age Model (CAM, Galbraith *et al.,* 2005) is a statistical approach used in OSL age-modelling that accounts for the variability in *Des* measurements and is used where samples are assumed to be well-bleached. The model is usually applied to a log-transformed distribution. CAM yields two measurements – the central dose which is the geometric mean of the *Des* distribution, and overdispersion, which quantifies the amount of spread in the *Des* that remains after measurement uncertainties are taken into account. The Minimum Age Model (MAM) (Galbraith and Laslett, 1993) is typically

used where sediments are suspected to have received insufficient light exposure to reset the luminescence signals in all grains prior to final deposition. It implies that the age derived from the youngest population of samples represents the true age of the of the sample. Lastly, the Finite Mixture Model (FMM; Galbraith and Green, 1990) assumes that there are discrete groups of *Des* populations in the samples related to separate deposition events that have subsequently been mixed. Each *Des* population is further assumed to have its own normal distribution, and the choice of the model should be guided by knowledge of the sedimentary environment and deposition elements (Jacobs *et al.,* 2006).

The central age model (CAM) has been applied to all samples in this study because the population of *Des* were not highly skewed and there was no evidence from the stratigraphic sections of sedimentary mixing. Examples of the distributions of these are presented as Abanico plots in Chapter 4 (Figure 4.4). To calculate minimum ages on the saturated samples, the (CAM) was used on unsaturated *De's* – this by definition biases the estimate towards an erroneously young age but provides a useful lower limit for the sample (Table 4.2)

3.5. Conclusion

This chapter has outlined the materials used and multiple methods followed in this project. Multi-proxy data collection enables detailed research with a corroboration of results from the different proxies to strengthen research. The chapter has provided reasons for choosing the specific sampling sites, described methods followed for

laboratory work and outlined steps followed to establish a robust chronology using radiocarbon and OSL dating.

Chapter 4:

Geomorphic evidence of Etosha Pan's late Quaternary evolution and depositional context of the marginal sand ridges

4.1. Introduction

This Chapter provides a chronology and interpretation of the landforms and sediments found at the western basin margin of Etosha Pan. It outlines new data from basin floor and ridge sediments to investigate 1) the chronology of Etosha basin development in the late Quaternary and 2) the timing and nature of ridge formation, geomorphology of Logan's Island and their palaeoenvironmental context. This was conducted to establish the geomorphological evolution of the landscape through an investigation of landforms and basin floor development.

One of the aims of this thesis is to establish a multi-proxy palaeoenvironmental reconstruction on the north-western side of Etosha Pan. The southern and eastern parts of the pan where flooding occurs today accumulates sediments from the rivers in the north including the Ekuma Delta. However, during the late Quaternary, Hipondoka *et al.* (2004) found that the Ekuma Delta was the main source of sediments in the west of the basin based on particle size data. In the current chapter, new data is presented that assists in building a more complete understanding of the late Quaternary evolution of the pan. Palaeoenvironmental inferences are made across two landforms: the lakebed itself and the sand ridges parallel to the modern-day pan, using OSL dating as an underpinning chronological framework. The dominant north-easterly wind that facilitates sediment transport across the pan also leads to sediment accumulation on the western end of the pan either directly through aeolian processes or indirectly by wave action (Hipondoka *et al.*, 2004).

To establish a robust dataset, several steps were taken to ensure quality control for the OSL dating as outlined in Chapter 3 (*Methods*). Single aliquot regenerative dose cycling (SAR) was used to establish equivalent doses, while ICP-MS provided data for dose rate calculations. Dating methods at Etosha have evolved over several decades of research. The chronological data comes from various techniques, with some older methods having been replaced by more accurate and precise modern approaches. This includes eight dates that were calculated using thermoluminescence dating (Buch and Zoller, 1992) which is associated with less precise ages. Due to limits on available sampling techniques, several studies were only able to sample the upper 250 cm on the sand ridges which may have biased these datasets to the Holocene (Brook *et al.*, 2007; Hipondoka *et al.*, 2014). These factors have previously limited understanding of the geomorphological evolution of the pan. However, with both instrumental and methodological advances in OSL, it is possible to date a larger number of samples, from a greater depth with more precision. This was the primary goal for this study. The present study allows for a more temporally extended assessment of the pan's sediment accumulation and mobility history in the context of fluvial and aeolian processes that operate on the pan over the long term. Therefore, this chapter provides results for the new chronological understanding of Etosha Pan evolution and palaeoenvironmental context based on 11 absolute ages attained through OSL dating.

4.2. Ridge and basin floor chronology

The OSL dating results (Table 4.1) ranged in age from 0.59 to 40.05 ka, with age uncertainties between 0.04 and 2.72 ka. These dates maintained chrono-stratigraphic order throughout both the lake basin and ridge sequences. The ridges have preserved

multiple phases of accumulation from 1 to 40 ka (Figure 4.1). The depositional ages from ETO 15/1 were sampled within the first metre from the surface, making them the shallowest ages on all ridges.

ETO 15/2 is the oldest ridge, with ages ranging between 40.05 ± 2.72 ka (Phase A) and 8.45 ± 0.64 ka (Phase E). Auguring was stopped after the first metre because a hard calcrete layer was encountered. The multi-grain quartz signals for the three bottom-most samples yielded saturated ages with 42 % of measured *Des*> 2D0, at which point the OSL signal no longer provides a reliable measure of the absorbed dose but nevertheless suggesting sediments were deposited during the Pleistocene (Table 4.2). ETO 15/3 from Logan's Island is the youngest of the ridges, dating mostly to the Holocene. The top-most luminescence age from ETO 15/1/1 (8.69 ± 0.2 ka) (Phase E) corresponds with that of ETO 15/2/1 (8.45 ± 0.64 ka) (Phase E) within errors, suggesting that the geomorphological activity was recorded by both ridges which are located further away from the modern-day shoreline.

Table 4.1: Chronology – OSL Results of samples with finite ages from this study (excluding saturated samples). CAM = Central Age Model.

Sample ID	Depth (m) (± 5%)	% K (±10%)	Th (ppm) (±10%)	U (ppm) (±10%)	Total Dose Rate (Gy/ka)	No. of Aliquots (Accepted/Total)	Dose Recovery	De (Gy)	Overdispersion (%)	**CAM Age (ka)**
ETO 15/1/1	0.5	0.638	3.351	0.019	1.043 ± 0.055	39/55		9.06 ± 0.71	49.02 ± 0.9	**8.69 ± 0.82**
ETO 15/1/2	1	0.551	2.804	0.034	0.935 ± 0.047	34/40	0.960 ± 0.04	17.29 ± 1.09	36.5 ± 0.77	**18.50 ± 1.49**
ETO 15/2/1	1	1.153	5.125	0.208	1.964 ± 0.096	38/42	0.935 ± 0.04	16.6 ± 1.0	35.26 ± 0.66	**8.45 ± 0.64**
ETO 15/2/2	1.2	0.579	4.525	0.181	1.36 ± 0.059	24/24		54.5 ± 2.8	24.56 ± 0.79	**40.05 ± 2.72**
ETO 15/3/1	0.3	1.225	7.29	0.365	2.530 ± 0.115	27/48	0.910 ± 0.05	5.09 ± 0.25	25.38 ± 0.67	**2.53 ± 0.115**
ETO 15/3/4	3	1.341	4.839	0.344	2.530 ± 0.115	25/36		12.8 ± 0.5	19.91 ± 0.58	**5.44 ± 0.35**
ETO 15/3/5	4	1.608	3.037	0.250	2.345 ± 0.28	27/48		14.0 ± 0.7	18.54 ± 4.23	**5.94 ± 0.76**
ETO 15/3/6	5	1.608	3.037	0.250	2.244	36/52		28.9 ± 2.3	47.52 ± 0.94	**12.86 ± 1.25**
ETO 19/5/1	0.08	1.147	12.253	2.188	2.51	19/23	0.967 ± 0.035	1.5 ± 0.10	24.68 ± 0.95	**0.59 ± 0.04**
ETO 19/5/2	0.26	1.798	5.983	1.409	2.501	30/46		56.5 ± 2.5	23.51 ± 0.58	**22.59 ± 1.59**
ETO 19/7/1	0.39	1.509	6.824	4.240	2.861	12/12	0.960 ± 0.04	68.7 ± 2.0	15.25 ± 0.41	**24.01 ± 1.34**

Table 4.7: Minimum ages of saturated samples from Etosha lakebed and sand ridges from the present study

Sample ID	Depth (m) (±5%)	% K (±10%)	Th (ppm) (±10%)	U (ppm) (±10%)	Total Dose Rate (Gy/ka)	Average 2D0 (Gy)	Environmental Dose Rate (Gy/ka)	Minimum Age (ka)
ETO 15/2/3	1.9	0.777	3.5	0.226	1.547	100.63 ± 1.574	1.547 ± 0.072	65.05 ± 3.19
ETO 15/2/5	3	0.699	4.74	0.384	1.855	97.64 ± 1.523	1.855 ± 0.083	52.64 ± 2.49
ETO 15/2/6	4	0.555	4.89	0.326	1.601	95.04 ± 1.488	1.601 ± 0.071	59.36 ± 2.79
ETO 19/7/3	0.88	0.206	1.241	0.544	0.578	112.99 ± 2.303	0.578 ± 0.028	195.48 ± 10.27
ETO 19/8/1	0.4	1.228	6.254	2.725	2.268	98.84 ± 1.499	2.268 ± 0.107	43.58 ± 2.16
ETO 19/8/2	0.64	0.687	5.048	2.573	1.665	100.71 ± 1.878	1.665 ± 0.073	60.49 ± 2.88
ETO 19/8/3	0.75	1.696	5.768	1.393	2.349	118.82 ± 2.437	2.349 ± 0.13	50.58 ± 2.99

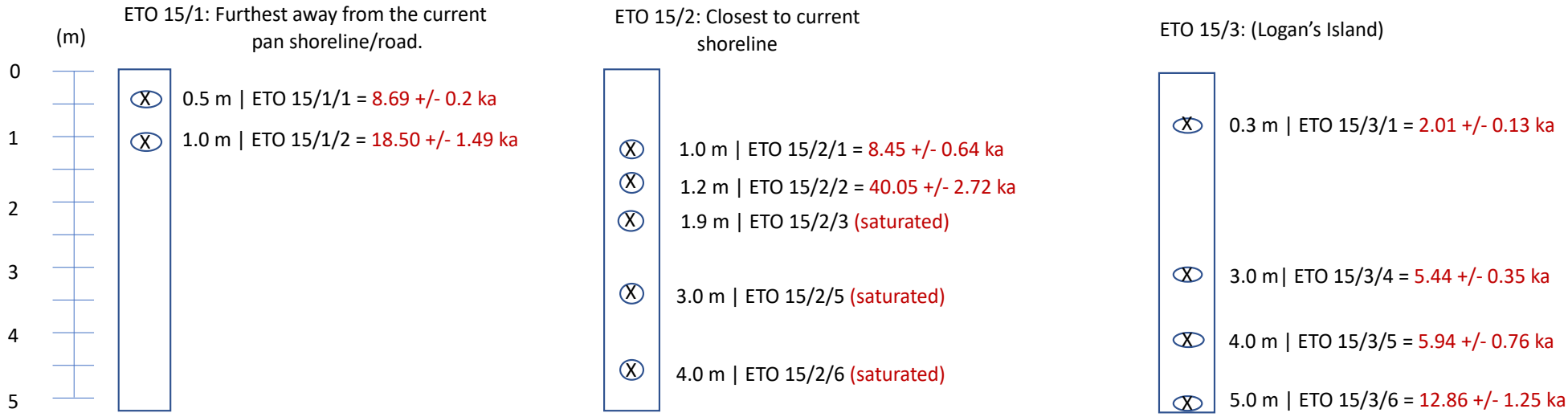

Figure 4.1: OSL data from subsamples collected using a hydraulic auger from three **sand ridges** namely: ETO 15/1, ETO 15/2, and ETO 15/3. Sand ridge ages (also known as 'lunette dunes' or 'shorelines' in other studies) range between 2.01 ± 0.13 ka to 40.05 ± 2.72 ka. OSL age data from sand ridges 1 to 3, with depths below the surface in metres. "ka" = thousand years before present/modern day. The ± values are the related uncertainties for each date. "saturated" means that the sample age was beyond the reliable range of quartz OSL dating.

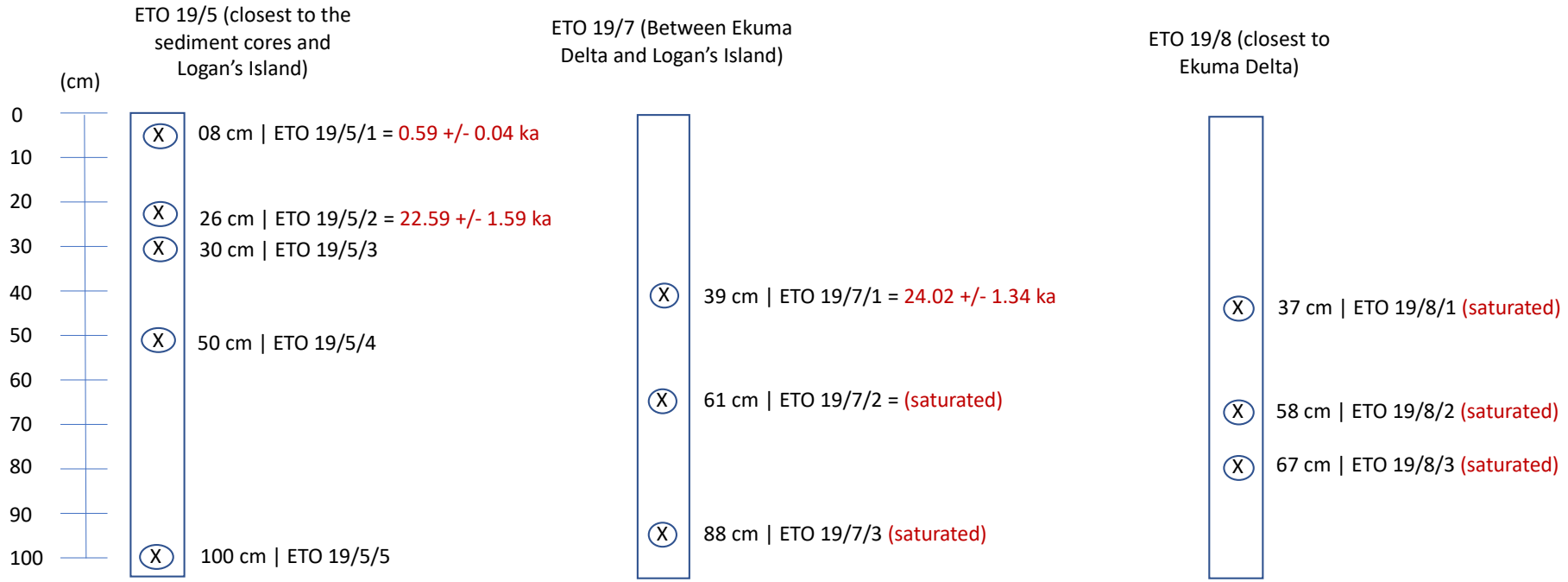

Figure 4.2: OSL ages of **lakebed** samples (pits) from Etosha from this study. Ages span from 0.59 ± 0.04 ka to 24.02 ± 1.34 ka and represent samples from 3 field sites, ETO 19/5, ETO 19/7 and ETO 19/8

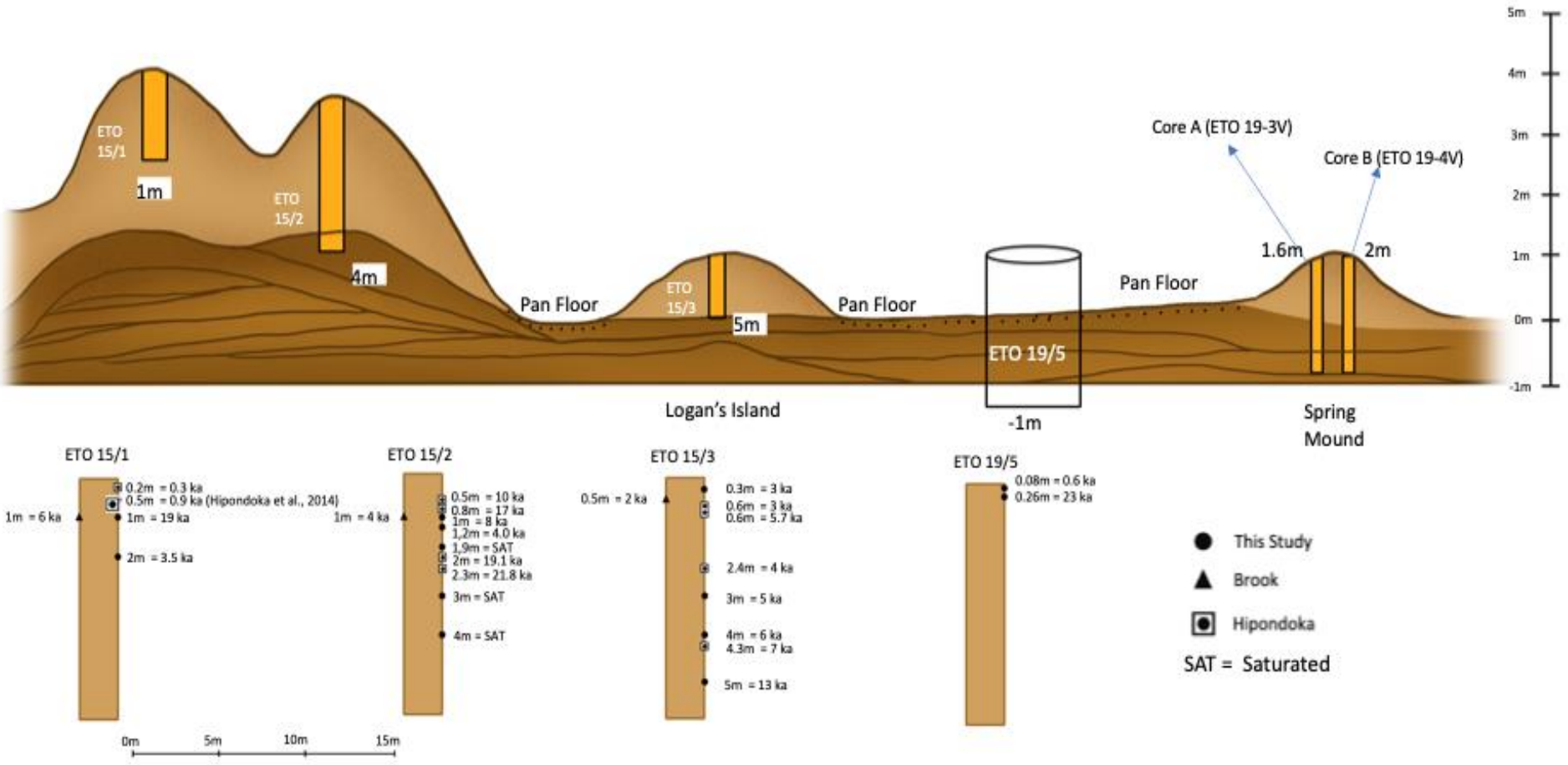

Figure 4.3: Cross-section of the north-western part of Etosha Pan showing sampled sites on the sand ridges, Logan's Island, ETO 19/5 and spring mound. OSL results are shown in brown bars comparing data from Brook *et al.* (2007), Hipondoka *et al.* (2014) and this study. Spring mound ages are presented in Chapter 5.

Depositional ages from the lakebed are varied, spanning 0.59 ± 0.4 ka at 8 cm depth in sampling site ETO 19/5, which is the youngest age in the dataset, to 24.02 ± 1.34 ka at 39 cm depth in sample ETO 19/7/1 (Figure 4.2). All samples from ETO 19/8 are saturated, similar to the two bottom-most samples in ETO 19/7 (Table 4.2 and Figure 4.3). The sorting of grain size in subsamples from the lakebed varies between poorly sorted and extremely poorly sorted, with ETO 19/8/2 containing the largest particle size (457 microns); which is very high compared to the mean grain size of ETO 19/5/2 of 103 microns and is dominated by extremely poorly sorted sandy clay (Table 4.3).

The Central Age Model (CAM) was selected because, in most of the samples, the logged *De*s display a tight cluster around a central value, which takes the form of a normal distribution (Figure 4.4 C). The central age model (Galbraith *et al.,* 1999) assumes the distribution of log *Des* values is normal and consistent with a range of values within a standard deviation (overdispersion) greater than that accounted for by measurement uncertainties. Dose recovery tests were conducted on one sample from each sampling location and showed good concordance, with all recovered *De's* falling within 10 % of laboratory administered doses (Figure 4.4). Overdispersion values (the degree of variation between logged *De's* beyond the measurement variation observed in dose recovery tests) are relatively high, ranging between 15 and 49 %. Although the Ekuma River has low-relief river discharge, seasonal flooding episodes can contribute to the rapid deposition of sediment. Another explanation is that clay cracking enables some sand grain movement during dry periods and that these grains can penetrate deeper sections when the pan is desiccated.

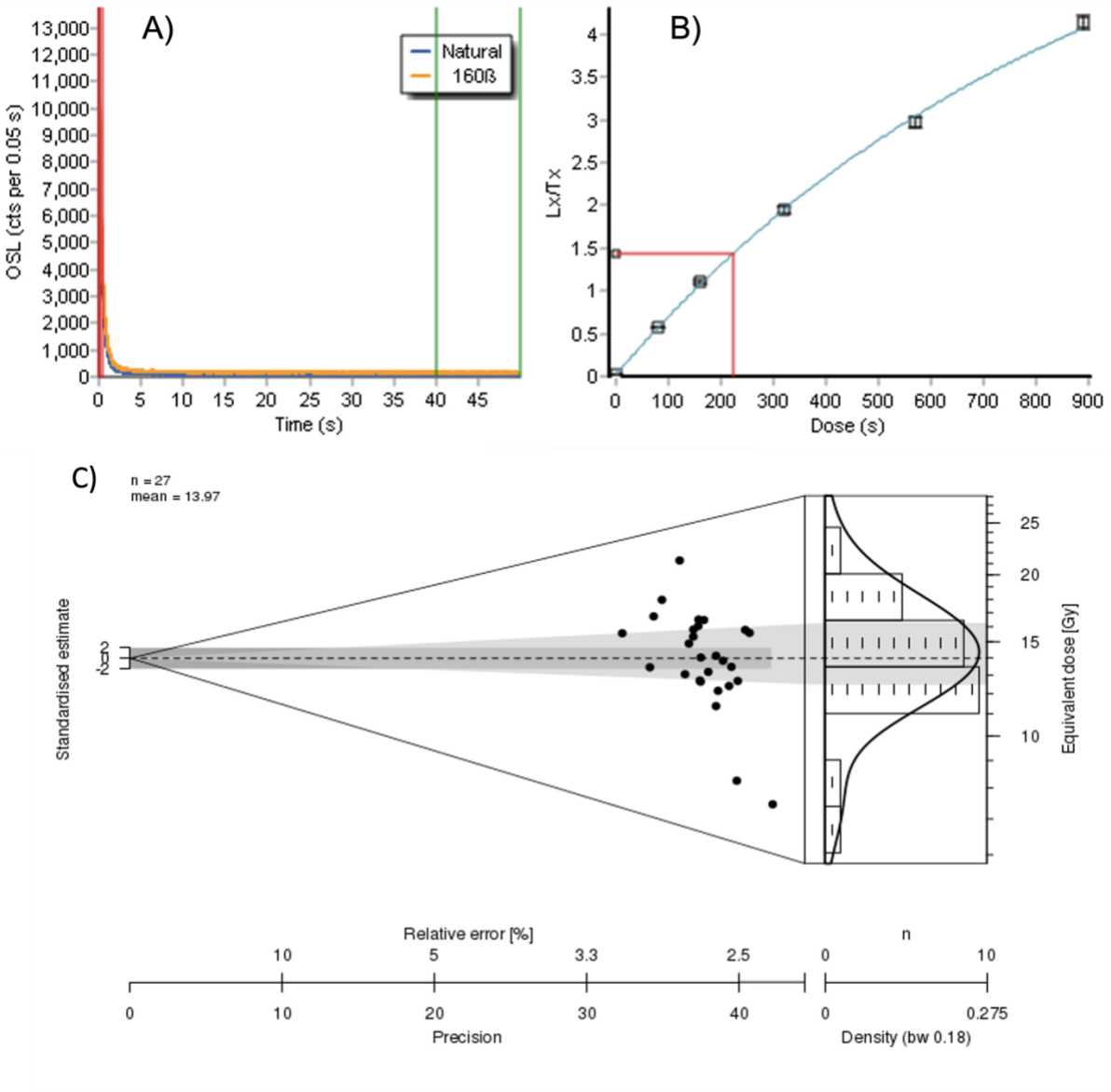

Figure 4.4: Dose response curve and aliquot regeneration data for ETO 19/3/5. (A) OSL signal decay with stimulation time showing >90 % of OSL reduction in OSL within the first four seconds. (B) OSL regenerative growth curve with laboratory-induced doses. Lx / Tx is the test dose-corrected ratio of the OSL signal. (C) Frequency distribution of Des measured on 27 aliquots.

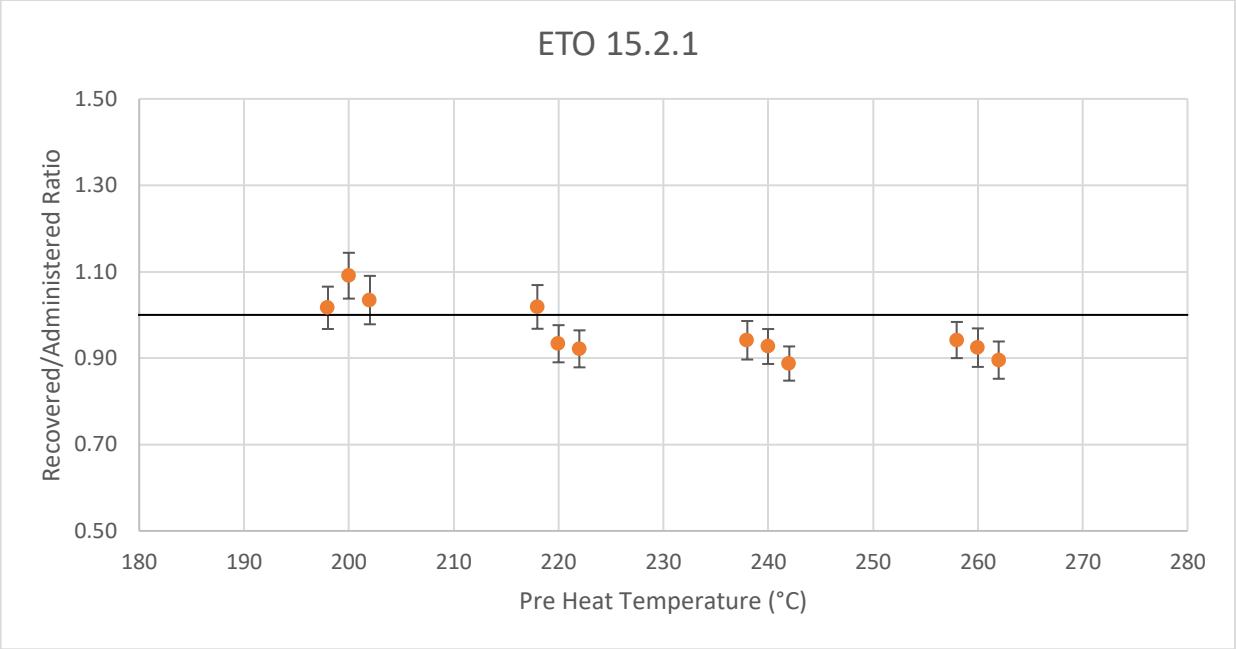

Figure 4.5: Preheat temperature test for sample ETO15/2/1 presented as a ratio of recovered to administered laboratory dose.

These results from the pre-heat temperature tests suggest that there is a slight but insignificant dependence on preheat temperature. Based on these experiments, a pre-heat temperature of 220 °C was used in this study. In addition, the recovery of administered doses lies principally within 10 % uncertainty suggesting the SAR protocol is effective in recovering laboratory doses (Figure 4.5).

Table 4.8: Grain size data for samples that underwent particle size analysis. Sand ridge sample grain size (from the 2015 field work) data were not available.

OSL Sample Name and Depth	Sample Type	Textural Group	Sediment type	Mean grain size (microns)	Mode 1 (microns)	Mode 2 (microns)
ETO 19/5/1 (8 cm)	Bimodal, Very Poorly Sorted	Clayey Sand	Fine Silty Fine Sand	132.2	150.2	4.75
ETO 19/5/2 (26 cm)	Polymodal, Extremely Poorly Sorted	Sandy Clay	Fine Sandy Clay	102.8	5.33	0.212
ETO 19/7/1 (39 cm)	Polymodal, Extremely Poorly Sorted	Sandy Clay	Very Fine Sandy Clay	180.6	59.81	7.53
ETO 19/7/3 (88 cm)	Unimodal, Poorly Sorted	Sand	Poorly Sorted Medium Sand	384.9	423.4	N/A
ETO 19/8/1 (37 cm)	Trimodal, Very Poorly Sorted	Clayey Sand	Fine Silty Medium Sand	237.7	377.4	5.98

ETO 19/8/2 (58 cm)	Unimodal, Poorly Sorted	Clayey Sand	Coarse Silty Medium Sand	456.9	423.4	N/A
ETO 19/8/3 (67 cm)	Trimodal, Extremely Poorly Sorted	Clayey Sand	Clayey Medium Sand	280.3	377.4	0.24

4.3. Sediment accumulation records in the total OSL dataset

Studies have been conducted to determine the geomorphic evolution of the Etosha Pan during the late Quaternary by Buch and Zoller (1992), Rust (1984), Buch and Rose (1996), Hipondoka *et al.* (2004), Brook *et al.* (2007) and Hipondoka *et al.* (2014). However, those studies were based on data from the basin margin sand. Sediment samples from this study capture additional episodes of deposition to at least 40 ka (Table 4.4), uniquely including samples from the Etosha pan floor, and therefore extending the dated range of existing geoarchives.

Table 4.9: Phases of deposition labelled from A-G where A is the oldest geomorphological unit and was likely deposited first among these samples. Seven sub-groups were found within the dataset determined through hierarchical cluster analysis. Cluster analysis is a frequently utilized tool in chronological studies to help interpret temporal pattens of deposition within discontinuous sediment deposition (e.g., Burrough *et al.*, 2007; 2009, Walsh *et al.*, 2021; Burrough *et al.*, 2022; Woor *et al.*, 2023). Most ages are within error margins and were used to make interpretations from these data (A-G).

Phase of deposition	CAM Age (ka)	Sample ID	Location
G	• 0.59 ± 0.76 • 2.01 ± 0.13	• ETO 19/5/1 • ETO 15/3/1	• Pan floor • Sand ridge
F	• 5.44 ± 0.35 • 5.94 ± 0.76	• ETO 15/3/4 • ETO 15/3/5	• Sand ridge • Sand ridge
E	• 8.45 ± 0.64 • 8.69 ± 0.2	• ETO 15/2/1 • ETO 15/1/1	• Sand ridge • Sand ridge
D	• 12.86 ± 1.25	• ETO 15/3/6	• Sand ridge
C	• 18.5 ± 2.72	• ETO 15/1/2	• Sand ridge
B	• 22.59 ± 1.59 • 24.02 ± 1.34	• ETO 19/5/2 • ETO 19/7/1	• Pan floor • Pan floor
A	• 40.05 ± 2.72	• ETO 15/2/2	• Sand ridge

The total dataset of the sampled sites ranges from 40 ± 2.72 ka (A) to 0.59 ± 0.04 ka (G) (Table 4.4). According to these data, the pan has recorded multiple phases of sediment accumulation at different times both on the lakebed and sand ridges. Phase A of deposition occurred on ETO 15/2/2 (sand ridge 2) with an age of 40.05 ± 2.72 ka at a depth of 1.2 m and is the oldest unit. Most of the deeper samples on the basin floor are saturated (ETO 19/7/2, ETO 19/7/3, ETO 19/8/1, ETO 19/8/2, ETO 19/8/3) (Table 4.2). This implies that either the samples saturate at c 40 ka, or that sediments

are missing due to, for example, deflation. Another possibility is that the 40 ka sediments rest on a much older surface that could, according to Miller *et al.* (2010), be Miocene. According to Buch (1996), deflationary processes begin to erode and lower the pan floor as environmental conditions change towards a drier climate or increased wind activity. The lowering of the pan floor leaves behind the former pan surface as a littoral surface with multiple littoral terraces at different elevations, each representing a former pan floor level.

The particle sizes of these saturated samples characterise them as poorly sorted sand, with the largest grain sizes on the record (Table 4.3). Sediments on the lakebed contain a large composition of silt and clay and feature some sandy layers below the current pan floor (Table 4.3). There are geomorphological processes that could have likely winnowed out the sediments before they got deposited on the north-western part of the pan and the ridges. This is evident in the improvement in sorting from Site 8 (at the river mouth) to Site 5 which is near the periphery. Site 5 though, being located near the spring, could have acted as a 'sediment trap' at different times in the past and therefore protected sediments from erosion and led to better sorting.

4.3.1. Lakebed since the Late Glacial Maximum (LGM)

The ages from ETO 19/7/1 (24.02 ± 1.34 ka) and ETO 19/5/2 (22.59 ± 1.59 ka) suggest that the north-western part of the basin was a hydrologically active system at least periodically able to sustain a lake body between 24 and 23 ka (Phase B). Some areas, particularly in the northern and eastern parts of Namibia (Gasse *et al.*, 2008), may have

experienced slightly wetter conditions than present compared to the western and southern regions. Moreover, with a record spanning the last 40 ka, Schuller *et al.* (2018) interpreted higher sedimentation and changes in geochemical proxies from 4 different salt pans in Namibia be indicative of wetter conditions and stronger winds during the LGM (23 - 19 ka) than today. This suggests that the wet period persisted possibly between 24 – 23 ka and 22 - 18 ka, spanning the entire LGM. Although the ages from the Etosha basin floor in this study are in good chronostratigraphic order, the record of sediment accumulation is discontinuous which could be caused by erosion from aeolian processes when the pan is dry. Additionally, sediments deeper than ETO 19/5/2 (26 cm) (on the lakebed) are saturated. This could support the hypothesis that the pan is very old and is an erosional landform with 50 m of clayey sediments below the current pan-floor (Stuart-Williams, 1992; Miller, 2010). These ages, however, show that although the pan have originated in the Miocene, it has sustained various lacustrine phases in the late Quaternary with erosion from wet and dry episodes. Etosha is known to be a key site for deflation in modern-day, with dust plumes sourced from the pan potentially reaching the Atlantic Ocean (Washington *et al.*, 2003). Where there is evidence of net sediment accumulation rather than sediment loss, it would suggest a radically different hydrological state than in modern day, presumably one which sustained a permanent or semi-permanent body of water. Therefore, Etosha has likely been an active lake system during the LGM, and this contrasts the hypothesis that it has had limited hydrological activity since the Miocene (e.g., Miller, 2010).

Further away from the spring, sample sites ETO19/7 and ETO 19/8, that become saturated from 86 cm at ETO 19/7/3, are close to the river delta with ages of 24.02 ± 1.34 ka at 39 cm. ETO 19/7/3 however reflects fundamentally different depositional conditions. It is pure sand with a modal grain size of 423.4 microns and traces of clay (4.2 %) (Table 4.3). ETO 19/7/3 has a mean grain size of 384.9 microns and is extremely poorly sorted. The period documented at 39 cm (ETO 19/7/1) (24.02 ± 1.34 ka) predates the LGM within errors and is the second-oldest date on the ridges.

The absence of ages does not necessarily preclude the deposition of sediments during earlier lake periods as erosion and deflation may have occurred. When conditions become wetter after a dry period, there is a greater amount of available sediment in the landscape so that transitions from dry to wet can be characterised by high, poorly sorted sediment loads. It is also at these times of transition that river systems tend to experience more flash floods (Walsh *et al.*, 2022). These two factors could explain the nature and timing of samples from ETO 19/7 as a fluvial deposit located near the mouth of a river system. Belz *et al.* (2020) identified a trend towards aridity during the Last Glacial Maximum which they stipulated to have occurred between 25 - 18 ka at Omongwa Pan in Namibia. The period was found to be characterized by increased sand content and reduced organic matter. This was attributed to various climate forcing mechanisms, including variations in solar insolation as well as the southward movement and increasing strength of the African tropical rain belt (Belz *et al.*, 2020).

Phase E of sediment deposition occurred between 8.45 ± 0.64 ka and 8.69 ± 0.2 ka. It seems to have affected Logan's Island (ETO 15/3), potentially because the wet area shrunk in extent and left the sediments of Ridge 3 exposed to both wind and water erosion. This helps to contextualise the geomorphological history of Logan's Island by asserting that, at least in the early Holocene, it was an active site of geomorphological processes.

Sample site ETO 19/8 is located 1 km east of the Ekuma Delta and all its samples are saturated. There is a marked increase in grain size within the lakebed samples as they get deeper and saturate. The mean grain size from the three samples in ETO 19/8 ranges between 237.7 to 456.9 microns and they are characterised as trimodal or unimodal clayey sand (Table 4.3). Moreover, the grain size data from ETO 19/8 varies from extremely poorly sorted to poorly sorted. At Etosha, poorly sorted sand at the river mouth is often associated with rapid flooding that could result from increased river discharge from the catchment (Hipondoka *et al.*, 2004). Increased precipitation could be influenced by an abrupt change in rainfall due to attenuation of a climate signal, or geomorphological changes upstream in southern Angola where the Cuvelai-Etosha Basin emerges. In addition, the Ekuma River mouth could act as a zone of sediment accumulation and/or removal which could at times result in the erosion of any younger sediments that could have been deposited during pan inundation or changes in aeolian processes. Sediment accumulation at the Ekuma would primarily be driven by the tributary rivers during times of extended rainfall or through aeolian processes depositing sediments with larger grain sizes. Alternatively, the site could be a Miocene

relict that continues to be exposed by erosion – it cannot be confirmed by these data due to the saturated samples.

4.3.2. Sand ridges and Logan's Island chronology

There is a debate about the formation of Logan's Island (where Ridge 3 is located), regarding whether it is a lunette or a strandline feature (Hipondoka *et al.*, 2014; Miller *et al.*, 2010). The data from the present study suggest that Ridge 3 (ETO 15/3), the innermost ridge, has a different sediment accumulation regime from the other two ridges. Ridge 3 is primarily a Holocene feature, evidenced by the upper 5 m of sediment accumulating since 12.86 ± 1.25 ka (ETO 15/3/6) (Phase D). As it is not on the extreme periphery, it would be influenced or shaped by the different pan-wide lake phases or increased aridity in the past. This young landform is evidence that Etosha has not remained as a uniform geomorphological unit since the Miocene. The data suggests that sediments have accumulated over different deposition periods. Ridge 3 was formed distinctly in the Holocene and may have been formed during times when the lake extent was smaller and shallower – shallow enough for the landform to have been on the edge, experience sediment aggradation and forming a shoreline. Ridge 1's accumulation history suggests two main periods of sediment deposition and mobility. In Phase C (ETO 15/1/2) (18.5 ± 2.72 ka), post LGM geomorphological activity is noted, isolating the first ridge and suggesting that it was breached during a period of high lake levels or increased regional moisture. An alternative explanation could be that, during phase C, the pan experienced stronger aeolian processes that eroded a part of ridge 1, exposing samples that were buried during the LGM.

Data from Hipondoka *et al.* (2014) with OSL ages of 3.1, 4.0 and 7.2 ka interpreted to indicate wet phases at Logan's Island add weight to these findings. Therefore, during higher lake phases, Logan's Island would be a small island or under water (depending on the depth of the water) and experiencing sediment mobilisation due to the hydrological changes. Furthermore, Brook *et al.* (2007) conducted their study on the pan's 'shorelines' and suggested that there were higher lake levels for Logan's Island during the period from 2.5 to 1.7 ka. Their findings, along with those from this study, suggest that the Holocene epoch at Etosha did not have stable lake conditions. Instead, it was dynamic site with fluctuating lake levels that likely exposed and redeposited sediments on the landforms.

Burrough *et al.* (2009) suggested that ridges in these types of environments should not be analysed as singular landforms, but as composites built from both wave-driven water action and aeolian processes which move lacustrine sediments into and within the shore zone. Therefore, in this study, the ridges are interpreted as a unitary dataset. Sediments accumulated of the edge of the pan as indicated by samples at ETO 15/1/1. The site recorded a hard calcrete 'blanket' starting at 1 m depth from the surface. This layer could be a 'lip' or extension of the old pan-floor below the large volume of sand on the ridges, that protrudes at the far-most ridge of the pan and is thus potentially saturated below that layer. Indeed, Hipondoka *et al.* (2004) found that massive concreted and nodular calcrete occurred at or near the surface towards the southern end of the sand ridges. This suggests that the southern part of the sand ridge system

has undergone significant carbonate cementation where pH fluctuations caused the precipitation of minerals. Calcrete was also encountered at a depth of 1.2 m on the outer dune profile at the 20 km transect (Ridge 1 or ETO 15/1 in this project) (Hipondoka *et al.* 2004). Another calcrete layer was encountered during coring at the spring mound in this study near site ETO 19/5. Coring was terminated at both core ends with one having a maximum of 2 m and the other at 1.6. m depth. This indicates that carbonate cementation is not limited to the surface and can occur at depth below the pan floor or could also be the result of a former water table. Netterberg (1978) suggested that, according to ^{14}C dating on calcretes, that the pan is older than 33 ka. However, to better constrain the age of the calcretes and the surface palaeosol, it has been of great value to use alternative dating techniques such as OSL dating combined with radiocarbon dating of organic material in the sediment cores and eggshells.

4.3.3. The role of the Kunene River in shaping Etosha's landscape evolution

As outlined in Chapter 2 (*Literature Review*), almost a century ago Wellington (1938) hypothesized that the Kunene River once flowed into the Etosha basin. Rust (1985) argued against the contribution of the Kunene River to Etosha's development i.e., the Kunene River had no connection to the Owambo basin where Etosha Pan is located. Their study highlighted that scarp retreat or pan edge retreat occurred under periodic phases of erosion. This idea infers that some aridity is required to build the sand ridges. In addition, the location of the ridges on the north-western edge of the pan and their relatively high relief (> 5 m above sea level) puts them directly in line with the north-easterly winds that blow across Etosha and potentially deposit wind-blown sediments

on the margins of the pan (Brook *et al.*, 2007). Wellington (1938) opposed Jaeger's (1926) proposition of Etosha being water-formed. They argued that because the margins are not continuous around the pan, and because aeolian processes are dominant in the area and form an essential part of the pan evolution, the terraces must be wind-formed and not remnants of a former lake (Wellington, 1938). The data in this Chapter suggest that water has played a major role in sustaining wet phases at the Etosha Pan, particularly during the LGM. However, these data can neither confirm nor reject the role of the Kunene in depriving the pan of essential fluvially sourced sediments or water that led to the demise of 'palaeolake' Etosha at 35 ka (Stuart-Williams, 1992; Hipondoka, 2005). This is due to the sampling being limited to the pan sediments and not upstream in the rivers flowing southward into the pan.

4.4. Conclusion

Overall, this study indicates that the Etosha basin has been a site of geomorphic dynamism over a long period, adding weight to the hypothesis that the pan had fluctuating hydrological activity during the Quaternary. There are numerous sediment samples with saturated OSL signals that date beyond 40 ka on the ridges and 23 ka on the lakebed. Large basin-filling events (seen through dated sediments on the marginal ridges) and increased river inflows into the basin evidenced by data from the north-western portion of the lakebed, operated in concert to sustain a long-term wet phase at Etosha Pan during the LGM (23 – 19 ka). There is evidence suggesting that sediment activation occurred during the earlier period of 24 to 22 ka. However, it is unclear from these data whether the period afterwards remained arid at the time, or

that the pan lost sediments from erosion by water action and therefore indicative of wet phases. Post LGM, only one OSL date is available from the sand ridges (ETO 15/3/6 = 12.86 ± 1.25 ka). This suggests that there was repeated aeolian deflation or extended erosion which prevented preservation of the sediment accrual (if any) during that period prior to the Holocene. Evidence from ETO 15/3 provides grounds for reconstructing Holocene geomorphological changes on the pan, which suggests extended hydrological and processes. In conclusion, this study has investigated lakebed sediments, which, for the first time have been dated to this depth and produced data suggesting that Etosha has not remained as an arid/erosional landform since the Miocene with no hydrological activity. It has an old clayey silted bedform, with intervening layers of poorly sorted sand due to sustaining wetter palaeoenvironmental changes during the LGM.

Chapter 5:

Palaeoecological insights from Etosha Pan

5.1. Introduction

Palaeoecological proxies are sensitive indicators of the climate and environmental conditions at their time of deposition and can reflect their post-deposition settings. They are widely used in studies of palaeoenvironmental reconstruction and continue to provide valuable insights into major ecological changes, and their response to changing climate. In southern Africa, terrestrial palaeoecological proxies have included rock hyrax middens (Chase *et al.*, 2009; Scott *et al.,* 1996), pollen (Quick *et al.*, 2018), diatoms (Kirsten *et al.*, 2018), and leaf wax n-alkanes (Carr *et al.*, 2014; Strobel *et al.*, 2019; Belz *et al.,* 2020). Historically, palaeoecological investigations in Namibia have mainly been comprised of the analysis of pre-Quaternary fossils. For example, at Etosha, Pliocene aged deposits were primarily found on the western end of the Oshigambo Peninsula (Pickford *et al.*, 2009). In addition to the fossils discovered, the remains of *Tragelaphus spekei,* also known as the sitatunga were found. The sitatunga is an aquaphilic bovid species that thrives in swampy and marshy habitats (Hipondoka *et al.*, 2006) and its preservation was considered to be evidence of wet climate conditions during the mid-Holocene.

This chapter presents and discusses results from three palaeoecological proxies that have been investigated in this research: diatoms, leaf-wax n-alkanes and avian eggshells. New palaeoecological evidence from two well-dated sediment cores of 2 m and 1.6 m depths from a spring mound on the pan floor were examined for their potential to reconstruct late Quaternary ecosystem changes. These data have proved to be helpful in understanding palaeoenvironmental change at Etosha and the changes

in water resource availability, since the last glacial maximum LGM (23 – 19 ka). These insights can be placed in relevant contexts when used in multi-proxy analyses. The successful application of ancient DNA analysis helped to reduce uncertainties in the different datasets discussed in this chapter. Furthermore, findings discussed in this chapter present a more complete and coherent palaeoecological reconstruction at Etosha Pan. A thorough analysis of the bulk sediments in the cores follows in Chapter 6.

5.2. Introduction to results

A new avian proxy was discovered during core-splitting of sediments from a spring mound on the Etosha pan-floor. A rich band of eggshell fragments, later found to be from the Greater Flamingo (*Phoenicopterus roseus*) through aDNA analysis, was identified and environmental inferences were drawn from analysis of both their geochemical data and their physical properties (Figure 5.1). Radiocarbon dating was used to constrain the timing of eggshell deposition. The first section of this chapter discusses the identification and geochemical analyses of flamingo eggshells, while the following section details findings from experiments conducted to analyse diatoms and leaf wax n-alkanes.

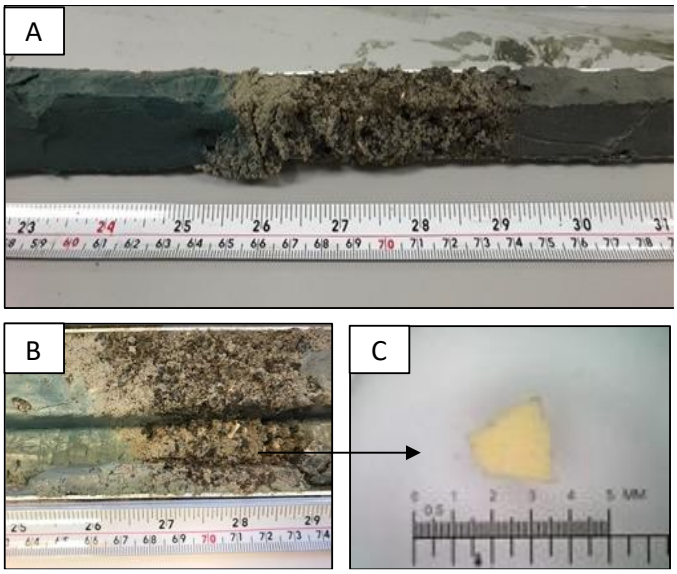

Figure 5.1: (A) – Eggshell fragments within sediment u-channel. (B) –Sediment Core A opened for subsampling and eggshell removal. (C) Sample of a macroscopic eggshell fragment.

5.3. Shell identification

Based on macroscopic analysis, the eggshell was initially thought to be from ostrich (*Struthio camelus*), a common bird species in southern Africa, and frequently represented in palaeoarchives (e.g., Kivisto *et al.*, 2016; Kandel *et al.*, 2005). However, during the analyses of $\delta^{13}C$ at the University of Cape Town Stable Isotopes Lab, the eggshell fragments were identified as being only about a third in thickness of those typically expected from ostrich eggshells. Under a 3D microscope, the fragments showed no surface deformation and excellent preservation (Figure 5.1 - C). To corroborate the macroscale species identification, eight samples were submitted for aDNA analysis at the University of Oxford's Wellcome Trust Palaeogenomics and Bio-Archaeology Research Network (PalaeoBARN). 13 shell subsamples were dated at

Research Laboratory for Archaeology and the History of Art (RLAHA) and iThemba Radiocarbon Dating laboratories to infer their depositional age.

It was found that all eggshell samples exhibited 100 % assignment probability to the greater flamingo (*Phoenicopterus roseus*) (Figure 5.2). The only exception (ETO 19-3V, 75 - 76 cm) still showed complete affinity to the flamingo genus *Phoenicopterus*, but species-level discrimination proved inconclusive, likely the result of lower endogenous DNA (0.1 %) (Figure 5.2). High abundances of prokaryotic genera adapted to brine (e.g., *Alcanivorax, Halobiforma, Haloterrigena, Natrialba, Paracoccus, Pseudomonas, Spirochaeta, Thioalkalivibrio*) or high temperature (e.g., *Acidihalobacter*) environments likely reflect true microbial diversity present in the Etosha Pan.

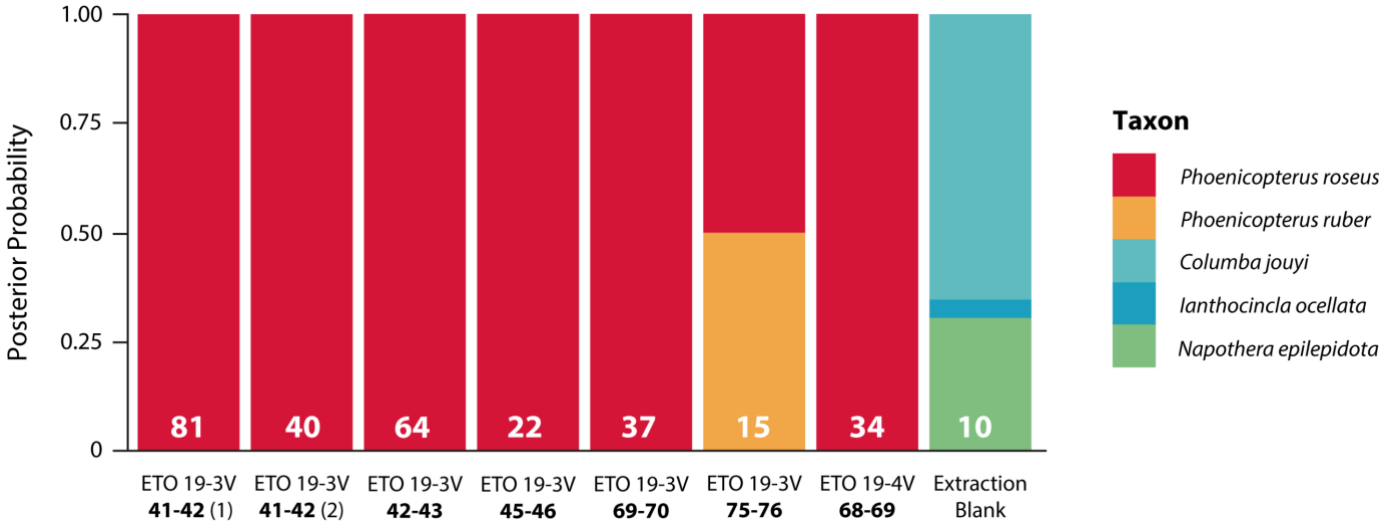

Figure 5.2: Taxonomic assignment posterior probabilities of eggshell fragments (including the DNA extraction blank) from the Etosha Pan. Numbers indicate the number of unique reads aligning to the reference mitochondrial genome. The highest number of unique reads align to the closest matching host mitochondrial genome is indicated for each sample.

5.4. Chronology

The BACON age-depth models for both sediment cores and eggshell found in them show deposition over the last 40 ka. Table 5.1 presents uncalibrated ages (years BP), sample depth (cm) as well as BACON modelling ages that have been calibrated and used for further interpretations in this study. The BACON modelling results for Core A are presented in Figure 5.3. Figure 5.4 (age model for Core B) demonstrates complex age-depth models with varied accumulation rates over the 25 ka period using data presented in Table 5.2. Also notable in Figure 5.4 (age model for Core B) are the larger uncertainties for the section from 55 – 85 cm, where two different ages on bulk sediments were obtained for the same depth (i.e., 55 cm). The two ages taken from 55 cm are 4,170 ± 71 BP and 5,130 ± 70 BP. During this period, the age-depth model gives conservative age estimations due to the greater uncertainties. These differences might be due to different organic compounds being dated from the same depth, sediment mixing or potential contamination of one of the samples. This could also be due to a higher number of dates obtained from Core B than for Core A.

Table 5.1: Radiocarbon dating results for Core A: ETO 19-3V including shell and bulk sediment samples. N= 9

Sample ID	Lab code	Age (BP)	Error (BP)	Depth (cm)	Sample Type	Min age (cal years BP)	Max age (cal years BP)	Median age (cal years BP)	$\delta^{13}C$ (‰ VPDB)	Standard error (‰ VPDB)
ETO19_3V_10_11cm	OxA-X-3172-17	5127	74	10	Sediment	5336	6402	5824	-19.34	1.19
ETO 19-3V 39-40cm_OES	OxA-41980	14083	37	39	Eggshell	12274	17343	16972	-3.73	0.42
ETO19_3V_45_46cm	OxA-X-3172-18	11240	240	45	Sediment	13150	17920	17242	-22.5	1.43
ETO19_3V_70_71cm	OxA-X-3144-39	14820	300	70	Sediment	18158	19150	18587	-24.29	1.76
ETO 19-3V 71-72cm_OES	OxA-41799	15553	45	71	Eggshell	18585	19340	18818	-2.98	0.16
ETO 19-3V 74-75cm	OxA-41981	25660	97	74	Eggshell	18895	20616	19544	1.13	0.34
ETO19_3V_85_86cm	OxA-X-3167-29	18010	140	85	Sediment	21148	22508	21850	-15.74	1.32
ETO19_3V_112_113cm	OxA-X-3178-12	27500	1200	112	Sediment	26296	31947	29316	-20.21	0.33
ETO19_3V_140_141cm	OxA-X-3178-13	28500	1600	140	Sediment	30883	37818	33937	-20.86	0.18

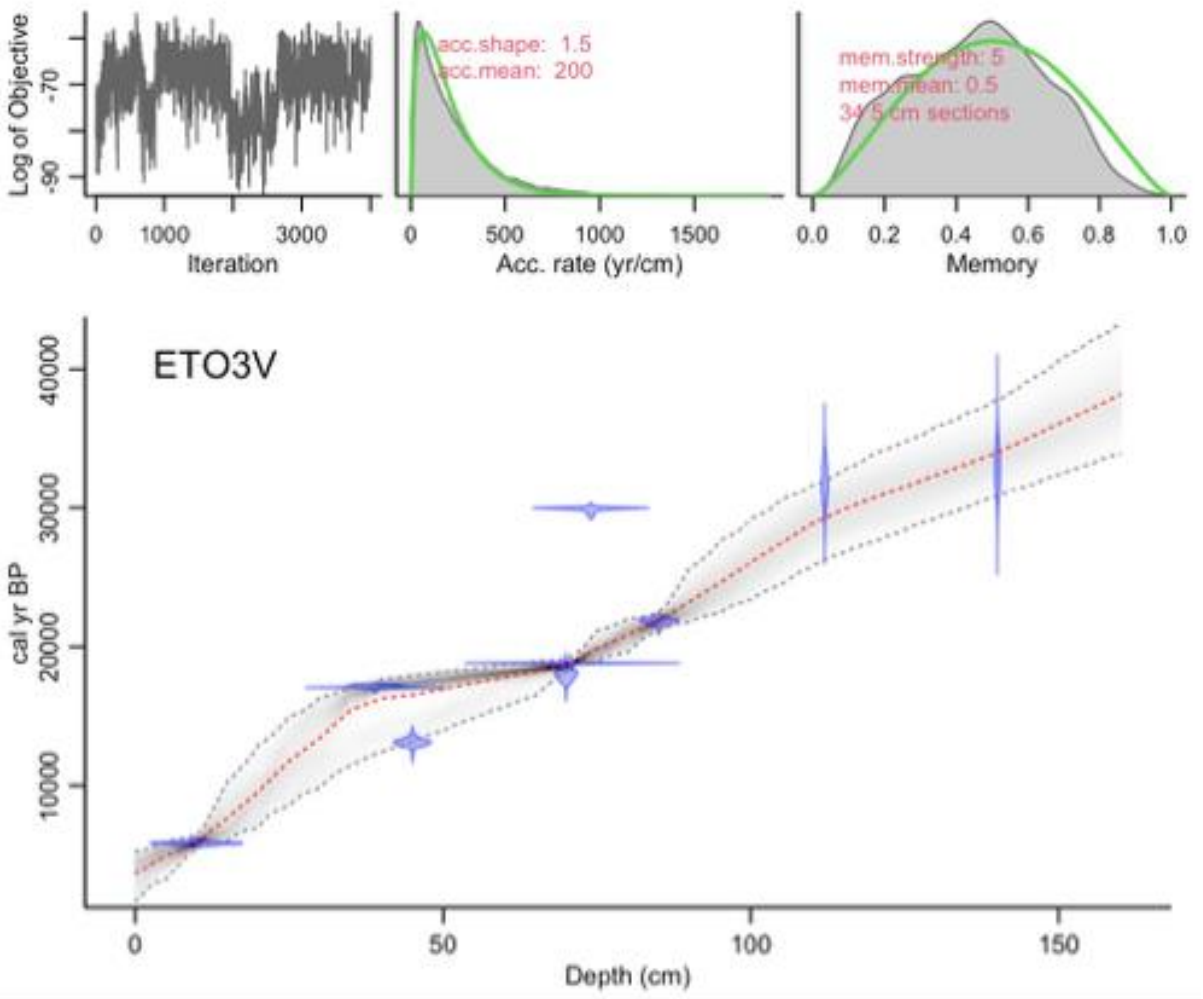

Figure 5.3: BACON age-depth model for sediment core A (ETO 19-3V) from Etosha Pan. The sedimentation history presented by the model suggests gradual deposition through time, with steady sedimentation rates between 163 and 80 cm. At 70 cm depth, there is a sharp change in sedimentation, whereby, the gradient is steeper and there was enhanced sediment input likely responding to climatic variability or major geomorphological changes upstream. Model parameters: The 163 cm core was divided into 55 sections of 3 cm each, with 0 cm corresponding to the year 2019. Accumulation shape = 1.5, Accumulation mean = 200 yr/cm, Memory strength = 5, Memory mean = 0.5. Ages were calibrated using the SHCal20 calibration curve (Hogg *et al*. 2020) in BACON (version 2.2).

Table 5.2: Radiocarbon Dating Results for Core B (ETO 19-4V) including shell and bulk sediment samples. N = 22

Sample ID	Lab code	Age (years BP)	1 Sigma Error (years BP)	Depth (cm)	Sample type	Min Age (cal years BP)	Max Age (cal years BP)	Median Age (cal years BP)	$\delta^{13}C$ (‰ VPDB)	Standard error (‰ VPDB)
ETO_12_13	IT-C-3044	3680	39	12	Sediment	3848	4208	4002	-21.3	0.47
ETO19_4V_31_32	IT-C-3024	3980	53	31	Sediment	4281	4794	4481	-21.6	0.51
ETO19_4V_55_56	IT-C-3023	4170	71	55	Sediment	5454	6091	5775	-21.5	0.55
ETO19_4V_55_56_B	IT-C-3043	5130	70	55	Sediment	5454	6091	5775	-21.5	0.61
ETO19_4V_69_70_NEIF	OxA-41982	8308	25	69	Eggshell	12524	12893	12733	-6.36	2.19
ETO19_4V_OES_69_70_iThemba	IT-C-3063	10830	52	69	Eggshell	12524	12893	12733	n/a	n/a
ETO_19_4V_70_71	IT-C-3032	14440	79	70	Sediment	12715	13341	12888	-24.0	1.86
ETO_19_4V_70_71_OES	IT-C-3039	11600	56	70	Eggshell	12715	13341	12888	n/a	n/a
ETO19_4V_71_72OE	IT-C-2831	10470	49	71	Eggshell	12790	13411	12965	-1.31	2.22
ETO19_4V_71_72	IT-C-3026	11020	73	71	Sediment	12790	13411	12965	-23.3	2.34
ETO19_4V_85-86OE	IT-C-2830	14270	80	85	Eggshell	13670	16152	15367	-2.90	2.16
ETO19_4V_85_86	IT-C-3025	15900	84	85	Sediment	13670	16152	15367	-22.7	2.56
ETO19_4V_86-88	IT-C-2824	16480	87	86	Sediment	13746	16171	15436	-21.2	2.66
ETO19_4V_91_92	IT-C-3031	13440	80	91	Sediment	13979	16309	15765	-21.7	2.67
ETO_110_111	IT-C-3041	12240	68	110	Sediment	14584	17011	16180	-19.3	2.56
ETO19_4V_127_128	IT-C-3028	16200	105	127	Sediment	15286	17600	16728	-19.7	2.50
ETO19_4V_164-165	IT-C-2811	15680	76	164	Sediment	17017	18426	17843	-17.1	2.36
ETO_185_186	IT-C-3042	19550	165	185	Sediment	17741	18734	18308	-22.0	2.44
ETO19_4V_196_197	IT-C-2737	15200	79	196	Sediment	18219	18872	18522	-22.8	2.11

ETO_OES_71-72 cm	n/a	n/a	n/a	71	Eggshell	12790	13411	12965	1.31	0.46
ETO_OES_83-84 cm	n/a	n/a	n/a	83	Eggshell	13544	15909	14876	-2.14	0.03
ETO_OES_84-86 cm	n/a	n/a	n/a	84	Eggshell	13670	16152	15367	-2.35	0.06

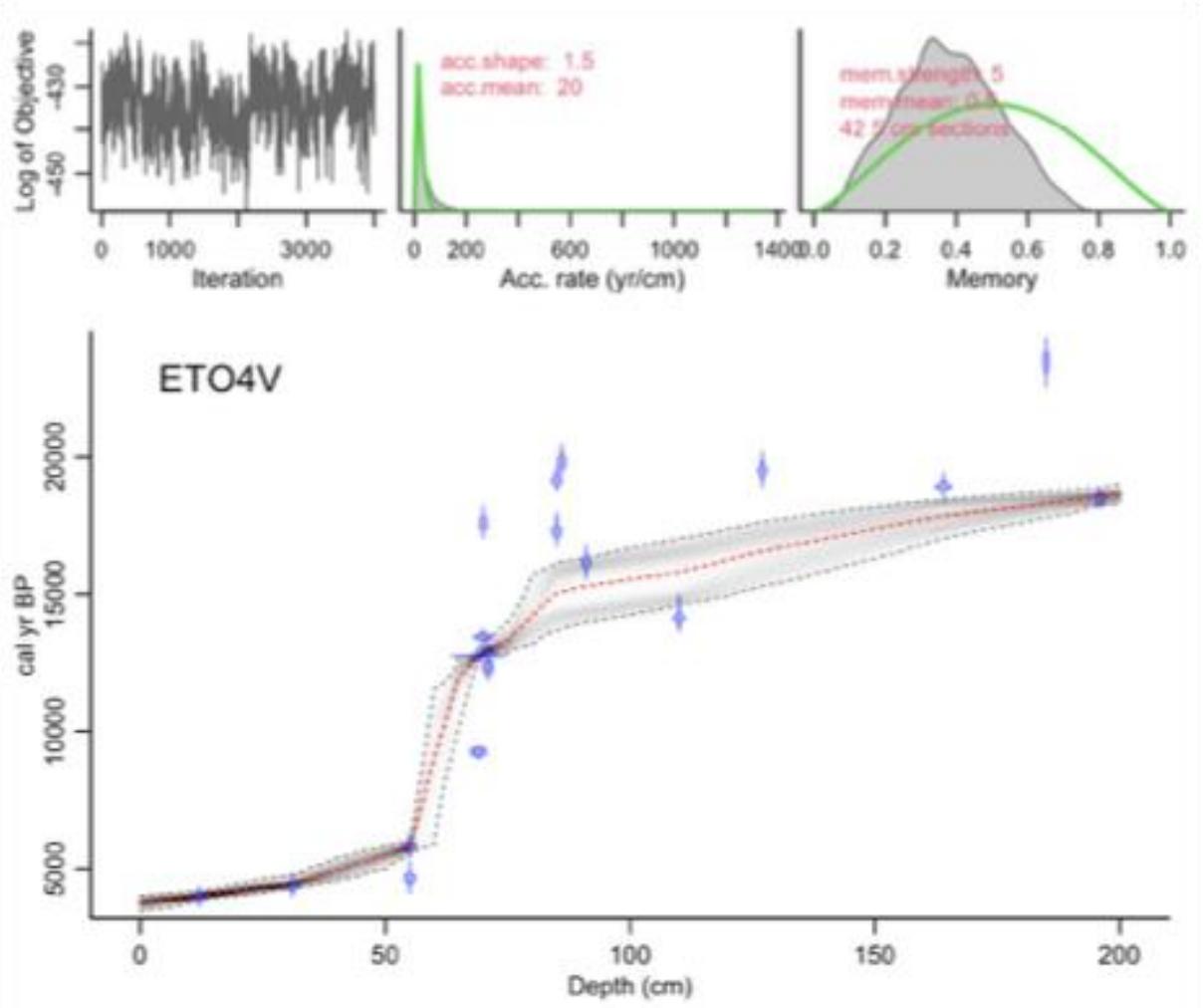

Figure 5.4: The BACON age-depth model for Core B. The age-depth relationship reveals a two-phase sedimentation history whereby the first phase (50 – 200 cm) indicates rapid sedimentation and possibly a high accumulation rate. The model shows greater uncertainties between 70 cm and 200 cm, while the period between 70 – 75 cm encapsulates greater certainty in the ages due to a higher number of samples at that depth. Moreover, it shows a distinct change in sedimentation rate at approximately 50 cm depth, with much slower accumulation rates in the upper portion of the core compared to the lower section. This could be the result of increased sedimentation from local sediment inputs that could have occurred under a wetter environmental regime with increased erosion. In contrast, the younger phase, represented by 0 – 50 cm has a considerably slower accumulation rate of sediments, possibly due to changes in lake levels or in response to regional climatic shifts with prolonged arid periods. Model parameters: Accumulation shape = 1.5, Accumulation mean = 20 yr/cm, Memory strength = 5, Memory mean = 0.5. Ages were calibrated using BACON age-depth modelling software (Version 2.2) using SHCal 2020 (Hogg *et al*., 2020).

5.5. Eggshell fragments individual calibrated ages and their stable isotopes.

Radiocarbon dating was successfully applied to the extracted shell fragments (Table 5.3). The data from shells in both sediment cores were then analysed using the 'rbacon' package from Blaauw *et al.* (2019) in the R Statistical Environment (v. 4.2.1; R Core Team, 2019) with the SHCal20 radiocarbon calibration curve (Hogg *et al.*, 2020). Age-depth models were created and illustrated the chronological history of the eggshells found in the sediment cores. Where there was no raw radiocarbon age on an eggshell, the equivalent age was used from the BACON age-depth model using the shell's depth. Therefore, where a $\delta^{13}C$ value was not available the sample was not taken to the next level of analysis. Hierarchical clustering was conducted on the modelled radiocarbon ages of the 11 samples analysed for $\delta^{13}C$ to assess whether there were significant groups or clusters of the data (Table 5.3). Hierarchical clustering was conducted on the modelled radiocarbon ages of the 18 samples analysed for $\delta^{13}C$ to assess whether there were significant groups or clusters of the data (Table 5.3). The results of hierarchical clustering are presented in Figure 5.5.

Table 5.3: $\delta^{13}C$ data for **18 individual eggshell fragments**. These results were used in the hierarchical clustering are presented in Figure 5.3.

Depth (cm)	Eggshell Fragment Sample ID on Dendrogram	Age ranges with their approximate 2 sigma ranges (95.4 % probability) (cal BP)	Modelled Median Age (cal BP)	$\delta^{13}C$ (‰ VPDB)	Standard error of $\delta^{13}C$
40	1	12,250 - 11,950	12,116	-2.02	0.46
41	2	12,450 – 12,150	12,322	-2.81	0.46
42	3	12,650 - 12,350	12,519	-4.18	0.47
65	4	12,150 -11,850	11,968	-3.64	0.48
66	5	12,300 - 12 000	12,172	-3.69	0.50
67	6	12,500 – 12,200	12,360	-4.65	0.57
67	7	17,850 - 17,500	17,689	-4.41	0.54
69	8	18,300 – 17,950	18,134	-5.45	0.57
70	9	13,050 - 12,750	12,913	-4.70	0.88
70	10	18,600 – 18,250	18,444	-7.26	0.612
71	11	13,150 - 12,850	13,005	-5.12	0.57
72	12	12,900 - 12,600	12,740	-6.32	0.62

72	13	19,250-18,850	19,069	-5.35	0.83
73	14	19,500 - 19,150	19,349	-3.76	0.58
74	15	13,150 – 12,850	13,005	-1.31	0.44
83	16	16,200 - 15,850	16,032	-2.14	0.05
84	17	16,750 – 16,400	16,570	-2.35	0.10
85	18	17,250 - 16,900	17,099	-2.60	0.46

5.6. Hierarchical clustering

Hierarchical clustering has been used here as a rigorous statistical tool to analyse periods of occupation and breeding of flamingos at the pan, and the data are presented in Table 5.3 above.

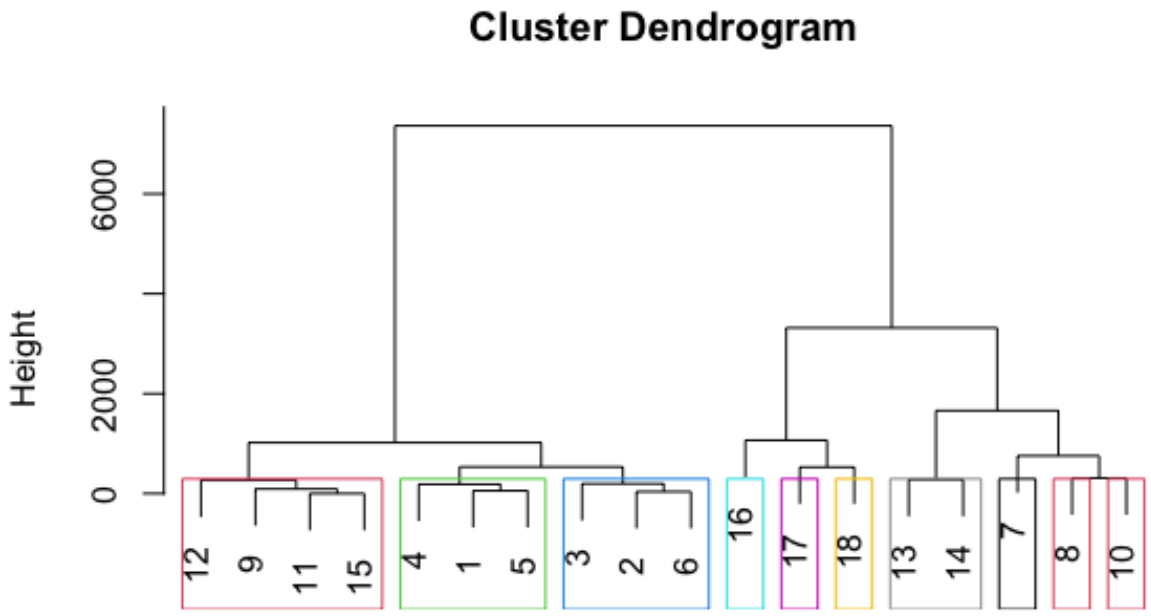

Figure 5.5: Hierarchical clustering dendrogram illustrating two optimal clusters for the flamingo egg-laying episodes. The numbers 1-18 represent individual eggshell fragment ages as shown in Table 5.3 above.

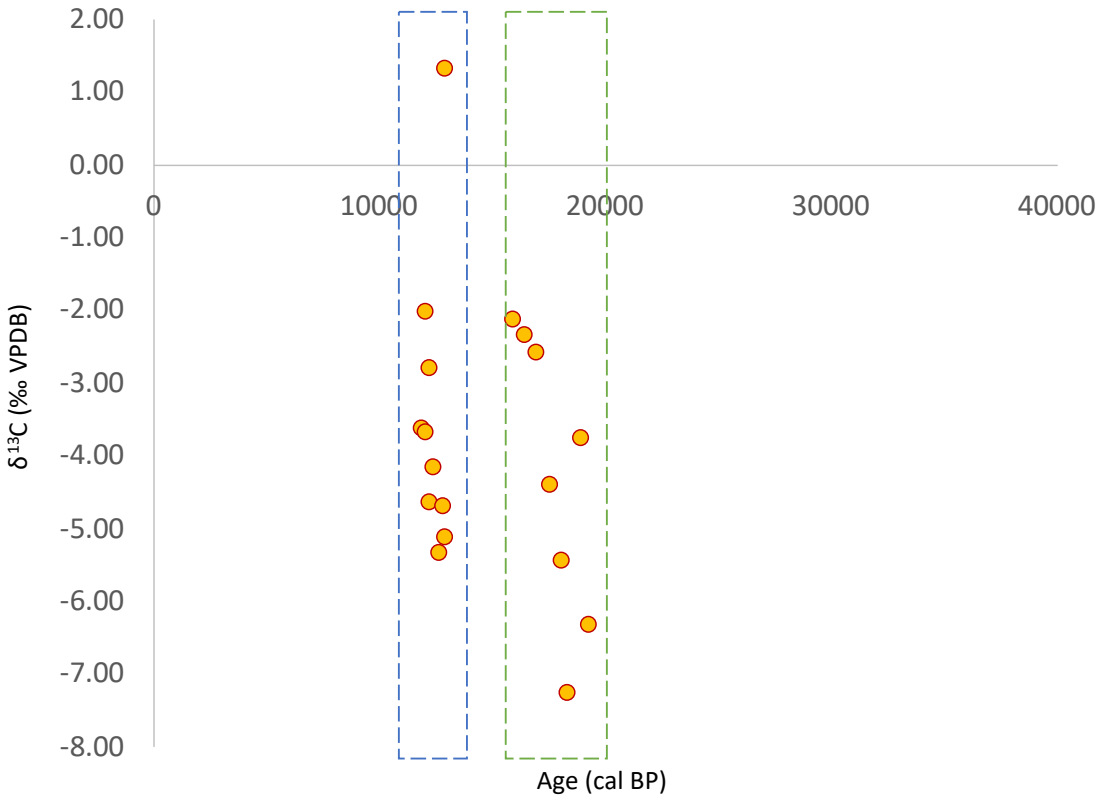

Figure 5.6: Results from the stable isotopes analyses against calibrated ages. Two groups with distinct deposition phases are noted with the two dotted rectangles drawn over the plot. Each dot represents an eggshell sample that was analysed for radiocarbon dating. The two clusters are derived from hierarchical clustering in Figure 5.5 above.

5.7. Sedimentological data

Figure 5.7 (below) presents the grain size data for the two cores. The sediment cores were sub-sampled at a 1 cm resolution forming continuous records. In total, about 360 samples were analysed using laser-granulometry. The primary trends of the grain size data lie in the relationships between the mean, sorting, depth and correlation between the different parts of the sediment cores. In Core, A, the strong correlation between depth and mean grain size (r=0.999) suggests progressive change in depositional environments and sources over time. The grain size is fining upwards, increasing from 38,179 µm at 163cm (~40 ka) depth, and 3,653 µm at the surface. The overall trend

here is that the site potentially experienced a change in depositional processes from higher energy in the past, and progressing to calmer conditions towards the modern-day. The sediments exhibit poor to moderate sorting, with a dominance of silt (80%), while sand is more variable. The sand content lies between 0 – 76.2% over the 40 k cal BP, indicating episodic periods of high-energy transport of sediment into the pan. In addition, Core A includes slightly larger uncertainties towards the bottom of the core at 32 k cal BP. The grain size data varied in two phases of the record whereby, from 35 k cal BP to 17 k cal BP, the mean grain size is 72.53 microns, driven by the large proportions of silt and clay. After 17 k cal BP, Core A records a marked increase in sand-sized particles, which continue to fluctuate until the present. The 22 sand-dominated samples e.g. there is a peak at 45 cm depth (4.7 – 5.6 k cal BP) with 76.2% sand, likely represent periods of increased precipitation with intermittent flooding, or enhanced wind activity.

Core B has a variable grain composition. The overall sediment characteristics is that it is composed of silt (47.8% average), with variable proportions of sand (25.5%) and clay (26.8%) over the 24 k cal BP period covered by the core. These high variability leads to poor sorting, with limited reworking, typical of an environment with fluctuating lake levels or changing depositional conditions. The grains have variability in each component indicating an environment with rapid changes. Sand variability: 17.5 % (high variability), Silt variability: 13.1 % (moderate variability) and Clay variability: 19.1 % (high variability). In the period between 24 and 15 k cal BP, there was a domination of fine-grains (~36 %) suggesting deeper lake conditions, stable water column potentially

under wetter conditions during the LGM. Between 15 and 8 ka, there is a steep increase in sand (50.8 % average), suggesting a more dynamic depositional environment, perhaps under a transitional period with complex interactions between precipitation, temperature and wind changes. There are 18 intervals of high sand where the proportions are >50% between 16-9 k cal BP. The high incursion of sand particles continues until about 2 k cal BP in both cores when the proportion of sand fell below 35 % until the present.

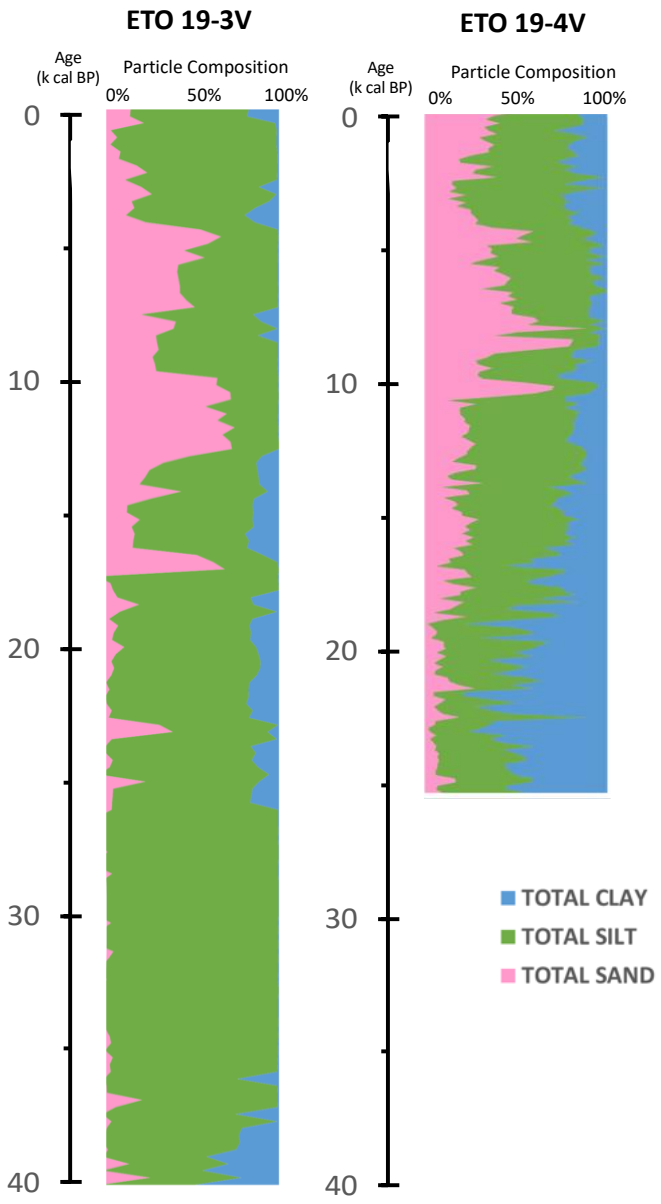

Figure 5.7: Particle size data taken at a 1 cm resolution plotted against ages modelled using BACON (version 2.2) in (RStudio version 2.3.9.1) (Blaauw and Christen, 2011). Core A (ETO 19-3V) and Core B (ETO 19-4V) are plotted using model-derived ages illustrated in Figure 5.3 and Figure 5.4.

The end-member model analysis (EMMA, see Chapter 3 for details, Section 3.3.2 on Page 31) for grain size data in both sediment cores suggests that there are three members: EM1, EM2 and EM3 (Figure 5.8). In Core A, EM1 (PC1) accounts for 57.34 %

variance with a positive loading on sand (0.73) and negative loadings in clay (-0.36) and silt (-0.24). The dominance of sand represents a high-energy depositional environment, likely resulting from increased precipitation and stronger fluvial inflows. EM1 was most dominant during the periods: 14 - 12 ka BP and 8.5 – 7 ka. The period 14 - 12 ka is characterised by the highest content of sand grains on the record, ranging between 70 - 76 % (mean = 71.2 %) with relatively stable contributions (standard deviation = 3.4 %). In addition, there was minimal silt content (<1 %) between 14 - 12 ka while the presence of clay was similarly limited during this period. Between 8.5 - 7 ka, sand content was still high (55 - 70 %) but variable (standard deviation = 14 %), while the silt component was moderate, and clay content remained low.

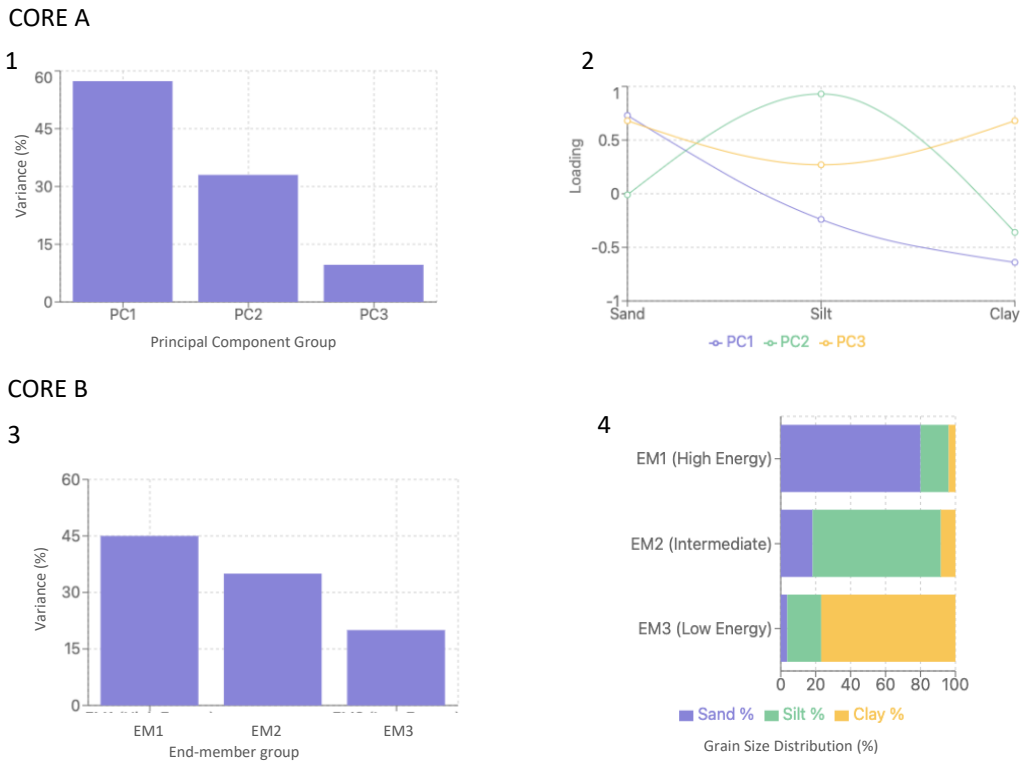

Figure 5.8: The end-member model analysis (EMMA) for grain size data in sediment Core A and B. 1 = Principal component groups for Core A showing the variance associated with each grain size group. 2 = Grain size loading ratios for silt, clay and sand. 3 = End-member groups for Core B particle size data. 4 = Grain size distribution by percentage in end-member groups. Core A had 161 samples at a 1 cm resolution. Core B had 194 samples analysed at a 1 cm resolution.

PC2 has a strong positive loading by silt (0.93) with minimal loading from sand (-0.6) and clay (-0.01) in Core A. Moreover, in Core A, EM2 likely represents a depositional environment with moderate energy and contributions from a variety of sediment sources. Such an environment is most prominent during the period 36 - 34 ka that features the highest silt proportions on the record. Overall, the two end-members (PC1 and PC2) are responsible for over 90.34 % variance. These two dominant endmembers suggest two distinct depositional processes whereby, EM1 in Core A accounts for deposition of a high energy geomorphological environment (with high levels of sand), and a moderate-energy environment represented by high silt contents evident in PC2. End member 3 (PC3) is most prominent in the period 36 - 34 ka (in Core A) and has moderate contributions from all components (Figure 5.8). PC3 might have occurred during transitional periods with mixed proportions of sand, silt and clay and minimal variations. Between 4 and 3.5 ka, silt and clay ratios are balanced, with minor proportions of clay (16 - 17 %) and moderate proportions of sand (15 - 30 %). This period represents stable conditions that are sustained during this period (4 – 3.5 ka) as reflected in both sediment cores.

Core B exhibits similar characteristics to those in Core A, including the presence of three endmembers. However, the contribution of sand in EM1 of Core B is less dominant (i.e., sand proportions exceed 60 % but do not reach the high values in Core A). EM1 in Core B represents 45 % of the variance instead of the 57.34 % in Core A. EM2 (silt-rich) accounts or 35 % of the variance, with 50 - 60 % silt component. This suggests moderate energy conditions from Core B, similar to Core A. EM3 (stable

mixed proportions of all grains) explains 20 % of the variance in Core B and has high clay enrichment (>40 %), likely resulting from low-energy depositional processes.

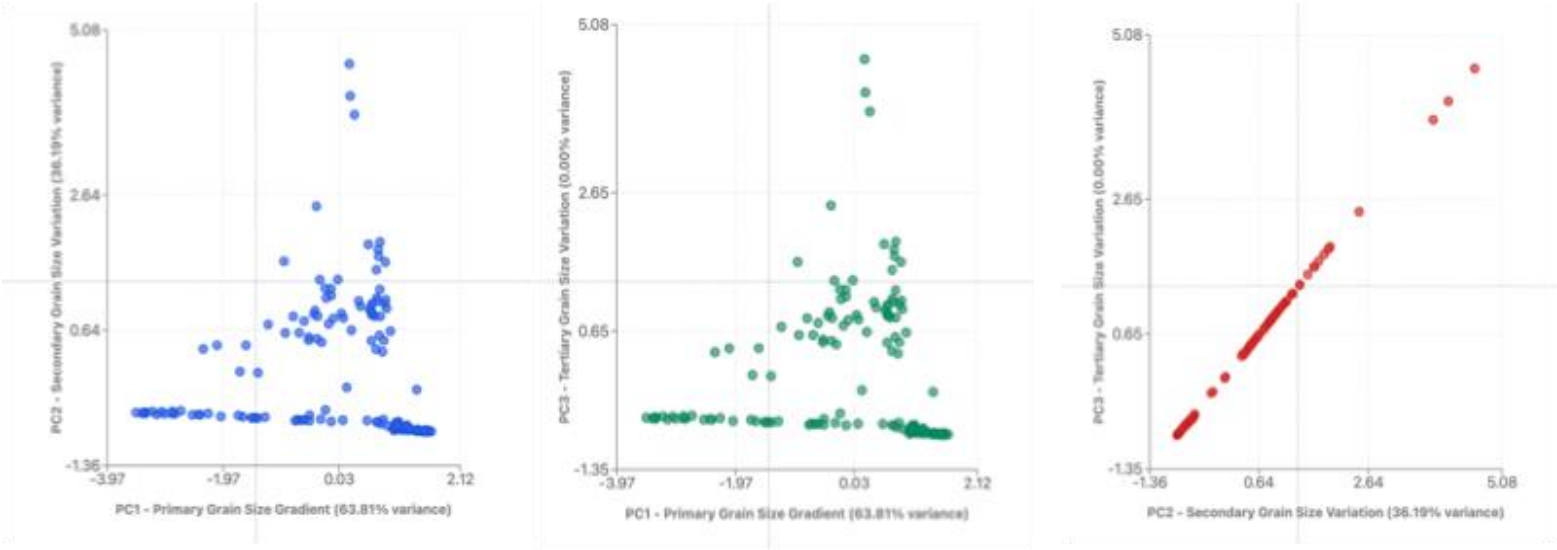

Figure 5.9: PCA biplot (PC1 vs PC2) of grain size data from Etosha Pan Core A, showing primary depositional gradient and secondary environmental variations (36.2% variance) with depth-related trends.

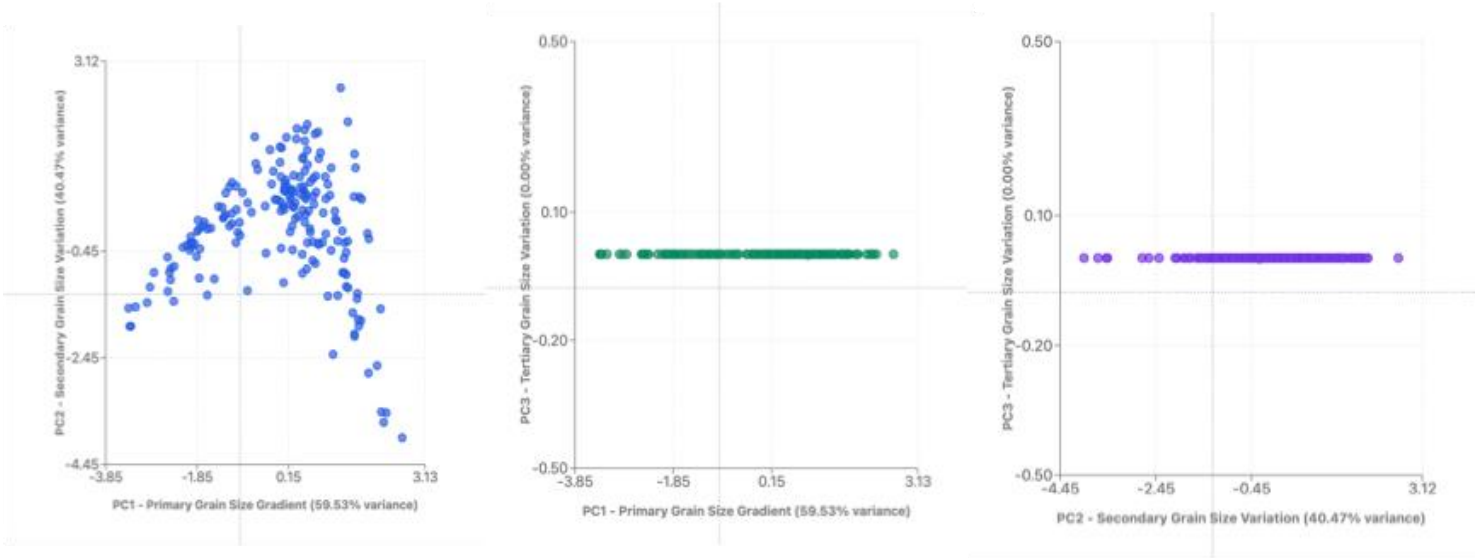

Figure 5.10: PCA biplot (PC2 vs PC3) of grain size data from Etosha Pan Core B, revealing secondary and tertiary environmental patterns independent of the main sand-silt-clay gradient.

PCA results suggest that there has been long term environmental evolution, potentially responding to regional climate shifts over the last 40 ka. PC1 contributes ~65% to the total variance and contains heavy loadings on coarser fractions (Figure 5.10). These correlate with End-member 1 that has sand enrichment and was likely derived from high energy transport processes such as increased fluvial inputs (Figure 5.8). The PC1 vs PC2 biplot demonstrates primary processes that were driven by varying proportions of sand-silt-clay and accounts for most variance (Figure 5.9 and Figure 5.10). Moreover, the biplot revealed environmental shifts that were not captured by the first principal component.

PC2 vs PC3 highlighted secondary and tertiary patterns in the grain size data that were independent of the primary gradient (Figure 5.8 for Core A, and Figure 5.9 for Core B). Moreover, the PC2 vs PC3 biplots account for ~15% of the variance and indicate long periods of environmental stability where the tighter clusters suggest that the site also experienced dynamic environmental change (Figure 5.9 for Core A, and Figure 5.10 for Core B). In addition, PC2 vs PC3 shows a linear set of sample points, suggesting that there is a unidirectional environmental process controlling sediment deposition and accumulation. This could be an indication that the sediments were responding to either a climate signal, changes in lake levels or both at different times.

The secondary gradient also reflects varied sorting of the sediments at different depths. These patterns were likely influenced by changes in deposition that could include

changing water levels or variation in transport mechanisms over time. These findings complement results from the EMMA analysis which suggested that sediment deposition at Etosha was not uniform over the last 40 ka (Figure 5.8). Moreover, it can be inferred from these results that aeolian processes were likely not the main contributor to long term sediment deposition at Etosha. This is supported by the coarse, extremely poorly sorted sand (Table 4.3) that is typical of flooding events during periods of increased fluvial activity.

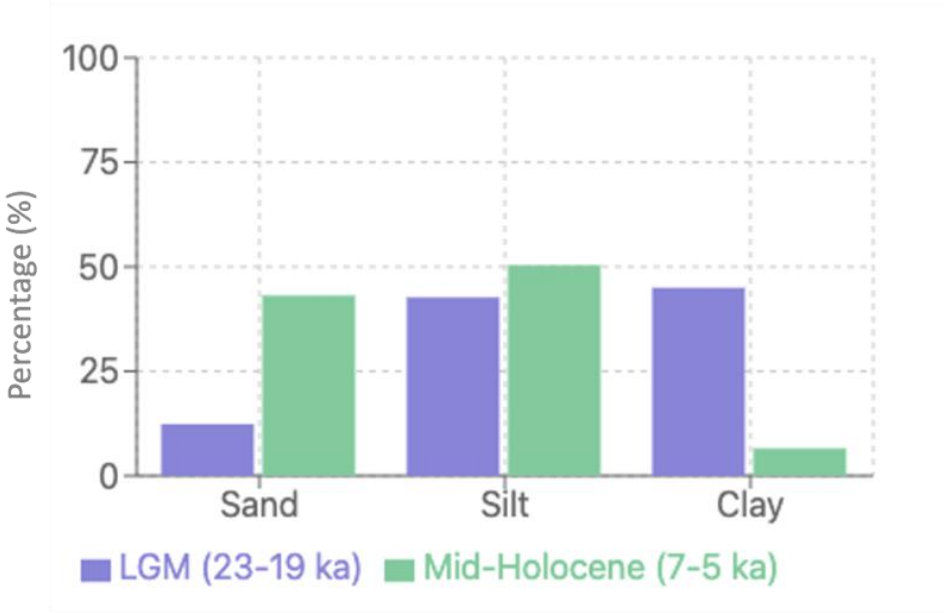

Figure 5.11: Mean grain size data comparison between LGM and Mid-Holocene from sediment cores A and B collected from the Etosha spring mound.

According to Figure 5.11, the mid-Holocene was characterised by greater proportions of sand (40 %), with low clay (10 %) and moderate amounts of silt. The last glacial maximum (LGM) on the other hand had 45 % clay, which is dominant and minor amounts of sand (15 %). One interpretation is that in dryland systems, the sand/silt/clay proportion often does not follow the typical temperate relationship with high energy,

and it is not always a straightforward correlation. Large amounts of sand being transported into a basin can sometimes reflect a wet period after a prolonged dry phase during which the fluvial systems deposited large amounts of sand. Silt and clay are typically deposited under lacustrine conditions once a stable lake body has formed. However, the data presented above suggest that stronger fluvial processes with high-energy transport deposited coarse, poorly sorted sediments into the system during the mid-Holocene than during the LGM. This suggests higher energy inputs for sands from shallower water, perhaps an intermittent lake body with riverine inputs. Furthermore, the abundance of clay during the LGM suggests deeper water, or a permanent water body with calm conditions and low-energy transport within a stable environment.

5.8. Other palaeoecological proxies

Palaeoecological proxies are important indicators of environmental change in different ecosystems such as freshwater lakes and estuaries. Proxies such as diatoms respond rapidly to shifts in variables such as water temperature and water chemistry (Ognjanova-Rumenova, 2008). In drylands, palaeoecological proxies are scarce, but when available, they can reflect changes in climate and lake levels in saline lakes (Fritz *et al.*, 2022). Others such as pollen, diatoms, leaf-wax n-alkanes and ostracods have been utilised in conducting research to reconstruct late Quaternary palaeoenvironments (as discussed extensively in Chapter 2). Below is a discussion of results from two experiments to explore other palaeoecological proxies in the Etosha sediment cores and other sediments on the pan-floor.

5.8.1. Diatoms

Diatoms are commonly found in lakes with varying salinity levels, but they are not always well preserved in sedimentary records, particularly in alkaline environments (Neumann *et al.*, 2010). Under x1000 magnification of the 8 samples taken from the two sediment cores, diatoms had not preserved at all in any of the slides apart from one slide which had one valve of an unknown *Pinnularia* species. But as there was just one valve, it was not possible to say if this grew in the palaeolake or was transported there and left behind.

5.8.2. Leaf-wax n-alkanes

There was a very low indication of the presence of leaf-wax n-alkanes in the sediment and floor-pan samples. Therefore, the analysis was adapted to using the Soxhlet method (Collins *et al.*, 2011) instead of the automated alkane extraction process as it is more adapted to extracting n-alkanes in samples with low concentrations. With the method applied, there was still no preservation of the n-alkanes in the sediment samples tested from 20 sample depths along both cores and other samples excavated from the pan floor. N-alkanes are relatively stable on Quaternary time scales and have been known to survive a range of potentially erosive environmental processes. However, they were not present in samples from Etosha. This could have occurred because exposure to long periods of extremely high or low pH conditions can alter and damage the n-alkanes. It could also be because inputs of leaf waxes to the site were very low given that there is sparse vegetation in that part of northern Namibia.

5.9. Flamingo breeding as a palaeoarchive of environmental change at Etosha

While the modern Etosha Pan hosts a wide variety of fauna and flora (Olivier and Olivier, 1993), there is limited information about the landscape in the past millennia, and on the nature of wildlife (if any) to have occupied the site. The stable isotopes data from the shells are not interpreted further in this research because there was no known study that had used flamingo shells to extract modern climate information that could act as an analogue to these new findings. In particular, factors that can affect carbon isotope fractionation of the $\delta^{13}C$ signal in eggshells including: the metabolic rate of the bird, its digestive physiology, nature of diet including its terrestrial range, amount of protein in the diet, and the processes related to pregnancy, lactation and/or egg-laying (e.g., Tieszen *et al.*, 1983). These factors are not fully researched or understood with regards to their implication on $\delta^{13}C$ data on flamingo eggshells. Emslie and Patterson (2007)'s work on penguin eggshells accumulated in the last 38 ka was achievable largely through access to sufficient research already conducted on penguin eggshells. The research based on prior experiments provided information about eggshell fractionation between diet, yolk membranes and outer shell material as it accumulates within 6 - 8 days (Emslie and Patterson, 2007). However, their research assumed that eggshells in the same sample depths were of similar age. One of the strengths of the present study is that no layer was generalised. Each of the 22 data points of the $\delta^{13}C$ values were analysed on a single eggshell fragment from both different and similar depths. The samples yielded data that demonstrated that even though shells may be collected from the same stratigraphic layer, they may not necessarily be of the same age (Table 5.3).

Therefore, instead of the $\delta^{13}C$ data, the presence, ages of deposition and identity of the shells form the basis of the interpretations. Moreover, the stable isotope values of the flamingo shells lie outside those from modern ostrich eggshells collected 40 km outside Etosha (with $\delta^{13}C$ values ranging between - 9.01 and -9.1 ‰), further corroborating evidence that the shells do indeed belong to a different species and not ostrich. Nevertheless, these results provided new insights into the post-LGM hydroclimate variation in this location with complex sources of atmospheric moisture sources.

5.9.1. Time periods of flamingo breeding at Etosha

According to the hierarchical clustering statistical model on the eggshell fragments (Figure 5.5), and radiocarbon data, the most apparent periods when flamingo breeding occurred in Phase 1: From 19,349 cal BP ($\delta^{13}C$= -3.76) to 16,032 cal BP ($\delta^{13}C$ = -2.14) (broadly concurrent with Heinrich Stadial 1), and Phase 2: From 13,005 cal BP ($\delta^{13}C$ = -1.31) to 12,116 cal BP ($\delta^{13}C$ = -2.02) (broadly concurrent with the Younger Dryas)

Three key sources of evidence point to specific hydrological conditions in the pan during these times. First, flamingo egg laying typically occurs on mud nests (approximately ~30 cm wide, ~20 cm high) when there is shallow water (Scott *et al.*, 2012; Barcelos-Silveira *et al.*, 2023). The combination of three factors - levelled topography, clay sediments with high salinity/alkalinity and seasonal water availability - creates an ideal breeding habitat for flamingos in Etosha Pan (del Hoyo *et al.*, 1992;

Berry, 2000). These conditions likely occurred on the pan and allowed flamingos to construct stable nests, access food resources, and maintain their social structure during the breeding season. In areas with high densities of flamingos, the lake sediments may undergo preferential compaction, especially at breeding sites making the sediments resistant to subaerial erosion (Scott *et al.*, 2012). Berry (1980) categorised three distinct climatic periods in Etosha based on average annual precipitation and temperature data: a. January to April: wet and hot season b. May to August: dry and cold season c. September to December: dry and hot season. Etosha Pan, like most of Namibia, is characterised as a summer rainfall area, with the majority of precipitation occurring during the summer months (Nicholson, 2000). The winter months in Etosha are dry, with little to no rainfall. Despite attempts to quantify rainfall requirements (Bigalke, 1959; Berry, 1972; Archibald and Nott, 1987; Krienitz *et al.*, 2016), the precise quantity of rainfall needed to sustain flamingo breeding at Etosha remains unclear (Simmons, 1996; McCulloch *et al.*, 2003; Cunningham and Jankowitz, 2010). Greater flamingos usually breed in summer which suggests that northern Namibia mostly received rainfall in the summer rather than winter during the periods of eggshell deposition.

Large, pan-wide inundations are unsuitable for flamingo breeding because the water can flood the nests (Sauer & Rocher 1966; Berry, 1972; Simmons, 1996). Therefore, it can be assumed that there was lower rainfall experienced after the LGM, during the egg-laying phases. It seems that flamingo breeding requires a complex interplay of brackish and fresh rainwater. This is because in recent history, flamingos are known

to have fled during the breeding season and abandoned their young at least three times by the year 1971 (Berry, 1972). This may be the result of flamingos initially being attracted to breed at the pan. However, due to higher evaporation rates, the pan dried out before breeding was complete. This adds weight to the fact that flamingos need some water to breed, but not too high or too low. The second flamingo breeding phase suggests that there were no full lacustrine conditions that could have, for example, built 2 to 3 m high shorelines on the west of the pan during those periods as suggested by Hipondoka *et al.* (2014). The maximum depth of water at the time would have to have been less than 15 cm (below the average height of the nests). Following this period, OSL data (9.70 ± 0.60 ka) from Hipondoka *et al.* (2014) show lacustrine conditions to have taken place until 10 ka with a shallow water body.

On the other hand, a drying climate might be responsible for the low water levels (probably less than ~15 cm in depth) that occurred at Etosha Pan during the periods of flamingo eggshell deposition. It is likely that the summer rainfall zone as described by Chase and Meadows (2007) shrunk or moved further east away from Etosha to deprive the pan of rainwater during the periods when the flamingos bred. Based on their sedimentological investigations on smaller pans in Namibia, Schuller *et al.* (2018) hypothesised that after the LGM, climatic changes were caused by large-scale spatial fluctuations in both summer and winter rainfall zones. These fluctuations led to variations in precipitation intensities and wind strengths and could explain the changes in precipitation observed at Etosha with a decreased summer rainfall zone extent during flamingo breeding.

In addition, the second line of evidence relates to the preservation of the eggshells and their DNA in an excellent condition, with no evident abrasion affecting the shell surfaces, which suggests that the shells were 'protected' (or kept away from erosional elements) since their deposition (Figure 5.1). This could be through the quick formation of mud - as can be expected from a spring - and the lack of disturbance such as from other animals trampling them, people fetching water, floods that could transport the shells to another location, flow of large-grained sediment deposits, or unfavourable climate conditions such as strong winds or extreme drought associated with aeolian deflation. All these could lead to the damage or transport of the shell fragments if they had influenced the site.

Thirdly, the microbial diversity from the aDNA analysis provided evidence of prokaryotes that are adapted to brine (*Alcanivorax, Halobiforma, Haloterrigena, Natrialba, Paracoccus, Pseudomonas, Spirochaeta, Thioalkalivibrio*) and to hot climates (*Acidihalobacter*) (Figure 5.2). Both these sets of microorganisms are essential for flamingos as they breed in semi-arid environments and consume organisms that are adapted to brackish water. The reconstruction of the Etosha pan-floor as highly alkaline is also supported by the absence of diatoms in the smear slides that were examined in this study. Diatom dissolution is known to occur when lacustrine conditions fluctuate around pH 9 (Barker, 1990).

5.10. Preservation of other palaeoecological proxies

As stated above, diatoms were not present in the samples taken from the sediment cores. This may indicate that although they were once growing in the lake, high water salinity and pH led to dissolution of their silicious frustules following death, leaving no trace of diatoms behind (North *et al.*, 2018). An alternative explanation is that diatoms were not able to grow in this lake, and instead primary production was driven by other algal groups such as cyanobacteria. It has been argued, by Schmidt *et al.* (2017) that this has been the case in the Makgadikgadi salt pans in Botswana, where diatom assemblages were analysed and the data were inferred to indicate extremely alkaline and oligohaline conditions in the Marine Isotope Stage 5 (MIS 5) (Schmidt *et al.*, 2017).

Diatom dissolution is highest in sodium carbonate solutions due to high pH levels (>9), which enhances the alteration or dissolution of silica (Fritz *et al.*, 2022). These processes can affect the total diatom abundance in sediments and the species composition, as different diatom species have varying sensitivities to dissolution and diagenesis. Thus, these results suggest that Etosha Pan, at least near the spring mound, probably had extremely high alkalinity that may have destroyed the diatom assemblages that are common in high-salinity environments. Similarly, there was little to no contribution of n-alkanes to the organic sedimentary signal. This may be due to the lack of terrestrial or aquatic plants in the basin or from surrounding areas which could have blown them into the pan during periods of strong aeolian processes. Another reason may be that the post-depositional environment is not suitable for the preservation of n-alkanes. However, other pans in Namibia have yielded sufficient leaf

wax alkanes to allow an in-depth palaeoclimate reconstruction at Koës Pan (Belz *et al.*, 2022).

5.11. Implications for palaeorainfall and pan inundation phases

To better understand the environmental history of a lake, it is crucial to consider both the hydrological changes and sedimentological characteristics such as grain-size distributions. The prevalence of fine silt and the absence of lake-shore components such as well-sorted sand grains in the sediments during flamingo nesting periods shed light on the dominant environmental conditions and sediment sources at those times (Figure 5.7). Moreover, the transportation of fines by endorheic rivers and their subsequent deposition on the pan provides insights into the paleogeography and hydrological processes of the region. The dominance of silt and clay in the pan sediments suggests that the pan hosted a low energy environment due to fine-grained sediments that indicates that the water flow was slow or stagnant, allowing silt and clay particles to settle out of suspension (Hipondoka, 2005). The sediments are largely sourced from drainage systems which used to be connected to the Kunene River and the Owambo-Etosha Basin (Hedberg, 1979; Buch & Trippner, 1997; Hipondoka, 2005).

Modern day Etosha experiences a significant water deficit, which can have negative implications for the ecosystem, water resources and human activities in the area. The seasonal distribution of rainfall, with a pronounced dry season during the winter months, also shapes the vegetation and wildlife dynamics in the region (Mucina *et al.,* 2006). The data presented in this Chapter suggests that Etosha Pan has experienced the

wettest climate conditions during the LGM (23 – 19 ka), followed by an extended period of decreased moisture (19 – 16 ka). The period covered by flamingo breeding presented in this chapter received less rainfall/inflow than the LGM, but not as low as modern day. This demonstrates that the palaeohydrological changes at Etosha were dynamic and this impacted the ability of wildlife to access and thrive on the pan.

Phase 1 of eggshell deposition reflects possible drying climate experienced at the site during the latter part of the LGM 19.35 to 16 k cal BP. A drying climate which possibly persisted to the latter part of the LGM, was likely influenced by the reduced mean annual precipitation and lower temperature that would limit evaporation and therefore result in lower-than-average rainfall. This interpretation of a dry phase is corroborated by the work of (Shi *et al.,* 1998). They found the northern Karoo to have been arid during the LGM based on palynological evidence characterised by high percentages of *Asteroideae* and *Chenopodiaceae* which are adapted to dry conditions Shi *et al.* (1998). This was based on their study on marine sediment core GeoB1023 off the west coast of Namibia and Angola and could signify that the drying climate was more widespread in the region.

There are differences in the amount of freshwater input received from the Ekuma Delta, the main inlet freshwater into the lake. This has probably led to variations in salinity that probably played a role in sustaining the low water levels in the past to allow flamingo nesting - assuming that the pan was responding to changes in local environmental conditions through river discharge and/or regional climate. Today, it

appears that the freshwater river discharge from the Ekuma Delta is diverted eastwards because of the tilt of the modern pan, with less water flowing to the western end of the pan. If these flow dynamics and changes occurred in the past, they could also be a reason for water quantity variation reaching the western part of the pan to allow for flamingo breeding. But this cannot be confirmed by the present study as sample collection occurred on the western end of the pan.

During periods of flamingo nesting at the lake during the two phases, the sediment grain-size distributions were primarily composed of fine silt (Figure 5.7). These sediments lacked the typical higher-energy characteristics of lake-shore components, such as sand or fine sand. According to the results of a geomorphic terrain analysis conducted by Hipondoka *et al.* (2004) the source of sandy particles at Etosha is the Ekuma delta. This suggests that the near absence of sand in the sediments during eggshell deposition indicates that the Ekuma delta was probably dry and not depositing sand as it would during flooding phases or from extended periods of aeolian deposition from surrounding areas. These sediments may have been derived from more distant locations or were the result of aeolian deposition. Therefore, it is likely that Etosha Pan did not experience full lacustrine conditions during the periods of flamingo breeding.

5.12. Comparison with other studies in the region

Brook *et al.* (2011) calibrated ages for stromatolite deposits on the east of Etosha range from 3 - 19 ka. The growth of stromatolites requires favourable moisture conditions, therefore, stromatolites found 8 m above the present pan's lowest point on the eastern

end of Etosha Pan near Poachers Point grew during that period (between 3 – 19 ka BP, Brook *et al.*, 2011). This suggested a transition in hydroclimate towards a wetter environment and signifies the existence of lacustrine conditions in the past. The new data presented in this Chapter indicate a dynamic change in lacustrine conditions, with low water levels occurring from Phase 1: from 19.35 – 16 k cal BP and from 13 k cal BP to 12,1 k cal BP. Dry LGM conditions were also observed from marine sediment cores investigated by Collins *et al.* (2011), where they interpreted bulk sediment sample carbon isotopic data to indicate a contraction of the African rain belt during the LGM which brought arid conditions to Namibia, presumably including areas east of the Namib Desert.

At Etosha, flamingo breeding continued after the LGM (Phase 1 and 2). The occupation phases presented here featured a climate that was drier than the LGM, while the period in between could be characterized by continued wet conditions similar to the period before eggshell deposition. Schuller *et al.* (2018) found supporting evidence at Omongwa Pan. Following the LGM (between 19 - 15 ka cal BP), where the palaeoclimate in the studied pans became drier, and aeolian transport decreased. Using evidence from the Tsauchab River, 630 km to the south, Brook *et al.* (2006)'s wet phase at c. 15 ka coincides with the gap in the flamingo eggshell record. It occurred after Phase 1 at Etosha, and no flamingo eggshells were preserved during that period. The shells could have been removed by fluvial processes if laid under a wetter climate. Alternatively, no breeding took place during that time due to expected full lacustrine

conditions that might have occurred if wetter conditions at c.15 ka (Brook *et al.*, 2006) were region wide.

The presence and preservation of shells and DNA, as well as ages of deposition of the flamingo eggshells from Etosha Pan gives us insight into the associated environmental conditions post the LGM period. Eggshell deposition likely occurred during drier summers, with low rainfall, decreased river discharge and a sustenance of a shallow water body. During those dry periods, the breeding flamingos most likely relied on freshwater from the spring (Brown, 1955). Therefore, these results align with some existing palaeoenvironmental reconstructions that have argued that dry conditions prevailed after the LGM in southwestern Africa.

5.13. Conclusion

Sedimentary archives are valuable tools for studying the changes in pan landscapes over time. These archives can include a variety of sedimentary deposits, such as those from cores, where layers of sediment deposited by fluvial processes during flooding events can provide information about past river dynamics and changes in sediment supply. In this Chapter, new data was presented and used to affirm changes in sediment deposition at Etosha Pan during and between seasonal flamingo breeding on the pan collected from two continuous sediment cores. The reconstructed palaeoenvironmental changes provided clues on local environmental conditions at Etosha since the late Pleistocene to Holocene periods. It is proposed here that

flamingo breeding occurred under relatively dry conditions, and this is likely due to the reduction in summer rainfall zone extent.

Chapter 6:

Reconstruction of lake level changes at Etosha Pan and their linked palaeoclimate mechanisms

6.1. Introduction

Due to its prevailing arid climate and the consequently limited opportunity for the preservation of organic material, northern Namibia has a scarcity of long, continuous records of sedimentological sources of data to reconstruct late Quaternary palaeoclimatic changes (Schuller *et al.*, 2018). As a result, testing the robustness of palaeoclimate modelling for past environmental and climatic change in southern Africa remains challenging, particularly regarding the reconstruction of past wet phases in modern-day dryland basins. Similar work has been conducted in pans in southern Africa. For example, Telfer and Thomas (2007) and Telfer *et al.* (2009) conducted research at Witpan, while Belz *et al.* (2020) focused their study at Omongwa Pan in Namibia and others as noted in Chapter 2 (*Literature Review*). However, these studies were focused on relatively smaller pans than Etosha, which limits their catchment sizes and excludes palaeoclimatic implications of atmospheric circulation systems that extend further than the pans. Etosha Pan is comparatively much larger in size (4 730 km^2) and offers an opportunity to investigate past wet phases resulting from a wide range of sources that contributes geomorphological deposits to the pan. Moreover, the position of Etosha, in northern Namibia and closer to the African rainbelt, allows for a closer comparison between the palaeoproxy data and model simulations for northern Namibia.

This Chapter aims to first reconstruct late Quaternary palaeohydrological change at Etosha, with a focus on periods characterised by wetter conditions than modern day. Secondly, the Chapter presents a robust chronological framework using radiocarbon

dating to constrain the timing of the wet phases and to compare those with existing palaeoclimate model reconstructions for southwestern Africa. $\delta^{13}C$ and radiocarbon data from bulk sediments are the key sources of data in this Chapter, and comparisons are made with two palaeoclimate mechanisms that are understood to have influenced Etosha's late Quaternary climate.

The present chapter suggests that, similar to most PMIP 3 model simulations (e.g., Engelbrecht *et al.*, 2019), the LGM palaeoclimate conditions at Etosha were wetter than modern-day. For the mid-Holocene (7 - 5 ka), palaeoclimate conditions have been wetter than for the modern day, but drier than the LGM (Engelbrecht *et al.,* 2019). In addition, the chapter assesses these findings against other records with respect to better identifying the coherence (or not) of hydrological responses to hypothesised regional and global drivers of palaeoclimate change. This has led to an improved understanding of the atmospheric circulation systems that influence moisture availability in the area and can help improve determinations of climate predictions for the future.

Interpretations of these $\delta^{13}C$ data refer to landscape changes of C_3/ C_4 vegetation in the Etosha Basin and their response to changing palaeoclimate conditions over the last 35 k cal BP. Sources of C_3 vegetation in this region include trees, shrubs and woody plants, while most grasses are usually C_4 (Still *et al.,* 2003). The nature of vegetation, whether they are C_3 or C_4 can be influenced by several factors including temperature, precipitation, seasonality and partial pressure of atmospheric CO_2

(Diefendorf *et al.,* 2010). In addition, stable carbon isotope composition values may also be a result of non-terrestrial aquatic sources including dissolved inorganic carbon (DIC), aquatic plants, plankton and algae (Cloern *et al.,* 2002). These factors are considered in making interpretations for the $\delta^{13}C$ data from the bulk sediment samples in this Chapter.

Chapter 2 outlined existing studies at Etosha Pan and how wet phases in the past had been reconstructed. This is particularly in reference to when Etosha's marginal sand ridges are interpreted as shoreline systems, regardless of whether the final accumulation of material is due to direct deposition by water (e.g., on a beach). It could also be through subsequent deposition by wind through material moved to the shore zone by wave action (Figure 6.1). In this Chapter, previously published records are compared with a new record produced in this study. This chapter achieves Objective 3 of the thesis which states: *To reconstruct palaeohydrological history of a spring mound on the basin floor by applying a range of geochemical and sedimentological analyses on sediment cores extracted from it (Chapter 5 and Chapter 6).*

6.2. Existing records of lacustrine phases at Etosha Pan over the last 25 k cal BP

Recent work conducted by De Cort *et al*. (2021) demonstrates the need for reliable proxy records from the Etosha Pan to assist with understanding late Quaternary palaeohydrological changes (Figure 6.1.) Reconstructions of past lake statuses in southern Africa often have large age uncertainties associated with their chronologies

(Figure 6.1; De Cort *et al.*, 2021). Both model and data-driven palaeohydrological records highlight the need for better palaeoclimate data to improve understanding of the impacts of climate drivers such as precession (Engelbrecht *et al.,* 2019). In addition, details of palaeoclimate conditions during the glacial and interglacial periods require a sediment record that extends further than the Holocene in order to understand the long-term behaviour of atmospheric circulation systems during the late Quaternary. This study of a unique record from Etosha, given its location and period of accumulation, has added data that can be used to test some of the hypotheses that have been put forward to explain the late Quaternary geomorphological evolution of the pan.

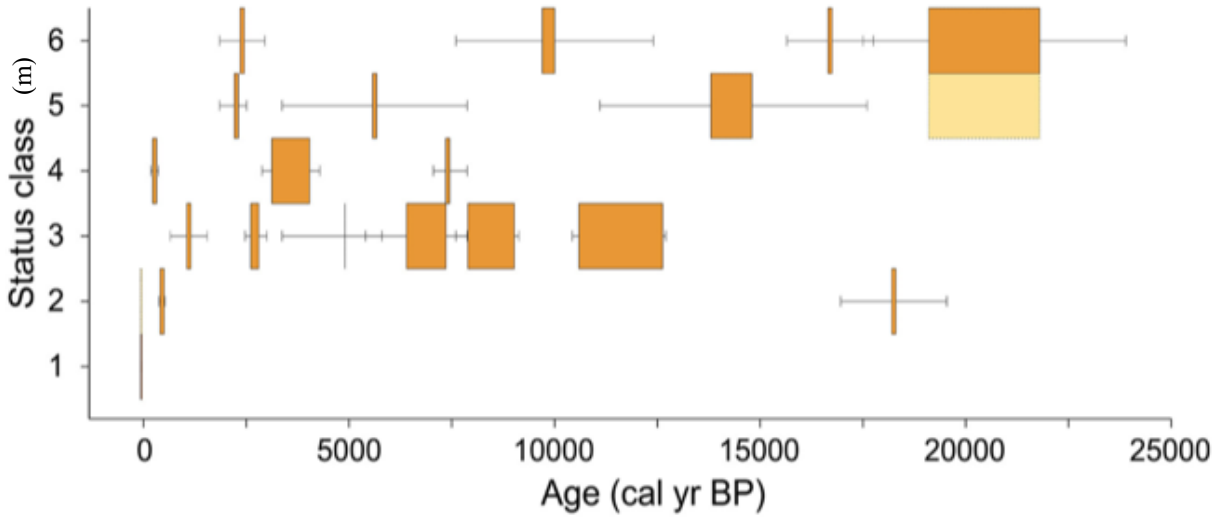

Figure 6.1: Summary of lake high stands from Etosha Pan since 25 k cal BP (De Cort *et al*., 2021). It is a statistical reanalysis of existing data that allows the continuity/gaps in the data to be better teased out. Status class refers to a relative lake level with 1 being lowest and 6 being highest. It assumes that the marginal basin ridges are shorelines. Whiskers represent the uncertainty associated with each high stand.

6.3. Results

In the present study, $\delta^{13}C$ data from sediment cores A and B at Etosha (Figure 6.4) range between (C_4) -15.74 ± 1.32 ‰ (21.85 k cal BP) and (C_3) –24.29 ± 1.76 ‰ (18.58 k cal BP) reflecting greater variability than in the Otjikoto record presented by Tabares *et al.* (2019). The oldest sample in this study occurs in Core A with an age of 33.98 k cal BP and a $\delta^{13}C$ value of (mixed C_3/C_4) -20.86 ± 0.18 ‰ (33.93 k cal BP). Following this, towards 29.32 k cal BP, it increases slightly to (mixed C_3/C_4) -20.21 ± 0.33 ‰ (29.32 k cal BP). At the start of the LGM around 23.50 k cal BP, the $\delta^{13}C$ values lie between (mixed C_3/C_4) -17.1 ± 2.36 ‰ (17.83 k cal BP) and (mixed C_3/C_4) -22.8 ± 2.11 and (mixed C_3/C_4) -22.0 ± 2.44 ‰ (18.52 k cal BP) as measured in Core A and B respectively. From 18 k cal BP, a decrease can be observed, leading to the lowest $\delta^{13}C$ values on the record in the early Holocene with values of as low as (C_3) -24 ± 1.86 ‰ (12.88 k cal BP). Following that period is an increase in the values towards the mid Holocene. During this period, $\delta^{13}C$ values of (mixed C_3/C_4) -19.3 ± 1.19 ‰ (5.82 k cal BP) are recorded in Core A and (mixed C_3/C_4) -21.5 ± 0.61 ‰ (5.34 k cal BP) from Core B.

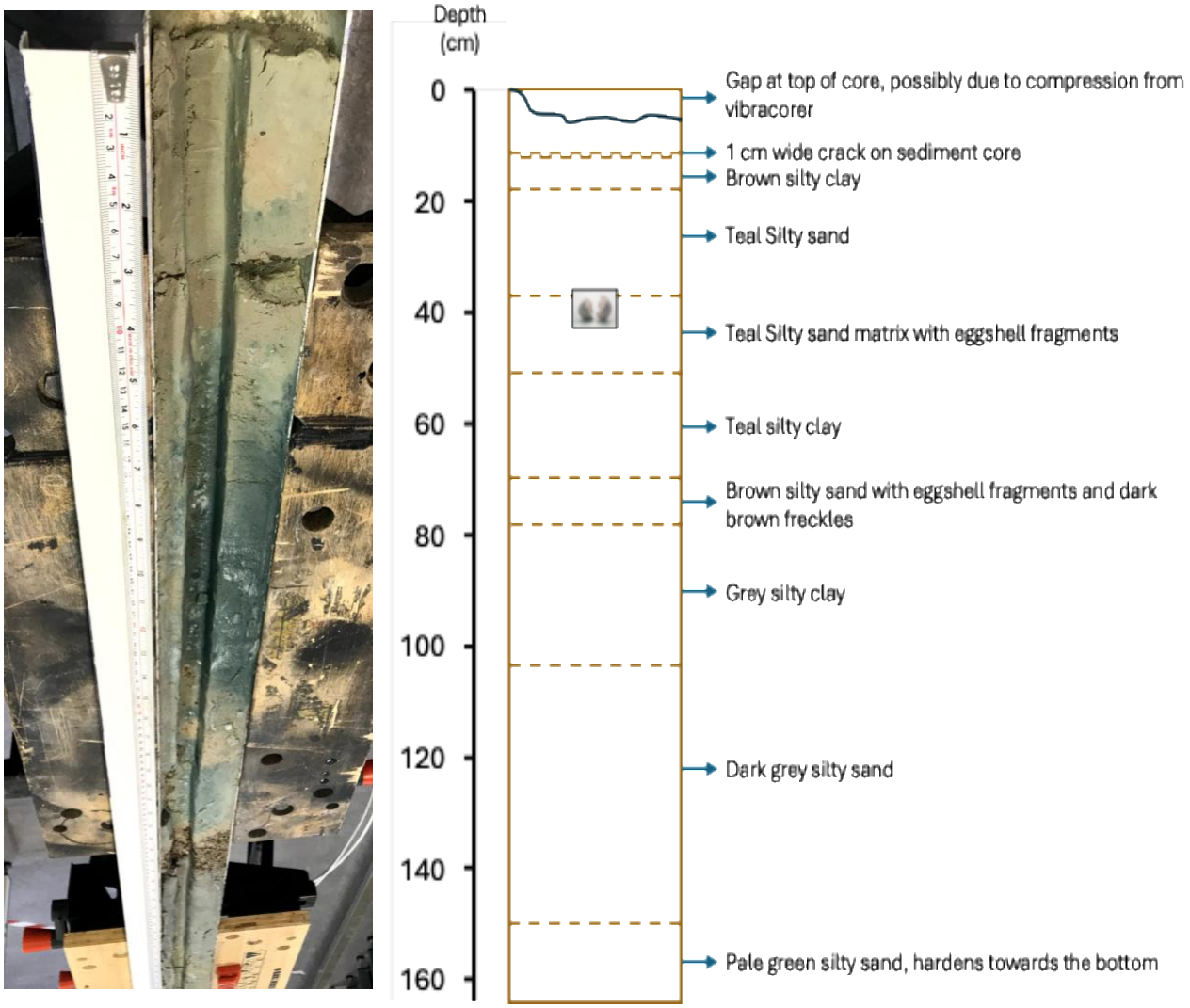

Figure 6.2: Photograph of sediment Core A (ETO 19-3V) (left) and a sediment stratigraphic description sheet of the same core (right). The 1.6-meter core shows distinct sedimentary layers reflecting changing depositional environments. The sequence begins with pale green silty sand at the base (160-150 cm depth), transitioning upward through dark grey silty sand (150-120 cm), grey silty clay (120-90 cm), and brown silty sand with eggshell fragments. The middle section contains teal silty clay (70-50 cm) and teal silty sand matrix with eggshell fragments (50-35 cm), followed by thick teal silty sand layer (35-20 cm). The upper portion consists of brown silty clay (20-15 cm) with a 1 cm wide crack visible in the sediment core, and a gap at the top (15-0 cm) possibly due to compression from the vibracorer. The presence of eggshell fragments in multiple layers suggests periodic occupation by flamingos, while the varied sediment types indicate fluctuating water levels and depositional conditions in this ephemeral lake system

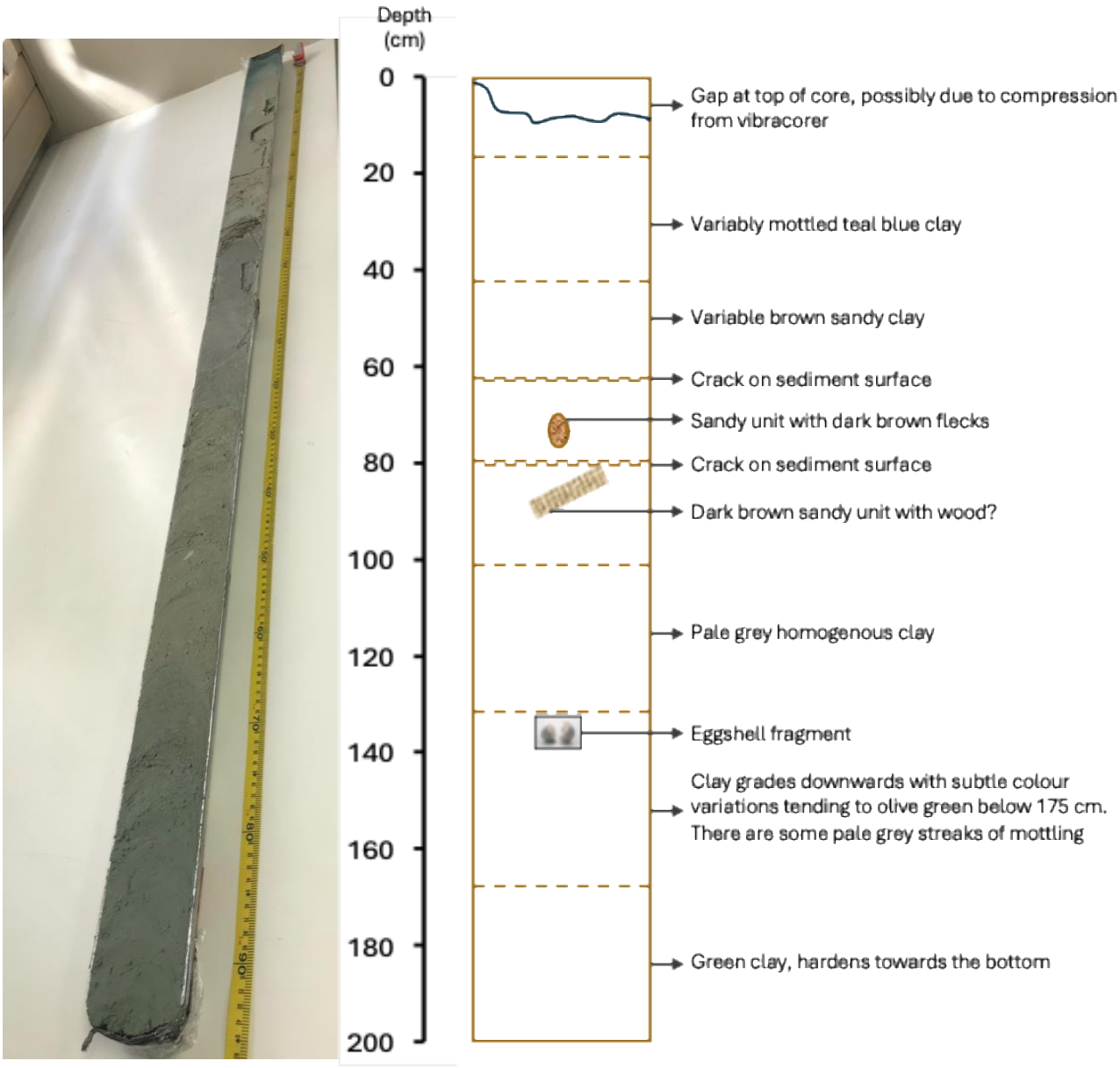

Figure 6.3: Photograph of sediment Core B (ETO 19-4V) (left) and a sediment description sheet of the same core (right). The 2-meter core displays a complex sequence of sedimentary units that are indicative of varying hydrological and depositional conditions in this ephemeral lake system. The basal unit consists of pale green silty sand that hardens towards the bottom (150-200 cm depth), overlain by dark grey silty sand (150-120 cm). The sequence continues upward through grey silty clay (120-90 cm), brown silty sand with eggshell fragments and dark freckles (90-70 cm). The middle section features teal silty sand matrix with eggshell fragments (50-35 cm), followed by teal silty sand (35-20 cm) and brown silty clay (20-15 cm). A 1 cm wide crack is visible in the upper sediment core, with a gap at the top (15-0 cm) likely resulting from compression during vibracore extraction. The recurring presence of eggshell fragments throughout multiple stratigraphic intervals suggests episodic occupation by the avian fauna, while the alternating clay, sand, and silt layers reflect fluctuating water levels and energy conditions characteristic of pan environments in semi-arid regions

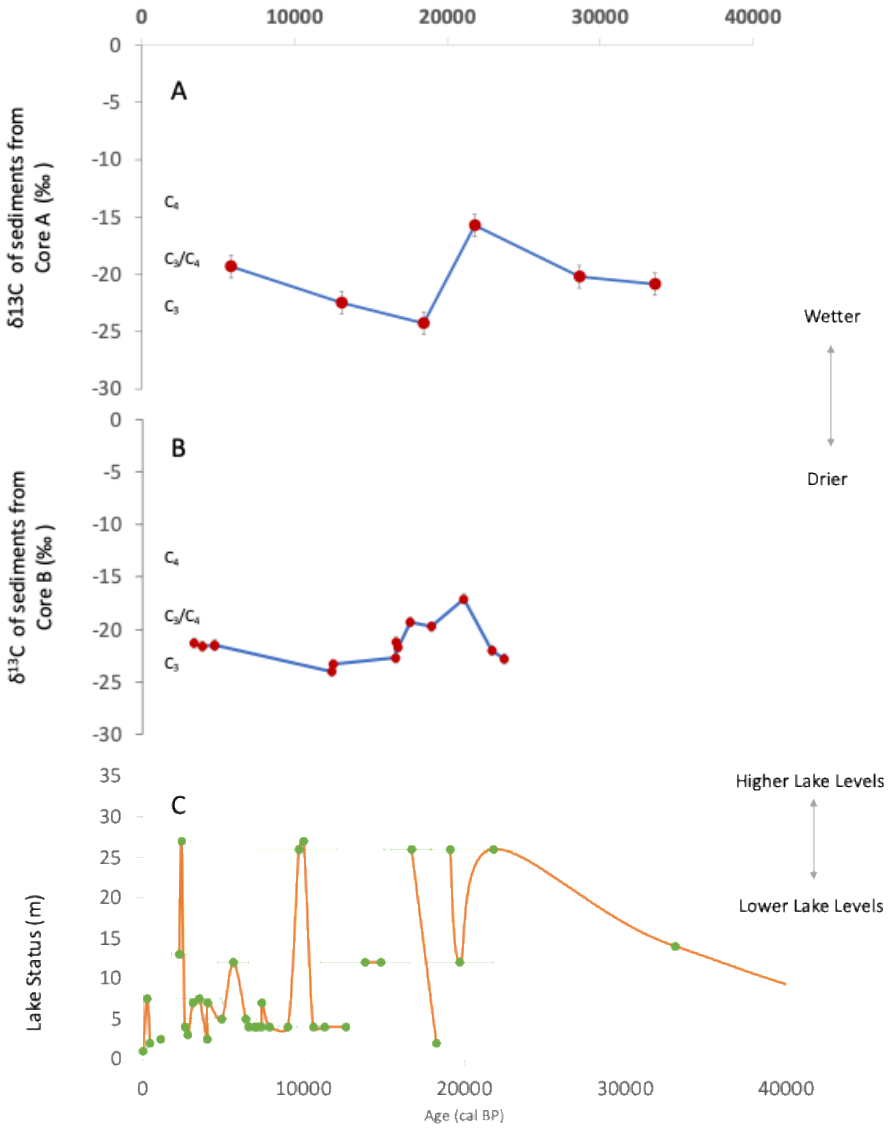

Figure 6.4: A and B = $\delta^{13}C$ of Core A and Core B, all expressed in VPDB (‰) and placed in comparison with C. The figure shows a summary of relative lake levels at Etosha Pan from de Cort *et al*. (2021) including data from Hipondoka *et al*. (2014), Brook *et al*. (2007) and Buch and Zoller (1992). Graphs A and B were constructed using radiocarbon ages, while Graph C includes both radiocarbon and OSL dating methods. Stable carbon isotopes analyses results are from Core A and Core B from the spring on the Etosha lakebed. In purple are the modern-day values of $\delta^{13}C$ with a value of 26 ‰ from both Tabares *et al*. (2019) and Belz *et al*. (2020). All $\delta^{13}C$ are in ‰ VPDB. Error bars reflect standard error of the $\delta^{13}C$ value

6.4. Modern-day $\delta^{13}C$ in Namibia

Tabares *et al.* (2019) examined historical $\delta^{13}C$ data on soil surface samples from Lake Otjikoto, 80 km south-east of Etosha in the same, savanna grassland, vegetation zone. Their study reconstructed vegetation dynamics on the landscape surrounding the lake using multi-proxy analyses (Tabares *et al.,* 2019). Tabares *et al.* (2019) found $\delta^{13}C$ data with a minimum of -27.0 ‰ and a maximum of -20.0 ‰ at a maximum depth of 30 cm at Lake Otjikoto. A bulk sediment-derived $\delta^{13}C$ value of -26.0 ‰ was observed for the year 1950, which is 0 on the cal BP time scale (Tabares *et al.*, 2019). Belz *et al.* (2020) also found a modern-day $\delta^{13}C$ value of -26.0 ‰ at a depth of 0.3 cm based on stable carbon isotopes in sediment core data from Omongwa Pan, 450 km south of Etosha. Concordance of these studies suggest that the modern-day $\delta^{13}C$ range was more widespread in Namibia, thus permitting comparisons among studies that use similar proxies. As the $\delta^{13}C$ values for modern day were similar in these two studies, it is probable that most of Namibia had similar $\delta^{13}C$ values including at Etosha.

6.5. Change in C_3/C_4 Vegetation.

Reconstructing palaeoclimatic changes using evidence from vegetation assemblages requires an understanding of the types of vegetation available in the landscape, and their response to changes in climate and the environment. C_4 plants are more adapted to arid conditions than C_3 plants due to physiological characteristics in their

photosynthetic pathways that help them to use water more efficiently (Ward *et al.,* 1999; Swap *et al.,* 2004). Furthermore, stable isotope ratios of carbon and oxygen in sediments and faunal remains can provide information about past environmental conditions (Lee-Thorp and Sponheimer, 2005). For example, carbon isotope ratios can indicate the relative proportions of C_3 and C_4 vegetation, which are associated with competitive success under different climatic conditions (Lee-Thorp *et al.*, 2007; Luyt *et al.*, 2000). The stable carbon isotope measurements in this study allowed quantifiable tracking of the vegetation community changes. However, interpretations of $\delta^{13}C$ values are complex in dryland environments and have tended to focus on relative aridity. Temperature or atmospheric partial pressure of CO_2 concentrations might also impact community assemblages at the glacial/interglacial scale. C_4 plants are more efficient in photosynthesis than C_3 plants under hot, dry conditions but not under cool, moist conditions (Osborne and Freckleton, 2009; Taylor *et al.,* 2014). However, C_4 plants (mainly grasses in this region) also don't do well under very arid conditions because they are mainly annual grasses that depend on seasonal rainfall. Previous studies have noted that in humid ecosystems, ample rain enables C_3 plants (more depleted $\delta^{13}C$) to dominate over C_4 (less depleted $\delta^{13}C$). In arid environments which have very little rain, C_4 grasses cannot seasonally establish so C_3 shrubs (more depleted $\delta^{13}C$) are prominent. However, in between these two extremes, good seasonal rains enable C_4 grasses (which are mostly annuals but can also include perennials) to be a regular, if not dominant, component of the ecosystem providing an elevated $\delta^{13}C$ signal. Chase *et al.* (2009) interpreted their data to reflect the proportion of C_3 plants (in this environment, generally trees and shrubs with average $\delta^{13}C$ values of about −26 ‰)

versus C_4 plants (mostly grasses and average $\delta^{13}C$ of about −12 ‰). Railsback *et al.* (2022) provide an interpretation using a speleothem from the Dante cave in northeast Namibia. Whilst noting the added complications associated with $CaCO_3$ precipitation, they also suggest that less depleted $\delta^{13}C$ is indicative of increasing C_4 grasses with increasing humidity with their $\delta^{13}C$ range between -17.8 and -16.1 ‰ (Railsback *et al.,* 2022). $\delta^{13}C$ in organic matter is considered to be an excellent indicator of vegetation assemblages (Vogts *et al.*, 2009; Carr *et al.*, 2014). Similarly, Belz *et al.* (2020) also inferred that at Omongwa Pan (700 km southeast of Etosha), less-depleted sediment organic $\delta^{13}C$ values point to a greater coverage of C_4 vegetation during periods of greater moisture availability on the landscape (e.g., increased seasonal precipitation). These interpretations of the $\delta^{13}C$ parameter are from different data sources i.e., speleothem (Railsback *et al.,* 2022) and pan sediments (Belz *et al.*, 2020), however, they follow similar mechanisms in terms of the interpretations, whereby there is reduced contribution of C_4 plants to the $\delta^{13}C$ signal during very arid palaeoclimate conditions. Most $\delta^{13}C$ values in the present study suggest a mosaic of mixed C_3 and C_4 vegetation, while modern day vegetation is largely C_3.

In the hyrax midden record discussed above from Spitzkoppe (Chase *et al.,* 2009), the carbon isotope ($\delta^{13}C$) values ranged between -23.4 ‰ and -17.0 ‰. These values were interpreted to primarily reflect variations in the hyrax diet composition between C_3 plants (trees and shrubs in this environment), that average around -26 ‰, and C_4 plants (grasses) which average around -12 ‰. In essence, the $\delta^{13}C$ fluctuations in the fossil hyrax middens indicate shifts in the proportion of trees/shrubs versus grasses

surrounding Spitzkoppe over time. More negative values represent periods when hyrax diet and the local landscape was dominated by C_3 bushes and trees, while less negative values mark times when C_4 grasses made up a larger part of vegetation cover and animal feeds. To avoid the complication with this, the present study instead refers to the $\delta^{15}N$ data from the Spitzkoppe study as the proxy has been utilised in a more consistent manner between studies.

By providing averaged histogram representations for rain forest and savanna C_3 plants in their study, Vogts *et al.* (2009) presented a more realistic representation of the $\delta^{13}C$ signal that would be found in sedimentary archives. Their study took into account the inherent averaging effect that occurs during post-depositional processes, which could be relevant to the sediment cores investigated in the present study (Vogts *et al.,* 2009). This averaging effect is a result of the mixing of plant organic matter from various growth settings and with different biological life histories. Sedimentary archives do not preserve the $\delta^{13}C$ signal of individual plants, but rather an average signal from a diverse mixture of plants that have contributed their organic matter to the archive over time (Vogts *et al.*, 2009). This makes them more suitable for reconstruction pan-wide palaeohydrological changes.

In this study, we follow the same interpretation as previous studies, more-enriched values of $\delta^{13}C$ infer an ecosystem with more coverage of C_4 grasses on the landscape due to increased seasonal rainfall. As present-day vegetation is dominated by C_3 vegetation, this can be interpreted as wetter than modern-day.

6.6. Lake status interpretation from Etosha $\delta^{13}C$ data

Using the Otjikoto record as an analogue to interpret $\delta^{13}C$ data from Etosha and considering the modern day $\delta^{13}C$ value of -26 ‰ derived from soil surface samples (Tabares *et al*., 2019), the data from this study suggest that Etosha Pan is significantly drier now than it was in the past 34 k cal BP (Figure 6.4). This is according to the $\delta^{13}C$ record presented in Figure 6.4 A and B. It is much drier today than during the LGM period, which can otherwise be identified as the wettest period on the record, as supported by the $\delta^{13}C$ measurements from both cores which were more C_4 enriched during the LGM.

6.7. Palaeoclimate conditions at Etosha Pan over the last 35 k cal BP

According to a reanalysis of regional dune system development by Thomas and Bailey (2017), the north Kalahari (to the east of Etosha) experienced limited dune accumulation during the LGM. Their study was interpreted to indicate reduced dryness and wetter conditions experienced during the LGM. During the mid-Holocene, fluvial activity from rivers on the west coast such as the Huab (Walsh *et al.*, 2022) point to increased humidity in the mid-Holocene period between 7 - 5 ka. The extent of the humidity or dryness in Namibia during the mid-Holocene and the growing suite of palaeoclimate models require more data to test model simulations and reconstruct past environmental conditions during both the LGM and mid-Holocene. Data from the above palaeoclimate studies suggest that there was spatial heterogeneity in Namibia, hence it is important to focus on relatively smaller areas (e.g., Etosha Pan) than to make region-wide conclusions.

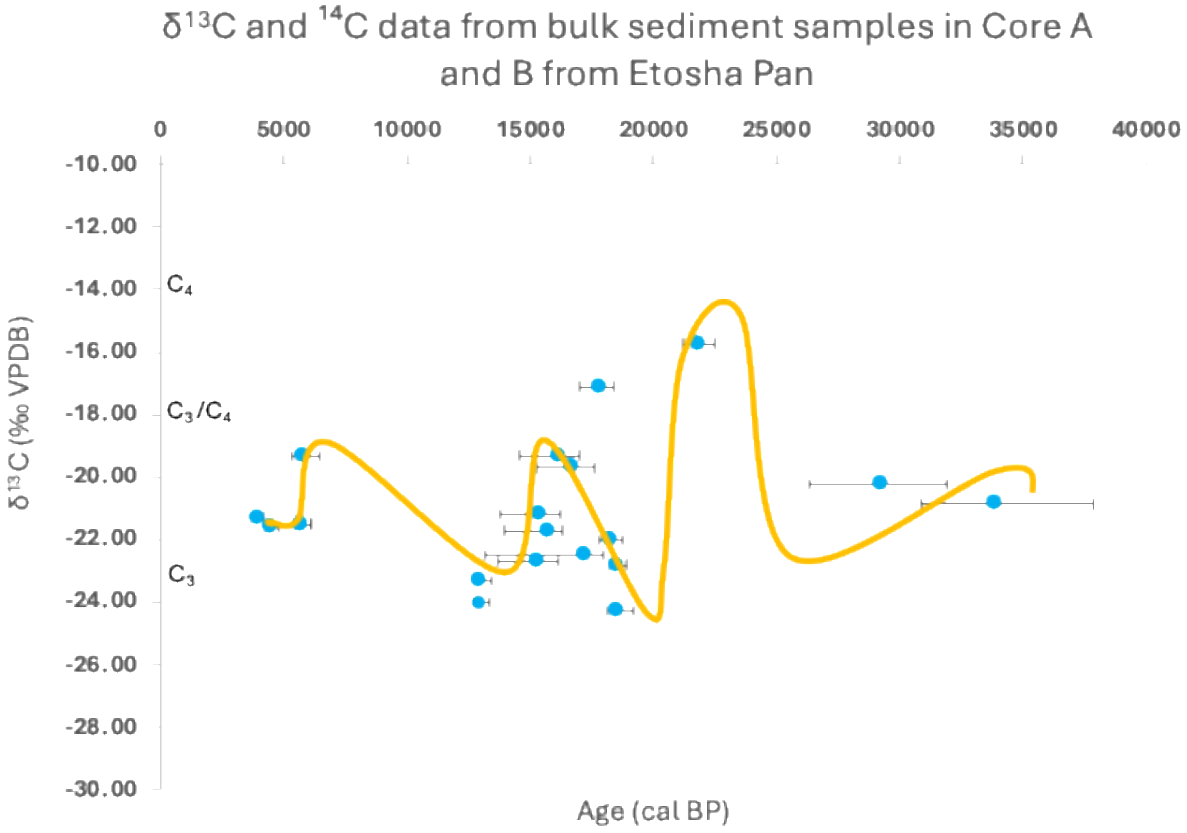

Figure 6.5: Carbon isotope record from Etosha Pan sediment cores over the past 35 ka. The orange line represents the fitted trend through the data points (blue circles) with 1 sigma errors from the BACON model. The record shows significant variability in $\delta^{13}C$ values ranging from approximately -12‰ to -26‰, with notable shifts indicating changes in vegetation composition and/or environmental conditions. More depleted $\delta^{13}C$ (e.g., -22 to -24‰) indicate C_3-dominated ecosystem while less depleted values indicate a dominance by C_4 vegetation.

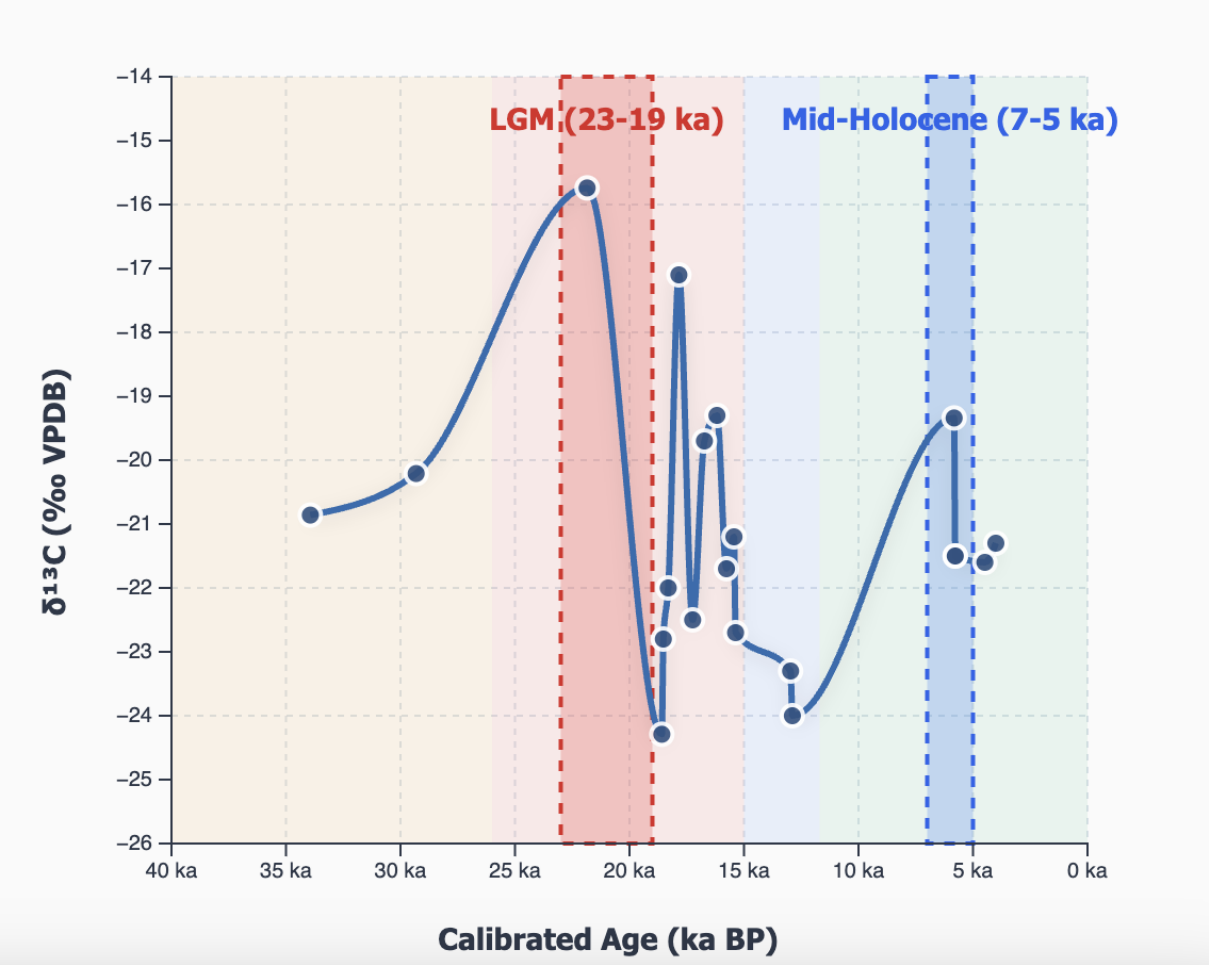

Figure 6.6: Carbon isotope record from Etosha Pan sediment cores showing paleoenvironmental changes over the past 35 ka**.** The data reveal distinct shifts in vegetation and/or atmospheric conditions. The LGM, (23-19 ka BP, red shaded area) is characterised by less negative $\delta^{13}C$ values (with a peak of -15.7 ‰), indicating an increase in C_4 vegetation. The overall trend reflects major transitions in the Etosha pan that were possibly driven by changes in regional and/or local paleoclimatic conditions.

The large range in $\delta^{13}C$ values (8.6 ‰) of the Etosha records indicates that, over time, the pan's ecosystem has been responded to climate variability, as indicated by shifts in C_3 and C_4 vegetation. Specifically, the late Pleistocene at Etosha, between 35 and 29 ka, had relatively stable $\delta^{13}C$ values that ranged between -21 to -20 ‰ with a mix

of C_3 and C_4 vegetation communities. The LGM period at Etosha was highly variable: the most extreme $\delta^{13}C$ values of -15.7 to -24.3 ‰ are observed, indicating an environment that was rapidly changing, perhaps due to the post-LGM deglaciation and the sudden change in temperatures and regional moisture. The high $\delta^{13}C$ of -15.7 ‰ was likely driven by an expansion in grasslands during peak glacial conditions. The period between the LGM and the mid-Holocene was moderately variable, with vegetation transitions captured by $\delta^{13}C$ values of between -21.2 and -24.0 ‰ and a dominance of C_3 vegetation. Following this, the mid-Holocene period has $\delta^{13}C$ values that ranged from -19.3 to -21.5 ‰, leaning more towards an enhanced domination of C4 vegetation which characterizes it as a humid period.

6.7.1. Etosha Pan during the late glacial maximum (LGM) (23 - 19 k cal BP)

Model simulations by Engelbrecht *et al.* (2019), suggest the LGM was characterised by wetter than modern-day climate across southern Africa. However, the model simulations also indicate variability in precipitation patterns based on orographic and ocean circulation influences. Similarly, the $\delta^{13}C$ data in this study suggests that the LGM was wetter than the modern-day at Etosha. The periods between 21.78 k cal BP and 19.46 k cal BP are characterised by high $\delta^{13}C$ values of -15.74 ± 1.32 ‰ and -19.7 ± 2.50 ‰ respectively, which indicate increased C_4 grasses indicative of wetter than present conditions when compared to a modern-day $\delta^{13}C$ value of -26.0 ‰. This would result in overall greater vegetation biomass on the landscape, with the C_4 grasses making marginal contributions to the $\delta^{13}C$ signal in the sediment cores, unlike during arid conditions. This suggests that during these periods (21.78 - 19.46 k cal BP),

the catchment of the Etosha might have been under a wetter climate and led to the greater discharge of water-lain sediments with in-wash of allochthonous organic material into the which could result in higher lake levels on the pan. However, an alternative or compounding explanation is that the regional vegetation was also affected by global $ppCO_2$ which was lower during the LGM (~ 180 ppm) in southern Africa (Bragg *et al.,* 2013). C_3 grasses are less efficient under low palaeoatmospheric $ppCO_2$ levels and warm conditions (Boom *et al.,* 2002). Therefore, the LGM was possibly cooler, with low CO_2 and therefore increased C_4 elements mixed with smaller a C_3 component.

Offshore marine cores analysed by Collins *et al.* (2014) resolved that the wettest period in this region of southern Africa in the last 140 ka was the LGM. More negative δD values of leaf-wax n-alkanes reported by Collins *et al.* (2014) suggest that during the last glacial period, the primary source of increased rainfall was the tropically sourced moisture sources, rather than the northerly-tracking winter-westerlies.

Belz *et al.* (2020) found an enrichment in deuterium within their biomarker record at Omongwa Pan during the LGM and concluded that winter rainfall was not a significant contributor to the moisture at Omongwa Pan during the last glacial. The same trend is observed at other time periods with wetter than modern-day climate on their record within the last 27 k cal BP. They argued that the source of precipitation remains more likely to have been derived from other sources, such as Indian Ocean summer rainfall (Belz *et al.*, 2020). Schuller *et al.* (2018) also interpreted increased sedimentation in

five southern Namibian pans to have resulted from higher precipitation. Therefore, the high sedimentation rate observed at Etosha during the LGM is likely driven by higher sediment inputs from the catchment carried through the Ekuma Delta during wet phases in summer (Figure 6.4). Wet conditions are recorded at 23 - 19 k cal BP at both Etosha and Omongwa, located 700 km, to the south. It is reasonable to assume that the same mechanism drove precipitation increases at both locations at this time, with intensification of austral summer tropical rain belt incursion the most probable cause (Collins *et al.*, 2014; Schuller *et al.,* 2018). Collins *et al.* (2014) also ascribed increases in $\delta^{13}C$ from core MD08-3167 to indicate increased summer wetness due to the intensification of the tropical rain belt over Namibia. Dynamics behind the southward shifting of the rainfall belt during spring and early summer are not yet fully understood (Nicholson, 2018). However, there are still unresolved questions around the seasonal migration of rainfall in southern Africa and what controls the timing of the rainfall belt's southward movement. Further examination of present-day seasonal rainfall transitions is required to better understand and predict potential future shift dynamics under climate change.

6.7.2. Etosha Pan during the mid-Holocene (7 to 5 k cal BP)

During the mid-Holocene, most simulations of the PMIP3 models indicate drier conditions in central and northern Namibia including Etosha Pan, when compared to pre-industrial climate conditions (Engelbrecht *et al.*, 2019). Wetter areas are confined to parts of the western coastal regions, while the interior, including Etosha Pan, seem to have experienced reduced precipitation minus evapotranspiration (Engelbrecht *et*

al., 2019; Liu *et al.*, 2019). Similarly, PMIP4-CMIP6 models suggest a drier mid-Holocene resulting from lower sea-surface temperatures that led to reduced advection of moisture and consequent increased aridity on land (Breierley *et al.*, 2020). In contrast, most evidence from the present study point to a wetter than present climate at Etosha. The $\delta^{13}C$ record from this study suggests though that the mid-Holocene was wetter than present, but drier than the LGM (Figure 6.6) with isotope values of -19.3 and -21.5 ‰ indicating C_3 vegetation with some mixed with C_3/ C_4 when compared to the modern analogue of -26 ‰. Previous interpretations have inferred that extended period of low sea surface temperature gradients between the tropics and subtropics, along with associated weaker trade winds during the mid-Holocene and a weakened Congo Air Boundary allowed moist Indian Ocean air masses to move into the Etosha Pan area, leading to more humid conditions and higher lake levels (Brook *et al.*, 2007). Their study was supported by OSL dating and they reported 3 brief periods of high lake status inferred from shoreline construction during 6,4, 6 - 5 and 4 ka (Brook *et al.*, 2007). This finding aligns with results from the present study that show higher $\delta^{13}C$ values indicating more moist-adapted C_3 vegetation. In addition, Brook *et al.* (2011) noted from stromatolite ages that spring flow on the east of Etosha Pan was much higher between 7 – 6.5 k cal BP. The present study furthers their findings with more precise dating and $\delta^{13}C$-based lake level reconstruction, and it complements the findings by Brook *et al.* (2011) that the pan sustained lacustrine conditions that were wetter than present-day. A wetter than present mid-Holocene was also suggested by Hipondoka *et al.* (2006) using fossils of an extinct ungulate found at the Ekuma Delta during the mid-Holocene (5 to 4.5 k cal BP).

6.7.3. Comparison with other terrestrial studies (rock hyrax middens) in Namibia

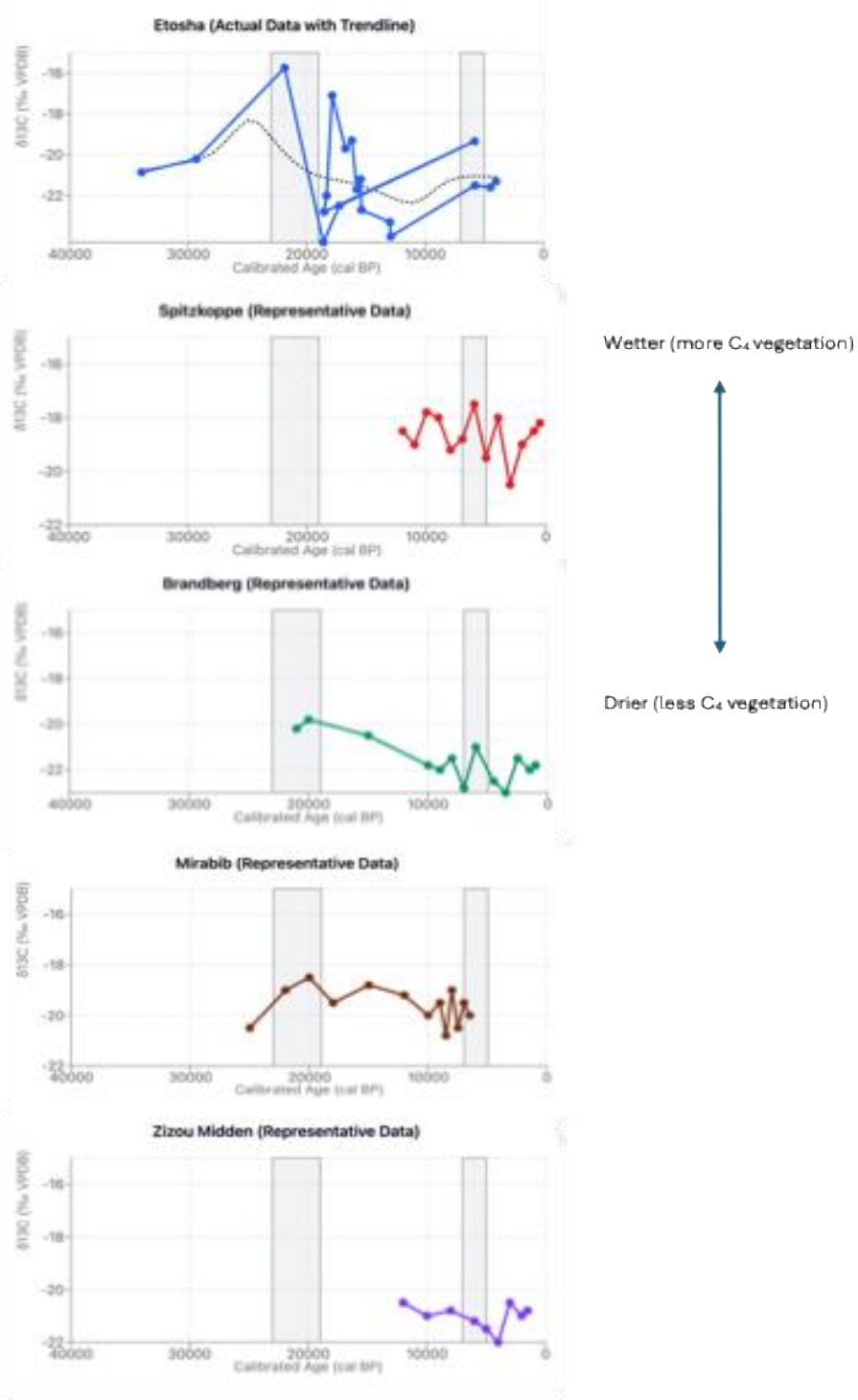

Figure 6.7: Composite diagram showing $\delta^{13}C$ data from Etosha Pan sediment cores compared with data from four rock hyrax midden sites in Namibia spanning 35 ka. The LGM (23-19 ka) and the mid-Holocene (7-5 ka) periods are highlighted in grey rectangles. The graphs are sourced from Etosha (This study), Spitzkoppe (Chase *et al*., 2009), Brandberg (Scott *et al*., 2004), Mirabib (Scott *et al*., 2008) and Zizou (Chase *et al*., 2019).

Key interpretations from Figure 6.7 shows that the Etosha records covered the longest period going further back into the late Pleistocene than the other four records. In addition, the trendline of the Etosha sediment cores indicates a prolonged wet period recorded with a larger coverage of C_4 vegetation composition from 35 to 19 ka. This period suggests that the LGM was wet and was followed by a transitional phase that likely featured a mix of C_3 and C_4 vegetation, with a trend towards aridity. The intermediate period underwent another rise in $\delta^{13}C$ values to -21 ‰, which is comparable to that of Spitzkoppe (Chase *et al.,* 2009) that also suggested a wetter-than-present mid-Holocene. In contrast, $\delta^{13}C$ data from Brandberg (Scott *et al.,* 2004) indicates that the diet of the rock hyrax middens was mostly composed of C_3 vegetation, and indicated progressive aridity from the mid-Holocene to the present (Figure 6.7). While the Etosha record demonstrates the greatest variability in the total time period covered, the Mirabib (Scott *et al.,* 2008) record shows moderate variability, however it accords with the reconstruction of Etosha's palaeovegetation changes that indicate a mid-Holocene that was wet, but not as wet as the LGM. Covering the shortest period, the Zizou (Chase *et al.,* 2019) midden suggests a mid-Holocene that is much drier than the present, with more negative values after the mid-Holocene.

Overall, these data imply that there were temporal and spatial variations in Namibia during the period covered. There is no uniform signal among all the sites, particularly during the LGM and the mid-Holocene. This suggests that each site may have been responding to complex regional and local shifts in palaeoclimate in different ways.

The datasets suggest that in general, terrestrial Namibia was mostly arid over the past 35 ka, with episodes of wetter periods that occurred at different points in time.

6.8. Conclusion

The data presented in this Chapter contribute a better understanding of LGM and mid-Holocene conditions at Etosha. Previous palaeoclimate studies had inferred that Etosha Pan over the last 25 ka was wet at both the LGM and the mid-Holocene (Brook *et al.,* 2007; Hipondoka, 2005; Hipondoka *et al.*, 2006). The present study aligns with these findings; however, the mid-Holocene was found to be drier than the LGM. On the other hand, most PMIP 3 palaeoclimate models over northern Namibia suggested wetter than modern-day LGM and mid-Holocene (Engelbrecht *et al.*, 2019) over the Etosha basin. The sedimentological and geochemical data presented in this study has helped to reconstruct palaeohydrological changes in the northern Namibia region. More precisely, the present study at Etosha suggests a mid-Holocene that is wetter than modern-day, but drier than the LGM. This suggests the tropical rain belt behaved differently (potentially wider in latitude extent and/or shifted southward) during the mid-Holocene (MH) period, which is also in agreement with model simulations from Williams *et al.* (2020) using HadGEM3-GC3.1. This study furthers the discussion by demonstrating that, while the mid-Holocene was wetter than present, it was not as wet as the LGM. This finding can be used in climate models to improve understanding of climate drivers over this region. The reconstruction in this study, based on data from the spring mound, has helped to achieve Objective 3 of this study.

Chapter 7 – Discussion

AIM: This project aims to generate a robust dataset to establish the chronology and palaeoenvironmental context of Etosha Pan through multi-proxy analyses of sediments on the lakebed and marginal sand ridge to reconstruct late Quaternary palaeoclimatic conditions of northern Namibia

7.1. Introduction

This project has advanced the current understanding on the late Quaternary geomorphological evolution of the Etosha Pan. The 11 finite OSL ages and 28 radiocarbon dates provided a chronological framework upon which to interpret the geomorphic changes on the basin during the period 40 ka to the modern-day (Chapter 4). Chapter 5 detailed palaeoecological insights from the pan and demonstrated the potential of flamingo eggshell fragments in reconstructing late Pleistocene environmental change. This is the first published record of flamingo eggshell with palaeoenvironmental potential in Namibia. In Chapter 6, evidence from stable carbon isotopes and particle size analyses underpinned by a robust radiocarbon dating dataset (28 radiocarbon ages) provided information that supports current palaeoclimate understanding of a wet LGM (23 - 19 ka), and mid-Holocene (7 – 5 ka) that is drier than the LGM and wetter than modern-day. The objective of this Chapter is to summarise and discuss findings from this study presented in the previous three Chapters (4,5,6) and linking these with wider palaeoenvironmental reconstruction records in the region. Key findings suggest that basin evolution occurred under the control of palaeoclimate changes that resulted in the formation of distinct geomorphological landforms. Moreover, the interplay between fluvial and aeolian

processes led to the development of sand ridge features that allowed palaeohydrological reconstruction on the pan since the late Pleistocene. The following section presents an assessment of the chronological framework adopted in this study. For the data comparison, the Chapter draws heavily on 2 studies that were also conducted on the western sand ridges of the pan i.e., Brook *et al.* (2007) and Hipondoka *et al.* (2014), as well as findings from Brook *et al.* (2011) who conducted radiocarbon dating on stromatolites from the east of Etosha Pan near Poacher's Point.

7.2. Assessment of chronological framework

OSL and radiocarbon dating have been used as rigorous chronological tools in this study. Few outliers and dating uncertainties were present in the radiocarbon models, possibly resulting from measurement and sampling uncertainties, or sediment reworking. Despite these challenges, the dual dating approach was applied successfully and has demonstrated great utility in setting a firm foundation upon which data in this study were analysed and interpreted.

7.2.1. Radiocarbon dating

Radiocarbon dating provided a continuum of ages based on Bayesian statistics and suggested that Core A covered the last 40 k cal BP. The accumulation history of Core B over the 2 m depth covered the last 25 k cal BP. During these periods, no visible break in sedimentation was observed on the sediment cores. The age-depth model (BACON) suggested that Core A had a varied relationship between age and depth, indicating that the accumulation rate was steady over the last 40 k cal BP. This may

be because of a microscopic stratigraphic hiatus that resulted from a break in sedimentation. Low dating resolution may have meant that breaks in sedimentation were unidentified so that the age depth model is an oversimplification. In these systems where deposition is rarely continuous and sedimentation rates may change radically, a very high sampling resolution is required in order to generate a robust age model.

Age reversals were also observed in Core B between 164 cm (15,680 ± 76 BP), 185 cm (19,550 ± 165 BP) and 196 cm (15,200 ± 79 BP). While these were excluded from the BACON model, they are valid and need to be considered in context. To overcome this, thin 5 cm sections were used to build the models, and these helped to smoothen out the age-reversals. These reversals may have occurred because of geomorphological processes associated with spring flow whereby older sediments may be introduced into the system perhaps from a raised underground water table, resulting in a reworking of sediments. During periods with strong aeolian processes, it is also likely that organic material within sediments may become redeposited after long periods of deflation. Similarly, when lake levels are higher, localised minor turbidity currents can lead to sediment reworking. It is not possible to exclude either of these processes based on the data available in this study.

Age-depth relations can also be influenced by how the BACON model treats outliers. Two samples from the same depth (55 cm) had different ages: 4,170 ± 71 and 5,130 ± 70 BP (Figure 5.4). These may be due to different organic compounds being dated from that depth or bioturbation processes that can rework sediments. Bayesian

statistics help in isolating outlier events and determining the likelihood of certain samples being outliers. Thus, the age models in this study can be utilised with confidence, because outliers and age-reversals were accounted for. In these cases, the calibration used in BACON were used, and the age-depth relationships, rather than individual calibration of samples using software such as Calib or OxCal. This is because, the Bayesian statistics used by BACON are more robust and take accumulation history into account when building the models. As such, BACON results were adopted in order to have consistency in the ages. High sampling resolutions were used for radiocarbon dating. A total of 28 ages were analysed for the entire 360 cm (sum of both cores' depths), which is roughly one date every 13 cm. This interval helped to sharpen the age-depth models.

7.2.2. OSL dating

Finite OSL ages in this study ranges between 0.59 to 40.05 ka with three distinct periods: (<1 ka): ETO 19/5/1 (0.59 ± 0.04 ka), (2-10 ka): ETO 15/1/1 (8.69 ± 0.82 ka), ETO 15/2/1 (8.45 ± 0.64 ka) and (>10 ka): ETO 15/2/2 (40.05 ± 2.72 ka). This dataset has older ages than those from Brook *et al.* (2007) and Hipondoka *et al.* (2014) and has thus extended the temporal coverage at the pan i.e., while Brook *et al.* (2007) found Holocene ages from the sand ridges (2.1 - 6.4 ka), Hipondoka *et al.* (2014) dated deposits that covered up to 22 ka on the same landforms. The present study though has better coverage of intermediate ages between those previously reported, suggesting more continuous deposition compared to the discrete periods from existing studies. However, there are some similarities among the three data sets: they have

preserved multiple phases of deposition including very recent (<1 ka) and mid-Holocene (2 - 8 ka). Moreover, these age-determination datasets have good precision levels (5 – 15 % relative errors). Methodologically, however samples from the present study have lower overdispersion values, than those from Hipondoka *et al.* (2014) which range from 20 – 63 % possibly due to poor bleaching, post-depositional mixing, aliquot size or varying values of sigma b used to calculate overdispersion. Regarding saturated OSL samples, this study has presented a broader range of minimum ages ranging between 50 ± 3 ka (ETO 19/8/3) and 195 ± 10 ka (ETO 19/7/3) indicating that the lakebed and ridges are likely much older than has been recorded by studies at Etosha thus far. In this way the present study has improved the quality and temporal coverage of OSL ages at Etosha, and these supplemented the radiocarbon data. Moreover, these ages form a firm base for the interpretations of different proxy data on both pan floor and sand ridges.

7.3. Proxy representation

Palaeoenvironmental reconstruction using proxies needs to take into consideration the fact that there are several factors that can affect how each proxy is represented in the sediment record. For example, at Etosha, northern areas at the main river inlets experience more rainfall and sediment input through fluvial processes than the southern areas. Increasing distance from fluvial sources can lead to some proxies becoming less represented on the sediment record (Walsh *et al.*, 2022). This would be different to proxies that can withstand flood frequencies occurring on the north of the pan and therefore become better preserved. In addition, historical changes in the

migration of river channels can also affect the distribution and representation of some proxies in the sediment record. Thus, these factors need to be considered when interpreting data from proxies.

7.3.1. Diatoms

The lack of preservation of diatoms on the north-western part of the pan does not provide conclusive grounds for geochemical and hydrological processes that took place on the entire pan. Diatoms can be used as a proxy for localised hydrological processes in lacustrine environments (Stanisch *et al.,* 2011; Pfister *et al.*, 2017) and are therefore unlikely to reflect regional changes in palaeoclimate. Moreover, the absence of diatoms in the record from the current study suggests that specific paleoenvironmental conditions that might have damaged the diatoms remain. For example, high pH and high levels of salinity can dissolve silica frustules (Barker *et al.,* 1994). In addition, salt crystallisation can lead to breaks in surface sediments which can lead to mechanical breakdown of diatoms, causing breaks in sedimentation. It would be worth probing similar aged sediments on the east of the pan to investigate whether the lack of preservation of diatom assemblages occurred on that part of the pan as well.

7.3.2. Stable carbon isotopes data

While bulk sediments of $\delta^{13}C$ generally represent regional changes in vegetation and thus moisture availability, their response differs in salt pans from other terrestrial environments (Beuning *et al.,* 2003; Belz *et al.,* 2020). Therefore, it is important to note that $\delta^{13}C$ interpretations are context-specific and can be improved by using multiple

proxies. The present study assumed that the $\delta^{13}C$ signal is a representative of vegetation changes and palaeorainfall patterns from the northern part of the Cuvelai-Etosha catchment area. $\delta^{13}C$ data in sedimentary basins can incorporate aquatic material, dissolved inorganic carbon, changes in partial pressure of atmospheric CO_2 and temperature (Campeau *et al.,* 2017). In this way the $\delta^{13}C$ serves as a reliable proxy that likely represented regional paleoenvironmental changes that also influenced changing lake levels on the pan and palaeoclimatic changes. The findings from $\delta^{13}C$ data were affirmed by sedimentological and radiocarbon data found in the same sediment cores.

7.3.3. Flamingo eggshell

18 flamingo eggshell fragments were analysed for $\delta^{13}C$ and, with the available radiocarbon data, produced information that enabled the reconstruction of flamingo breeding on the western part of Etosha Pan. These data suggests that flamingo breeding occurred at an extended temporal resolution from 19.5 – 19.15 k cal BP to 16.2 – 15.85 k cal BP and from 13.15 – 12.85 k cal BP to 12.25 – 11.95 k cal BP. The shells were found in both sediment cores, implying that their breeding site was expanded around and potentially beyond the spring.

7.4. Biological indicators

Poor preservation of diatoms and n-alkanes suggests that the pan experienced alkaline, arid and high temperature, strong aeolian process or other environmental conditions that prohibited their preservation. It is likely that both were present during

periods of high lake levels as they are associated with aquatic environments. The availability of $\delta^{13}C$ data, however, created an avenue for reconstructing vegetation changes in relation to palaeoclimate conditions that influence their coverage on the landscape.

7.4.1. Vegetation changes and productivity

$\delta^{13}C$ data from bulk sediment served as a reliable proxy in this study as they helped to reconstruct vegetation changes over the last 40 ka and highlighted wet conditions during key periods such as the LGM and the mid-Holocene (Figure 6.6). This is critical information that assists in understanding the pan's ecological histories and lake level changes which can provide information about the pan's relationships with broader palaeoclimatic changes in the region.

$\delta^{13}C$ data on flamingo eggshell fragments were successfully collected, however, they were not interpreted further due to the lack of an existing study that contextualises the changes in $\delta^{13}C$ of the shells in relation to palaeoenvironmental changes. Future studies can examine this relationship closely to help deepen understanding of flamingo breeding and the clues they can provide about environmental changes. Uncertainties in this proxy can be influenced by preservation biases and post-depositional alterations, and these cannot be excluded using data provided in this study. To an extent, preservation of these shells was facilitated by breeding processes of flamingos that involve the birds trampling on the shell-bearing mud to build their nests. This compacted substrate very likely helped to preserve the shells over time. In future, other

studies could sample sites closer to the spring to have a better estimation of the size of the flocks, changes in $\delta^{13}C$ and $\delta^{18}O$ and further examine water chemistry and palaeoenvironmental reconstruction changes represented by the shells and sediment matrices where they are preserved.

Pollen is another an excellent indicator of vegetation changes in palaeoenvironmental reconstruction studies; however, it is often not preserved in sites based in the drylands of southern Africa. Investigation of pollen spores in the Etosha sediment record was outside the objectives of this study. Perhaps in future, pollen preservation can be investigated in the sediment cores or from other locations on the pan. Moreover, changes in pollen over time can help to distinguish between local and regional signals because Etosha Pan is largely unvegetated.

7.4.2. Microbial activity

aDNA analysis assisted in isolating the greater flamingo as the main species that bred on the pan during those periods. Phase 1: ~19 k cal BP to 16 k cal BP and Phase 2: From 13 k cal BP to 12 k cal BP (Figure 5.5). Furthermore, it provided information on microbial activity preserved on the eggshell fragments which helped in reconstructing eco-system changes on the pan. *Alcanivorax, Halobiforma, Haloterrigena, Natrialba, Paracoccus, Pseudomonas, Spirochaeta, Thioalkalivibrio* and *Acidihalobacter* species which are adapted to arid, saline and high temperature environmental conditions were found during the aDNA analysis and helped reconstruct the water chemistry during the times of flamingo breeding that are preserved in the sediment record (Figure 5.2).

Perhaps in future, it would be worth investigating the presence of and changes in other biological indicators such as biomarker and ostracod assemblages that can provide information about lake levels and other hydrological responses of the pan to changing palaeoclimatic changes.

7.5. Sedimentological indicators

Grain size distributions were well preserved in the sediment cores and helped to understand changes in depositional energy during wet vs. dry periods. The data were processed through rigorous statistical methods in Gradistat version 9.1 (Blott and Pye, 2001). Both cores were sampled at 1 cm resolution to unveil sedimentological changes on the lakebed over the last 40 k cal BP at a finer resolution (Figure 5.7). Each OSL sample from ETO 19/5, ETO 19/7 and ETO 19/8 were also analysed for grain size changes. Grain size data for the sand ridge samples from ETO 15/1, ETO 15/2 and ETO 15/3 were not available. Microscopic stratigraphic discontinuity (chronological hiatus) likely occurred as suggested by radiocarbon dating results between 85 cm (eggshell), 85 cm (bulk sediment and 86 cm (bulk sediment) (14270 ± 80 BP, 15900 ± 84 BP and 16480 ± 87 BP respectively) in Core B. While the BACON model smoothened them out and eliminated the outliers, this discontinuity has a palaeoclimatic significance in that it represents sediment loss during those periods and can create a gap in interpretations during that period.

At Etosha, sand is primarily deposited through fluvial and aeolian processes (Hipondoka *et al.*, 2004). These can be differentiated by the sorting of sediments,

whereby, the Ekuma Delta would discharge large amounts of poorly sorted sand during floods, while aeolian processes typically deposit finer, well-sorted sediments. Overall, fluvial grain sizes are more varied near the deltas as grain size decreases from proximal-to-distant ends of the river channels (Weismann *et al.*, 2015; Carbonneau *et al.*, 2005).

For the OSL samples in sampling sites ETO 19/7 and ETO 19/8 near the Ekuma Delta, the coarse particles were poorly to extremely poorly sorted, suggesting that they were likely deposited during rapid floods (Figure 5.7). Therefore, the periods with increasing poorly sorted sand can be characterised as periods of higher lake levels with high depositional energy likely arising from increased rainfall upstream. Sediments from these periods (minimum OSL ages of 195 ± 10 ka in ETO 19/7/3 and 43 ± 2 ka in ETO 19/8/1) contain low sand contribution, suggesting a decreased role of the Ekuma Delta, a drier climate and weaker fluvial processes. An alternative explanation is that, while deposition of sand was low, aeolian processes could have eroded geomorphological evidence and limited the accumulation of sandy particles.

7.6. Reconstruction of hydrological changes and lake level fluctuations

The suite of proxies utilised in this study enabled the identification of key environmental phases where they confirm major geomorphological and palaeoclimate changes. Below is a summary of the major periods where changes were identified from the records analysed.

7.6.1. Asynchronous proxy responses from 40 to 33 ka

The OSL and $\delta^{13}C$ data from this study exhibit asynchronous responses during the period 40 to 33 ka. Firstly, the radiocarbon data (Figure 5.3 and Figure 5.4) suggest that the spring was above the water level during this period and possibly formed calcrete from the carbonate-rich groundwater precipitating on the pan's surface under high evaporative conditions (Nash and McLaren, 2003). This implies that Etosha had extremely low lake levels during this period. Similarly, more depleted $\delta^{13}C$ data (e.g., -20.86 ‰ at 34 ka) suggests that the period was drier than the LGM and Holocene. However, endmember 3 (Figure 5.8) from EMMA grain size data is enriched in clay (>40 %) during this period, suggesting a low energy depositional context. This end-member (3), accounting for 9.66 % of the variance in Core A and 20 % in Core B, is most dominant in the 36 - 34 ka period. This suggests a calm environment, with deep and still water conditions that enabled fine particles to settle out of suspension. During this period, it is likely that there was minimal wave action as observed in shallow coastal lagoons in semi-arid areas (Renaut *et al.,* 2023). These sedimentological data thus contrast $\delta^{13}C$ data which rather suggest drier conditions. The asynchronous proxy response might result from time lags in $\delta^{13}C$ response to ecosystem changes or sediment mixing during dry/wet periods or during periods of extensive aeolian deflation.

7.6.2. Wet LGM with a deep lake (23 to 19 ka)

As cited in Chapter 2, Brook *et al.* (2007) estimated that Etosha sustained high lake levels ranging between 8 - 20 m in the late Pleistocene. The present study improves on this reconstruction by contributing an age estimation of 23 - 19 ka period (LGM),

when the pan sustained high lake levels. Sedimentological data from this study also affirm the reconstruction that the pan indeed was under a wet, stable environment with 85 to 90 % well-sorted silt content. The negative loading in sand represented by EM1 suggests that there was major reduction in high energy transport mechanisms (Figure 5.8) during the LGM. This could result from reduced fluvial or aeolian processes that contribute sand to Etosha Pan. During this period, EM2 (silt rich) dominated the sediments signifying a low energy depositional environment. This is consistent with stable high lake levels sustained by low energy sediment transport to the site suggested by $\delta^{13}C$ data (Figure 6.4). During the LGM, $\delta^{13}C$ values were the highest observed on the record captured by both cores (between -15.74 to -19.7 ‰ during 23 - 19 ka period). The lake would need to have been deep enough for organic matter to accumulate and settle. During a much wetter climate, coverage by C_3 vegetation and C_4 grasses would increase on the landscape, making a greater contribution to the $\delta^{13}C$ signal than during dry conditions when they are limited (Railsback *et al.*, 2022).

In the present study, the variable sand input (9 – 13 %) during the LGM is noted and likely represents minor sand deposition by complex aeolian and fluvial processes. Furthermore, the ridges ETO 15/2 and ETO 15/3 may have been under water when extremely high lake levels breached the margins of ETO 15/1, to have recorded sediment activation, likely by water, during the 19 ka period i.e. ETO 15/1 (2.3 m = 19 ka, this study) and ETO 15/1 (2 m = 19 ka from Hipondoka *et al.* (2014), indicating that the wet phase lasted for much of the LGM. On the lakebed, these higher lake levels were recorded earlier through samples ETO 19/5/2 (0.26 m = 23 ka) and ETO 19/7/1

(0.39 cm = 24 ka). ETO 15/3 (Logan's Island) appears to have been sensitive to varying lake levels in the past, that led to poor preservation of sediments older than 12 ka. This is supported by findings from this study, and that of Hipondoka *et al.* (2014), which demonstrated that ETO 15/3 is primarily a Holocene landform.

Compared to the Etosha Pan, at Kuiseb river during the LGM (23 – 19 ka), aggradation of fine-grained flood sediments was observed near the Homeb silts and were interpreted as episodic back-flooding that formed embayment (Tooth *et al*., 2006). This is in agreement with the moist climate that formed a deep lake at Etosha during the LGM from the present study. In addition, Vogelsang *et al.* (2010) identified faunal and floral data from Apollo 11 which provided key evidence for a cool and wet LGM due to reduced evapotranspiration under a cooler climate.

7.6.3. Transition from LGM to early Holocene

The deglacial transition (19 - 11.7 ka) in Southern Africa is characterised by complex patterns that involve increasing insolation, rising sea surface temperatures and southward retreat of the southern hemisphere westerlies (Cohen and Tyson, 1995; Tyson *et al.,* 2001; Chase *et al.*, 2009). The sedimentological data in this study suggests that the deglacial transition at Etosha followed similar trends of warming and enhanced precipitation. During this period, there is a gradual increase of EM1 (sand enriched) contribution that controls 65 - 90 % of the variance, highlighting the importance of sediments with higher energy such as increased fluvial processes resulting from a wetter climate (Figure 5.8). Moreover, PC1 biplots complements these findings with a variance of ~65 % that contains coarser sand grains in comparison to

clay and silt. The secondary pattern exhibited by PC2 vs PC3 suggest an environment that is driven mostly by a uniform process, which in this case is likely to be sand grains deposited by higher energy transport processes under a wetter palaeoclimate regime (Figure 5.9 and Figure 5.10).

Furthermore, sediments from this study recorded flamingo breeding between 19 ka and 16 ka which suggested that water levels fluctuated allowing nest sites to be constructed during seasonally lower phases (Figure 5.6). Smith and Mason (1991) concluded that the Poachers Point Formation was formed from different environmental conditions: flooding and erosion during dry phases that are as arid as modern-day. Flamingos need shallow water for breeding, so in those periods, the pan would not be inundated for long periods with large volumes of water. However, the sand ridges on the western margin of the basin, probably acted as shorelines during the LGM in response to changing climatic conditions recorded by fluctuating lake levels (Brook *et al.*, 2007; Hipondoka *et al.*, 2014).

In the latter half of the post LGM deglacial, the reduction of moisture into the driest period observed in the record is evidenced by the dryness in suggested by $\delta^{13}C$ data from Core B's bulk sediments which decrease continuously until 11 ka. However, the pan was not completely dry during this period. Evidence for this is that flamingo breeding returns at 13 - 11 ka, suggesting shallower lake levels than during the wet LGM. The period 10 - 8 ka is intriguing: ETO 15/1 from the marginal ridges recorded two ages (9 ka and 10 ka both at 0.5 m) and ETO 15/2 had an age of 8 ka. It is likely

that ETO 15/3 (Logan's Island) was under water, with ETO 15/1 and ETO 15/2 acting as shorelines. Alternatively, the ridges might have been affected by strong aeolian processes that mobilised sediments on all three ridges around a dry pan. The data available in this study cannot ascertain which of two processes dominated the site during this period.

According to Brook *et al.* (2007), sediments on the pan floor surface are older than 13 ka, as their OSL dates from near Logan's Island was at a minimum age of 13 ka. Brook *et al.* (2007) interpreted this age to refer to a period in the past when the pan was drier and inundated less regularly than in the modern-day. Indeed, the pan floor at this location is much older than 13 ka as evidenced by an age of 40 ka from ETO 15/2/2 at 1.2 m depth. This period is coeval with some findings from Namibian caves from which other researchers were able to extract evidence of palaeoclimatic change. In their study of stalagmite Orum-1 from Orumana cave in the northern Namibia, Railsback *et al.* (2016) interpreted less-depleted $\delta^{13}C$ values between 20 – 14.5 ka to indicate dry climate conditions to have taken place under the influence of a northward shift of the tropical rain belt, leaving northern Namibia dry. Furthermore, Phase 4 of the Orumana speleothem by Railsback *et al.* (2016) indicates that the LGM was analysed using multiple proxies including stable isotope ratios of carbon and oxygen indicated greater precipitation in Northwest Namibia which also concurs with findings from the present study. Railsback *et al*. (2016) further found a trend towards arid conditions after the LGM. At Etosha, the period after the LGM was transitionary with varied grain size and occasional flamingo breeding in shallow water, indicating that the environmental

conditions were changing with varied lake levels at Etosha. In addition, the frequency of speleothem and tufa U-series dating ages from caves in the Otavi mountains (located approximately 300 km southeast of Etosha) suggested the water table was lowered by an average of 12 m, indicating that the 13 – 10 ka period was dry, compared to majority of the mid and late Holocene (Brook *et al.*, 1998).

7.6.4. Early to mid-Holocene lake levels higher than modern day pan extent

The next phase of sand deposition recorded after that period, located only 0.2 m above the modern day surface, is of Holocene age and occurs at 8.45 ± 0.6 ka. This period coincides with a sample age of 8.69 ± 0.2 ka taken from Ridge 1 (ETO 15/1/1 at 0.5 m) and suggests that there was palaeoenvironmental change on the pan, different to the preceding one. As explained in Chapter 2, a study by Brook *et al.* (2007) found that Etosha experienced basin inundation between 7 - 5 ka. The authors argued that these phases took place under a wetter climate and probably not due to geomorphological changes in the catchment areas that would change stream flows and could lead to greater moisture on the pan. Hipondoka *et al.* (2014), also using OSL dating, found the period 7 - 5 ka to be wetter, which coincides with the first period identified by Brook *et al.* (2007). OSL ages from outer and inner ridges (ETO 15/1 and ETO 15/2 in the study) led to their conclusion that the Etosha experienced a mid-Holocene wetness (Brook *et al.*, 2007). Their data also showed that the outer ridge (ETO 15/1), which has a greater height than the other two (ETO 15/2 and ETO 15/3), appears to be much older than the inner ones. Moreover, an OSL age during this period at Etosha was 5.4 ± 0.6 ka so this shoreline was likely formed in the middle Holocene at 5 m depth on the outer ridge (ETO 15/1) (Brook *et al.*, 2007).

There is no record of flamingo breeding in the spring mound cores at Etosha during the mid-Holocene (Figure 5.6). Flamingos generally breed at the same site over many generations, a phenomenon known as philopatry (Brown, 2008; Balkiz *et al.*, 2010) and this could explain the presence of the eggshells at the spring over thousands of years. However, the lack of preservation of flamingo eggshells during this period cannot be concluded upon. It is important to take caution when interpreting depositional or post-depositional settings at a site for palaeoecological proxies when no evidence is available. Evidence from the bulk sediment cores $\delta^{13}C$ data in this study suggests that the mid-Holocene was drier than the LGM, but not as dry as modern-day. Yet the driving forces of flamingo breeding at Etosha remain poorly understood (as established in Chapter 5). Berry (1972) reported that more than 50,000 flamingos in 1971 AD were breeding on the western part of the pan, and a slightly less number on the east. Perhaps the higher water levels on the east were too high for the flamingos compared with the west. It could also be because flamingos did not breed at Etosha during this time, presumably because drier conditions prevailed shortly after the LGM. Another interpretation could be that they didn't breed on the western part of the pan during this time. Perhaps they bred on the eastern part of the pan. However, the sites are over 100 km away from each other, it is therefore difficult to make inferences on that part of the pan, especially given that there is a modern-day eastwards rainfall gradient in Etosha, and across the country.

Compared to the high silt content during the LGM, grain size data during the mid-Holocene has moderate contributions from all three endmembers (Figure 5.11) Firstly, the mid-Holocene has a much-reduced clay content (~15 – 20 %) which suggest an increase in energy transport of the sediment deposits (Figure 5.11). Silt fraction (~45 – 50 %) accounts for about half of the sediment load while sand increases to 40 % during the mid-Holocene. High sand proportions suggest greater fluvial and aeolian processes, the former likely to result from increased seasonal precipitation. This would have caused changes in the water body extent, likely to shallower lake levels than those experienced during the LGM due to more variable palaeoclimate conditions. Moreover, the OSL data from Logan's Island at 3 and 4 m depths (Figure 4.1) suggest that sediment activation occurred during ~ 6 ka.

When comparing the Etosha records with other data from regional fluvial records, the studies are in agreement about the mid-Holocene (7 -5 ka) that was wetter than modern day. For instance, at the Huab river petrographic and heavy mineral compositional assemblages suggested that mid-Holocene humidity activated sediment stores across the catchment under a wetter climate regime (Walsh *et al*., 2022). Moreover, the study found that during the mid-Holocene the Kuiseb river's behaviour sustained flow in a well-defined channel (Heine and Heine, 2002). Furthermore, OSL ages and lithostratigraphic analysis from Srivastava *et al*. (2017) suggested that wetter conditions occurred in the form of flash floods from ~6 ka at the Homeb silt deposits. Reorganisation of atmospheric circulation systems in the region is the most probable cause of the palaeohydrological changes observed on the record.

7.6.5. Late Holocene

While this study has not produced data between 4 ka and 0.6 ka, two relatively recent ages suggest that the Etosha Pan continues to be a dynamic hydrological system, with the driest conditions on the record. ETO 15/2 (at 0.2 m) had an age of 0.3 ka (1724 AD) while ETO 19/5/1 (at 0.08 m) produced an age of 0.6 ka (1424 AD). Moreover, recent deposits documented by Hipondoka *et al.* (2014) from Etosha sand ridge 1 (ETO 15/2) in this study were dated to 0.3 ka at 50 cm depth. These indicate periodic activation of Etosha Pan's sediments, and it is likely that the pan's current geomorphological configuration as an ephemeral lake system was concluded during the late-Holocene. These processes possibly occur through what was hypothesized as the seasonal erosional processes that continue to excavate the pan with erosion from water in the summer, and aeolian deflation in the dry winters (Miller *et al.*, 2008).

Furthermore, during the late-Holocene, better hydraulic sorting and flash flood lithofacies at the Huab River indicated reduced river flow with increasing arid climate conditions until modern day (Walsh *et al*., 2022). This finding accords with grain size data from the presented study that suggests that progressive aridity occurred in the region after the mid-Holocene. In addition, Late Holocene occupation was also noted around 2 ka onwards at the Apollo 11 rockshelter suggesting climate conditions that were different from the period prior (mid-Holocene) (Vogelsang *et al*., 2010).

Further south, OSL ages from fluvial sediments from the Tsauchab River indicated wetter conditions between 0.9 and 0.3 ka (Brook *et al.*, 2006), In addition, the period

0.6 - 0.3 ka was described as humid according to dendrochronological records and calcrete radiocarbon dates from the Kuiseb River (Yamagata and Mizuno, 2005). Furthermore, using petrography, mineralogy and stable isotopes of carbon and oxygen analyses at Dante cave, Voarinstoa *et al.* (2016) resolved that the hydroclimate between ca. 1660 – 1710 and ca. 1790 – 1830 was cooler and wetter than modern-day. Their data were interpreted to suggest that southward migration of the tropical rain belt led to longer summers with higher precipitation in the recent past. In addition, arid conditions and/or higher wind velocity is documented in the Kuiseb valley near Gobabeb by encroaching dune sand into the valley about 300 – 400 years ago (Mizuno & Kotaro, 2003). These may have been triggered by human use through cattle feeding that might reduce surface vegetation, making the dunes more prone to erosion and water loss. These studies, with overlaps in some dates, suggest that northern Namibia was responding to changes in a progressively drier palaeoclimate in the recent past.

7.6.6. Comparison with local records from Etosha

Petrographic and isotopic data from the stromatolites at Poacher's Point helped in reconstructing humid phases in the pan. These data were interpreted to represent long periods of pan inundation during the Holocene Climate Optimum (9 - 5 ka) (Smith and Mason, 1991). Rust (1984) also reported ages of 11,900 ± 100 cal BP from a lacustrine carbonate and 9,300 ± 100 cal BP for a spring carbonate from Namutoni, on the south-eastern margin of the pan. Both ages were interpreted to represent phases of higher lake levels at the start of the Holocene. Rust (1984) obtained radiocarbon dates from 42,400 to 39,300 cal BP and 32,200 to 30,300 cal BP for oncoids and calcretes from Poachers Point on the east of the pan with very high $\delta^{13}C$ values reported ranging

between +2.8 and +4.4 ‰. These values were interpreted to represent a period when the pan underwent extremely evaporative conditions with little photosynthesis. Based on the above findings, Rust (1984) argued that the pan had an extensive lake phase at 40 ka. Pan flooding was restricted to that period and continued decreasing until modern-day (Rust, 1984). However, these dates can be unreliable because of the 'hard-water effect' and the incorporation of 'old' carbon that would have formed the deposits, thus making the ages appear older than they actually are (Brook *et al.*, 2011). Miller (2008) suggested that the stromatolites are of Miocene age: however, there was no data provided to support this. Moreover, palaeoenvironmental reconstruction of stromatolites were problematic because researchers interpreted the ages differently as some ages were from carbonates (Hipondoka, 2005).

Comparing this finding with data from the present study, a deep lake occurred during the LGM, but these data cannot provide conclusions about preceding lake levels as the data only go up to 40 ka. Furthermore, the present study has helped to improve chronology the of the pan by dating organic material from the lakebed (both bulk sediment samples and eggshell fragments) which were mostly in chronostratigraphic order and helped to overcome the problems with dating calcrete.

Hipondoka *et al.* (2004) measured particle size and carbonate content on sand ridges with increasing distance of 0 - 60 km away from the Ekuma Delta and reported that the sand ridges (referred to as lunette dunes in their study), were formed by unconsolidated sand that entered the pan via the Ekuma Delta. This contrasted

hypothesis that the pan had aeolian origins. River delta deposition is the main source of the sand input on the sand ridges (Hipondoka *et al.,* 2004). They concluded that the pan is older than the Kalahari cover sands that form the upper part of the sand ridges. Indeed, OSL ages from the present study confirmed that the pan floor is older than the cover sands on the ridges.

In addition, based on their particle size analysis, Hipondoka *et al.* (2004) found that there was a southward fining of sediments from the Ekuma Delta to towards the southern rim of the sand ridges. This helped to exclude the pan-floor as a primary source of sediment input to the ridges (Hipondoka *et al.*, 2004). The present study had a smaller spatial resolution on the sand ridges and therefore did not investigate sediment relationships between the northern and southern parts of the ridges. Similar to the present study, Hipondoka *et al.* (2006) found the mid-Holocene at Etosha was wetter than present between 5 - 4.5 k cal BP based on the discovery of sitatunga (*Tragelaphus spekei)* faunal remains which are known to thrive in swampy conditions (Hipondoka *et al.,* 2006).

7.7. Comparison with other southern African palaeoclimate records

Overall, the new Etosha palaeoenvironmental record from the present study aligns with most regional records and forcing mechanisms relating to insolation and migrations of the tropical rain belt. As outlined in Chapter 2, Belz *et al.* (2020) conducted a palaeoclimatic reconstruction study using biomarkers to investigate climatic shifts recorded in the sediments of Omongwa Pan. Their study interpreted low δ2H values of n-alkanes to evidence against the influence of winter rainfall at their study site during

the LGM. The present study also found wet conditions during the LGM but lacked a proxy to distinguish between summer and winter rainfall zones. Furthermore, their study suggests that summer rainfall through the southward migration of the tropical rain belt was the key source of precipitation over the last 27 ka.

Similar climatic shifts to a short-wet period during Heinrich Stadial 1 (HS1) (18 - 14.8 ka) were found between the Omongwa and Etosha records. Flamingo breeding occurred on the western part of the Etosha Pan during HS1, suggesting that summer rainfall was a key contributor to moisture on the pan. This is further supported by increases in sand content (Core A and B) that likely resulted from moderate-energy depositional environment from higher rainfall to sustain the shallow water conditions (Figure 5.7). In addition, n-alkane and n-alkanol distributions at Omongwa Pan suggested that there was a greater coverage of C_4 vegetation on the landscape during HS1. The alignment in palaeohydrological change between the Omongwa and Etosha Pan records during HS1 suggest a similar source of rainfall, likely summer rainfall. Stable carbon isotope data in stalagmite LH4 from Lobatse II cave (~900 km from Etosha) recorded enhanced precipitation during the LGM that was interpreted as a consequence of increased winter rainfall (Holmgren and Shaw, 1999). This finding, which contrasts that of Belz *et al.* (2020) highlights the need for more studies in the region to help disentangle local from regional palaeoenvironmental signals and more information to resolve conflicting datasets.

Collins *et al.* (2014) found humid conditions during the LGM from lower leaf wax δ D and higher $\delta^{13}C$ values in their marine core MD08-3167. Their evidence suggested that Namibia's increased precipitation during the LGM was sourced from tropical systems and not winter westerlies. The three records (Collins *et al.*, 2014; Belz *et al.*, 2020, this study) collectively highlight the importance of summer rainfall in southwestern Africa during the LGM.

The break in sedimentation at Tsodilo hills (~500 km east of Etosha in Botswana) was interpreted to indicate that dry conditions took place at the lake during the LGM (Thomas *et al.*, 2003). Furthermore, Thomas *et al.* (2003) found no evidence of hydrological activity during the mid-Holocene. In contrast, Geppert *et al.* (2021) inferred shoreline building and a lake high stand at Tsodilo Hills during the LGM to indicate wetter conditions. These findings were from sedimentological, geophysical and genetic information from prior studies which affirmed that increases in fish consumption during the LGM indicated occupation by humans near the lake during that period (Geppert *et al.,* 2021). The different palaeoenvironmental interpretations at Etosha and Tsodilo hills during the LGM and mid-Holocene may have occurred due to spatial heterogeneity or because shifting rainfall zones that would have brought increased moisture to reach Etosha and Tsodilo Hills.

Moreover, the Brandberg Massif Mountain which Scott *et al.* (2004) analysed $\delta^{13}C$ of rock hyrax middens, indicated a reduction in woody vegetation and arboreal pollen during the LGM which were interpreted as reflecting different environmental conditions

(e.g. than during the Holocene), through a shift from woody vegetation to small shrubs and diverse plant communities. The cooler conditions were compared to the lower lying foreland of the Huns Mountain, where the Apollo 11 is located (Vogelsang *et al.*, 2010). Vogelsang *et al.* (2010) suggest these conditions may explain the lesser importance of woody taxa during the LGM.

Finally, $\delta^{15}N$ data from rock hyrax middens at Spitzkoppe (~400 km southwest from Etosha) suggested that humid conditions took place during the mid-Holocene (6.9 - 6.7 ka), citing strong solar forcing as a key modulator of humidity at the site (Chase *et al.*, 2009). At Etosha, the current study also found wet conditions during the mid-Holocene although they were drier than the LGM. This similarity could be explained by the increasing importance of Indian ocean-sourced moisture during this time. Increased insolation in southwestern Africa during this period is not depicted by the current dataset. It might have been such that the tropical rain belt migrated southwards to reach both Spitzkoppe and Omongwa Pan.

7.8. Conclusion

At Etosha, an early study by Buch and Zoller (1992) had suggested that the sand ridges had an aeolian formative history, that they were formed during dry periods, and therefore making them lunette dunes. Hipondoka *et al.* (2014) on the other hand, interpreted them to be shorelines which represented formation under a palaeoclimate regime with greater precipitation than modern-day. Brook *et al.* (2007), also referring to them as shorelines, suggested that the lake level was between 8 - 20 m higher than

present prior to the Holocene. While it has not produced an estimation of lake levels to a specific height during wet periods, the flamingo breeding phases captured here suggest that during shallow pan inundation, the pan probably sustained maximum depth of ~15 cm depth to avoid flooding flamingo nests. This helps to improve the wet/dry binary of palaeoclimate reconstructions on the pan, and instead suggests an average lake depth during transitionary periods with distinct water chemistry. This project has also provided an avenue for further investigations exploring the use of flamingo eggshells to extract palaeoenvironmental change in this arid environment when other proxies (such as leaf waxes and diatoms) are not available. It remains imperative to collect further pan sediments for investigation in order to better understand the sediment dynamics across the pan itself. Perhaps other locations, further away from the Ekuma Delta, might have preserved sediments from earlier than 40 ka that are not saturated.

In summary, this study proposes that Etosha Pan experienced a major high stand during the LGM. The high stand was characterised by high silt proportions which suggested calm palaeoenvironmental conditions that allowed settling of fine grains and increased organic material accumulation within a deep lake. A major drop in lake levels occurred to reach shallow levels during HS1 as evidenced by the return in flamingo breeding on the western part of the pan. This shallow water body had likely resulted from reduced moisture from regional atmospheric circulation systems. Following this period, there was a continued shift from lower to higher energy sediment transportation systems sustaining a second but shallower high stand with greater fluvial sediments

than during the LGM. These interpretations are further supported by vertical and lateral distribution of sediments that have been dated from the lakebed and marginal sand ridges, as well as changes in sediments characteristics. The changes from a deep lake (LGM), a shallow lake (mid-Holocene) and the modern day pan environment imply transitions between different aquatic habitats that gave rise to some of the faunal remains that have been discovered on the pan including flamingo eggshells.

With the evidence produced above, it can be concluded that Etosha Pan has been a dynamic system with varying lake levels in the late Quaternary. In this way, the proposal here is that Etosha Pan has been a palaeolake from as early as 40 ka with fluctuating pan lake extent in agreement with Brook *et al.* (2007) and Hipondoka *et al.* (2014). Furthermore, while the palaeoenvironmental context of the sand ridges remain contested, the present study has provided evidence of them acting as shorelines at different periods in the past. Their role during arid periods, however, is yet to be confirmed.

Chapter 8 - Conclusion

8.1. Introduction

Pans have recently become significant in paleoclimate research to understand long term climate and environmental change in drylands (Telfer *et al.,* 2009; Genderjahn *et al.*, 2017; Schmidt *et al.*, 2017; Schuller *et al.,* 2018; Franchi *et al.,* 2022). In particular, they act as geoarchives, storing information that is helpful in reconstructing environmental changes and the atmospheric circulation systems that influence them on millennia time scales. This study has demonstrated that Etosha Pan can provide clues on late Quaternary palaeoenvironmental change and palaeoclimatic shifts, with implications for regional climate dynamics. This Chapter will summarise the main findings from this study, lay out the key contributions to the literature and demonstrate the level to which the objectives were met.

This project investigated a range of proxies from the sediments in the western area of the pan. Techniques from palaeoecology, sedimentology and advanced chronology methods (OSL and radiocarbon dating) were utilised to better understand the geomorphological history of the Etosha Pan and surrounding localities. Together, these proxies captured different palaeoclimate signals, thus strengthening the evidence to build a more comprehensive picture of Etosha Pan's lake-level reconstruction and associated hydrological changes. As more proxy data becomes available, the information can help to accurately model past palaeoclimate changes on a regional level.

This study has produced 11 finite OSL dates with the largest temporal coverage at Etosha Pan thus far (from 40 ka to the present). Previous OSL studies on the pan mainly covered the Holocene (see, for example, Brook *et al.* (2007) and Hipondoka *et al.* (2014)). This study is also the most continuous record from Etosha Pan as it covers intervals in between the discrete periods found by previous studies (e.g., Brook *et al.*, 2007; Hipondoka *et al.*, 2014). One of the main findings is that higher precipitation during the LGM and the mid-Holocene were strongly controlled by summer rainfall arising from the southward migration of the African tropical rain belt during the LGM and mid-Holocene. In addition, a brief wet period with shallow lake levels during Heinrich Stadial 1 (HS1) (19 - 16 ka) is suggested by a flamingo breeding phase on the pan between 19 - 16 ka, as well as the sedimentological data.

8.2. Methodological contributions

This is the first study to sub-sample and analyse sediments from the Etosha lakebed. Most studies only sampled the sand ridges on the western parts of the pan (e.g., Buch and Zoller, 1992; Buch and Rose, 1996; Brook *et al.*, 2007; Hipondoka *et al.*, 2014), while others applied radiocarbon dating to calcretes on the east (e.g., Rust, 1984; Brook *et al.*, 2011). Secondly, this study is the first known in Namibia, and perhaps elsewhere, to use flamingo eggshell as a novel proxy for palaeohydrological reconstruction. Moreover, ancient DNA analyses on the flamingo eggshells are a new contribution to understanding late Quaternary ecosystem changes in this arid region. If adopted by future studies, it can provide valuable information to better understand biodiversity changes in palaeoenvironmental reconstructions. In addition, the present

study improved the chronology of the pan's geomorphological history by using a dual approach of OSL and radiocarbon dating at the Etosha Pan which proved helpful in reconstructing palaeoenvironmental changes. Finally, high resolution sedimentological data collection (1 cm sub-sampling on the sediment cores) and analysis took place in this study, while previous studies had not collected sediment cores on the pan or the sand ridges. Bulk sediment core samples provided $\delta^{13}C$ data which were helpful in reconstructing vegetation assemblages, and their associated palaeoclimatic changes.

8.3. Regional significance

The periods of flamingo nesting and breeding contributed new information to affirm the role of the African tropical rain belt in influencing summer rainfall in Namibia during the LGM (Chapter 5). Similar trends were observed in previous studies by Schefuß *et al.* (2011), Collins *et al. (2014*), and Belz *et al.* (2020), suggesting that the palaeoclimatic conditions occurred more regionally. In addition, the data in this study contributes to understanding the dynamics of Etosha Pan, its catchment area and it gives clues into the late Quaternary geomorphological evolution of large pans in southern Africa. Furthermore, the new lake high stands can contribute information to help improve palaeoclimate modelling projects such as Paleoclimate Modelling Intercomparison Project (PMIP) and Coupled Model Intercomparison Project (CMIP) (Chapter 6).

As explained in Chapter 2, two main hypotheses have been put forward to describe Etosha's late Quaternary geomorphological evolution. One school of thought argues that Etosha is a desiccated palaeolake with fluctuating lake levels in response to a

changing climate (Brook *et al.*, 2007; Hipondoka *et al.*, 2014). Moreover, these researchers interpret the marginal sand ridges to have acted as shorelines during periods of high lacustrine phases. The other hypothesis regards the pan as an erosional landform with long term deflationary processes under semi-arid climate (Jaegar, 1926; Buch and Rose, 1996; Beugler-Bell and Buch, 1997; Miller, 2008). The latter hypothesis argues that the sand ridges are lunette dunes formed during arid periods. However, neither of these hypotheses were formed using data collected from the lakebed. Instead, their studies were based on the marginal sand ridges.

This thesis, on the other hand, was designed to generate data and contribute to this debate by sampling both sand ridges and the lakebed. Samples from the western part of the pan allowed data comparisons and integration between the landforms (ridges and lakebed) and the spring mound. Multi-proxy data from the present study suggest that the pan had different lake phases over the last 40 ka. These changes are attributed to moisture availability in the regional atmospheric circulation systems during periods of high or low lake levels. This supports the hypothesis of Etosha as a palaeolake over the last 40 ka. However, the present study cannot exclude the role of aeolian deflation over long term periods at Etosha. Furthermore, the present study utilised OSL and radiocarbon dating which do not generally provide ages that go as far back as the Miocene. In this way, the study was not designed to contribute to the discussion of Etosha Pan experiencing extensive erosion with similar semi-arid climate since the Miocene. However, with the reconstructed high lake statuses of the pan under a wetter

climate than modern day, results from the present study suggest that Etosha Pan was less arid during the LGM and the mid-Holocene.

8.4. Achievement of study objectives

Thesis Aim: *To generate a robust dataset to establish the chronology and palaeohydrology of Etosha Pan through multi-proxy analyses of sediment cores, lakebed and marginal ridge sediments to reconstruct late Quaternary palaeoenvironmental change in northern Namibia.*

By achieving the following objectives, this project has met the aim in the following ways:

Objective 1:

Produce a new, robust chronology of sedimentary accumulation of the Etosha Pan floor and of the marginal sand ridges using modern dating protocols (OSL and Radiocarbon Dating) (Chapter 4)(Chapter 5).

- OSL and ^{14}C data are presented in Chapter 4 and Chapter 6 respectively. These data were collected and analysed at a high level of precision and have laid a firm foundation for the geomorphic interpretations.

Objective 2:

To characterise the nature and stratigraphy of pan floor sediments, and thereby environmental controls on their accumulation, at four sites on the north-western end of the pan. This objective aligns with informing the timing and nature of the development

of the three sand ridges parallel to the modern-day shoreline of the Etosha Pan (Chapter 4) (Chapter 6).

- The study achieved one part of objective 2 in that the stratigraphy of lakebed sediments was described. The available OSL ages enabled a robust chronological dataset indicating age depth relationships between the sand ridges. However, due to saturation of the OSL ages, it was not possible to determine the timing of sediment accumulation and their environmental controls on the deeper samples.

Objective 3:

To reconstruct the palaeohydrological and palaeoecological history of a spring mound on the basin floor by applying a range of geochemical and sedimentological analyses on sediment cores extracted from it (Chapter 6).

- Objective 3 was successfully met with a rich geochemical and sedimentological dataset extracted from sediment Core A and B. $\delta^{13}C$ data preserved in the bulk sediments assisted in reconstructing the palaeoenvironmental history indicating periods of high and shallow lake phases in the last 40 ka.

Objective 4:

To establish a record of palaeohydrological change within Etosha Pan through integration of the data from a transect on the west including sand ridge, basin floor and spring mound sediments and their respective chronologies (Chapter 7).

- In Chapter 7 data from ETO 15/1, ETO 15/2, ETO 15/3, ETO 19/5 and Core A and B were analysed and used to integrate the main findings of this thesis. Through this transact, it was possible to confirm major periods of pan-wide environmental change and to give insights into intra-basin geomorphological processes.

Objective 5:

To establish and contextualise the new palaeoenvironmental record from Etosha Pan within the growing regional record established from recent literature (Chapter 7).

- Results from this study were comparable with those from other local and regional studies such as from pans in the Kalahari (e.g., Belz *et al.*, 2020) and the marine core study by Collins *et al.* (2014). In Chapter 6, palaeoenvironmental reconstruction of lake statuses was improved by assigning a narrower age range to the hypothesised deep lake to have occurred during the LGM period. This new information has improved understanding of shifting rainfall zones during the late Quaternary in northern Namibia, as already cited by Schuller *et al.* (2018).

8.5. Future Research

There is great potential for Etosha Pan sediments to provide new information that can add different dimensions and improve understanding of northern Namibia's palaeoclimatic changes. Today Etosha lies within an arid geographical zone of Namibia, and past studies have found it challenging to successfully apply radiocarbon

dating. However, the pan has demonstrated that the sediments on the western margins are dateable, as shown in existing studies that targeted them out of scientific curiosity as outlined in earlier Chapters. It could be helpful to extend this to the other lakebed sediments to uncover hydrological changes from the lakebed using multiple proxies. In addition, future research can include collecting sediment cores from nearby pans with smaller catchment where it might be easier to distinguish between environmental and climatic signals. Moreover, it would be of great scholarly value to conduct an in-depth study on how flamingo eggshell stable isotope ratios vary in response to environmental change. This could serve as a blueprint to assist data interpretations in future palaeoenvironmental studies that may also discover flamingo shells in their sediment records.

9. References

Aitken, M.J. 1985. *Thermoluminescence Dating*. London, Academic Press Inc.

Archibald, T.J. and Nott, T.B., 1987. The breeding success of flamingoes in Etosha National Park, 1986. *Madoqua*, 15 (3), pp.269-270.

Avery, D.M., 1993. Last Interglacial and Holocene altithermal environments in South Africa and Namibia: micromammalian evidence. *Palaeogeography, Palaeoclimatology, Palaeoecology*, 101 (3-4), pp.221-228.

Balkiz, Ö., Bechet, A., Rouan, L., Choquet, R., Germain, C., Amat, J.A., Rendón-Martos, M., Baccetti, N., Nissardi, S., Özesmi, U. and Pradel, R., 2010. Experience-dependent natal philopatry of breeding greater flamingos. *Journal of Animal Ecology*, 79 (5), pp.1045-1056.

Barcelos-Silveira, A., Dentzien-Dias, P., Francischini, H. and Schultz, C.L., 2023. Registration, morphology and taphonomy of feeding structures produced by Chilean Flamingos (Phoenicopterus chilensis) in a lagoonal/barrier depositional system in southern Brazil. *Journal of South American Earth Sciences*, 127, pp.104396.

Bard, E. and Rickaby, R.E., 2009. Migration of the subtropical front as a modulator of glacial climate. *Nature*, 460 (7253), pp.380-383.

Bateman, M.D., Holmes, P.J., Carr, A.S., Horton, B.P. and Jaiswal, M.K., 2004. Aeolianite and barrier dune construction spanning the last two glacial–interglacial cycles from the southern Cape coast, South Africa. *Quaternary Science Reviews*, 23 (14-15), pp.1681-1698.

Baxter, A.J. and Meadows, M.E., 1999. Evidence for Holocene sea level change at Verlorenvlei, western cape, South Africa. *Quaternary International*, 56 (1), pp.65-79.

Bell, W.T. 1979. Thermoluminescence dating: Radiation dose-rate data, *Archaeometry*, 2, pp.243–245.

Belz, L., Schüller, I., Wehrmann, A., Köster, J. and Wilkes, H., 2020. The leaf wax biomarker record of a Namibian salt pan reveals enhanced summer rainfall during the Last Glacial-Interglacial Transition. *Palaeogeography, Palaeoclimatology, Palaeoecology*, 543, pp.109561.

Beugler-Bell, H. & Buch, M.W., 1997. Soils and soil erosion in the Etosha National Park, northern Namibia. *Madoqua*, 1997 (1), pp.91-104.

Beuning, K.R., Talbot, M.R., Livingstone, D.A. and Schmukler, G., 2003. Sensitivity of carbon isotopic proxies to paleoclimatic forcing: A case study from Lake Bosumtwi, Ghana, over the last 32,000 years. *Global Biogeochemical Cycles*, 17 (4), pp.1-10

Beyer, M., Hipondoka, M., Hamutoko, J. & Wanke, H. 2018. Water resources in the Cuvelai-Etosha Basin. In: Climate change and adaptive land management in southern Africa – assessments, changes, challenges, and solutions (ed. by Revermann, R., Krewenka, K.M., Schmiedel, U., Olwoch, J.M., Helmschrot, J. & Jürgens, N.), pp. 84-85, *Biodiversity & Ecology*, 6, Klaus Hess Publishers, Göttingen & Windhoek.

Bianchi, C. and Gersonde, R., 2004. Climate evolution at the last deglaciation: the role of the Southern Ocean. *Earth and Planetary Science Letters*, 228 (3-4), pp.407-424.

Bista, I., Carvalho, G.R., Walsh, K., Seymour, M., Hajibabaei, M., Lallias, D., Christmas, M. and Creer, S., 2017. Annual time-series analysis of aqueous eDNA reveals ecologically relevant dynamics of lake ecosystem biodiversity. *Nature communications*, 8 (1), p.14087.

Blaauw, M, Christen, J.A. 2011. Flexible paleoclimate age-depth models using an autoregressive gamma process. *Bayesian Anal*, 6, pp.457–474

Blaauw, M., Christen, J.A., Aquino Lopez, M.A., Esquivel Vazquez, J., Gonzalez, O.M., Belding, T., Theiler, J., Gough, B. and Karney, C., 2019. rbacon: Age-depth modelling using Bayesian statistics. *R package version*, 2 (9.1).

Blaauw, M. and Christen, J. A. 2021. rbacon: Age-Depth Modelling using Bayesian Statistics. R package version 2.5.7.

Boggs, S. 2012. *Principles of sedimentology and stratigraphy*. 5th edn. Boston: Pearson Prentice Hall.

Blott, S.J. and Pye, K., 2001. GRADISTAT: a grain size distribution and statistics package for the analysis of unconsolidated sediments. *Earth surface processes and Landforms*, *26* (11), pp.1237-1248

Bond, G., Heinrich, H., Broecker, W., Labeyrie, L., McManus, J., Andrews, J., Huon, S., Jantschik, R., Clasen, S., Simet, C. and Tedesco, K., 1992. Evidence for massive discharges of icebergs into the North Atlantic Ocean during the last glacial period. *Nature*, 360 (6401), pp.245-249.

Boom, A., Marchant, R., Hooghiemstra, H. and Damsté, J.S., 2002. CO2-and temperature-controlled altitudinal shifts of C_4-and C_3-dominated grasslands allow reconstruction of palaeoatmospheric pCO2. *Palaeogeography, Palaeoclimatology, Palaeoecology*, 177 (1-2), pp.151-168.

Bourke, M.C., Child, A. and Stokes, S., 2003. Optical age estimates for hyper-arid fluvial deposits at Homeb, Namibia. *Quaternary Science Reviews*, 22 (10-13), pp.1099-1103.

Braconnot, P., Harrison, S.P., Kageyama, M., Bartlein, P.J., Masson-Delmotte, V., Abe-Ouchi, A., Otto-Bliesner, B. and Zhao, Y., 2012. Evaluation of climate models using palaeoclimatic data. *Nature Climate Change*, 2 (6), pp.417-424.

Braconnot, P., Otto-Bliesner, B., Harrison, S., Joussaume, S., Peterchmitt, J.Y., Abe-Ouchi, A., Crucifix, M., Driesschaert, E., Fichefet, T., Hewitt, C.D. and Kageyama, M., 2007. Results of PMIP2 coupled simulations of the Mid-Holocene and Last Glacial Maximum–Part 2: feedbacks with emphasis on the location of the ITCZ and mid-and high latitudes heat budget. *Climate of the Past*, 3 (2), pp.279-296.

Bragg, F.J., Prentice, I.C., Harrison, S.P., Eglinton, G., Foster, P.N., Rommerskirchen, F. and Rullkötter, J., 2013. Stable isotope and modelling evidence for CO 2 as a driver of glacial–interglacial vegetation shifts in southern Africa. *Biogeosciences*, 10 (3), pp.2001-2010.

Braun, K., Bar-Matthews, M., Ayalon, A., Zilberman, T., & Matthews, A. 2020. Modelling the effects of CO_2 on C_3 and C_4 grass competition during the mid-Pleistocene transition in South Africa. *Scientific Reports*, 10, pp.16149

Brierley, C.M., Zhao, A., Harrison, S.P., Braconnot, P., Williams, C.J., Thornalley, D.J., Shi, X., Peterschmitt, J.Y., Ohgaito, R., Kaufman, D.S. and Kageyama, M., 2020. Large-scale features and evaluation of the PMIP4-CMIP6< i> midHolocene</i> simulations. *Climate of the Past*, 16 (5), pp.1847-1872.

Bristow, C.S., Lancaster, N. and Duller, G.A.T., 2005. Combining ground penetrating radar surveys and optical dating to determine dune migration in Namibia. *Journal of the Geological Society*, 162 (2), pp.315-321.

Brock, F., Higham, T., Ditchfield, P. and Ramsey, C.B., 2010. Current pretreatment methods for AMS radiocarbon dating at the Oxford Radiocarbon Accelerator Unit (ORAU). *Radiocarbon*, 52 (1), pp.103-112.

Broecker, W.S. & Walton, A. 1959. The geochemistry of C14 in fresh-water systems. *Geochimica et Cosmochimica Acta*, 16, 15-38.

Brook, G., Cowart, J., Marais, E.M. 1996. Wet and dry periods in the southern African summer rainfall zone during the last 300 kyr from speleothem, tufa and sand dune age data. *Palaeoecology of Africa*, 24, pp.147-158

Brook, G., Railsback, L., Marais, E.M. 2011. Reassessment of carbonate ages by dating both carbonate and organic material from an Etosha Pan (Namibia) stromatolite:

evidence of humid phases during the last. *Quaternary International*, 229 (1-2), pp. 24-37.

Brook, G.A., Cowart, J.B. and Brandt, S.A., 1998. Comparison of Quaternary environmental change in eastern and southern Africa using cave speleothem, tufa and rock shelter sediment data. In Brook, G.A., Cowart, J. B., and Brandt, S.A. (Eds), *Quaternary Deserts and Climatic Change*, pp. 239-249. CRC Press.

Brook, G.A., Cowart, J.B. and Marais, E., 1996. Wet and dry periods in the southern African summer rainfall zone during the last 300 kyr from speleothem, tufa and sand dune age data. *Palaeoecology of Africa*, 24, pp.147-158.

Brook, G.A., Marais, E., Srivastava, P. & Jordan, T. 2007. Timing of lake-level changes in Etosha Pan, Namibia, since the middle Holocene from OSL ages of relict shorelines in the Okondeka region. *Quaternary International*, 175 (1), pp.29–40.

Brook, G.A., Railsback, L.B. and Marais, E., 2011. Reassessment of carbonate ages by dating both carbonate and organic material from an Etosha Pan (Namibia) stromatolite: evidence of humid phases during the last 20 ka. *Quaternary International*, 229 (1-2), pp.24-37.

Brown, L.H., 1955. The breeding of lesser and greater flamingoes in East Africa. *Journal of East African Natural History*, 22, pp.159-162.

Brown, L.H., 1971. The breeding behaviour of the lesser flamingo Phoeniconaias minor. *Ibis*, 113 (2), pp.147-172.

Brown, T.A. and Barnes, I.M., 2015. The current and future applications of ancient DNA in Quaternary science. *Journal of Quaternary Science*, 30 (2), pp.144-153.

Buch, M.W. & Rose, D. 1996. Mineralogy and geochemistry of the sediments of the Etosha Pan Region in northern Namibia: a reconstruction of the depositional environment. *Journal of African Earth Sciences*, 22 (3), pp.355-378

Buch, M.W. and Zöller, L., 1992. Pedostratigraphy and thermoluminescence-chronology of the western margin-(Lunette-) dunes of Etosha Pan, Northern Namibia. *Wurzburger Geographische Arbeit*, 84, pp.361-84.

Buch, M.W., 1997. Etosha Pan-the third largest lake in the world? *Madoqua*, 1997 (1), pp.49-64.

Buch, MW & Trippner, C., 1997. Overview of the geological and geomorphological evolution of the Etosha region, northern Namibia. *Madoqua*, 1997 (1), pp.65-74.

Burrough, S.L. & Thomas, D.S.G. 2009. Geomorphological contributions to palaeolimnology on the African continent. *Geomorphology*, 103 (3) pp. 285-298

Burrough, S.L. and Thomas, D.S., 2013. Central southern Africa at the time of the African Humid Period: a new analysis of Holocene palaeoenvironmental and palaeoclimate data. *Quaternary Science Reviews*, 80, pp.29-46.

Burrough, S.L., 2022. *The Makgadikgadi basin*. In Eckardt, F., (Ed) Landscapes and Landforms of Botswana, pp.77-90, Cham: Springer International Publishing.

Burrough, S.L., Thomas, D.S., Allin, J.R., Coulson, S.D., Mothulatshipi, S.M., Nash, D.J. and Staurset, S., 2022. Lessons from a lakebed: unpicking hydrological change and early human landscape use in the Makgadikgadi basin, Botswana. *Quaternary Science Reviews*, 291, pp.107662.

Burrough, S.L., Thomas, D.S.G. & Bailey, R.M. 2009. Mega-Lake in the Kalahari: A Late Pleistocene record of the Palaeolake Makgadikgadi system. *Quaternary Science Reviews*, 28 (15–16), pp.1392–1411.

Caley, T., Peeters, F.J., Biastoch, A., Rossignol, L., Van Sebille, E., Durgadoo, J., Malaizé, B., Giraudeau, J., Arthur, K. and Zahn, R., 2014. Quantitative estimate of the paleo-Agulhas leakage. *Geophysical Research Letters*, 41 (4), pp.1238-1246.

Campeau, A., Wallin, M.B., Giesler, R., Striegl, R.G., Kokfelt, U., Humborg, C., Scheller, J., Nilsson, M.B., Karlsson, J. and Laudon, H. 2017. Multiple sources and sinks of dissolved inorganic carbon across Swedish streams, refocusing the lens of stable C isotopes, *Scientific Reports*, 7, pp.9158.

Capo, E., Giguet-Covex, C., Rouillard, A., Nota, K., Heintzman, P.D., Vuillemin, A., Ariztegui, D., Arnaud, F., Belle, S., Bertilsson, S. and Bigler, C., 2021. Lake sedimentary DNA research on past terrestrial and aquatic biodiversity: Overview and recommendations. *Quaternary*, 4 (1), pp.6.

Carr, A.S., Boom, A. and Chase, B.M., 2010. The potential of plant biomarker evidence derived from rock hyrax middens as an indicator of palaeoenvironmental change. *Palaeogeography, Palaeoclimatology, Palaeoecology*, 285 (3-4), pp.321-330.

Carr, A.S., Boom, A., Chase, B.M., Meadows, M.E. and Grimes, H.L., 2015. Holocene sea level and environmental change on the west coast of South Africa: evidence from plant biomarkers, stable isotopes and pollen. *Journal of Paleolimnology*, 53, pp.415-432.

Carr, A.S., Boom, A., Grimes, H.L., Chase, B.M., Meadows, M.E. and Harris, A., 2014. Leaf wax n-alkane distributions in arid zone South African flora: Environmental controls, chemotaxonomy and palaeoecological implications. *Organic Geochemistry*, 67, pp.72-84.

Carrión, J.S., Scott, L. and Vogel, J.C., 1999. Twentieth century changes in montane vegetation in the eastern Free State, South Africa, derived from palynology of hyrax dung middens. *Journal of Quaternary Science: Published for the Quaternary Research Association*, 14 (1), pp.1-16.

Chambers, R. L., & Upchurch, S. B. 1979. Multivariate analysis of sedimentary environments using grain-size frequency distributions. *Mathematical Geosciences*, 11 (1), 27–43.

Chase, B., 2009. Evaluating the use of dune sediments as a proxy for palaeo-aridity: a southern African case study. *Earth-Science Reviews*, 93 (1-2), pp.31-45.

Chase, B.M. and Meadows, M.E., 2007. Late Quaternary dynamics of southern Africa's winter rainfall zone. *Earth-Science Reviews*, 84 (3-4), pp.103-138.

Chase, B.M. and Quick, L.J., 2018. Influence of Agulhas forcing of Holocene climate change in South Africa's southern Cape. *Quaternary Research*, 90 (2), pp.303-309.

Chase, B.M., Boom, A., Carr, A.S. and Reimer, P.J., 2022. Climate variability along the margin of the southern African monsoon region at the end of the African Humid Period. *Quaternary Science Reviews*, 291, pp.107663.

Chase, B.M., Boom, A., Carr, A.S., Carré, M., Chevalier, M., Meadows, M.E., Pedro, J.B., Stager, J.C. and Reimer, P.J., 2015. Evolving southwest African response to abrupt deglacial North Atlantic climate change events. *Quaternary Science Reviews*, 121, pp.132-136.

Chase, B.M., Carr, A.S., Boom, A., Tyrrell, G. and Reimer, P.J., 2023. Linking upwelling intensity and orbital-scale climate variability in South Africa's winter rainfall zone: Insights from a ~70,000-year hyrax midden record. *Quaternary Science Advances*, 12, pp.100110.

Chase, B.M., Chevalier, M., Boom, A. and Carr, A.S., 2017. The dynamic relationship between temperate and tropical circulation systems across South Africa since the last glacial maximum. *Quaternary Science Reviews*, 174, pp.54-62.

Chase, B.M., Meadows, M.E., Carr, A.S. & Reimer, P.J. 2010. Evidence for progressive Holocene aridification in southern Africa recorded in Namibian hyrax middens: Implications for African Monsoon dynamics and the "'African Humid Period.'" *Quaternary Research*. 74 (1), pp.36–45.

Chase, B.M., Meadows, M.E., Scott, L., Thomas, D.S.G., Marais, E., Sealy, J. and Reimer, P.J., 2009. A record of rapid Holocene climate change preserved in hyrax middens from southwestern Africa. *Geology*, 37 (8), pp.703-706.

Chase, B.M., Niedermeyer, E.M., Boom, A., Carr, A.S., Chevalier, M., He, F., Meadows, M.E., Ogle, N. and Reimer, P.J., 2019. Orbital controls on Namib Desert hydroclimate over the past 50,000 years. *Geology*, 47 (9), pp.867-871.

Chase, B.M., Quick, L.J., Meadows, M.E., Scott, L., Thomas, D.S. and Reimer, P.J., 2011. Late glacial interhemispheric climate dynamics revealed in South African hyrax middens. *Geology*, 39 (1), pp.19-22.

Cheung, M.C., Zong, Y., Wang, N., Aitchison, J.C. and Zheng, Z., 2015. δ13Corg and n-alkane evidence for changing wetland conditions during a stable mid-late Holocene climate in the central Tibetan Plateau. *Palaeogeography, Palaeoclimatology, Palaeoecology*, 438, pp.203-212.

Chevalier, M. and Chase, B.M., 2015. Southeast African records reveal a coherent shift from high- to low-latitude forcing mechanisms along the east African margin across last glacial–interglacial transition. *Quaternary Science Reviews,* 125, 117–130.

Clark, P.U., Dyke, A.S., Shakun, J.D., Carlson, A.E., Clark, J., Wohlfarth, B., Mitrovica, J.X., Hostetler, S.W. and McCabe, A.M., 2009. The last glacial maximum. *Science*, 325 (5941), pp.710-714.

Cloern, J. E., Canuel, E. A., & Harris, D. 2002. Stable carbon and nitrogen isotope composition of aquatic and terrestrial plants of the San Francisco Bay estuarine system. *Limnology and Oceanography,* 47 (3), 713-729

Cohen, A.L. and Tyson, P.D., 1995. Sea-surface temperature fluctuations during the Holocene off the south coast of Africa: implications for terrestrial climate and rainfall. *The Holocene*, 5 (3), pp.304-312.

Collins JA, SchefuB E, Heslop D, Mulitza S, Prange M, *et al.* 2011. Interhemispheric symmetry of the tropical African rainbelt over the past 23000 years. *Nat Geosci* 4, pp.42-45.

Collins, J.A., Schefuß, E., Govin, A., Mulitza, S. & Tiedemann, R. 2014. Insolation and glacial-interglacial control on southwestern African hydroclimate over the past 140000 years. *Earth and Planetary Science Letters*, 398, pp. 1–10.

Cooke, R.U. and Warren, A., 2023. *Geomorphology in Deserts*. University of California Press.

Cowling, R.M. 1983. The occurrence of C3 and C4 grasses in fynbos and allied shrublands in the South Eastern Cape, South Africa. *Oecologia* 58, 121–127

Crump, S.E., 2021. Sedimentary ancient DNA as a tool in paleoecology. *Nature Reviews Earth & Environment*, 2 (4), pp.229.

de Cort, G., Chevalier, M., Burrough, S. L., Chen, C. Y., & Harrison, S. P. 2021. An uncertainty-focused database approach to extract spatiotemporal trends from qualitative and discontinuous lake-status histories. *Quaternary Science Reviews*, 258.

De Lecea, A.M., 2016. *Benguela upwelling*. Available at: https://seaview.u-bordeaux.fr/Scenarios-Case-studies/Benguela-upwelling (Accessed: 14 April 2025).

Dee, S.G., Morrill, C., Kim, S.H. and Russell, J.M., 2021. Hot air, hot lakes, or both? Exploring mid-Holocene African temperatures using proxy system modeling. *Journal of Geophysical Research: Atmospheres*, 126 (10), pp. 2020JD033269.

del Hoyo, J., Elliott, A., Sargatal, J. and Christie, D.A., 1992. Handbook of the Birds of the World. 17 vols. *Lynx Edicions: Barcelona*.

Demenocal, P., Ortiz, J., Guilderson, T., Adkins, J., Sarnthein, M., Baker, L. and Yarusinsky, M., 2000. Abrupt onset and termination of the African Humid Period: Rapid climate responses to gradual insolation forcing. *Quaternary Science Reviews*, 19 (1-5), pp.347-361.

Diefendorf, A. F., Mueller, K. E., Wing, S. L., Koch, P. L., & Freeman, K. H. 2010. Global patterns in leaf 13C discrimination and implications for studies of past and future climate. *Proceedings of the National Academy of Sciences,* 107 (12), 5738-5743

Dietze, E., Hartmann, K., Diekmann, B., IJmker, J., Lehmkuhl, F., Opitz, S., Stauch, G., Wünnemann, B., & Borchers, A. 2012. An end-member algorithm for deciphering modern detrital processes from lake sediments of Lake Donggi Cona, NE Tibetan Plateau, China. *Sedimentary Geology*, 243-244, 169-180.

Dietze, E., Maussion, F., Ahlborn, M., Diekmann, B., Hartmann, K., Henkel, K., Kasper, T., Lockot, G., Opitz, S., & Haberzettl, T. 2022. Application of end-member modelling to grain-size data: Constraints and limitations. *Sedimentology*, 69 (2), 845-863.

Dimopoulos, E.A., Carmagnini, A., Velsko, I.M., Warinner, C., Larson, G., Frantz, L.A. and Irving-Pease, E.K., 2022. HAYSTAC: A Bayesian framework for robust and rapid

species identification in high-throughput sequencing data. *PLoS Computational Biology*, 18 (9), pp.1010493.

Djurhuus, A., Closek, C.J., Kelly, R.P., Pitz, K.J., Michisaki, R.P., Starks, H.A., Walz, K.R., Andruszkiewicz, E.A., Olesin, E., Hubbard, K. and Montes, E., 2020. Environmental DNA reveals seasonal shifts and potential interactions in a marine community. *Nature Communications*, 11 (1), pp.254.

Du Plessis, N., Chase, B.M., Quick, L.J. and Meadows, M.E., 2021. A Late Holocene pollen and microcharcoal record from Eilandvlei, southern Cape coast, South Africa. In *Quaternary Vegetation Dynamics, Gosling, W.D., Lezine, A. and Scott. L. (Eds),* 35, pp. 293-300. CRC Press.

Duller, G.A.T., 2003. Distinguishing quartz and feldspar in single grain luminescence measurements. *Radiation measurements*, 37 (2), pp.161-165.

Duller, G.A.T. 2008. Single-grain optical dating of Quaternary sediments: why aliquot size matters in luminescence dating. *Boreas*, 37 (4), 589-612

Dupont, L.M., Kim, J.H., Schneider, R.R. and Shi, N., 2004. Southwest African climate independent of Atlantic Sea surface temperatures during the Younger Dryas. *Quaternary Research*, 61 (3), pp.318-324.

Durcan, J.A., Roberts, H.M., Duller, G.A.T. and Alizai, A.H., 2010. Testing the use of range-finder OSL dating to inform field sampling and laboratory processing strategies. *Quaternary Geochronology*, 5 (2-3), pp.86-90.

Dussex, N., Bergfeldt, N., de Anca Prado, V., Dehasque, M., Díez-del-Molino, D., Ersmark, E., Kanellidou, F., Larsson, P., Lemež, Š., Lord, E. and Mármol-Sánchez, E., 2021. Integrating multi-taxon palaeogenomes and sedimentary ancient DNA to study past ecosystem dynamics. *Proceedings of the Royal Society B*, 288 (1957), p.20211252.

Eckardt, F.D., Bryant, R.G., McCulloch, G., Spiro, B. & Wood, W.W. 2008. The hydrochemistry of a semi-arid pan basin case study: Sua Pan, Makgadikgadi, Botswana. *Applied Geochemistry*. 23 (6),1563–1580.

Eckardt, F.D., Livingstone, I., Seely, M. and Von Holdt, J., 2013. The surface geology and geomorphology around Gobabeb, Namib Desert, Namibia. *Geografiska Annaler: Series A, Physical Geography*, 95 (4), pp.271-284.

Ecker, M., Kelley, D. and Sato, H., 2020. Modelling the effects of CO_2 on C_3 and C_4 grass competition during the mid-Pleistocene transition in South Africa. *Scientific Reports*, 10 (1), p.16234.

Ehleringer, J.R., Cerling, T.E. and Helliker, B.R., 1997. C4 photosynthesis, atmospheric CO2, and climate. *Oecologia*, 112 (3), pp.285-299.

Ellis, R. P., Vogel, J. C., Fuls, A. 1980. Photosynthetic pathways and the geographical distribution of grasses in South West Africa/Namibia. *S Afr J Sci* 76, pp.307–314.

Emslie, S.D. and Patterson, W.P., 2007. Abrupt recent shift in δ13C and δ15N values in Adélie penguin eggshell in Antarctica. *Proceedings of the National Academy of Sciences*, 104 (28), pp.11666-11669.

Engelbrecht, F.A., Marean, C.W., Cowling, R.M., Engelbrecht, C.J., Neumann, F.H., Scott, L., Nkoana, R., O'Neal, D., Fisher, E., Shook, E. and Franklin, J., 2019. Downscaling last glacial maximum climate over southern Africa. *Quaternary Science Reviews*, 226, p.105879.

Flower, R.J. and Ryves, D.B., 2009. Diatom preservation: differential preservation of sedimentary diatoms in two saline lakes. *Acta Botanica Croatica*, 68 (2), pp.381-399.

Folk, R. L. and Ward, W. C. 1957. Brazos River bar: A study in the significance of grain size parameters. *Journal of Sedimentary Petrology*, 27 (1), 3-26.

Franchi, F., Cavalazzi, B., Evans, M., Filippidou, S., Mackay, R., Malaspina, P., Mosekiemang, G., Price, A. and Rossi, V., 2022. Late Pleistocene–Holocene palaeoenvironmental evolution of the Makgadikgadi Basin, Central Kalahari, Botswana: New evidence from shallow sediments and ostracod fauna. *Frontiers in Ecology and Evolution*, *10*, p.818417.

Fritz, S.C., 2022. Salinity and climate reconstruction from diatoms in continental lake deposits. *Earth Systems and Environmental Sciences.* Reference Module in Earth Systems and Environmental Sciences. Elsevier.

Galbraith, R.F. and Green, P.F., 1990. Estimating the component ages in a finite mixture. *International Journal of Radiation Applications and Instrumentation. Part D. Nuclear Tracks and Radiation Measurements*, 17 (3), pp.197-206.

Galbraith, R.F. and Laslett, G.M., 1993. Statistical models for mixed fission track ages. *Nuclear Tracks and Radiation Measurements*, 21 (4), pp.459-470.

Galbraith, R.F., Roberts, R.G., Laslett, G.M., Yoshida, H., Olley, J.M., Galbraith, R.F., Olley, J.M., Yoshida, H. and Laslett, G.M. 1999. Optical dating of single and multiple grains of quartz from Jinmium rock shelter, Northern Australia: *Archaeometry*, 41 (2): 339–364,

Gärtner, A., Hofmann, M., Zieger, J., Sagawe, A., Krause, R., Stutzriemer, M., Gesang, S., Gerdes, A., Marko, L., Lana, C. and Linnemann, U., 2022. Implications for sedimentary transport processes in southwestern Africa: a combined zircon morphology and age study including extensive geochronology databases. *International Journal of Earth Sciences*, 111 (3), pp.767-788.

Gasse, F., 2000. Hydrological changes in the African tropics since the Last Glacial Maximum. *Quaternary Science Reviews*, 19 (1-5), pp.189-211.

Gasse, F., Barker, P., Gell, P.A., Fritz, S.C. and Chalie, F., 1997. Diatom-inferred salinity in palaeolakes: an indirect tracer of climate change. *Quaternary Science Reviews*, 16 (6), pp.547-563.

Genderjahn, S., Alawi, M., Kallmeyer, J., Belz, L., Wagner, D. and Mangelsdorf, K., 2017. Present and past microbial life in continental pan sediments and its response to climate variability in the southern Kalahari. *Organic Geochemistry*, 108, pp.30-42.

Gersonde, R., Crosta, X., Abelmann, A. and Armand, L., 2005. Sea-surface temperature and sea ice distribution of the Southern Ocean at the EPILOG Last Glacial Maximum—a circum-Antarctic view based on siliceous microfossil records. *Quaternary Science Reviews*, 24 (7-9), pp.869-896.

Geyh, M.A. and Eitel, B., 1997. Radiometric dating of young and old calcrete. *Radiocarbon*, 40 (2), pp.795-802.

Geyh, M.A. and Heine, K., 2014. Several distinct wet periods since 420 ka in the Namib Desert inferred from U-series dates of speleothems. *Quaternary Research*, 81 (2), pp.381-391.

Gil-Romera, G., Scott, L., Marais, E. and Brook, G.A., 2007. Late Holocene environmental change in the northwestern Namib Desert margin: new fossil pollen evidence from hyrax middens. *Palaeogeography, Palaeoclimatology, Palaeoecology*, 249 (1-2), pp.1-17.

Gingele, F.X. 1996. Holocene climatic optimum in Southwest Africa - Evidence from the marine clay mineral record. *Palaeogeography, Palaeoclimatology, Palaeoecology*. 122 (1–4), pp.77–87.

Gordon, N., García-Rodríguez, F. and Adams, J.B., 2012. Paleolimnology of a coastal lake on the Southern Cape coast of South Africa: Sediment geochemistry and diatom distribution. *Journal of African Earth Sciences*, 75, pp.14-24.

Goudie, A.S. and Wells, G.L., 1995. The nature, distribution and formation of pans in arid zones. *Earth-Science Reviews*, 38 (1), pp.1-69.

Goudie, A. and Viles, H. 2015. Koes and the Nature and Origin of Pans. In: Landscapes and Landforms of Namibia. *World Geomorphological Landscapes*, Springer, Dordrecht.

Goudie, A.S., 1991. *Pans*. Progress in Physical Geography, 15 (3), pp.221-237.

Grealy, A., Rawlence, N.J. and Bunce, M., 2017. Time to spread your wings: a review of the avian ancient DNA field. *Genes*, 8 (7), p.184.

Grobler, B.A., Franklin, J., Marean, C.W., Gravel-Miguel, C. and Cowling, R.M., 2023. The importance of C_3 and C_4 grasses and CAM shrubs in the Greater Cape Floristic Region under contemporary and Last Glacial Maximum climates. *Quaternary Science Reviews*, 318, pp.108294.

Gudka, M., Davies, J., Poulsen, L., Schulte-Herbrüggen, B., MacKinnon, K., Crawhall, N., Henwood, W.D., Dudley, N. and Smith, J., 2014. Conserving dryland biodiversity: a future vision of sustainable dryland development. *Biodiversity*, 15 (2-3), pp.143-147.

Guérin, G. 2013. Luminescence Dating, Dose Rates. In Rink, W.J. and Thompson, J. (Eds), *Encyclopedia of scientific dating methods*, pp. 1–6. Springer Netherlands, Dordrecht

Haddon, I., 1999. Isopach Map of the Kalahari Group. *(No Title)*. Council for Geoscience, Pretoria, South Africa

Haddon, I.G. and McCarthy, T.S., 2005. The Mesozoic–Cenozoic interior sag basins of Central Africa: the late-Cretaceous–Cenozoic Kalahari and Okavango basins. *Journal of African Earth Sciences*, 43 (1-3), pp.316-333.

Haug, G.H., Hughen, K.A., Sigman, D.M., Peterson, L.C. and Rohl, U., 2001. Southward migration of the intertropical convergence zone through the Holocene. *Science*, 293 (5533), pp.1304-1308.

Hedberg, R.M., 1979. *Stratigraphy of the Ovamboland Basin, South West Africa* (Vol. 24). University of Cape Town, Department of Geology.

Heine, K., 1982. The main stages of the late Quaternary evolution of the Kalahari region, southern Africa. *Palaeoecology of Africa and the Surrounding Islands*, 15, pp.53-76.

Heine, K. and Heine, J.T. 2002. A paleohydrologic reinterpretation of the Homeb Silts, Kuiseb River, central Namib Desert (Namibia) and paleoclimatic implications. *Catena*, 48 (1-2), 107-130

Henderson, G.M., 2002. New oceanic proxies for paleoclimate. *Earth and Planetary Science Letters*, 203 (1), pp.1-13.

Hillary S. R., L. Railsback, B. L., Liang, F. Brook, G.A., Marais, E. Hardt, B.F. Cheng, H. and Edwards, L.R. 2013. A petrographic and geochemical record of climate change over the last 4600 years from a northern Namibia stalagmite, with evidence of abruptly wetter climate at the beginning of southern Africa's Iron Age. *Palaeogeography, Palaeoclimatology, Palaeoecology,* 376, pp.149-162.

Hipondoka, M.H., 2005. *The Development and Evolution of Etosha Pan, Namibia*, Doctoral Dissertation, Universität Würzburg.

Hipondoka, M.H., Busche, D. and Kempf, J., 2004. Source of Lunette Dune Sediments: A Geomorphic Terrain Analysis Approach in Etosha National Park, Namibia (Zur Herkunft von Lunettedünen-Sedimenten im Etoscha-Nationalpark, Namibia). *Erdkunde*, 58 (3), pp.212-220.

Hipondoka, M.H.T., Jousse, H., Kempf, J. and Busche, D., 2006. Fossil evidence for perennial lake conditions during the Holocene at Etosha Pan, Namibia: news and views. *South African Journal of Science*, 102 (3), pp.93-95.

Hipondoka, M.H.T., Mauz, B., Kempf, J., Packman, S., Chiverrell, R.C. and Bloemendal, J., 2014. Chronology of sand ridges and the Late Quaternary evolution of the Etosha Pan, Namibia. *Geomorphology*, 204, pp.553-563.

Hoetzel, S., Dupont, L.M. and Wefer, G., 2015. Miocene–Pliocene vegetation change in south-western Africa (ODP Site 1081, offshore Namibia). *Palaeogeography, Palaeoclimatology, Palaeoecology*, 423, pp.102-108.

Hogg, A. G., Heaton, T. J., Hua, Q., Palmer, J. G., Turney, C. S., Southon, J., Bayliss, A., Blackwell, P. G., Boswijk, G., Ramsey, C. B., Pearson, C., Petchey, F., Reimer, P., Reimer, R., & Wacker, L. 2020. SHCal20 Southern Hemisphere Calibration, 0–55,000 Years cal BP. *Radiocarbon,* 62 (4), 759-778.

Holmgren, K. and Shaw, P., 1997. Palaeoenvironmental reconstruction from near-surface pan sediments: an example from Lebatse pan, southeast Kalahari, Botswana. *Geografiska Annaler: Series A, Physical Geography*, 79 (1-2), pp.83-93.

Holmgren, Karen and Shaw, P., 1999. A late Pleistocene palaeoenvironmental record from Lobatse II Cave. *Botswana Notes & Records*, 31 (1), pp.73-82.

Horisk, K.E., Ivory, S.J., McCorriston, J., McHale, M., Al Mehri, A., Anderson, A., Anderson, R.S. and Al Kathiri, A.A., 2023. Vegetation dynamics in Dhofar, Oman, from

the Late Holocene to present inferred from rock hyrax middens. *Quaternary Research*, 116, pp.12-29.

Horne, D.J., Holmes, J.A., Rodriguez-Lazaro, J. and Viehberg, F.A., 2012. Ostracoda as proxies for Quaternary climate change: overview and future prospects. *Developments in Quaternary Sciences*, 17, pp.305-315.

Hou, J., D'Andrea, W.J. and Huang, Y., 2008. Can sedimentary leaf waxes record D/H ratios of continental precipitation? Field, model, and experimental assessments. *Geochimica et Cosmochimica Acta*, 72 (14), pp.3503-3517.

Howard, E. and Washington, R., 2019. Drylines in southern Africa: Rediscovering the Congo air boundary. *Journal of Climate*, 32 (23), pp.8223-8242.

Hughes, P.D., Gibbard, P.L. and Ehlers, J., 2013. Timing of glaciation during the last glacial cycle: evaluating the concept of a global 'Last Glacial Maximum'(LGM). *Earth-Science Reviews*, 125, pp.171-198.

Huntley, B.J. (2019) 'Angola in Outline: Physiography, Climate and Patterns of Biodiversity', in Huntley, B.J., Russo, V., Lages, F. and Ferrand, N. (eds.) *Biodiversity of Angola: Science & Conservation: A Modern Synthesis*. Cham: Springer, pp. 15-42

Huntsman-Mapila, P., Ringrose, S., Mackay, A.W., Downey, W.S., Modisi, M., Coetzee, S.H., Tiercelin, J.J., Kampunzu, A.B. and Vanderpost, C., 2006. Use of the geochemical and biological sedimentary record in establishing palaeo-environments and climate change in the Lake Ngami basin, NW Botswana. *Quaternary International*, 148 (1), pp.51-64.

Ikhane, P. R., Oladipo, O. V., & Oyebolu, O. O. 2019. Predicting the depositional environments and transportation mechanisms of sediments using granulometric parameters, bivariate and multivariate analyses. *GeoScience Engineering*, 65 (1), 11–28.

Inglis, G.N., Bhattacharya, T., Hemingway, J.D., Hollingsworth, E.H., Feakins, S.J. and Tierney, J.E., 2022. Biomarker approaches for reconstructing terrestrial environmental change. *Annual Review of Earth and Planetary Sciences*, 50 (1), pp.369-394.

Jackson, S.T. and Williams, J.W., 2004. Modern analogs in Quaternary paleoecology: here today, gone yesterday, gone tomorrow?. *Ann. Rev. Earth Planet. Sci.*, 32 (1), pp.495-537.

Jacobs, Z., Hayes, E.H., Roberts, R.G., Galbraith, R.F. and Henshilwood, C.S., 2013. An improved OSL chronology for the Still Bay layers at Blombos Cave, South Africa: further tests of single-grain dating procedures and a re-evaluation of the timing of the Still Bay industry across southern Africa. *Journal of Archaeological Science*, 40 (1), pp.579-594.

Jaeger, F. 1926. *Die Etoschapfanne*. Mitteilungen aus dem Deutschen Schutzgebieten, 34 (1), pp.1–22.

James, R., Washington, R., Abiodun, B., Kay, G., Mutemi, J., Pokam, W., Hart, N., Artan, G. and Senior, C., 2018. Evaluating climate models with an African lens. *Bulletin of the American Meteorological Society*, 99 (2), pp.313-336.

Jenks, M.A., Ashworth, E.N. and Janick, J., 1999. Plant epicuticular waxes: function, production, and genetics. *Hortic Rev*, 23, pp.1-54.

Johnson, B.J., Fogel, M.L. and Miller, G.H., 1998. Stable isotopes in modern ostrich eggshell: a calibration for paleoenvironmental applications in semi-arid regions of southern Africa. *Geochimica et Cosmochimica Acta*, 62 (14), pp.2451-2461.

Jokisch, A. and Urban, W., 2012, April. Lessons learned from the integration of local stakeholders in water management approaches in central-northern Namibia. In *EGU General Assembly Conference Abstracts,* pp.9335.

Joo, Y.J., Soreghan, A.M., Madden, M.E.E. and Soreghan, G.S., 2018. Quantification of particle shape by an automated image analysis system: a case study in natural sediment samples from extreme climates. *Geosciences Journal*, 22, pp.525-532.

Joussaume, S., Taylor, K.E., Braconnot, P.J.F.B., Mitchell, J.F.B., Kutzbach, J.E., Harrison, S.P., Prentice, I.C., Broccoli, A.J., Abe-Ouchi, A., Bartlein, P.J. and Bonfils, C., 1999. Monsoon changes for 6000 years ago: results of 18 simulations from the Paleoclimate Modeling Intercomparison Project (PMIP). *Geophysical Research Letters*, 26 (7), pp.859-862.

Kageyama, M., Albani, S., Braconnot, P., Harrison, S.P., Hopcroft, P.O., Ivanovic, R.F., Lambert, F., Marti, O., Peltier, W.R., Peterschmitt, J.Y. and Roche, D.M., 2017. The PMIP4 contribution to CMIP6–Part 4: Scientific objectives and experimental design of the PMIP4-CMIP6 Last Glacial Maximum experiments and PMIP4 sensitivity experiments. *Geoscientific Model Development*, 10 (11), pp.4035-4055.

Kageyama, M., Braconnot, P., Bopp, L., Caubel, A., Foujols, M.-A., Guilyardi, E., Khodri, M., Lloyd, J., Lombard, F., Mariotti, V., Marti, O., Roy, T. and Woillez, M.-N., 2013. Mid-Holocene and Last Glacial Maximum climate simulations with the IPSL model—part I: comparing IPSL_CM5A to IPSL_CM4, *Climate Dynamics*, 40 (9-10), pp. 2447-2468.

Kandel, A.W. and Conard, N.J., 2005. Production sequences of ostrich eggshell beads and settlement dynamics in the Geelbek Dunes of the Western Cape, South Africa. *Journal of Archaeological Science*, 32 (12), pp.1711-1721.

Karin, Holmgren., Julia, A., Lee-Thorp., Gordon, R., J., Cooper., Katarina, Lundblad., T., C., Partridge., Louis, Scott., Riashna, Sithaldeen., A., Siep, Talma., P., D., Tyson. 2003. Persistent millennial-scale climatic variability over the past 25,000 years in Southern Africa*. Quaternary Science Reviews,* 22 (21), 2311-2326.

Kirkels, F., de Boer, H., Concha Hernández, P., Martes, C., van der Meer, M., Basu, S., Usman, M. and Peterse, F., 2022. Carbon isotopic ratios of modern C_3 and C_4 vegetation on the Indian Peninsula and changes along the plant–soil–river continuum; implications for (paleo-) vegetation reconstructions. *Biogeosciences Discussions*, 2022, pp.1-34.

Kirsten, K., 2014. *Late Holocene diatom community responses to climate variability along the southern Cape coastal plain, South Africa*. PhD Thesis, University of Cape Town.

Kirsten, K.L., Haberzettl, T., Wündsch, M., Frenzel, P., Meschner, S., Smit, A.J., Quick, L.J., Mäusbacher, R. and Meadows, M.E., 2018. A multiproxy study of the ocean-atmospheric forcing and the impact of sea-level changes on the southern Cape coast, South Africa during the Holocene. *Palaeogeography, Palaeoclimatology, Palaeoecology*, 496, pp.282-291.

Kivisto, S.A., Dewar, G. and Finkelstein, S., 2016. *Evaluating paleoenvironmental and landscape mobility dynamics: stable isotope and strontium isotope analyses of ostrich eggshell at Spitzkloof Rockshelter*. Master's Thesis, University of Toronto.

Kuechler, R.R., Schefuß, E., Beckmann, B., Dupont, L. and Wefer, G., 2013. NW African hydrology and vegetation during the Last Glacial cycle reflected in plant-wax-specific hydrogen and carbon isotopes. *Quaternary Science Reviews*, 82, pp.56-67.

Kumar, M., Dashora, M., Kumar, R., Dubey, S. K., Gupta, P., & Kumar, A. 2022. Deciphering Depositional Environment of Playa Lakes Using Grain Size Parameters in the Arid and Semi-Arid Region of Rajasthan, India. *Agriculture*, 12 (12), 2043.

Lambeck, K., Rouby, H., Purcell, A., Sun, Y. and Sambridge, M., 2014. Sea level and global ice volumes from the Last Glacial Maximum to the Holocene. *Proceedings of the National Academy of Sciences*, 111 (43), pp.15296-15303.

Lancaster, N., 1986. Grain-size characteristics of linear dunes in the southwestern Kalahari. *Journal of Sedimentary Research*, 56 (3), pp.395-400.

Lang, S.C., Payenberg, T.H.D., Reilly, M.R.W., Hicks, T., Benson, J. and Kassan, J., 2004. Modern analogues for dryland sandy fluvial-lacustrine deltas and terminal splay reservoirs. *The APPEA Journal*, 44 (1), pp.329-356.

Last, W.M., 2002. Geolimnology of salt lakes. *Geosciences Journal*, 6, pp.347-369.

Lawson, M.P. and Thomas, D.S.G., 2002. Late Quaternary lunette dune sedimentation in the southwestern Kalahari Desert, South Africa: Luminescence Based Chronologies of Aeolian Activity. *Quaternary Science Reviews*, 21 (7), pp.825-836.

Lee-Thorp, J.A. and Ecker, M., 2015. Holocene environmental change at Wonderwerk Cave, South Africa: Insights from stable light isotopes in ostrich eggshell. *African Archaeological Review*, 32, pp.793-811.

Lee-Thorp, J.A. and Sponheimer, M., 2005. Opportunities and constraints for reconstructing palaeoenvironments from stable light isotope ratios in fossils. *Geological Quarterly*, 49 (2), pp.195-204.

Leterme, S.C., Prime, E., Mitchell, J., Brown, M.H. and Ellis, A.V., 2013. Diatom adaptability to environmental change: a case study of two Cocconeis species from high-salinity areas. *Diatom Research*, 28 (1), pp.29-35.

Levin, N.E., Brown, F.H., Behrensmeyer, A.K., Bobe, R. and Cerling, T.E., 2011. Paleosol carbonates from the Omo Group: Isotopic records of local and regional environmental change in East Africa. *Palaeogeography, Palaeoclimatology, Palaeoecology*, 307 (1-4), pp.75-89.

Lindahl, T., 1993. Instability and decay of the primary structure of DNA. *Nature*, 362 (6422), pp.709-715.

Lindeque, M. and Archibald, T.J. 1991. Seasonal wetlands in Ovambo and the Etosha National Park. *Madoqua,* 1991 (2), pp. 129–133.

Liu, S., Jiang, D. and Lang, X., 2019. Mid-Holocene drylands: A multi-model analysis using Paleoclimate Modelling Intercomparison Project phase III (PMIP3) simulations. *The Holocene*, 29 (9), pp.1425-1438.

Liu, X., Colman, S.M., Brown, E.T., Minor, E.C., Li, H., Liu, X., Colman, S.M., Brown, Á.E.T., *et al.* 2013. Estimation of carbonate, total organic carbon, and biogenic silica content by FTIR and XRF techniques in lacustrine sediments. *J. Paleolimnology*, 50, pp.387–398.

Lombard, M. and Högberg, A., 2018. The Still Bay points of Apollo 11 rock shelter, Namibia: an inter-regional perspective. *Azania: Archaeological Research in Africa*, 53 (3), pp.312-340.

Luetkemeier, R., Stein, L., Drees, L. & Liehr, S. 2017. Blended Drought Index: Integrated Drought Hazard Assessment in the Cuvelai-Basin. *Climate*. 5 (3), pp.51.

Lukich, V., Cowling, S. and Chazan, M., 2020. Palaeoenvironmental reconstruction of Kathu Pan, South Africa, based on sedimentological data. *Quaternary Science Reviews*, 230, p.p.106153.

Luyt, J., Lee-Thorp, J.A. and Avery, G., 2000. New light on Middle Pleistocene west coast environments from Elandsfontein, Western Cape Province, South Africa. *South African Journal of Science*, 96 (7), pp. 399-402.

Ma, L., Wu, J., Abuduwaili, J. and Liu, W., 2016. Geochemical responses to anthropogenic and natural influences in Ebinur Lake sediments of arid Northwest China. *PloS One*, 11 (5), p.p.0155819.

Mahan, S.A., Rittenour, T.M., Nelson, M.S., Ataee, N., Brown, N., DeWitt, R., Durcan, J., Evans, M., Feathers, J., Frouin, M. and Guérin, G., 2023. Guide for interpreting and reporting luminescence dating results. *Bulletin*, 135 (5-6), pp.1480-1502.

Mapani, B., Shikangalah, R., Mapaure, I. and Musimba, A., 2021. Dichrostachys cinerea growth rings as natural archives for climatic variation in Namibia. In *African Handbook of Climate Change Adaptation,* (pp. 2433-2446). Cham: Springer International Publishing.

Marker, M.E., and Holmes, P.J. 1995. Lunette dunes in the northeast Cape, South Africa, as geomorphic indicators of palaeoenvironmental change. *Catena,* 24, 259-273.

Mather, A., 2007. Arid environments. *Environmental Sedimentology*, pp.144-189.

McCulloch, G. and Irvine, K., 2004. Breeding of greater and lesser flamingos at sua pan, botswana, 1998–2001. *Ostrich-Journal of African Ornithology*, 75 (4), pp.236-242.

Meadows, M.E. and Holmes, P.J., 2018. Quaternary environmental change. In, Holmes, P. and Boardman, J. (Eds), *Southern African Landscapes and Environmental Change,* (pp. 275-294). Routledge. London.

Meadows, M.E., 2014. Recent methodological advances in Quaternary palaeoecological proxies. *Progress in Physical Geography*, 38 (6), pp.807-817.

Mendelsohn, J., Jarvis, A. and Robertson, T., 2013. *A Profile and Atlas of the Cuvelai-Etosha Basin*. Raison, John Mein, Windhoek.

Mendelsohn, J., Jarvis, A., Roberts, C., & Robertson, T. 2002. *Atlas of Namibia: A Portrait of the Land and its People*. David Philip Publishers, Cape Town.

Meyer, M. and Kircher, M., 2010. Illumina sequencing library preparation for highly multiplexed target capture and sequencing. *Cold Spring Harbor Protocols*, 2010 (6), pp.448.

Meyers, P.A., 1997. Organic geochemical proxies of paleoceanographic, paleolimnologic, and paleoclimatic processes. *Organic Geochemistry*, 27 (5-6), pp.213-250.

Middleton, N. 2011. *The Forgotten Billion: MDG Achievement in the Drylands*. New York: United Nations Development Programme.

Milewski, R., Chabrillat, S. and Behling, R., 2017. Analyses of recent sediment surface dynamic of a Namibian Kalahari salt pan based on multitemporal landsat and hyperspectral hyperion data. *Remote Sensing*, 9 (2), pp.170.

Miller, G.H., Beaumont, P.B., Deacon, H.J., Brooks, A.S., Hare, P.E. and Jull, A.J.T., 1999. Earliest modern humans in southern Africa dated by isoleucine epimerization in ostrich eggshell. *Quaternary Science Reviews*, 18 (13), pp.1537-1548.

Miller, R. McG., 2008. *The Geology of Namibia: Upper Palaeozoic to Cenozoic*., vol. 3. Ministry of Mines and Energy, Geologic Survey, Windhoek.

Miller, R.M., Pickford, M. and Senut, B. 2010. The geology, palaeontology and evolution of the Etosha Pan, Namibia: Implications for terminal Kalahari deposition. *South African Journal of Geology*, 113 (3), pp.307-334.

Mizuno, K. and Yamagata, K., 2005. Vegetational Succession and Plant Use in Relation to Environmental Change along the Kuiseb River in the Namib Desert. pp.35-50. *African Study Monograph*, Supplementary Issue, 30, pp.3-14

Moore, A., Blenkinsop, T. and Cotterill, F., 2009. Southern African topography and erosion history: plumes or plate tectonics? *Terra Nova*, 21 (4), pp.310-315.

Mucina, L., Rutherford, M.C. and Powrie, L.W., 2006. Logic of the map: Approaches and procedures. *The vegetation of South Africa, Lesotho and Swaziland. Pretoria: South African National Biodiversity Institute*, 19, pp.12-29.

Müller, W. and Fietzke, J., 2016. The role of LA–ICP–MS in palaeoclimate research. *Elements*, 12 (5), pp.329-334.

Munday, C., Engelstaedter, S., & Washington, R. 2021. African Low-Level Jets and Their Importance for Water Vapor Transport and Rainfall. *Geophysical Research Letters*, 48 (2).

Munsell, A.H., 2000. *Munsell soil color charts*. Gretagmacbeth. New Windsor, New York.

Murray, A.S., and Wintle, A.G. 2000. Luminescence dating of quartz using an improved single-aliquot regenerative-dose protocol. *Radiation Measurements*, 32 (5-6), 57-73.

Murray-Wallace, C.V., Richter, J. and Vogelsang, R., 2015. Aminostratigraphy and taphonomy of ostrich eggshell in the sedimentary infill of Apollo 11 Rockshelter, Namibia. *Journal of Archaeological Science: Reports*, 4, pp.143-151.

Murray, A., Arnold, L.J., Buylaert, J.P., Guérin, G., Qin, J., Singhvi, A.K., Smedley, R. and Thomsen, K.J., 2021. Optically stimulated luminescence dating using quartz. *Nature Reviews Methods Primers*, 1 (1), pp.72.

Mwilima, F.J., 2008. Practical reality of media freedom: an examination of the challenges facing the Namibian media. *Global Media Journal-African Edition*, 2 (2), pp.128-131.

Nash, D.J., Meadows, M.E. & Gulliver, V.L. 2006. Holocene environmental change in the Okavango Panhandle, northwest Botswana. *Quaternary Science Reviews*, 25 (11–12), pp.1302–1322.

National Research Council, Division on Earth, Life Studies, Board on Earth Sciences and Committee on the Importance of Deep-Time Geologic Records for Understanding Climate Change Impacts, 2011. *Understanding Earth's Deep Past: Lessons from Climate Future*. National Academies Press.

Netterberg, F., 1978. Dating and correlation of calcretes and other pedocretes. *South African Journal of Geology*, 81 (3), pp.379-391.

Neumann, F.H., Scott, L., Bousman, C.B. and Van As, L., 2010. A Holocene sequence of vegetation change at Lake Eteza, coastal KwaZulu-natal, South Africa. *Review of Palaeobotany and Palynology*, 162 (1), pp.39-53.

Newsham, A.J. and Thomas, D.S., 2011. Knowing, farming and climate change adaptation in North-Central Namibia. *Global Environmental Change*, 21 (2), pp.761-770.

Nhiwatiwa, T., & Dalu, T. 2017. Seasonal variation in pans in relation to limno-chemistry, size, hydroperiod, and river connectivity in a semi-arid subtropical region. *Physics and Chemistry of The Earth,* 97, 37-45.

Niang, I., Ruppel, O. C., Abdrabo, M. A., Essel, A., Lennard, C. & Padgham, J. 2014. Africa. In: V. R. Barros (Ed.), *Climate Change 2014: Impacts, Adaptation, And Vulnerability*. Part B: Regional Aspects. Contribution Of Working Group ii to the Fifth Assessment Report Of The Intergovernmental Panel On Climate Change. 1199–1265. Cambridge, United Kingdom and New York, NY: Cambridge

Nicholson, S.E. 2000. The nature of rainfall variability over Africa on time scales of decades to millenia. *Global and Planetary Change*. 26 (1–3), pp.137–158.

Nicholson, S.E., 2018. The ITCZ and the seasonal cycle over equatorial Africa. *Bulletin of the American Meteorological Society*, 99 (2), pp.337-348.

Niespolo, E.M., Sharp, W.D., Tryon, C.A., Faith, J.T., Lewis, J., Ranhorn, K., Mambelli, S., Miller, M.J. and Dawson, T.E., 2020. Carbon, nitrogen, and oxygen isotopes of ostrich eggshells provide site-scale Pleistocene-Holocene paleoenvironmental records for eastern African archaeological sites. *Quaternary Science Reviews*, 230, p.106142.

Ning, S. and Dupont, L.M., 1997. Vegetation and climatic history of southwest Africa: a marine palynological record of the last 300,000 years. *Vegetation History and Archaeobotany*, 6, pp.117-131.

Njagi, D.M., Routh, J., Olago, D. and Gayantha, K., 2021. A multi-proxy reconstruction of the late Holocene climate evolution in the Kapsabet Swamp, Kenya (East Africa). *Palaeogeography, Palaeoclimatology, Palaeoecology*, 574, p.110475.

Norström, E., Risberg, J., Gröndahl, H., Holmgren, K., Snowball, I., Mugabe, J.A. and Sitoe, S.R., 2012. Coastal paleo-environment and sea-level change at Macassa Bay, southern Mozambique, since c 6600 cal BP. *Quaternary International*, 260, pp.153-163.

North, S.M., Stockhecke, M., Tomonaga, Y. and Mackay, A.W., 2018. Analysis of a fragmentary diatom record from Lake Van (Turkey) reveals substantial lake-level

variability during previous interglacials MIS7 and MIS5e. *Journal of Paleolimnology*, 59, pp.119-133.

Oba, G., 2014. *Climate Change Adaptation in Africa: an Historical Ecology*. Routledge.

Ognjanova-Rumenova, N., 2008, October. Palaeoenvironment and archaeology: the use of diatom analysis in archaeology. In, Kostov, R.I., Gaydarska, B., and Gurova, M (Eds) *Geoarchaeology and Archaeomineralogy, Proceedings of International Conference*, pp. 29-30. October 2008, Sofia, Publishing House, Sofia, pp. 291-294.

Olivier, W., Olivier, S. 1993. *A Guide to Namibian Game Parks*. Longman Namibia, Windhoek

Osborne, C.P. and Freckleton, R.P., 2009. Ecological selection pressures for C_4 photosynthesis in the grasses. *Proceedings of the Royal Society B: Biological Sciences*, 276 (1663), pp.1753-1760.

Oskam, C.L., Haile, J., McLay, E., Rigby, P., Allentoft, M.E., Olsen, M.E., Bengtsson, C., Miller, G.H., Schwenninger, J.L., Jacomb, C. and Walter, R., 2010. Fossil avian eggshell preserves ancient DNA. *Proceedings of the Royal Society B: Biological Sciences*, 277 (1690), pp.1991-2000.

Otto-Bliesner, B.L., Brady, E.C., Zhao, A., Brierley, C.M., Axford, Y.L., Capron, E., Govin, A., Hoffman, J.S., Isaacs, E., Kageyama, M. and Scussolini, P., 2021. Large-scale features of Last Interglacial climate: results from evaluating the lig127k simulations for the Coupled Model Intercomparison Project (CMIP6)-Paleoclimate Modeling Intercomparison Project (PMIP4). *Climate of the Past*, 17 (1), pp.63-94.

Partridge, T.C. and Maud, R.R., 2000. Macro-scale geomorphic evolution of southern Africa. *Oxford Monographs on Geology and Geophysics*, 40, pp.3-18.

Pereira, C., Couto, F. T., Salgado, R., & Gernandt, L. 2024. Drivers of seasonal rainfall variability over the Angolan and Namibian plateaus. *International Journal of Climatology*, 44 (5), 1751-1766

Peter and Braxmeier, H. 2020. Map of Cunene River. https://maps-for-free.com, CC BY-SA 2.0, https://commons.wikimedia.org/w/index.php?curid=88424882

Pickford, M., 2000. Neogene and Quaternary vertebrate biochronology of the Sperrgebiet and Otavi Mountainland, Namibia. *Communications of the Geological Survey of Namibia*, 12, pp.359-365.

Pickford, M., Senut, B., Hipondoka, M., Person, A., Segalen, L., Plet, C., Jousse, H., Mein, P., Guérin, C., Morales, J. and Mourer-Chauviré, C., 2009. Mio-plio-Pleistocene geology and palaeobiology of Etosha Pan, Namibia. *Communications of the Geological Survey of Namibia,* 14, pp.95-139.

Pinter, N., Scott, A.C., Daulton, T.L., Podoll, A., Koeberl, C., Anderson, R.S. and Ishman, S.E., 2011. The Younger Dryas impact hypothesis: A requiem. *Earth-Science Reviews*, 106 (3-4), pp.247-264.

Pokras, E.M. & Mix, A.C. 1985. Eolian evidence for spatial variability of late Quaternary climates in tropical Africa. *Quaternary Research*. 24 (2), pp.137–149.

Prescott, J.R. and Stephan, L.G., 1982. The contribution of cosmic radiation to the environmental dose for thermoluminescence. In *Pact*, 6, pp. 17-25.

Pye, K. and Blott, S.J., 2004. Particle size analysis of sediments, soils and related particulate materials for forensic purposes using laser granulometry. *Forensic Science International*, 144 (1), pp.19-27.

Quick, L.J., Chase, B.M., Meadows, M.E., Scott, L. and Reimer, P.J., 2011. A 19.5 kyr vegetation history from the central Cederberg Mountains, South Africa: palynological evidence from rock hyrax middens. *Palaeogeography, Palaeoclimatology, Palaeoecology*, 309 (3-4), pp.253-270.

Quick, L.J., Chase, B.M., Wuendsch, M., Kirsten, K.L., Chevalier, M., Maeusbacher, R., Meadows, M.E. and Haberzettl, T., 2018. A high-resolution record of Holocene climate and vegetation dynamics from the southern Cape coast of South Africa: pollen and microcharcoal evidence from Eilandvlei. *Journal of Quaternary Science*, 33 (5), pp.487-500.

Quick, L.J., Meadows, M.E., Bateman, M.D., Kirsten, K.L., Mäusbacher, R., Haberzettl, T. and Chase, B.M., 2016. Vegetation and climate dynamics during the last glacial period in the fynbos-afrotemperate forest ecotone, southern Cape, South Africa. *Quaternary International*, 404, pp.136-149.

Railsback, L. B., Kraft, S., Liang, F., Brook, G. A., Marais, E., Cheng, H., & Edwards, R. L. 2019. Control of insolation on stalagmite growth, rainfall, and migration of the tropical rain belt in northern Namibia over the last 100 kyr, as suggested by a rare MIS

5b-5c stalagmite from Dante Cave. *Palaeogeography, Palaeoclimatology, Palaeoecology,* 535. pp.109348

Railsback, L.B., Brook, G.A., Liang, F., Marais, E., Cheng, H. and Edwards, R.L., 2016. A multi-proxy stalagmite record from northwestern Namibia of regional drying with increasing global-scale warmth over the last 47 kyr: The interplay of a globally shifting ITCZ with regional currents, winds, and rainfall. *Palaeogeography, Palaeoclimatology, Palaeoecology*, 461, pp.109-121.

Railsback, L. B., Liang, F., Brook, G. A., Cheng, H., and Edwards, R. L. 2022. Additional multi-proxy stalagmite evidence from northeast Namibia supports recent models of wetter conditions during the 4.2 ka Event in the Southern Hemisphere. *Palaeogeography, Palaeoclimatology, Palaeoecology*, 586. pp.110756

Rawlence, N.J., Lowe, D.J., Wood, J.R., Young, J.M., Churchman, G.J., HUANG, Y.T. and Cooper, A., 2014. Using palaeoenvironmental DNA to reconstruct past environments: progress and prospects. *Journal of Quaternary Science*, 29 (7), pp.610-626.

Reimer, R.W. and Reimer, P.J. 2024 *CALIBomb* [Computer program]. Available at: http://calib.org (Accessed: 5 December 2024).

Renaut, R.W. and Owen, R.B., 2023. Lake processes and sedimentation. In, Renaut R, W., Owen, R.B (Eds). *The Kenya Rift Lakes: Modern and Ancient: Limnology and Limnogeology of Tropical Lakes in a Continental Rift*. pp. 129-160. Berlin, Heidelberg: Springer Berlin Heidelberg.

Revéret, A., Rijal, D.P., Heintzman, P.D., Brown, A.G., Stoof-Leichsenring, K.R. and Alsos, I.G., 2023. Environmental DNA of aquatic macrophytes: The potential for reconstructing past and present vegetation and environments. *Freshwater Biology*, 68 (11), pp.1929-1950.

Roberts, H.M., Durcan, J.A. and Duller, G.A., 2009. Exploring procedures for the rapid assessment of optically stimulated luminescence range-finder ages. *Radiation Measurements*, 44 (5-6), pp.582-587.

Rollinson, H. 2014. *Using Geochemical Data: Evaluation, Presentation, Interpretation.* Routledge, New York.

Rosenthal, Y., 2007. Chapter nineteen elemental proxies for reconstructing Cenozoic seawater paleotemperatures from calcareous fossils. *Developments in Marine Geology*, 1, pp.765-797.

Rossignol-Strick, M. 1985. Mediterranean Quaternary sapropels, an immediate response of the African monsoon to variation of insolation. *Palaeogeography, Palaeoclimatology, Palaeoecology*, 49 (3–4), pp.237–263.

Rothwell, R.G. and Croudace, I. 2015. *Twenty Years of XRF Core Scanning Marine Sediments: What Do Geochemical Proxies Tell* Us? In, Croudace I.W. and Rothwell, R, G. (Eds). Micro-XRF Studies of sediment cores, Springer, Dordrecht. pp.25–102.

Rousseeuw, P.J., 1987. Silhouettes: a graphical aid to the interpretation and validation of cluster analysis. *Journal of Computational and Applied Mathematics*, 20, pp.53-65.

Rozanski, K., Araguás-Araguás, L. and Gonfiantini, R., 1993. Isotopic patterns in modern global precipitation. *Geophysical Monograph Series*, 78, pp.1-36.

Rust, U. 1984. Geomorphic evidence of Quaternary environmental changes in Etosha, South West Africa/Namibia. in C. Vogel (ed.) *Late Cainozoic Palaeoclimates of the Southern Hemisphere: Proceedings of the SASQUA International Symposium*. Rotterdam: Balkema, pp.279–286.

Rust, U., 1985. Die Entstehung der Etoschapfanne im Rah- men der Landschaftsentwicklung des Etosha Nationalparks (nrrdliches Stidwestafrika/Namibia). *Modoqua*, 14, pp.197-266.

Rutherford, M.C., Mucina, L. and Powrie, L.W., 2006. Biomes and bioregions of southern Africa. *The Vegetation of South Africa, Lesotho and Swaziland*, In, Mucina L. and Rutherford, M.C. (Eds), SANBI, Pretoria, pp.30-51.

Ryan, W.B., Carbotte, S.M., Coplan, J.O., O'Hara, S., Melkonian, A., Arko, R., Weissel, R.A., Ferrini, V., Goodwillie, A., Nitsche, F. and Bonczkowski, J., 2009. Global multi-resolution topography synthesis. *Geochemistry, Geophysics, Geosystems*, 10 (3).

Safriel, U., Adeel, Z., Niemeijer, D., Puigdefabregas, J., White, R., Lal, R., Winslow, M., Ziedler, J., Prince, S., Archer, E. and King, C., 2005. Dryland systems. In *Ecosystems and human well-being: current state and trends* Hassan, R., Scholes, R. and Ash, N (Eds), pp. 623-662. Island Press. Washington, DC.

Sauer, E.F. and Rochér, C.J., 1966. *Flamingo nests and eggs on Etosha Pan, South West Africa*. SWA. Wissenschaftliche Gesellschaft, Windhoek.

Schefuß, E., Kuhlmann, H., Mollenhauer, G., Prange, M. & Pätzold, J. 2011. Forcing of wet phases in southeast Africa over the past 17,000 years. *Nature*, 480 (7378), pp 509–512.

Schefuß, E., Schouten, S. and Schneider, R.R. 2005. Climatic controls on central African hydrology during the past 20,000 years. *Nature*, 437 (7061), pp.1003–1006.

Schmidt, I., Ossendorf, G., Bubenzer, O., Henselowsky, F., Luyt, J., Sealy, J. and Hensel, E., 2023. Pockenbank, Namibia. In, Beyin, A., Wright, DK., Wilkins, J and Olszewski, D.I. (Eds), *Handbook of Pleistocene Archaeology of Africa: Hominin Behavior, Geography, and Chronology,* pp. 897-911. Cham: Springer International Publishing.

Schmidt, M., Fuchs, M., Henderson, A.C.G., Kossler, A., Leng, M.J., Mackay, A.W., Shemang, E. and Riedel, F. 2017. Paleolimnological features of a mega-lake phase in the Makgadikgadi Basin (Kalahari, Botswana) during Marine Isotope Stage 5 inferred from diatoms. *Journal of Paleolimnology*, 58 (3), pp.373–390.

Schüller, I. and Wehrmann, A., 2016. Age Determinations of Witpan Sediment Sequence (Northern Cape, South Africa) by 14C dating of TOC Bulk Samples. In supplement to Schuller, I., Belz, L., Wilkes, H. and Wehrmann, A., 2018. Late Quaternary shift in southern African rainfall zones: sedimentary and geochemical data from Kalahari pans. *Zeitschrift für Geomorphologie*, 61 (4), pp.339-362.

Schuller, I., Belz, L., Wilkes, H. and Wehrmann, A., 2018. Late Quaternary shift in southern African rainfall zones: sedimentary and geochemical data from Kalahari pans. *Zeitschrift für Geomorphologie*, 61 (4), pp.339-362.

Schüller, I., Belz, L., Wilkes, H. and Wehrmann, A., 2022. Kalahari Pans: Quaternary Evolution and Processes of Ephemeral Lakes. In, Eckhardt, F (Ed), *Landscapes and Landforms of Botswana* (pp. 167-178). Cham: Springer International Publishing.

Schwarz, E. 1920. *The Kalahari or thirstland redemption*. Maskew Miller, Cape Town.

Schmidt, I., Ossendorf, G., Hensel, E., Bubenzer, O., Eichhorn, B., Gessert, L., Gwasira, G., Henselowsky, F., Imalwa, E., Kehl, M. and Rethemeyer, J., 2016. New investigations at the Middle Stone Age site of Pockenbank Rockshelter, Namibia. *Antiquity*, 90 (353), pp.2.

Scott, L., 1996. Palynology of hyrax middens: 2000 years of palaeoenvironmental history in Namibia. *Quaternary International*, 33, pp.73-79.

Scott, L., Cooremans, B., de Wet, J. S., and Vogel, J. C. 1991. Holocene environmental changes in Namibia inferred from pollen analysis of swamp sediments: the Otjikoto Lake record. *Palaeogeography, Palaeoclimatology, Palaeoecology*, 84 (1-4), 175-188.

Scott, L., Marais, E. and Brook, G.A., 2004. Fossil hyrax dung and evidence of Late Pleistocene and Holocene vegetation types in the Namib Desert. *Journal of Quaternary Science: Published for the Quaternary Research Association*, 19 (8), pp.829-832.

Shaamhula, L.V., Smit, H.A.P. and van der Merwe, J., 2021. Community responses to the annual flooding (efundja) in the Cuvelai-Etosha basin, Northern Namibia. *International Journal of Disaster Risk Reduction*, 61, pp.102372.

Shaw, P.A. and Bryant, R.G., 2011. Pans, playas and salt lakes. *Arid zone geomorphology: process, form and change in drylands*, In, D.S.G. Thomas (Ed). Arid Zone Geomorphology. John Wiley and Sons, pp.373-401.

Shi, N., Dupont, L.M., Beug, H.J. and Schneider, R., 1998. Vegetation and climate changes during the last 21 000 years in SW Africa based on a marine pollen record. *Vegetation History and Archaeobotany*, 7, pp.127-140.

Shikangalah, R.N., 2020. The 2019 drought in Namibia: an overview. *Journal of Namibian Studies: History Politics Culture*, 27, pp.37-58.

Singarayer, J. S., & Burrough, S. L. 2015. Interhemispheric dynamics of the African rainbelt during the late Quaternary. In *Quaternary Science Reviews*, 124, pp. 48–67.

Singarayer, J.S., Valdes, P.J. and Roberts, W.H., 2017. Ocean dominated expansion and contraction of the late Quaternary tropical rainbelt. *Scientific Reports*, 7 (1), pp.9382.

Singh, C. K., Singh, C. K., Kumar, P., Kumar, A. and Mukherjee, S. 2015. Depositional Environment in Great Indian Desert Using Grain Size Parameters and its Chemical Characterization. *Journal of The Geological Society of India*, Geological Society of India, 86 (4), pp.412–420.

Smith, A.J. and Palmer, D.F., 2012. The versatility of Quaternary ostracods as palaeoclimate proxies: comparative testing of geochemical, ecological and biogeographical approaches. In, D.J. Horne, J.A. Holmes, J. Rodriguez-Lazaro, F. Viehberg (Eds.), Ostracoda as Proxies for Quaternary Climate Change, *Developments in Quaternary Science*, 17, Elsevier, pp.183-203

Smith, A.M. and Mason, T.R., 1991. Pleistocene, multiple-growth, lacustrine oncoids from the Poacher's point formation, Etosha Pan, northern Namibia. *Sedimentology*, 38 (4).

Stanish, L.F., Nemergut, D.R. and McKnight, D.M., 2011. Hydrologic processes influence diatom community composition in Dry Valley streams. *Journal of the North American Benthological Society*, 30 (4), pp.1057-1073.

Still, C. J., Berry, J. A., Collatz, G. J., & DeFries, R. S. 2003. Global distribution of C3 and C4 vegetation: Carbon cycle implications. *Global Biogeochemical Cycles*, 17 (1)

Stone, A., Zeng, Y., Yu, L., Van Der Ploeg, M. and Wanke, H., 2022. Reconstructing rainfall using dryland dunes: Assessing the suitability of the southern Kalahari for unsaturated zone hydrostratigraphies. *Frontiers in Earth Science*, 10, pp.1034671.

Stone, A.E.C., 2013. Age and dynamics of the Namib Sand Sea: A review of chronological evidence and possible landscape development models. *Journal of African Earth Sciences*, 82, pp.70-87.

Street-Perrott, F.A., Barker, P.A., Swain, D.L., Ficken, K.J., Wooller, M.J., Olago, D.O. and Huang, Y., 2007. Late Quaternary changes in ecosystems and carbon cycling on

Mt. Kenya, East Africa: a landscape-ecological perspective based on multi-proxy lake-sediment influxes. *Quaternary Science Reviews*, 26 (13-14), pp.1838-1860.

Strobel, P., Kasper, T., Frenzel, P., Schittek, K., Quick, L.J., Meadows, M.E., Mäusbacher, R. and Haberzettl, T., 2019. Late Quaternary palaeoenvironmental change in the year-round rainfall zone of South Africa derived from peat sediments from Vankervelsvlei. *Quaternary Science Reviews*, 218, pp.200-214.

Strunk, A., Olsen, J., Sanei, H., Rudra, A. and Larsen, N.K., 2020. Improving the reliability of bulk sediment radiocarbon dating. *Quaternary Science Reviews*, 242, pp.106442.

Stuart-Williams, V., 1992. Overall tectonics, modern basin evolution and groundwater chemistry of the Owambo Basin. In *Abstracts, Kalahari Symposium, Geological Society of Namibia, Windhoek* (pp. 3-9).

Stute, M. and Talma, A.S., 1998. Glacial temperatures and moisture transport regimes reconstructed from noble gases and δ 18 O, Stampriet aquifer, Namibia. *Isotope Techniques in the Study of Past and Current Environmental Changes in the Hydrosphere and the Atmosphere*. Proceedings of Vienna Symposium 1997, IAEA, Vienna, SM-349/53, pp.307–328

Stuut, J.B.W., Prins, M.A., Schneider, R.R., Weltje, G.J., Fred Jansen, J.H. & Postma, G. 2002. A 300-kyr record of aridity and wind strength in southwestern Africa: Inferences from grain-size distributions of sediments on Walvis Ridge, SE Atlantic. *Marine Geology* 180 (1–4), pp.221–233.

Sullivan, S., Dieckmann, U. and Lendelvo, S. eds., 2024. *Etosha Pan to the Skeleton Coast: Conservation Histories, Policies and Practices in North-West Namibia*. Open Book Publishers.

Swap, R.J., Aranibar, J.N., Dowty, P.R., Gilhooly III, W.P. and Macko, S.A., 2004. Natural abundance of ^{13}C and ^{15}N in C_3 and C_4 vegetation of southern Africa: patterns and implications. *Global Change Biology*, 10 (3), pp.350-358.

Tabares, X., Zimmermann, H., Dietze, E., Ratzmann, G., Belz, L., Vieth-Hillebrand, A., Dupont, L., Wilkes, H., Mapani, B. and Herzschuh, U., 2020. Vegetation state changes in the course of shrub encroachment in an African savanna since about 1850 CE and their potential drivers. *Ecology and Evolution*, 10 (2), pp.962-979.

Taylor, S.H., Ripley, B.S., Martin, T., De-Wet, L.A., Woodward, F.I. and Osborne, C.P., 2014. Physiological advantages of C_4 grasses in the field: a comparative experiment demonstrating the importance of drought. *Global Change Biology*, 20 (6), pp.1992-2003.

Telfer, M.W. and Thomas, D.S.G., 2007. Late Quaternary linear dune accumulation and chronostratigraphy of the southwestern Kalahari: implications for aeolian palaeoclimatic reconstructions and predictions of future dynamics. *Quaternary Science Reviews*, 26 (19-21), pp.2617-2630.

Telfer, M.W., Thomas, D.S.G., Parker, A.G., Walkington, H. and Finch, A.A., 2009. Optically Stimulated Luminescence (OSL) dating and palaeoenvironmental studies of

pan (playa) sediment from Witpan, South Africa. *Palaeogeography, Palaeoclimatology, Palaeoecology*, 273 (1-2), pp.50-60.

Thomas, D.S. and Bailey, R.M., 2017. Is there evidence for global-scale forcing of Southern Hemisphere Quaternary desert dune accumulation? A quantitative method for testing hypotheses of dune system development. *Earth Surface Processes and Landforms*, 42 (14), pp.2280-2294.

Thomas, D.S. and Burrough, S.L., 2012. Interpreting geoproxies of late Quaternary climate change in African drylands: Implications for understanding environmental change and early human behaviour. *Quaternary International*, 253, pp.5-17.

Thomas, D.S., Brook, G., Shaw, P., Bateman, M., Haberyan, K., Appleton, C., Nash, D., McLaren, S. and Davies, F., 2003. Late Pleistocene wetting and drying in the NW Kalahari: an integrated study from the Tsodilo Hills, Botswana. *Quaternary International*, 104 (1), pp.53-67.

Thomas, D.S.G., 1987. Discrimination of depositional environments using sedimentary characteristics in the Mega Kalahari, central southern Africa. *Geological Society, London, Special Publications*, 35 (1), pp.293-306.

Tierney, J.E., Russell, J.M. and Huang, Y., 2010. A molecular perspective on Late Quaternary climate and vegetation change in the Lake Tanganyika basin, East Africa. *Quaternary Science Reviews*, 29 (5-6), pp.787-800.

Tieszen LL, Boutton TW, Tesdahl KG, Slade NA. 1983. Fractionation and turnover of stable carbon isotopes in animal tissues: Implications for $\delta^{13}C$ analysis of diet. *Oecologia,* 57 (1-2), pp.32-37.

Tooth, S., Nanson, G.C., and Bourke, M.C. 2006. Depositional environment and OSL chronology of the Homeb silt deposits, Kuiseb River, Namibia. *Quaternary Research*, 65 (3), 478-491.

Tooth, S. and McCarthy, T.S. 2007. Wetlands in drylands: geomorphological and sedimentological characteristics, with emphasis on examples from southern Africa. *Progress in Physical Geography*, 31 (1), pp.3-41.

Tovar, C., Breman, E., Brncic, T., Harris, D.J., Bailey, R. and Willis, K.J., 2014. Influence of 1100 years of burning on the central African rainforest. *Ecography*, 37 (11), pp.1139-1148.

Trippner, C., 1997. Salt content as an eco-pedological limiting factor in soils of the Etosha National Park, northern Namibia. *Madoqua*, 1997 (1), pp.105-113.

Tyson, P. D. 1986, *Climatic Change and Variability in Southern Africa*, Oxford University Press, Cape Town, 220 pp

Tyson, P.D. and Gatebe, C.K., 2001. The atmosphere, aerosols, trace gases and biogeochemical change in southern Africa: A regional integration: START Regional Syntheses. *South African Journal of Science*, 97 (3), pp.106-118.

Urrego, D.H., Sánchez Goñi, M.F., Daniau, A.L., Lechevrel, S. and Hanquiez, V., 2015. Increased aridity in southwestern Africa during the warmest periods of the last interglacial. *Climate of the Past*, 11 (10), pp.1417-1431.

van Zinderen, B., 1967. Upper Pleistocene and Holocene stratigraphy and ecology on the basis of vegetation changes in sub-Saharan Africa. W.W. Bishop, J.D. Clark (Eds.), Background to Evolution in Africa, University of Chicago Press, Chicago, pp.125-147

van Zinderen Bakker, E.M., 1984. Palynological evidence for late Cenozoic arid conditions along the Namibia coast from Holes 532 and 530A, Leg 75, Deep Sea Drilling Project. *Initial Reports of the Deep Sea Drilling Project*, 75, pp.763-768.

Viles, H.A. and Goudie, A.S., 2013. Weathering in the central Namib Desert, Namibia: controls, processes and implications. *Journal of Arid Environments*, 93, pp.20-29.

Voarintsoa, N.R.G., Brook, G.A., Liang, F., Marais, E., Hardt, B., Cheng, H., Edwards, R.L. and Railsback, L.B., 2017. Stalagmite multi-proxy evidence of wet and dry intervals in northeastern Namibia: Linkage to latitudinal shifts of the Inter-Tropical Convergence Zone and changing solar activity from AD 1400 to 1950. *The Holocene*, 27 (3), pp.384-396.

Vogelsang, R., 2008. The Rock Shelter Apollo 11—Evidence of Early Modern Humans in South-western Namibia. *Heritage and Cultures in Modern Namibia—In-depth Views of the Country*, (Eds) Limpricht, C. and Biesele, M. Klaus Hess Publisher, pp.183-92.

Vogelsang, R., Richter, J., Jacobs, Z., Eichhorn, B., Linseele, V. and Roberts, R.G., 2010. New excavations of Middle Stone Age deposits at Apollo 11 Rockshelter, Namibia: stratigraphy, archaeology, chronology and past environments. *Journal of African Archaeology*, 8 (2), pp.185-218.

Vogts, A., Moossen, H., Rommerskirchen, F. and Rullkötter, J., 2009. Distribution patterns and stable carbon isotopic composition of alkanes and alkan-1-ols from plant waxes of African rain forest and savanna C_3 species. *Organic Geochemistry*, 40 (10), pp.1037-1054.

Vossmerbäumer, H., 1974. Grain-size data of some aeolian sands: Inland dunes in Franconia (southern Germany), Algeria and Iran, a comparison. *Geologiska Föreningen i Stockholm Förhandlingar*, 96 (3), pp.261-274.

Walsh, E., Caracciolo, L., Ravidà, D., Burrough, S. and Thomas, D., 2022. Holocene fluvial depositional regimes of the Huab river, Skeleton coast, Namibia. *Earth Surface Processes and Landforms*, 47 (7), pp.1820-1844.

Ward, J.D., 1987. *The Cenozoic succession in the Kuiseb valley, central Namib Desert* (Vol. 9). Geological Survey, Department of Economic Affairs.

Ward, J.K., Tissue, D.T., Thomas, R.B. and Strain, B.R., 1999. Comparative responses of model C_3 and C_4 plants to drought in low and elevated CO_2. *Global Change Biology*, 5 (8), pp.857-867.

Washington, R., Todd, M., Middleton, N.J. and Goudie, A.S., 2003. Dust-storm source areas determined by the total ozone monitoring spectrometer and surface observations. *Annals of the Association of American Geographers*, 93 (2), pp.297-313.

Weissmann, G.S., Hartley, A.J., Scuderi, L.A., Nichols, G.J., Owen, A., Wright, S., Felicia, A.L., Holland, F. and Anaya, F.M.L., 2015. Fluvial geomorphic elements in modern sedimentary basins and their potential preservation in the rock record: a review. *Geomorphology*, 250, pp.187-219.

Wellington, H. 1938. The Kunene river and the Etosha plain. *South African Geographical Journal,* 20 (1): pp 21-32.

Wendt, W. E.1976. Art mobiler from the Apollo 11 cave, South West Africa: Africa's oldest dated works of art. *South African Archaeological Bulletin*, 31, pp.5-11.

Williams, C.J., Guarino, M.V., Capron, E., Malmierca-Vallet, I., Singarayer, J.S., Sime, L.C., Lunt, D.J. and Valdes, P.J., 2020. CMIP6/PMIP4 simulations of the mid-Holocene and Last Interglacial using HadGEM3: comparison to the pre-industrial era, previous model versions and proxy data. *Climate of the Past*, 16 (4), pp.1429-1450.

Wingate, V.R., Phinn, S.R. and Kuhn, N., 2019. Mapping precipitation-corrected NDVI trends across Namibia. *Science of the Total Environment*, 684, pp.96-112.

Wintle, A.G. and Murray, A.S., 2006. A review of quartz optically stimulated luminescence characteristics and their relevance in single-aliquot regeneration dating protocols. *Radiation measurements*, 41 (4), pp.369-391.

Wintle, A.G., 1997. Luminescence dating: laboratory procedures and protocols. *Radiation measurements*, 27 (5-6), pp.769-817.

Wintle, A.G., 2008. Luminescence dating: where it has been and where it is going. *Boreas*, 37 (4), pp.471-482.

Woor, S., Thomas, D.S., Parton, A. and Leenman, A., 2023. Morphology and controls of the mountain-front fan systems of the Hajar Mountains, south-east Arabia. *Earth-Science Reviews*, 237, pp.104316.

Wright, V.P., 2007. Calcrete. In, Nash D.J. and McLaren S.J. (Eds), *Geochemical sediments and landscapes*, Blackwell Publishing Ltd, pp.10-45.

Wündsch, M., Haberzettl, T., Cawthra, H.C., Kirsten, K.L., Quick, L.J., Zabel, M., Frenzel, P., Hahn, A., Baade, J., Daut, G. and Kasper, T., 2018. Holocene environmental change along the southern Cape coast of South Africa–Insights from the Eilandvlei sediment record spanning the last 8.9 kyr. *Global and Planetary Change*, 163, pp.51-66.

Yamagata, K. and Mizuno, K., 2005. Landform development along the middle course of the Kuiseb River in the Namib Desert, Namibia. *African Study Monographs. Supplementary Issue*, 30, pp.15-25.

Yanes, Y., Wolf, D. and Faust, D., 2019. Paleoenvironmental reconstruction and sedimentary processes in Drylands. *Quaternary Research*, 91 (1), pp.1-3.

Yang, Y., Yang, Y., Gao, S., Gao, S., Zhou, L., Zhou, L., Wang, Y., Li, G., Wang, Y. P., Han, Z., & Jia, P. 2017. Classifying the sedimentary environments of the Xincun Lagoon, Hainan Island, by system cluster and principal component analyses. *Acta Oceanologica Sinica*, 36 (4), 64–71.

Yokoyama, Y., Lambeck, K., De Deckker, P., Johnston, P. and Fifield, L.K., 2000. Timing of the Last Glacial Maximum from observed sea-level minima. *Nature*, 406 (6797), pp.713-716.

Zhu, B., Wang, X., Yu, J., Rioual, P., Zhang, Y. and Wang, P., 2016. Late Quaternary Environmental Change in The Namibia of Southern Africa. In, Sherman, W., Edition 7 of Handbook on Africa: Challenges and Issues of the 21st Century, *Journal of Earth Science & Climatic Change*, Nova, pp.119.

Ziegler, M., Simon, M.H., Hall, I.R., Barker, S., Stringer, C. and Zahn, R., 2013. Development of Middle Stone Age innovation linked to rapid climate change. *Nature Communications*, 4 (1), pp.1905.